11-30-2018

Genomic Imprinting and X Chromosome Dosage Compensation in Domestic Ruminants

Jingyue Duan
jingyue.duan@uconn.edu

Genomic Imprinting and X Chromosome Dosage Compensation in Domestic Ruminants

Jingyue (Ellie) Duan, Ph.D.

University of Connecticut, 2018

Abstract

In diploid cells, genes are presumed to be expressed from both alleles to maintain gene dosage for normal development. However, a small number of genes reach haplosufficiency even with only one functional allele per cell. Most of these genes are regulated through genomic imprinting and X chromosome inactivation (XCI). DNA methylation is an essential epigenetic regulation for developmental programming in embryogenesis and play crucial roles in genomic imprinting and XCI. This dissertation presents 1) effects of maternal diets on genome imprinting in fetal sheep (Chapter Two), 2) dosage compensation of the X chromosomes in bovine germline, embryos and somatic tissues (Chapter Three), 3) Whole genome DNA methylation in bovine in vivo preimplantation development (Chapter Four). In chapter two, we report the first throughput study of genomic imprinting in sheep and report the identification of 13 new imprinted genes as well as demonstrating that maternal diets affect expression of imprinted genes in fetuses. Our results determine maternal diets influence imprinted gene expression while the parental-of-origin expression pattern was not affected, further suggesting that gene expression levels and imprinted patterns may be regulated through different epigenetic mechanisms. In chapter three, we reported the up-regulation of X chromosome in bovine germline, embryos and somatic tissues, supporting a balanced expression between a single active X and autosome pairs. However, deviating from Ohno's theory, dosage compensation to rescue X haploinsufficiency appears to be an incomplete process for expressed genes but a complete process for "dosage-sensitive" genes. In chapter four, we adopted the scWGBS-seq method to comprehensive profile 5-MeC in single-cytosine

resolution in bovine sperm, immature oocyte, *in vivo/vitro* mature single oocyte, and *in vivo* developed 2-, 4-, 8-, 16-cell single embryos. We observed global demethylation during bovine embryo cleavage up to 8-cell stage and *de novo* methylation at 16-cell stage. Our results refined the current knowledge on bovine embryo DNA methylation dynamics and provide valuable resources for future studies.

Title Page

Genomic Imprinting and X Chromosome Dosage Compensation in Domestic Ruminants

Jingyue (Ellie) Duan

B.S., Sichuan University, P.R. China, 2014

M.S., University of Connecticut, U.S.A, 2017

A Dissertation

Submitted in Partial Fulfillment of the

Requirements for the Degree of

Doctor of Philosophy

at the

University of Connecticut

2018

Approval Page

Doctor of Philosophy Dissertation

Genomic Imprinting and X Chromosome Dosage Compensation in Domestic Ruminants

Presented by

Jingyue (Ellie) Duan, B.S., M.S.

Major Advisor _____
Dr. Xiuchun (Cindy) Tian

Associate Advisor_____
Dr. Ion Mandoiu

Associate Advisor_____
Dr. Lynn Kuo

Associate Advisor_____
Dr. Michael O'Neill

University of Connecticut

2018

DEDICATION

This dissertation is dedicated to my first biology teachers in the middle school, late Mr. Liewen Yang, who asked me what is cloning.

ACKNOWLEDGMENTS

I would like to express my deepest gratitude to my major advisor Dr. Xiuchun (Cindy) Tian for your instruction, encourage and support. Thank you for believe in me and motivate me to overcome challenges over the past four years. Your patient guidance helps me become a skilled and independent scientist. You are not only an advisor of my research but also a mentor of my life. Through you, I see the life of a creative, ingenuity, intelligent female scientist, and I see an independent, strong, caring, supportive mother. You are a person inspired me the most in my life, what I have learned from you are invaluable. Thank you.

I would like to thank my committee members Dr. Ion Mandoiu, Dr. Lynn Kuo, and Dr. Michael O'Neill, for your help, support and insight. Thank you for your instruction in data analysis, statistical analysis and biological knowledge. Thank you for your valuable feedback and comments that made my dissertation thesis possible.

I would like to thank all my collaborators in my projects, for your help in making these projects possible. Dr. Nathaniel Jue, Dr. Rachel O'Neill, Wei Shi, Dr. Sahar Seesi, Fahad AlQahtani, Dr. Sadie Marjani, Dr. Isabelle Hue, Dr. Amanda Jones, Dr. Sambhu Pillai, Dr. Maria Hoffman, Dr. Sarah A Reed, Dr. Kristen Govoni, Dr. Steve Zinn. Thank you for your help and expert advice in statistical analysis, computational approaches, experimental design and providing the valuable samples used in the experiment. I would like to thank the Animal science department main office, graduate students, and faculty for your kindness and support.

To my current and previous fellow graduate students, post-doc and visiting scholars, Lang Sun, Liqi An, Dr. Zongliang Jiang, Linkai Zhu, Kaleigh Flock, Ling Wang, Dr. Kanokwan Srirattana, Elizabeth Johnson, Shyann Williams, Lindsay Bavone, Taiye Adakole, Dr. Rashid Ali, Dr. Chuanjie Zhang, Chang Huang, Jacob Ricker, Cabrera Juan, Qian Du, Dr. Delun Huang, Dr.

Mingyuan Zhang, Dr. Limin Wang, Dr. Huan Yang, Dr. Junhe Hu, and Dr. Junli Zhu. Thank you for sharing your expertise with me in the lab, and for your support, help and friendship in my life. A special thanks to Dr. Zongliang Jiang, Kaleigh Flock, Dr. Mingyuan Zhang, Elizabeth Johnson for your collaboration and lab experiment expertise in two projects present in my dissertation, without your help, I couldn't achieve this much.

I would like to thank my previous advisor Dr. Qun Sun, Life Science College vice dean Dr. Yun Zhao in Sichuan University (SCU) and CAHNR dean Dr. Cameron Faustman. Thank you for initiating the 3+1 exchange program between SCU and UCONN. I would like to thank Dr. Robert Milvae, Dr. Kumar Venkitanarayanan, Dr. Hedley Freake for recruiting me in this exchange program. This was a life-changing experience in my undergrad senior year. I got more opportunities to learn and to see the world.

Lastly, I would also like to thank my family and friends for your love and support. Shanglong, thank you for loving me, taking care of me, understanding me, and supporting me through every challenge. Mom and Dad, thank you for always encouraging me to pursue my dream and believing in me. Dear friends, Suiyuan, Qianyue, Ruixuan, Manqian, and Xiaogang, thank you for being my friends. I have been friends with some of you since primary school, it means so much to me that we support each other achieve our goals and follow our dreams. Thank you for being there for me through this journey.

Table of contents

List of Common Abbreviations

5caC: 5-carboxylcytosine
5fC: 5-formylcytosine
5hmC: 5-hydroxymethylcytosine
5mC: 5-methylcytosine
cDNA: complementary deoxyribonucleic acid
CTCF: CCCTC binding factor
DNA: deoxyribonucleic acid
DNA-seq: DNA sequencing
DNMT: DNA methyltransferase
EGA: embryonic genome activation
FPKM: fragments per kilobase of exon per million fragments mapped
GEO: gene expression omnibus
GO: gene ontology
ICM: inner cell mass
ICR: imprinting control region
IVF: *in vitro* fertilization
LOS: large offspring syndrome
mRNA: messenger ribonucleic acid
MZT: maternal to zygotic genome transition
NGS: next generation sequencing
PCR: polymerase chain reaction
PGC: primordial germ cell
RNA: ribonucleic acid
RNA-seq: RNA sequencing
RRBS: reduced representation bisulfite sequencing
SNPs: single nucleotide polymorphisms
TAB-seq: ten-eleven-translocation -assisted bisulfite sequencing
TE: trophectoderm
TET: ten-eleven-translocation
TPM: transcripts per million
WGBS: whole genome bisulfite sequencing
XCI: X chromosome inactivation
Xi: inactivate X chromosome
Xic: X-inactivation center

List of Tables and Figures

List of Tables

Chapter 2

Chapter 3

List of Figures

Chapter 2

Chapter 3

Chapter 4

List of Supplementary Tables

Chapter 2

Chapter 3

Chapter 4

List of Supplementary Figures

Chapter 2

Chapter 3

Chapter 4

Chapter One

Introduction

1.1. Epigenetics

The term ‘epigenetics’ was first coined by Waddington, who defined epigenetics as a bridge that connects between genotype and phenotype (Waddington, 1942). In a broad view, epigenetics phenomenon is the transmittable changes governed by modifications on the chromatin rather than the alterations of the DNA sequences (Goldberg et al., 2007). These changes include DNA methylation, post-translational modification of histone tails (methylation, acetylation, phosphorylation, etc.), chromatin remodeling and noncoding RNAs (Kaikkonen et al., 2011; De Majo and Calore, 2018). Within all cells of the body, the DNA sequences are almost identical, while the epigenetic modifications are very different in different cell types (Canovas and Ross, 2016). Epigenetics modifications are not only mitotically transmitted, but also may affect several generations (Rakyan et al., 2003; Dolinoy et al., 2007). They mainly exerts their effects via regulation of gene expression (O’Neill, 2015). During development and cell differentiation, epigenetic markers reinforce cell-fate and form barriers that keep the cell specification in an irreversible process (Shi and Wu, 2009). However, robust and genome-wide epigenetic erasure, known as epigenetic reprogramming, occurs at two stages of mammalian development: post-fertilization pre-implantation embryogenesis and primordial germ cell specification (Gao et al., 2017). During these events, the epigenetic information is reset to the ground state, from which differentiation of more advanced cell linage occurs with new epigenetic markers (Seisenberger et al., 2012; Hackett and Surani, 2013).

Epigenetics modifications regulate many cellular process, such as proliferation, differentiation, cell cycle (Guo et al., 2015), cancer development (Sharma et al., 2010; Jansson and Lund, 2012), chromatin architecture (Choy et al., 2010; Siddiqi et al., 2010), genomic imprinting and X chromosome inactivation (Lyon, 1993; Ohlsson et al., 2001; Lee, 2003), all

through regulations of gene expression (Handy et al., 2011). Epigenetic marks vary by genome locations, different types of epigenetics modifications and chromatin accessibility associate with different states of transcription (Cao et al., 2018). For example, methylation of the fifth carbon of cytosine (5mC) within CpG island in a gene promoter reduces gene expression by recruiting repressors or inhibiting the binding of transcription factors (Siegfried et al., 1999; Moore et al., 2013), whereas DNA methylation in gene body is associated to gene active transcription (Suzuki and Bird, 2008; Yang et al., 2014). Enrichment of histone lysine methylation can correlate to either chromatin silencing (H3K9me3, H3K27me3 and H4K20me3) or transcription activation (H3K4me3, H3K36me3 and H3K79me3) (Vakoc et al., 2006; Black et al., 2012; Hyun et al., 2017). Acetylation modification of histone tails, such as H3K27ac and H4K16ac, is generally associated with open chromatin favoring gene expression (Morales and Richard-Foy, 2000; Clayton et al., 2006).

High throughput next generation sequencing (NGS) has provided detailed and comprehensive views of epigenetics modifications, such as DNA methylation, histone modification and chromatin architectures, on a genome scale (Meaburn and Schulz, 2012; Shen et al., 2014). To study DNA methylation, Whole Genome Bisulfite Sequencing (WGBS) is the gold standard method (Li et al., 2010a). It could detect the methylated CpG and calculate DNA methylation level in a high throughput manner (Lister et al., 2009; Li et al., 2010a, 2010b). Sodium bisulfite treatment changes unmethylated cytosines to thymines without altering the methylated cytosines, and NGS allows quantification of changes at the single cytosine level (Li et al., 2010a). Other methods to detect and quantify DNA methylation levels include Reduced Representation Bisulfite Sequencing (RRBS) (Smith et al., 2009), MethylC-sequencing (MethylC-seq) (Urich et al., 2015) and Methylated DNA Immunoprecipitation Sequencing

(MeDIP-seq) (Bock et al., 2010). Tet-assisted Bisulfite Sequencing (TAB-seq) has been developed for mapping and quantifying 5-hydroxylmethylcytosinces (5hmC), a Ten-eleven-translocation (TET) oxidation derivative of 5mC, at a single-base resolution on a genome-wide scale (Yu et al., 2012). Moreover, Chromatin Immunoprecipitation-Sequencing (ChIP-seq) combines ChIP and NGS for genome-wide DNA-protein interaction (Terrenoire et al., 2010). ChIP-seq generates high-resolution profiles of histone modifications in the genome (O'Geen et al., 2011). To determine the higher order spatial organization of the genomes and chromatin, a robust technology Chromosome Conformation Capture (3C) technology is developed (Wit and Laat, 2012). The 3C method studies the 'one-to-one' interaction between selected pairs of sequences (Denker and Laat, 2016). Several variations of the 3C technology have been developed, such as 'one-to-all' 4C (circularized 3C) (Dekker, 2006), 'many-to-many' 5C (3C carbon copy) (Dostie and Dekker, 2007), and 'all-to-all' Hi-C technology (Belton et al., 2012). Additionally, Chromatin Interaction Analysis with Paired-End-Tag (ChIA-PET) technology combines the 3C technology with ChIP-seq, and enables the enrichment and observation of rare specific interactions mediated by specific chromatin factors (Fullwood et al., 2009).

1.2. Preimplantation embryonic development

Preimplantation embryonic development starts with fertilization, undergoes cell cleavage, morula formation, blastulation, and ends with implantation (Shi and Wu, 2009). Fertilization takes place in the ampulla of the oviduct, and is followed by rapid cell proliferation in one cell embryo – zygote (Niakan et al., 2012). While the embryo travels down the oviduct to the uterus, three rounds of cleavages occur and produce the totipotent blastomeres (8-cell stage), which hold the potential to form all cell types in embryo and extra-embryonic membranes (O'Neill, 2015). When the embryo enters the uterine environment, compaction begins. Embryonic compaction is

the first critical morphological event during embryogenesis and forms the morula stage embryo (White et al., 2016). The blastomeres in the morula develop the axis of polarity, they relocate to form inner and outer cells and start to express differential cell fate markers (Johnson and Ziomek, 1981). The first cellular differentiation occurs at the blastulation stage and cells specify into two populations: the inner cell mass (ICM) and the trophectoderm (TE) (Marikawa and Alarcón, 2009). The ICM consists of pluripotent cells that can develop to all cell types of the embryo, while TE cells have restricted developmental potentiality that could only form the extra-embryonic membranes (De Paepe et al., 2014). At the late blastocyst stage, the embryo matures and hatches from the outer membrane (zona pellucidae), and gains the implantation capability (Wang and Dey, 2006).

A unique feature of preimplantation embryonic development is that the early embryos almost entirely dependent on the maternal subcellular organelles and maternally stored mRNAs and proteins (Li et al., 2010c). These maternal components are loaded into a matured oocyte during the oogenesis, directing the first mitotic divisions and specifying cell fate and patterning (Tadros and Lipshitz, 2009). When the maternal mRNAs are gradually degraded while the robust activation of the embryonic genome (EGA) initiate, the maternal to zygotic genome transition (MZT) starts (Lee et al., 2014). The timing of EGA has been described as species specific: this happens at the 2-cell stage in mice and 8- to 16-cell stage in humans and domestic species, including cattle, sheep, pigs, rabbits (Telford et al., 1990). Recent whole transcriptome analysis indicated that the EGA in bovine *in vivo* produced embryos at the 4- to 8-cell stage (Kues et al., 2008; Jiang et al., 2014). The activation of the genome is accompanied by the alteration of chromatin structure and a drastic initiation of gene expression (Vastenhouw et al., 2010; Funaya and Aoki, 2017).

1.3. DNA methylation

In mammals, methylation of DNA is an essential epigenetic regulation with a key role during embryo development and germline differentiation (Canovas et al., 2017). It is essential in chromatin compaction (Choy et al., 2010), heterochromatin formation (Rountree and Selker, 2010), gene silencing (Curradi et al., 2002), transposon element repression (Slotkin and Martienssen, 2007), genomic imprinting (Li et al., 1993), and X chromosome inactivation (in females) (Sharp et al., 2011).

Stable inheritance of tissue-specific DNA methylation patterns during DNA replication and cell division are maintained by DNA methyltransferase 1 (DNMT1) (Hata et al., 2002) and its cofactor UHRF1 (Bostick et al., 2007). Mutation of *DNMT1* results in the global loss of methylation and embryonic lethality (Li et al., 1992). Another form of DNMT1 is DNMT1o, which has similar function to DNMT1, it is specific to oocyte and preimplantation embryos (Ko et al., 2013). Members of the DNMT3 protein family (DNMT3A, DNMT3B, and DNMT3L) are primarily responsible for the DNA *de novo* methylation in pre-implantation embryos (Chédin, 2011). DNMT3A and DNMT3B are the active enzymes for DNA *de novo* methylation. DNMT3L interacts with DNMT3A or DNMT3B, is required for the establishment of methylation on imprinted genes in germ cell development, and lacks enzymatic activity (Hata et al., 2002). Moreover, expression data indicates that *DNMT3A* and *DNMT3B* are highly expressed during germ cell development and blastocyst stage, and *DNMT3L* is highly expressed in embryonic stem cells (Chédin, 2011).

The DNA demethylation process can be either active or passive (Kohli and Zhang, 2013). Active DNA demethylation is a cell replication independent process (Hahn et al., 2014). This process is catalyzed by Ten-eleven-translocation enzymes (TET1, TET2, TET3) mediated 5-

methylcytosine (5mC) oxidation. The product of this active demethylation is 5-hydroxymethylcytosine (5hmC), which is a prominent intermediate epigenetic marker in the cytosine demethylation (Auclair and Weber, 2012). TETs can further oxidize 5hmC to 5-formylcytosine (5fC) and 5-carboxylcytosine (5caC) (Ito et al., 2011). TET3-dependent oxidation of 5mC has been found in demethylation of both the paternal and maternal genomes after fertilization (Canovas et al., 2017). On the other hand, the presence of a strong inhibitor of DNMT1 catalyzation, 5hmC, results in passive DNA demethylation over subsequent cell replication cycles (Valinluck and Sowers, 2007; Bhutani et al., 2011).

There are two major developmental dynamic reprogramming events of DNA demethylation (Gao et al., 2017). One in primordial germ cells (PGCs) specification and another in pre-implantation embryo stage development (Canovas et al., 2017). In mice, PGCs lineages originate from the epiblast of the embryo and commit to germline at embryonic day 6.5 (E6.5). Therefore, they have to erase the somatic fate epigenetic marks (Hayashi et al., 2007; Seisenberger et al., 2013). Around E10.5 to E11.5, the fetal gonadal sex is determined (Leitch et al., 2013) and PGCs are migrating into the developing genital ridge (Bao and Bedford, 2016). At the genital ridge, PGCs undergo virtually complete genomic DNA demethylation (Hanna et al., 2018), and establish the sex-specific epigenetic signatures and transcription profiles, which further enable the meiotic maturation process of male and female germ cells and then gametes (Smallwood and Kelsey, 2012). In sperms, the paternal genome DNA is highly methylated and exchanged most of its histone protein to protein protamine, which allows DNA to be compactly packaged into sperm head (Balhorn et al., 2000). In contrary, most of DNA methylation sites in oocyte are distinctly located over the intragenetic region of active genes (Kobayashi et al., 2012; Tomizawa et al., 2011; Veselovska et al., 2015). The reprograming of both male and female

PGCs is mediated by DNA demethylases and methyltransferases with remodeling of histone marks, the parent-specific-imprints are added as a results of reprograming (Hanna and Kelsey, 2014).

After oocyte fertilized by sperm, another drastic reprogramming occurs in the zygote stage (Messerschmidt et al., 2014). A distinct asymmetric DNA demethylation occurs on paternal and maternal pronucleus in the same cytoplasm (Iqbal et al., 2011). Paternal genome undergoes a rapid and active remodeling, starting with replacing the protamine to acetylated histones (Reik et al., 2001), following by global DNA demethylation, which actively catalyze the 5mC to 5hmC by Ten-eleven-translocation (TET) dioxygenase (Gu et al., 2011; Iqbal et al., 2011). Previous study demonstrated that the maternal genome demethylation is mainly passive replication-dependent dilution of 5mC, in the absence of DNMT1 (Rougier et al., 1998; Oswald et al., 2000). However, recent genome wide methylation profiles the presence of 5hmC in the female pronuclei (Bakhtari and P. J. Ross, 2014; Wang et al., 2014), indicating the active demethylation also onset. Additionally, some genes, such as imprinted genes, their germline differentially methylated regions (gDMRs) are resistant to the demethylation process in a parent-of-origin specific manner (Sanz et al., 2010; Stewart et al., 2016). At blastocyst stage, DNA methylation reaches the basal level and starts to establish *de novo* methylation, while the first cell differentiation occurs (Smallwood and Kelsey, 2012).

DNA methylation status is more dynamic in embryos and germlines than in somatic cells (Smith et al., 2012). Classical studies by immunofluorescence analysis of 5mC, H3K4me3 and H3K9me2 modifications have revealed a conserved genome DNA demethylation in embryo among many species, including mouse, rat, rabbit, pig, human, and cow (Lepikhov et al., 2008).

Recent studies used more precise techniques, such as RRBS, WGBS, or TAB-seq, are able to profile 5mC and 5hmC in high resolution (Canovas et al., 2017).

1.4. Genomic imprinting

Mammals are diploid organisms which have two matched sets of chromosomes inherited from both parents (Barlow and Bartolomei, 2014). Diploidy has many genetic beneficial such as protection organisms from somatic mutation and heterozygous advantage (Otto and Gerstein, 2008). Most of genes have the same potential for their parental copies to be active, while a few hundred of the total ~25,000 genes are expressed in a parent-of-origin-specific manner. These genes only have one single parental allele expressed, they are termed "imprinted" (Bartolomei and Ferguson-Smith, 2011). However, although only small number of genes have been categorized as imprinted genes, they have very dramatic effects in the phenotype (Ishida and Moore, 2013).

Genomic imprinting is an epigenetic regulatory phenomenon that have been first described in 1980s by the Solter and Surani laboratories (Surani and Barton, 1983; Surani et al., 1984). Their uniparental embryo experiments revealed that both parental genome are required for a normal mammalian development (Lyon, 1993). In maternal uniparental embryos (gynogenotes or pathogenotes), embryonic tissues develop normally, but the extraembryonic tissue fail to grow, whereas paternal uniparental embryos (androgenotes) develop dominantly extraembryonic lineages. These results suggested that there might be conflicts between parentally inherited genes influence the embryo development (Moore and Haig, 1991). This pioneer study formed the basis for the notion that the paternal genome is non-equivalent and non-interchangeable (Piedrahita, 2011).

Since monoallelic expression increased vulnerability to recessive mutations, the evolution of genomic imprinting is still an mystery (Tian, 2012). The co-presence of genomic imprinting and placenta indicates its function in controls nutrition flow from mother to fetuses (Piedrahita, 2011). Numerous hypotheses have attempted to explain the evolutionary origin and the meaning of genomic imprinting (Morison et al., 2005). Currently, there are four plausible evolutionary theories, including 1) kinship or parental genetic conflict hypothesis (Haig and Graham, 1991; Moore and Haig, 1991), 2) ovarian time bomb hypothesis (Varmuza and Mann, 1994; Weisstein et al., 2002), 3) X-linked sex-specific selection hypothesis (Iwasa and Pomiankowski, 2001; Van Cleve and Feldman, 2007), and 4) sexually antagonistic selection hypothesis (Wolf and Hager, 2006; Fairbairn et al., 2007). Among these theories, the most popular one is kinship or parental genetic conflict hypothesis, which considers the genetic imprinting is a selective advantage by which paternally expressed genes involved in resource extraction (more resources flow from mother to enhance fetal growth), while maternally expressed genes in conserve resources (restrain the maternal resources flow to fetus) (Haig, 1992). For instances, paternal genes (i.e. *IGF2*, *PEG1*, *PEG3*, *RASGRF1*, *DLK1, DIO3, MAGEL2, HYMAL,* and *PLAG11*) are tend to promote fetal growth, whereas maternal genes play as growth inhibitor (i.e. *IGF2R*, *GNAS*, *CDKN1C*, *H19*, *GRB10,* and *PHLDA2*) to increase mother's chance for future offspring (Barlow and Bartolomei, 2014). Despite the essential fetal growth and development regulation functions, imprinted genes also involved in behavior after birth, such as nurturing behaviors (*PEG1* and *PEG3*), milk ejection, caring of newborns (Piedrahita, 2011). However, with increasing number of imprinted genes have been identified recently, all hypotheses were challenged of fitting in all imprinted gene functions (Morison et al., 2005). Moreover, recent study generated the tissue-specific map for genomic imprinted genes and found that near all genes that imprinted in early

embryonic development were either retain or totally lost their parent-of-origin expression in adults (Babak et al., 2015).

One intriguing characteristic of imprinted genes are they tend to locate in one megabase clusters. 163 (Blake et al., 2010) mouse imprinted genes have been mapped to 17 chromosomes and in 16 clusters that contain two or more genes (Wan and Bartolomei, 2008). All clusters contain imprinting control regions (ICRs) that regulate the entire domain through differentially methylated CpG islands between two parental chromosomes (Wutz et al., 1997) or at least one long noncoding RNA (ncRNA) that mediates chromatin repression (Pauler et al., 2007). Another mechanisms for imprinted gene regulation are through histone markers such as H3K27me3, or by CCCTC binding factor (CTCF) binds insulator to block the shared enhancer element (Engel and Bartolomei, 2003).

To date, there are 255 imprinted genes in mammals have been identified or predicted, mostly in humans (114) (Morison et al., 2001) and mice (163), very fewer were in farm animals. However, only 51 imprinted genes are common between humans and mice. The high level of discordance between these two species indicate the need for more comparative data (Morison et al., 2005). Therefore, identification of the full catalog of imprinted genes in non-model mammalian species will greatly facilitate the understanding of the evolutionary roles of genomic imprinting (Wang and Clark, 2014).

1.5. X chromosome dosage compensation

In diploid mammals, maintenance of the correct gene dosage is essential for normal cellular function and development (Graves and Disteche, 2007). Aneuploidies were responsible for 46.3% of spontaneous abortions in humans (Jia et al., 2015). Few (~0.3%) live-born babies with aneuploidies on one of the four gene-poor chromosomes Y (577 genes), 21 (756 genes), 18

(988 genes), or 13 (1,381 genes), or on the relatively large X chromosomes (2,158 genes) (Hassold and Hunt, 2001) (gene counts including coding and non-coding gens are from human current genome assembly GRCh38.p11: https://www.ncbi.nlm.nih.gov/genome/51?genome_assembly_id=322645.) Live born babies with milder phenotypes effects of X chromosome aneuploidies were found in Turner syndrome (XO females, 1/2,500) or Klinefelter syndrome (XXY males, 1/660) than mortal autosomal aneuploidies (Payer and Lee, 2008). What made X chromosome aneuploidies are more tolerant than other chromosomes?

From book Sex Chromosomes and Sex-Linked Genes (Ohno, 1966).

"During the course of evolution, an ancestor to the placental mammals must have escaped a peril resulting from the hemizygous existence of all the X-linked genes in the male by doubling the rate of product output of each X-linked gene. Once this step was accomplished, the female no longer needed two X's in her somatic cells. Hence, the dosage compensation mechanisms by random inactivation of one or the other X evolved."

Dr. Susumu Ohno hypothesized that to solved the dosage imbalance of X-linked genes in males, upregulation of X-linked genes in the heterogametic sex would be necessary to return its gene expression to the levels from the normal diploid autosomes. X upregulation in female is counteracted by inactivation of a single X chromosome in every cell, to balances gene dosage between males and females as well as X and autosome (Ohno, 1966). Both X chromosome expression upregulation and X chromosome inactivation (XCI) are necessary components of the dosage compensation mechanism in mammals. Which one was developed first, or coevolved, is still unknown (Payer and Lee, 2008).

X-chromosome inactivation, the process by which one of two X chromosomes in mammalian female somatic cells is transcriptional inactivated (Lyon, 1961), equalizing the X chromosome dosage to the mammalian XY males (Erwin and Lee, 2008). Although, this chromosome-wide silencing has been studied for six decades, the underlying mechanisms still remain poorly understood (Augui et al., 2011). There are two forms of XCI: imprinted and random (Jeon et al., 2012). Imprinted XCI refer to the inactivation of the paternal X chromosome during early female embryo cleavage stage (Okamoto and Heard, 2006). The imprinted X chromosome was proposed to inherit from the paternal germ line and transmitted to the zygote (Huynh and Lee, 2003). After the first differentiation in blastocyst, the imprinted XCI is maintained in the outer trophectoderm (TE) cells, which developed to extra-embryonic tissues, while the inner cell mess (ICM), where the fetus come from, the XCI erased and then reestablished at a random manner (Payer et al., 2011). Random XCI is achieved by a series of events, including: counting, choice, initiation, spreading and maintenance (Avner and Heard, 2001). The region that cis-regulate the XCI on the inactivate X (Xi) is called 'X-inactivation center' (*Xic*) (Van Bemmel et al., 2016). This 1 Mb region contains several key noncoding (nc) genes that regulate XCI, including *Xist*, *Tsix*, *Xite*, *RepA*, *DXPas34* and *Jpx*/*Enox* (Tian et al., 2010). *Xist* encodes a 17kb noncoding RNA exclusively from the Xi and initiate the chromosome-wide silencing (Lee, 2009). *Tsix* is a 40-kb *Xist* antisense ncRNA that transcribe on active X (Xa), preventing the *Xist* transcribe and coating on that chromosome (Lee and Lu, 1999). These two pairs of sense-antisense ncRNA predominate the regulation of long-range chromatin on X chromosome (Lee, 2009).

Unlike XCI, which has been actively studied for over a half century, the testing for X chromosome upregulation only achievable in recent decades when the transcriptome wide

analysis become available (Nguyen and Disteche, 2006). Various tests have been performed in a number of species, results were more or less support for Ohno's hypothesis (Prothero et al., 2009). Supporters for this hypothesis was testing only a subset of genes, such as actively expressed genes (Deng et al., 2011), large protein-coding genes (Pessia et al., 2012), or ubiquitously expressed house-keeping genes (Sangrithi et al., 2017). Hyperactive of these genes reached an X:Autosome expression ratio close to or higher than 1 in somatic cells. Therefore, they were considered as "dosage-sensitive" genes that could subject to doubling the expression (Pessia et al., 2014). However, there are also studies refute Ohno's theory. Lin et al (2012). argued that due to the unavailability of the ancestral proto-X (X) and proto autosomes (A), most of current tests were indirectly compared between the present-day X (X) and present-day autosome (A) and were thus inconclusive. They claimed that by directly comparing human X with X orthologs identified from chicken, the expression of X-linked genes is roughly half. Additionally, proteomics studies in mammals also provided conflicting results for testing the Ohno's hypothesis. The mice proteomics data had X:A ratio of 1 (Deng et al., 2011), whereas humans data had 0.5 (Lin et al., 2012).

The debate of Ohno's hypothesis is still going on, mostly in humans, mice, drosophila or other model species. Testing for dosage compensation in non-model organisms, such as bovine and sheep, could provide more general conclusions and help with develop new hypotheses (Chandler Christopher H., 2017).

1.6. Effect of maternal nutrition on fetal epigenetics and development

Fetal developmental programming is largely influenced by intrauterine environmental factors, including stress, disease, uterine capacity, and maternal nutrition (Hoffman et al., 2017). Among them, maternal nutrition is the major factor that can induce permanent changes with

lifelong consequences (Godfrey and Barker, 2001). Poor maternal nutrition can be caused by excess or reduced nutrients during gestation (Pillai et al., 2016). For examples, management practices such as flushing can lead to over-nutrition, whereas inadequate feeding due to seasonal variations can cause nutrition restriction (Wu et al., 2006).

It has been found that poor maternal nutrition during gestation can influence fetal body size (Reynolds et al., 2010), muscle and adipose tissue gene expression (Peñagaricano et al., 2014), as well as skeletal muscles fiber composition and development (Reed et al., 2014) in offspring. Moreover, epigenetic modifications, including DNA methylation, histone modification, and microRNA, were also changed in the fetal tissues (Vickers, 2014). Similarly, human metastable epialleles, which are variably expressed in genetically identical individuals, have also been persistently changed in epigenetic by maternal nutritional status in early pregnancy (Dominguez-Salas et al., 2014). Therefore, more and more evidences for associations between maternal nutrition and transcriptomic/epigenomic alterations of fetal genome (Lan et al., 2013).

Chapter Two

Effects of Maternal Nutrition on the Expression of Genomic Imprinted Genes in Ovine Fetuses

Published in Epigenetics, 2018, DOI: 10.1080/15592294.2018.1503489

(Duan J.E., Zhang M., Flock K., Al Seesi S., Mandoiu I., Jones A.K., Johnson E., Pillai S.M., Hoffman M.L., McFadden K., Jiang H., Reed S.A., Govoni K.E., Zinn S.A., Jiang Z. & Tian X.C.)

2.1. Abstract

Genomic imprinting is an epigenetic phenomenon of differential allelic expression based on parental origin. To date, 263 imprinted genes have been identified among all investigated mammalian species. However, only 21 have been described in sheep of which 11 are annotated in the current ovine genome. Here we aim to 1) use DNA/RNA high throughput sequencing to identify new monoallelically expressed and imprinted genes in day 135 ovine fetuses, and 2) determine whether maternal diet (100%, 60%, or 140% of National Research Council Total Digestible Nutrients) influences expression of imprinted genes. We also reported strategies to solve technical challenges in the data analysis pipeline. We identified 80 monoallelically expressed, 13 new putative imprinted genes, and five known imprinted genes in sheep using the 263 genes stated above as a guide. Sanger sequencing confirmed allelic expression of seven genes, *CASD1, COPG2, DIRAS3, INPP5F, PLAGL1, PPP1R9A* and *SLC22A18.* Among the 13 putative imprinted genes, five were localized in the known sheep imprinting domains of *MEST* on chromosome 4, *DLK1/GTL2* on chromosome 18 and *KCNQ1* on chromosome 21, and three were in a novel sheep imprinted cluster on chromosome 4 known in other species as *PEG10/SGCE*. The expression of *DIRAS3, IGF2, PHLDA2,* and *SLC22A18* was altered by maternal diet, albeit without allelic expression reversal. Together, our results expanded the list of sheep imprinted genes to 34 and demonstrated that while the expression levels of four imprinted gene were changed by maternal diet, the allelic expression patterns were un-changed for all imprinted genes studied.

Keywords: Genomic imprinting; Allelic-specific gene expression; Maternal nutrition; Ovine

2.2. Introduction

Genomic imprinting refers to the epigenetic phenomenon that certain genes are expressed in a parent-of-origin-specific manner and play critical roles in fetal growth as well as post-natal development and metabolism (Bartolomei and Ferguson-Smith, 2011). The imprinted alleles are silenced or reduced in expression compared to the non-imprinted and expressed alleles (O'Doherty et al., 2015a). Imprinted genes tend to be located in clusters. Those in the same cluster are usually regulated by the same imprinting control region (ICR) (Koerner et al., 2009). Several mechanisms are involved in the control of allelic expression, including DNA allelic methylation, non-coding RNA and/or histone modifications (Delaval and Feil, 2004). Genomic imprinting is an evolutionary puzzle because monoallelic expression can expose deleterious recessive mutations, which are normally protected by diploidy (Wilkins and Haig, 2003). However, imprinting may have a selective advantage because it has been maintained throughout mammalian evolution (Tian, 2012). The identification of the full catalog of imprinted genes in different mammalian species will greatly facilitate the understanding of the evolutionary roles of genomic imprinting (Wang and Clark, 2014).

To date, 186 (Andergassen et al., 2017; Blake et al., 2010) and 112 (Morison et al., 2001) (http://www.geneimprint.com/site/genes-by-species) imprinted genes have been identified in mice and humans, respectively. However, only 49, 25, and 21 have been reported in cattle (Chen et al., 2016), pigs (Bischoff et al., 2009) and sheep (O'Doherty et al., 2015a; Wei et al., 2014), respectively. Although the general properties and regulations of imprinting are conserved across species (Hanna and Kelsey, 2014), the identities of imprinted genes often are not. For example, only 51 imprinted genes are common between humans and mice. Therefore, it is imperative to identify imprinted genes in each specific species.

Next generation sequencing (NGS) technologies, including genome-wide DNA sequencing (DNA-seq) and transcriptome-wide RNA sequencing (RNA-seq), have been increasingly utilized for in-depth analysis and detection of novel imprinted genes in both humans and mice (Barbaux et al., 2012; Luedi et al., 2007; Wang et al., 2011). While high throughput, such studies require completion of genome sequencing and annotation, intensive bioinformatics and careful independent validation (e.g. Sanger sequencing) to reduce false positives (Chen et al., 2016; DeVeale et al., 2012; Wang and Clark, 2014). The recent completion of the sheep genome and improved annotation abilities provide a great opportunity to identify new imprinted genes in this understudied species.

Poor maternal nutrition, either over- or restricted feeding during pregnancy (Hoffman et al., 2017), has been shown to cause abnormal DNA methylation and expression of a few imprinted genes such as *IGF2R* and *H19* in ovine fetuses (Lan et al., 2013). NGS, however, has the power to simultaneously determine expression changes of all known imprinted genes, which has yet to be conducted in sheep. The objectives of this study were to identify new sheep imprinted genes and to investigate the impact of maternal diets on the expression of all ovine imprinted genes by fetal organs at days 135 of gestation, when the fetuses undergo rapid growth and ample fetal samples can be collected.

2.3. Materials and Methods

2.3.1. Tissue sample collection

All animal protocols (Jones et al., 2016; Pillai et al., 2017) were reviewed and approved by the University of Connecticut Institutional Animal Care and Use Committee. Animal breeding, feeding and sample collection were described in Pillai et al., 2017. Briefly, Western white-faced ewes (n=12) were mated with Dorset rams (n=4). Ewes were individually housed beginning 20 days after mating. Pregnancy was confirmed by ultrasound at day 28.5 ± 0.4 of gestation (Jones et al., 2016) if a ewe was not re-marked by a ram; day 0 represents the initial marking of the ewe by the ram. On day 30 of gestation, pregnant ewes were randomly assigned to control 100% (Con), restricted 60% (Res) or overfed 140% (Over) based on the National Research Council (NRC) total digestible nutrients (TDN) for ewes pregnant with twins. Ewes were euthanized at day 135 of gestation (n = 4 per diet), and 15 fetuses were used (Con: n=7, including 3 sets of twins; Res: n=4; Over: n=4). Brain, kidney and lung samples were collected from all fetuses. Whole blood samples were obtained from the four rams. Tissues were flash frozen in liquid nitrogen and were stored at -80°C until RNA extraction.

2.3.2. Whole genome DNA- and RNA-sequencing

Genomic DNA of ram whole blood samples and fetal tissues were isolated using Qiagen DNeasy Blood & Tissue Kits (Qiagen, 69504). The ram DNA was sent to Novogene (Novogene Co., Ltd) for library preparation and sequencing. In brief, the DNA-seq library was prepared using the Illumina Truseq Nano DNA HT sample preparation kit (Illumina, FC-121-4003) with a 350 bp target insert size. Libraries were sequenced with 2 × 150 bp paired-end reads on HiSeq 2000 platform (Illumina). On average, 186.7 million raw read pairs were obtained for genotyping from each ram.

Total RNA was extracted from day 135 fetal brain, lung and kidney, using Trizol and RNAeasy kit (Qiagen, 74104) with three quality controls: NanoDrop (Thermo Fisher Scientific), agarose gel electrophoresis and Qubit 2.0 (Thermo Fisher). Library preparation was carried out using TruSeq RNA library prep kit (Illumina, RS-122-2001, RS-122-2002), which selected mRNA using Oligo d(T) with magnetic beads and built 2 × 75 bp paired-end cDNA libraries. The libraries were quantified using real-time PCR. Agilent 2100 Bioanalyzer (Agilent) was used to assess the size distribution and to determine the RNA integrity number (RIN) in each sample (**Table S5**). All RNA samples for sequencing had the RIN value greater or equal to 7. Overall, we obtained 2,149 million raw sequencing reads that passed filtering from three sequencing runs of 45 fetal tissue samples. A total of 1,160, 576 and 413 million raw sequencing reads that passed filtering were obtained for sequencing runs 1, 2 and 3, respectively. An average of 23.8 million read pairs per sample was generated on a NextSeq 500 System (Illumina).

2.3.3. SNP calling from DNA- and RNA-seq data

We adapted the computational pipeline from the SNPiR (single nucleotide polymorphisms (SNPs) in RNA-seq data) (Chen et al., 2016; Piskol et al., 2013) to solve several technical challenges in the identification of monoallelically expressed genes from RNA-seq data. Among those challenges are alignment bias of RNA-seq reads and filtering potential false positive SNPs. Heterozygosity can increase mapping bias because a read from the non-reference allele is considered a mismatch, resulting in a low mapping rate (Wang and Clark, 2014). To minimize such alignment bias to the reference allele in the genome, we artificially built a pseudo-genome (named “alternative genome”) by flipping the reference/alternative alleles in all SNP sites based on known sheep dbSNP (sheep 9940). Raw genomic DNA-seq reads were trimmed by Trimmomatic (version 0.33) (Bolger et al., 2014) to remove the universal sequencing

adaptors of Illumina with a minimum Phred score of 20 and minimal length of 30 bp. We then mapped the filtered DNA-seq reads using Hisat2 aligner (version 2.0.5) (Pertea et al., 2016) to both sheep reference genome Oar_v4.0 and the alternative genome. Only uniquely aligned reads were kept. The mapped reads and mapping rates of rams and fetuses in the two genomes were summarized in **Table S6**. The Picard Tool Mark Duplicates (2.12.0) ([CSL STYLE ERROR: reference with no printed form.]) was used to remove the PCR duplicates. SNVQ (NGS Tools version 2.0.0) (Duitama et al., 2012) was used to accurately detect the SNPs in the ram genome. To reduce potential false positive calls, the following parameters were used for SNP filtering (**Figure 1**): 1) a minimum quality score of 50 at the SNP position, 2) a minimum of three reads aligned at the SNP using both the reference and alternative genomes, 3) reversed genotypes of called SNP when reference/alternative genomes were switched (e.g., A/G in reference genome; while G/A in alternative genome), 4) SNP present and consistent with that in the sheep dbSNP (sheep 9940) database, and 5) SNP located in an exon.

Methods similar to the DNA-seq analysis for trimming, mapping and duplication removal were used for the RNA-seq data. The SNPs in fetuses were called at the individual fetus level, i.e., RNA-seq reads in the three tissue samples (brain, kidney and lung) of the same fetus were pooled to increase read coverage at each SNP site. The same SNP filtering criteria were applied as in the ram DNA-seq data.

2.3.4. Identification of informative SNPs

After genotyping SNPs of both the rams and their fetuses, we designated SNPs that were homozygous in the rams but heterozygous in their respective fetuses as informative SNPs (SNP1 in **Figure S1**). We then assigned the reads to the two parental alleles using Samtools mpileup

(version 1.4) (Li, 2011) and averaged the allele-specific read counts using the reference/alternative genomes.

2.3.5. Differential allele-specific gene expression and statistical analysis

When calculating the allele-specific gene expression (**Figure 1**), we only used informative SNPs that had total read counts of 20 or greater from each of the two parental alleles. This is because low read coverage may have a large variance in differential allelic expression estimation, potentially generating false positive differences (Wang and Clark, 2014). We then identified the expressed parental allele of all SNPs in the same gene and removed genes which contained discordant parental allele expression (i.e., a mixture of maternally and paternally expressed informative SNPs in the same gene). Next we aggregated the allele-specific reads for all informative SNPs in each gene to increase the sensitivity of imprinted gene prediction, as previously suggested (Chen et al., 2016), and pooled allelic expression of the same gene in biological replicates. The Fisher's exact test was used to examine if an allele was expressed by more than 70% of total read counts from both alleles combined with a false discovery rate (FDR) ≤ 0.05.

2.3.6. Mammalian imprinted gene lists

The known mammalian (human, mouse, bovine, sheep and pig) imprinted genes were obtained from three well-defined databases, including Imprinted Gene Database, (http://www.geneimprint.com/site/genes-by-species). Catalogue of Parent of Origin Effects (http://igc.otago.ac.nz/Search.html) and Mouse Book database (http://www.mousebook.org/imprinting-gene-list). Additionally, we incorporated 18 novel imprinted genes identified recently in mice (Andergassen et al., 2017) and 23 in bovine (Chen et

al., 2016) to create a more current and comprehensive list of imprinted genes (**Table S2**). This list was used to limit the number of imprinted genes found in the sheep.

2.3.7. Differential gene expression analysis across maternal diets

RNA-seq reads from 15 fetuses (Con: n=7; Res: n=4; Over: n=4) were trimmed and aligned to Oar_v4.0 using Hisat2 version 2.0.5 aligner (Pertea et al., 2016). The percentages of mapped reads for all samples are summarized in **Table S7** and the average multiple aligned rate is 90.3%. IsoEM version 1.1.5 (Nicolae et al., 2011a) was used to quantify levels of gene expression to transcripts per kilobase million (TPM) using default parameters. TPM normalizes for gene length first and then for sequencing depth. This unit was preferred to RPKM because it normalizes transcriptome sizes. When comparing levels of gene expression across different samples, TPM allows more appropriate comparisons (Soneson et al., 2015). Differentially expressed genes (DEGs) between Con and Over or Con and Res were determined using IsoDE version 2 (Al Seesi et al., 2014). The test was preformed separately in brain, kidney and lung. In each comparison, genes were deemed differentially expressed if they showed a P-value < 0.05 and Confident log2 fold change (FC) > 1. DEGs that are in the lists of sheep known/putative imprinted genes (**Table 2**), the 80 monoallelically expressed genes (**Table S8.1**), and the mammalian known imprinted genes (**Table S8.2)** were subsequently pulled from the total DEG list.

2.3.8. Sanger sequencing

The DNA of fetuses and their respective rams and the cDNA of the specific fetal tissue in which the gene was expressed monoallelically were all amplified by PCR. All primers used are in **Table S9**. The PCR products were sent to Eton Bioscience for Sanger sequencing.

2.3.9. Data access

The raw read FASTQ files for DNA/RNA-seq reads and informative SNP averaged read count files are available at Gene Expression Omnibus (GEO https://www.ncbi.nlm.nih.gov/geo/) under the accession number GSE111306.

2.4. Results

2.4.1. High throughput identification of informative single nucleotide polymorphisms

Using single nucleotide polymorphisms (SNPs), the parental origin of an allele in the fetus can be assigned. Informative SNPs are those 1) present in mRNAs (expressed), 2) homozygous in ram and heterozygous in fetuses, and 3) expressed at read counts of 20 or greater. They are essential in determining the origin of a parental allele of genes. However, mapping at SNP locations can introduce alignment bias towards the reference alleles because the reads of the alternative alleles may be treated as mismatches and discarded by the mapping tool (Wang and Clark, 2014). To minimize such bias, we artificially built a pseudo-genome (named "alternative genome") by flipping the reference/alternative alleles at all SNP sites from the dbSNP database (sheep 9940) of the sheep reference genome. DNA-seq reads of rams and RNA-seq reads of their respective fetuses were aligned to both the reference and alternative genomes for SNP calling (**Figure 1**). By comparing the homozygous SNPs in each ram to the heterozygous SNPs in his fetuses, we identified a total of 146,487 unique informative SNPs (represented by SNP1 in **Figure S1**). These informative SNP were annotated to 15,298 genes, yielding on average of 9.6 informative SNPs per gene. The parental origins of these informative SNPs were determined using the rams' genotypes as shown in **Figure S1**. To further reduce alignment bias, we used Samtools mpileup (version 1.4) (Li, 2011) to calculate the allele-specific read counts for each informative SNP which were then averaged between the two genomes. Using this approach, we successfully reduced the mapping bias at informative SNP locations to < 1% (**Figure 2**).

2.4.2. Allele-specific gene expression

Fisher's exact test was programmed to identify genes with allelic expression bias of ≥ 70% which also had a read coverage ≥ 20 at each informative SNPs in at least one tissue type. We

identified 4,537 such allelic-differentially expressed genes with a q-value < 0.05. Eighty of these genes had significant allelically biased expression of the same parental alleles in all examined tissues (brain, kidney and lung) and were thus classified as monoallelically expressed (**Table S1**). Among these, 19 and 61 preferentially expressed the paternal and maternal alleles, respectively. To decrease potential false positives, we conservatively used previously identified imprinted gene as a guide. By combining all imprinted genes in the human, mouse, cow, pig and sheep we obtained a total of 263 unique imprinted genes, 119 of which have been annotated in the sheep genome (**Table S2**). Between these 119 and the 4,537 allelic differentially expressed genes, 18 were common and eight and ten were paternally and maternally expressed, respectively (**Table 1**). Five of the 18 were known to be imprinted in sheep, the other 13 were known to be imprinted in other species and were here designated as putatively imprinted (**Table 1**). Although there are 21 previously reported imprinted genes in sheep, only 11 of them are annotated in Oar_v4.0. Therefore 5 out of 11 (45.6%) of imprinted genes were verified using just three tissues at one developmental stage. Each of the 18 genes were individually inspected using the Integrative Genomics Viewer (IGV) (Robinson et al., 2011) to confirm their correct alignments. Read counts from parental alleles of informative SNPs within the genes in each tissue were summarized in **Table S3**. Nine of these–*COPG2, GATM, GRB10, IGF2R, INPP5F, PEG3, PON3, PPPIR9A* and *WARS*–had more than three informative SNPs that showed significant differential allelic expression in multiple tissues and animals, firmly demonstrating their consistent parent-of-origin specific expression status, and therefore mostly likely imprinted.

The rest of the 80 monoallelically expressed genes may include genes that are only imprinted in sheep. Using the list of known imprinted genes as a guide, however does not allow

us to make such determination. Yet this conservative approach avoids any potential false positives while expanding ovine imprinting information.

2.4.3. Validation of the putative imprinted genes

To confirm the 13 putative imprinted genes identified above, we quantified their allelic expression using an independent method–Sanger sequencing. PCR products of seven genes: maternally expressed *CASD1*, *COPG2*, *PPP1R9A* and *SLC22A18* (**Figure 3**) and paternally expressed *DIRAS3*, *INPP5F* and *PLAGL1* (**Figure 4**) were successfully generated and their allelic expression patterns were verified. The other six genes could not be independently verified by this alternative approach because of the close proximity of informative SNPs to the edge of exons and difficulty in primer design.

2.4.4. A novel imprinted cluster in sheep

Most of imprinted genes were found to reside in clusters of approximately one megabase (Bartolomei and Ferguson-Smith, 2011), therefore, discovery of novel imprinted genes often uses the already established clusters as a guide (Chen et al., 2016). We generated a genome visualization of the known ovine imprinted, monoallelically expressed and putative imprinted genes identified in our analysis (**Figure 5**). The 80 monoallelically expressed genes were mostly distributed sporadically throughout the genome. Due to the limited information on imprinted clusters in sheep, we do not exclude the possibility that some of the 80 monoallelically expressed genes may be located in imprinted clusters yet to be identified.

Among the 13 putative imprinted genes, maternally expressed genes *CASD1, PPP1R9A* and paternally expressed *PON3* formed a novel sheep imprinted cluster located close to but not in the sheep known maternally expressed domain *MEG1/GRB10* (**Figure 6**). This novel large imprinted cluster had been characterized as *PEG10/SGCE* in the mouse (Ono et al., 2003) and

human (Monk et al., 2008), indicating it is conserved and likely important in development (Nakabayashi et al., 2004). Moreover, *COPG2* and *WARS* are located in the *MEST* domain and *DLK1/GTL2* domain on chromosomes 4 and 18 (which also contains five other known imprinted genes; **Figure 6**), respectively. *PHLDA2, SLC22A18* and *KCNQ1* are located in *KCNQ1* domain, next to *IGF2/H19* domain on chromosome 21, known to be imprinted in sheep (**Figure 6**). The remaining five genes are located sporadically throughout the sheep genome and their associations with imprinted clusters, if any, are yet to be defined.

2.4.5. Tissue-specific Expression of imprinted genes in fetal organs

Imprinted genes have unique tissue- and developmental stage-specific expression patterns. Nearly all are established during fetal development (Babak et al., 2015) (Thurston et al., 2008). Day 135 of gestation in sheep corresponds to the maximal fetal growth which allows ample tissue quantities (Peñagaricano et al., 2014). To be conservative and avoid false positives, we did not intend to identify genes imprinted in some but not in other tissues in this study. We did, however, determine the tissue-specific expression levels of imprinted genes in control (Con) fetuses (**Figure 7**), overfed (Over) and restricted (Res) fetuses (**Figure S2, Table S4.2**).

Expression levels (Transcripts Per Million (TPM); **Table S4**) of sheep known (**Figure 7**) and putative coding imprinted (**Figure 7**) genes in the brain, kidney, and lung of fetuses from mothers of control diet exhibited tissue-specificity. The fetal mitogen *IGF2*, for example, was expressed at the highest level in the lung and kidney among all imprinted genes. The genes *DLK1* and *GATM* in the kidney, *DIRAS3*, *INPP5F* and *BLCAP* in the brain were also among the highest expressed. While the tissue-specific expression of imprinted genes (Baran et al., 2015) have been reported previously in various species, they were mostly conducted using real time PCR which only gives relative values, while TPM from RNA-seq provides a close estimate to

the absolute expression values after correcting for transcriptome size and gene length, allowing the visualization of expression differences among different genes across samples.

2.4.6. Effects of maternal nutrition on expression of imprinted genes in ovine fetuses

We compared the allelic expression of the 18 imprinted genes in fetal organs from the three maternal nutrition groups (**Table 1**). Although not all 18 had informative SNPs or expression values in all groups, no allelic expression reversal was observed in any fetal organ under any nutrition status. However, maternal nutrition did affect the levels of expression of the imprinted genes *DIRAS3*, *IGF2, PHLDA2,* and *SLC22A18,* in fetal organs (**Table 2 & Figure S2**). Specifically, the paternally expressed *IGF2* gene, which promotes fetal growth (Reik et al., 2000), was down-regulated in the brain of fetuses from mothers of restricted diet (Res) compared to controls (Con). The maternally expressed *PHLDA2* was also down-regulated in fetal brains but up-regulated in fetal lungs of both Res and overfed (Over) groups compared to Con. This gene has been shown to be involved in placental growth (Frost and Moore, 2010) and its overexpression led to low birth weight in humans (Lewis et al., 2012). The paternally expressed *DIRAS3* and maternally expressed *SLC22A18* are inhibitors for cell proliferation and growth (Huang et al., 2009c; Zhang et al., 2015), and were both down-regulated in lungs of the Res group and kidneys of the Over group compared to controls, respectively. Interestingly, three of the four affected genes-*PHLDA2, SLC22A18*, and *IGF2*- are located near the imprinted cluster of *KCNQ1* and *IGF2/H19* on chromosome 21, indicating this domain is highly responsive to maternal diet changes.

2.5. Discussion

Genomic imprinting in sheep is an under-developed area of research, despite the importance of the sheep in agriculture in many regions of the world and its frequent use as a model for human pregnancy and fetal development (Barry and Anthony, 2008). Our study is the first to employ NGS and bioinformatics to identify sheep imprinted genes and the effects of maternal diets on fetal imprinting. We identified 80 genes that consistently monoallelically expressed the same parental allele more than the other in all fetal tissues from all treatment groups. These 80 contain potential candidate imprinted genes in the sheep for future studies. Recent NGS studies identified more than 1,300 imprinted loci in mouse brain (Gregg et al., 2010a, 2010b), however, most were due to false positives (DeVeale et al., 2012). To avoid such problems, we used the combined list of imprinted genes from all studied species to conservatively guide our data-mining. This approach, however, does not permit us to discover genes that are only imprinted in the ovine. Nonetheless, the list is the most comprehensive by combining information from five species and the conservative method generated five sheep known and 13 new putative imprinted genes, increasing the prior list of 21 by as much as 62%. Our results demonstrate the power of bioinformatics in genomic imprinting studies.

2.5.1. Imprinted domains

A unique feature of genomic imprinting is that imprinted genes tend to cluster as a result of long-range regulation by the imprinting control regions (Bartolomei and Ferguson-Smith, 2011). In sheep, the previously identified 21 imprinted genes are mostly clustered on chromosomes 18 and 21. From the 13 new putative imprinted genes, we identified a new sheep imprinted cluster on chromosome 4 (**Figure 6**), known as the *PEG10/SGCE* domain in humans (Kainz et al., 2007), mice (Wiley et al., 2008) and bovine (Chen et al., 2016). Unfortunately, we

did not have informative SNPs to study the expression of the two core genes, *PEG10/SGCE,* in this domain. Putative new imprinted genes *CASD1*, *PPP1R9A* and *PON3* were located in this large imprinting domain. The imprinted status of these three genes was supported by many informative SNPs from multiple tissues and animals in our data, strong evidence for their parental expression bias. All three are maternally expressed in mice (Babak et al., 2008) and located adjacent to the paternally expressed *SGCE* and *PEG10* (Ono et al., 2003). *CASD1*, like other maternally expressed genes in this domain such as *CALAR*, is highly expressed in the brain and encodes for a glycosyl transferase (Babak et al., 2008). However, in humans, *CASD1* and *PON3* are biallelically expressed (Monk et al., 2008), and *PPP1R9A* is imprinted in skeletal muscle but not in the brain (Nakabayashi et al., 2004). The data in sheep are more similar to those in the mouse (Babak et al., 2008). Although *CASD1* was expressed in all three tissues studied (**Figure 7**), only the kidney had sufficient read counts at this informative SNP for the determination of maternal allele expression. This pattern of expression was also confirmed by Sanger sequencing. *PPP1R9A* is important for early development of extraembryonic tissues (Nakabayashi et al., 2004) and is similarly expressed in all tissues examined (**Figure 7**). *PON3* belongs to an enzyme family associated with high-density lipoprotein that is believed to protect against the onset of atherogenesis (Ono et al., 2003). Although it was nearly negligible in the brain and kidney, it was highly expressed in the lung in ovine fetuses (**Figure 7**). Such expression was also observed in human tissues (Fagerberg et al., 2014).

COPG2 was located in the *MEST* cluster on chromosome 4 (**Figure 6**), which was previously known as the *MEST/COPG2* imprinted domain in humans and mice (Lee et al., 2000). The maternal allele of *COPG2* gene is expressed in mice but the human *COPG2* escapes genome imprinting although it is adjacent to the *MEST* gene (Yamasaki et al., 2000). In bovine, *COPG2*

was found to biallelically express in fetal tissues (Khatib, 2005). However, in our analysis of ovine fetuses, *COPG2* showed preferential expression from the maternal allele in both brain and lung. Such lack of conservation of genomic imprinting in closely related species may lead to challenges and modification of the currently most plausible imprinting hypothesis - "the parental conflict hypothesis" (Khatib, 2005) because not all imprinted genes fit in this model.

Our analysis placed the gene *WARS* near the *DLK1/GTL2* imprinting domain on chromosome 18 (**Figure 6**), which also contains the widely-studied sheep Callipyge (*CLPG*) locus (Jiang and Yang, 2009), expressed from the dominant paternal allele (Freking et al., 2002). Six other imprinted genes have been identified in this region: paternally expressed *DLK1, DAT,* and *RTL1* (also known as *PEG11*), and maternally expressed *GTL2* (also known as *MEG3), PEG11AS* and *MEG8.* Another paternally expressed gene *BEGAIN*, albeit located 138kb proximally from the imprinted *DLK1* gene, is not controlled by the ICR of the *DLK1/GTL2* domain (Smit et al., 2005). Paternally expressed *WARS* is located 150kb downstream of *BEGAIN* in sheep and encodes for a protein linking amino acids with nucleotide triplets in tRNA. It is believed to be one of the first proteins that appeared in evolution [provided by RefSeq, Jul 2008]. In the mouse *WARS* is also paternally expressed (DeVeale et al., 2012). However, it may not be controlled by the *DLK1/GTL2* LRCE in the sheep due to its relative location to the gene *BEGAIN* (**Figure 6**).

Three other putative imprinted genes, *SCL22A18*, *PHLDA2* and *KCNQ1*, are located on chromosome 21 (**Figure 6**) in the *KCNQ1* domain, which contains several maternally expressed genes (Lewis et al., 2006; Umlauf et al., 2004). In our analysis, these three ovine genes also showed preferential expression from the maternal allele. The region is highly involved in fetal growth regulation (Reik et al., 2000) and was found to be affected by maternal diet in our study.

Although members of this cluster are subjected to regulation by the same ICR, their expression levels varied dramatically. For example, *PHLDA2* situates close to the *KCNQ1* gene, yet they had the highest and lowest expression levels, respectively, in the kidney among all imprinted genes (**Figure 7**). This may suggest that allelic expression pattern and overall gene expression levels are regulated by different mechanisms.

2.5.2. Effects of maternal diets on expression of imprinted gene

Maternal stressors induce changes in expression of the fetal genome which can permanently alter the offspring's physiology, development, metabolism and growth (Wu et al., 2006) as reported in mice and rats (Cooney et al., 2002; Waterland et al., 2008). Understanding the effect of poor maternal nutrition in ovine fetal development is not only relevant to agriculture (Begum et al., 2012), but also to modeling for human pregnancy and fetal development. Restricted and over-feeding of pregnant ewes were found to alter gene expression (Peñagaricano et al., 2014). As seasonal breeders, ewes enter pregnancy in late fall or early winter, and usually have sufficient food in both quantity and quality. During late gestation when fetal growth is the most rapid, however, food becomes scarce, leading to nutrition restriction. Alternatively, the practice of flushing before and during the breeding season can result in overfeeding (Wu et al., 2006). Such nutrient imbalance has been shown to severely impair fetal and placental development (Wu et al., 2006). Interestingly, we found most of the disturbed gene expression were located in the *KCNQ1* and *IGF2/H19* clusters, consistent with the role of *IGF2* as a major fetal growth regulator (Demetriou et al., 2014). Diets of pregnant ewes containing different starch/fiber/protein portions have been shown to change the CpG methylation levels of specific imprinted genes such as *IGF2R* and *H19* (Lan et al., 2013). Our data also showed that despite the dramatic maternal diet changes, the allelic expression pattern was not affected, further suggesting

that gene expression levels and imprinted patterns may be regulated through different epigenetic mechanisms.

2.5.3. Recommendations for future throughput imprinting studies

First, to avoid false positives raised by potential allelic drop-outs during amplification-based RNA-seq library preparation (Jennings et al., 2017), we conservatively removed heterozygous SNPs between nucleotides that were not complementary even though parents were homozygous for the nucleotides (e.g., GG in fetus and TT in ram, SNP2 in **Figure S1**). This filtering reduced the numbers of informative SNP per gene. It is suggested that a non-amplification based hybrid capture NGS may circumvent this issue in library preparation (Jennings et al., 2017). Moreover, a number of informative SNPs were located too close to the edge of exons, making it difficult to design PCR primers. Consequently, validating them by Sanger sequencing proved difficult. Under this circumstance, new animals with different informative SNPs can be used. Allelic drop-outs may also affect PCR of Sanger sequencing. Digital Droplet PCR for absolute quantification of target informative SNPs may avoid this problem (Gutiérrez-Aguirre et al., 2015).

Second, a number of SNPs that were heterozygous in fetuses were also heterozygous in the parents (e.g., CA in fetus and CA in ram, SNP3 in **Figure S1**). These SNPs were not informative which reduced the number of informative SNPs and partially caused the lack of confirmation of the 6 known imprinted genes in the sheep genome. Alleviating this problem requires more animals with different genetic background, as well as a better version of sheep genome annotation.

Thirdly, most studies for the discovery of imprinted genes employ reciprocal crosses between two closely related strains/breeds/species. While this design generates high frequencies

of informative SNPs, parental allelic expression may be caused by species differences, not just imprinting. To overcome this problem, increasing the number of crosses from animals of the same species is the most relevant and preferred design.

Fourthly, cis-expression quantitative trait loci (eQTL) confers monoallelic expression in all crosses. Even using known mammalian imprinted genes as a guide, we cannot rule out that the putative imprinted genes may contain eQTL. On the other hand, the list of 80 monoallelically expressed genes likely contain more imprinted genes in addition to eQTL because they consistently expressed the same parental allele among several different crosses. Nonetheless, reciprocal crosses are necessary to firmly distinguish these two types of monoallelic expression.

Lastly, in the original experimental design, we included the fetal cotyledons because many genes are only imprinted in the placenta. However, cotyledon samples are mostly contaminated with caruncles (Bridger et al., 2007). We also found similar cross contaminations in our samples and were not able to include them in our study. Therefore, other strategies such as microdissection or single-cell RNA-seq have to be used in order to reliably study placental imprinting.

Table 1. Summary of the confirmed/putative imprinted genes in sheep

Treatment	Control group			Overfed group			Restricted group		
Tissues	Brain	Kidney	Lung	Brain	Kidney	Lung	Brain	Kidney	Lung
BEGAIN	ND	91%	100%	-	-	-	-	-	-
BLCAP	-	-	-	79%	80%	85%	-	-	-
DIRAS3	-	-	-	-	-	-	80%	87%	ND
INPP5F	97%	ND	70%	98%	ND	ND	97%	ND	ND
PEG3	86%	85%	86%	88%	87%	86%	84%	86%	88%
PLAGL1	ND	100%	86%	-	-	-	-	-	-
PON3	ND	73%	ND	ND	ND	75%	ND	78%	76%
WARS	74%	72%	ND	ND	74%	70%	78%	73%	ND
CASD1	-	-	-	ND	30%	ND	ND	29%	ND
COPG2	11%	27%	ND	17%	21%	ND	20%	29%	29%
GATM	29%	30%	29%	19%	25%	ND	ND	28%	ND
GRB10	ND	19%	25%	29%	23%	22%	ND	26%	18%
GTL2	-	-	-	0	0	24%	-	-	-
IGF2R	ND	4%	16%	ND	9%	10%	ND	8%	7%
KCNQ1	-	-	-	ND	ND	19%	ND	20%	ND
PPP1R9A	ND	ND	24%	ND	23%	ND	28%	21%	23%
SLC22A18	ND	ND	18%	ND	30%	ND	-	-	-
PHLDA2	-	-	-	-	-	-	ND	27%	ND

'-': no informative SNPs in this animal at this gene. 'ND': expression of the informative SNP is Not Detectable (read counts lower than 20; not reliable for allelic expression determination).
Pink or blue: exclusively/predominately expressing the maternal or the paternal allele. Numbers: % of paternal allele expression [paternal allele reads/(paternal allele reads+ maternal allele reads)]. Genes in bold: previously known sheep imprinted genes.

Table 2. Levels of differentially expressed imprinted genes in tissues of fetal sheep from mothers of different nutrition

Tissue	Genes	Control (TPM)	Overfed (TPM)	Log_2 FC*	Restricted (TPM)	Log_2 FC*
Brain	*PHLDA2*	19.36	0.44	-1.71	0.47	-6.32
Brain	*IGF2*	23.61	38.3	0.69	5.22	-2.07
Kidney	*SLC22A18*	16.40	9.55	-1.24	10.56	-0.64
Lung	*PHLDA2*	0.19	8.28	6.58	1.31	2.23
Lung	*DIRAS3*	3.06	2.37	-0.37	1.28	-1.11

FC*: fold change over the expression levels in controls. Log_2 FC: calculated by using bootstrapping and considered significant if greater than 1.

Figure 1. Data analysis pipeline used in this study

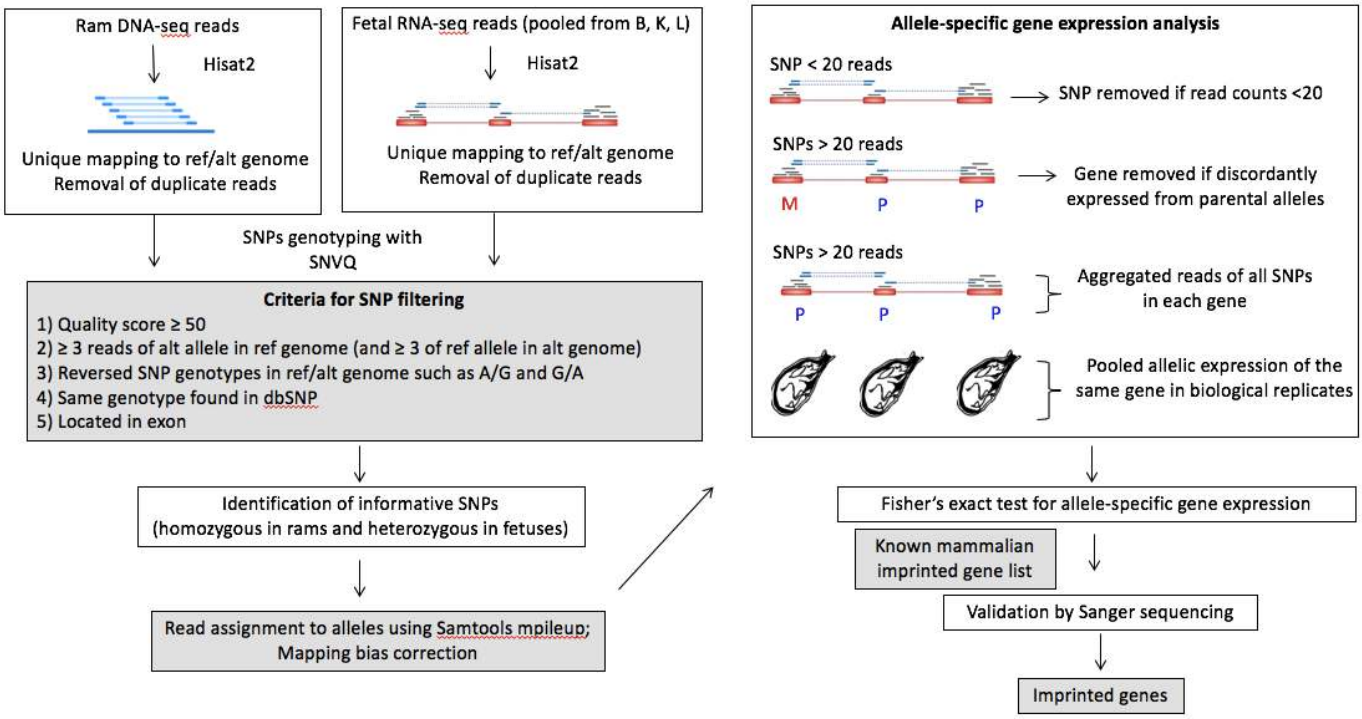

Left panels are the bioinformatics pipeline for SNP calling and informative SNPs identification. Right panels show the determination of monoallelically expressed genes in ovine fetuses and validation of putative imprinted genes. Details are presented in sections of Materials and Methods: SNP calling from DNA- and RNA-seq data, Identification of informative SNPs, and Differential allele-specific gene expression and statistical analysis. SNP: single nucleotide polymorphism; ref: reference genome; alt: alternative genome; B: Brain; K: Kidney; L: Lung; dup: duplication; M: maternally expressed; P: paternally expressed. Blue and red boxes: genomic DNA and exons; blue lines with blue boxes: RNA sequence reads; dash lines: mapped gaps in RNA-seq reads; Hisat2: Alignment software; SNVQ: SNP calling software; Samtools mpileup: software to assign read counts to alleles.

Figure 2. Correction of the RNA-seq alignment bias in the genome

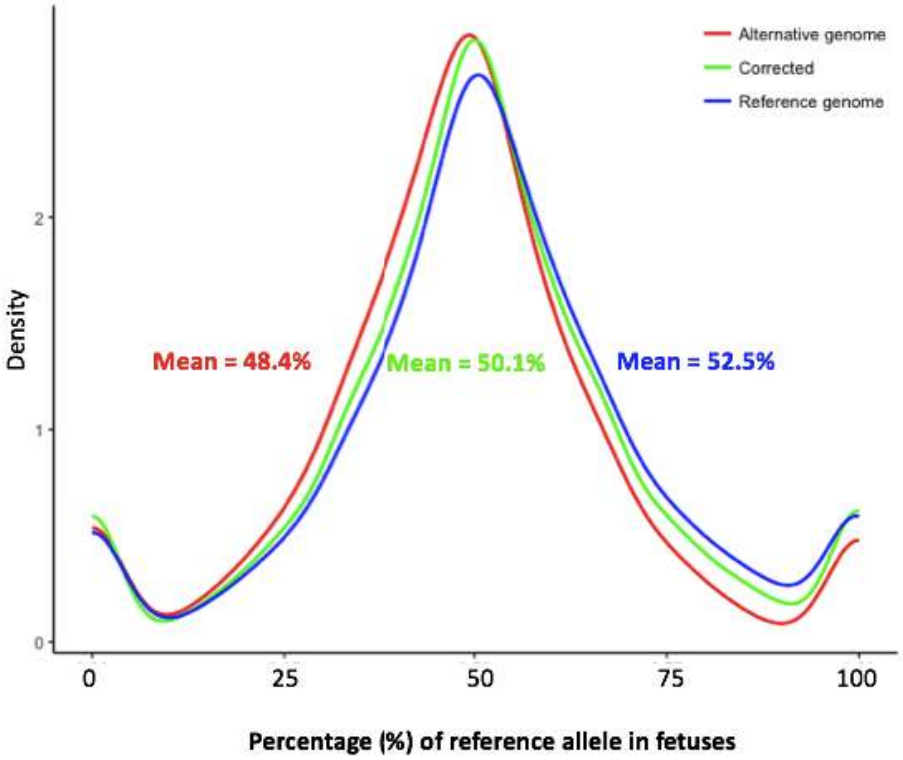

Density plot of the percentage of reference allele's read counts in the reference genome (blue), alternative genome (red), and after alignment bias correction (green).

Figure 3. Validation of putative imprinted genes (maternally expressed) using ram and fetal DNA as well as fetal cDNA: *CASD1, COPG2, PPP1R9A,* and *SLC22A18*

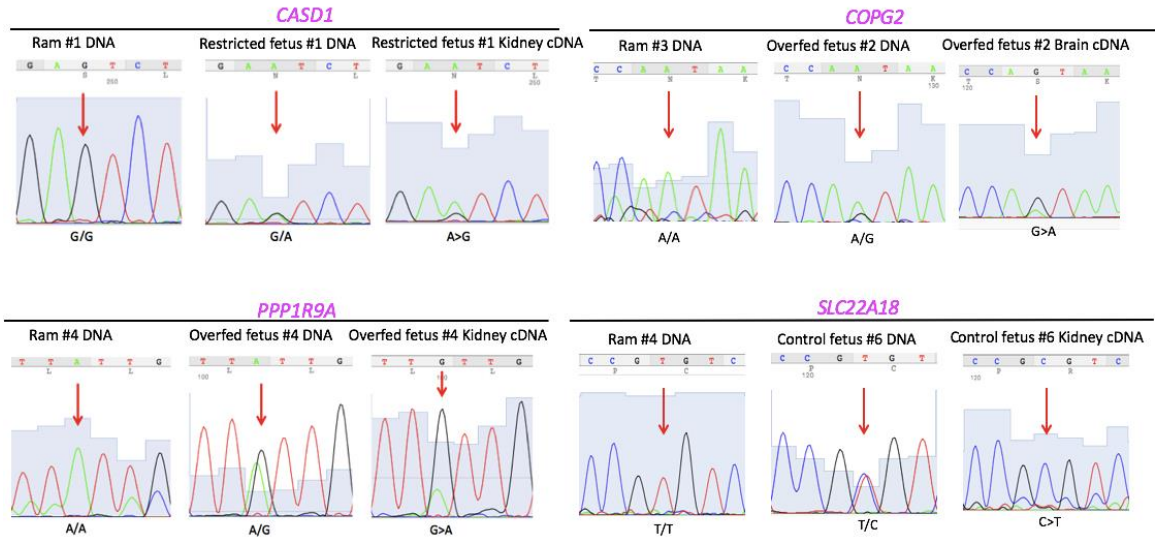

Red arrows: locations of the informative SNPs. All SNPs were confirmed homozygous in rams and heterozygous in fetuses. Gene expression in cDNA of fetal tissues were allelically biased.

Figure 4. Validation of putative imprinted genes (paternally expressed) using ram and fetal DNA as well as fetal cDNA: *DIRAS3, INPP5F*, and *PLAGL1*

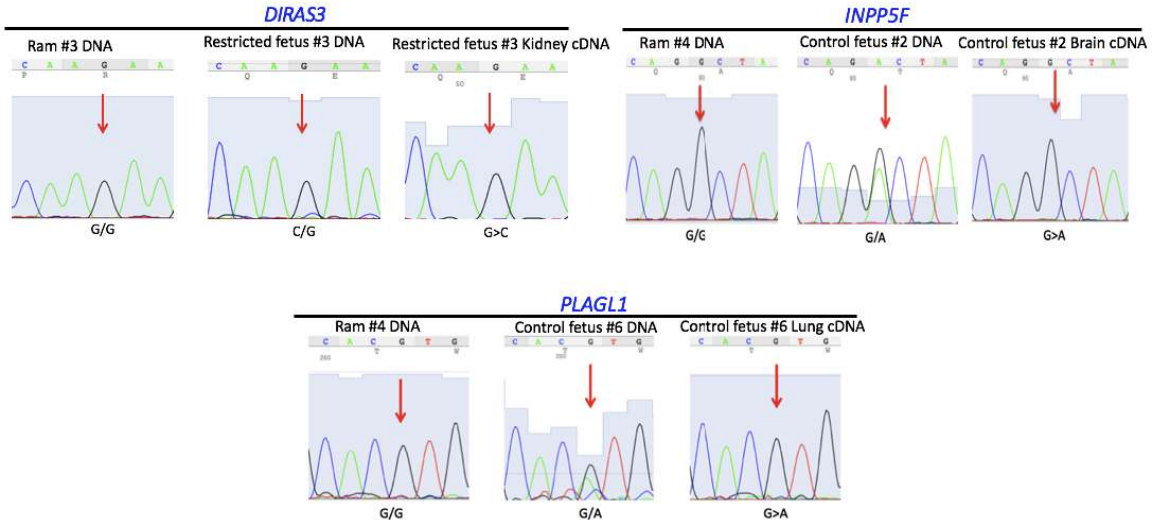

Red arrows: locations of the informative SNPs. All SNPs were confirmed homozygous in rams and heterozygous in fetuses. Allelic expression was determined using cDNA from fetal tissues.

Figure 5. Visualization of the 11 known sheep imprinted genes in the ovine genome Oar_v4.0 annotation (orange)

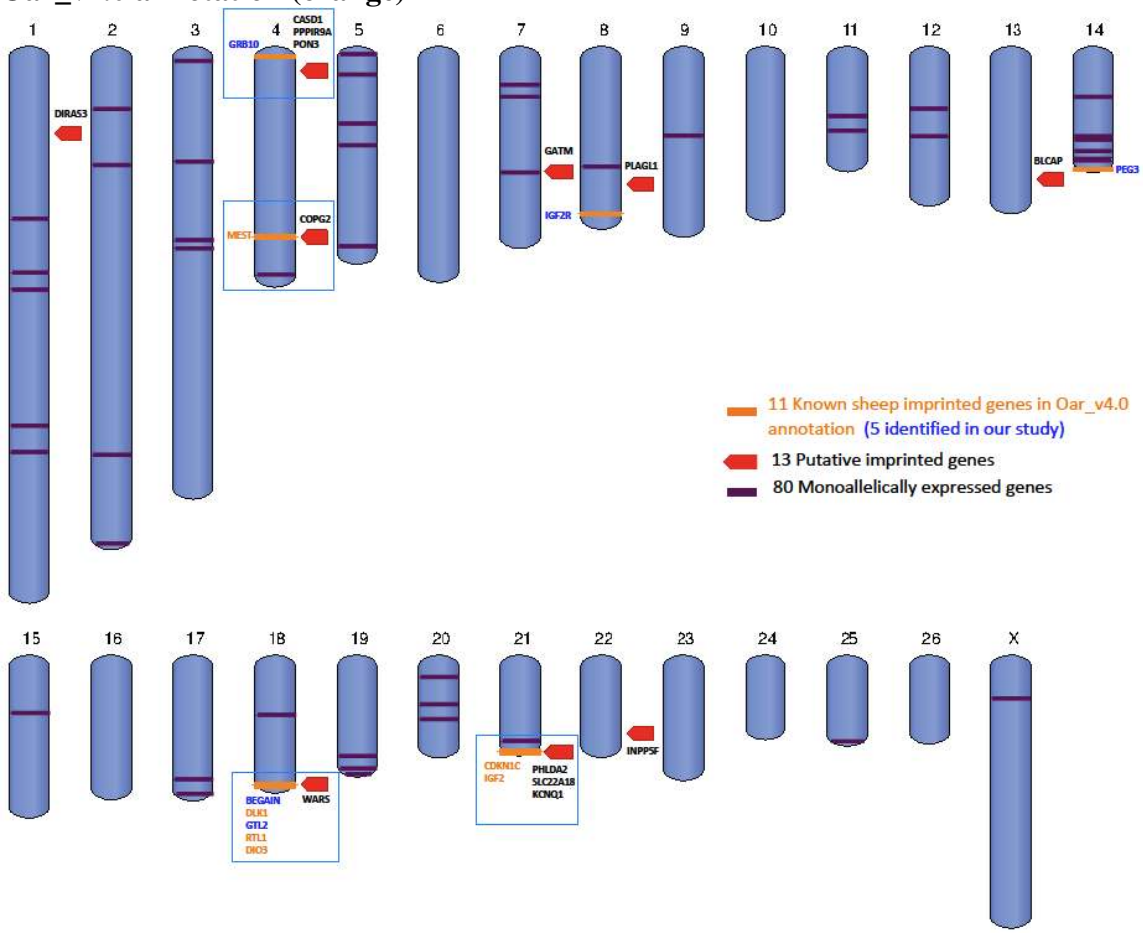

The five genes verified in our study (orange mark, blue text), the 13 putative imprinted genes identified here (red mark), the 80 monoallelically expressed genes (purple lines, some are overlapped), and the four imprinted clusters (blue boxes).

Figure 6. Genes and their parental expression patterns in the four imprinted clusters in sheep

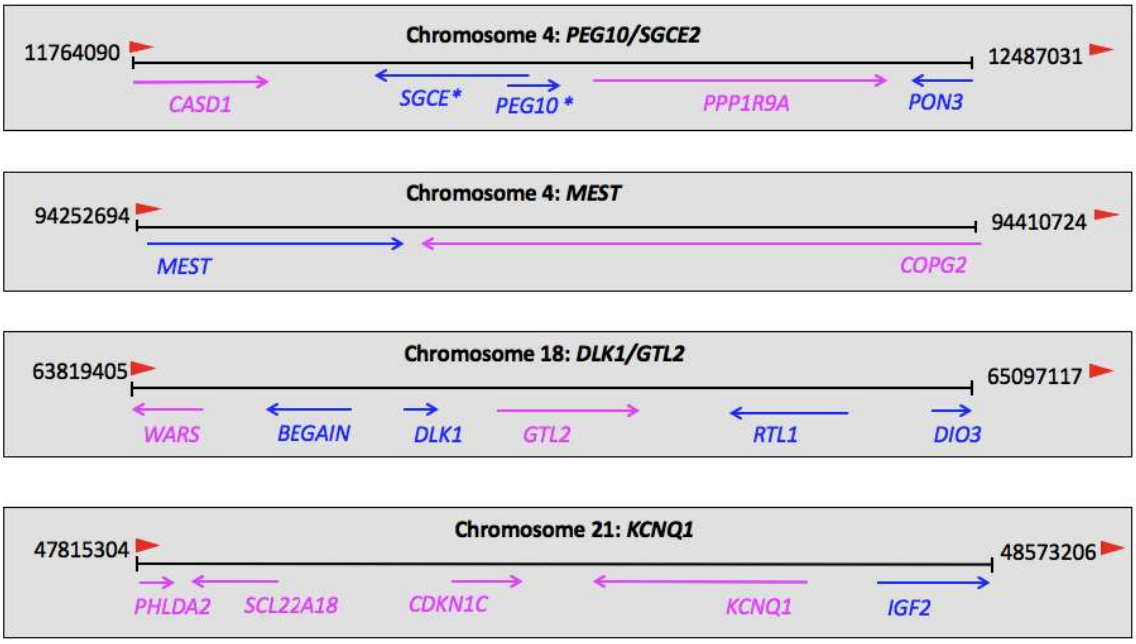

Pink: maternally expressed; blue: paternally expressed. Arrow indicates the gene expression direction. *known imprinted in humans/mice.

Figure 7. Expression levels (Transcripts Per Million, TPM±SD) of sheep imprinted genes in the brain, kidney, and lung tissue of day 135 ovine fetuses from ewes fed a control diet

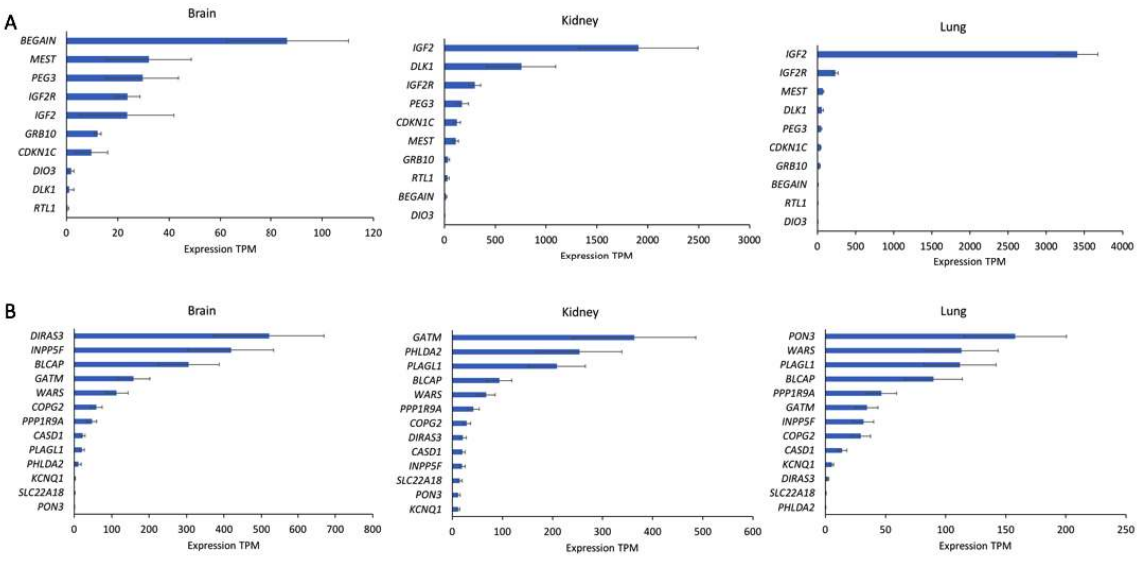

A. The 10 coding and previously known imprinted genes in the sheep genome. B. The 13 putative imprinted genes identified in our study.

2.6. Supplementary information

Table S1.1. Summary of the 80 monoallelically expressed genes in sheep

Treatment	Control group				Overfed group				Restrict group		
Tissuetype	Brain	Kidney	Lung		Brain	Kidney	Lung		Brain	Kidney	Lung
ACOT13	84%	85%	88%		83%	79%	84%		88%	81%	82%
C2H9orf3	77%	75%	76%		73%	85%	75%		75%	76%	74%
CCBL1	96%	83%	90%		85%	91%	85%		86%	89%	87%
CHMP2A	93%	92%	92%		94%	91%	94%		89%	95%	94%
EIF2S3	88%	91%	83%		89%	90%	91%		90%	87%	89%
EIF4G1	88%	92%	84%		91%	90%	87%		93%	92%	84%
GNAQ	76%	79%	81%		77%	77%	77%		78%	78%	77%
ITGB5	83%	80%	82%		100%	91%	79%		86%	84%	80%
LOC101108797	86%	84%	85%		84%	81%	86%		79%	86%	85%
LOC105602948	84%	89%	92%		84%	90%	94%		89%	90%	94%
LOC106991149	81%	92%	94%		89%	88%	93%		85%	92%	91%
NES	77%	72%	75%		79%	74%	78%		79%	79%	83%
PARG	91%	83%	81%		82%	78%	80%		76%	78%	80%
PEG3	86%	85%	86%		88%	87%	86%		84%	86%	88%
PPP2R1A	91%	94%	89%		92%	94%	90%		92%	89%	93%
RWDD1	76%	76%	78%		79%	77%	79%		81%	83%	82%
SAFB	81%	77%	77%		81%	75%	74%		81%	81%	83%
SON	79%	76%	78%		83%	78%	74%		82%	79%	79%
UBB	87%	85%	85%		87%	85%	85%		86%	81%	83%
ABHD16A	18%	23%	12%		17%	21%	26%		22%	30%	27%
ALDH2	18%	28%	27%		15%	25%	29%		23%	26%	27%
APOE	13%	20%	14%		11%	8%	25%		16%	9%	19%
ARCN1	9%	19%	13%		7%	4%	19%		17%	11%	13%
ARFGEF1	14%	22%	20%		11%	25%	29%		8%	20%	21%
ARL2BP	22%	16%	14%		20%	7%	10%		22%	13%	22%
ATP5G1	13%	20%	18%		10%	16%	22%		12%	17%	26%
AUP1	13%	20%	18%		16%	17%	21%		15%	16%	19%
BBS4	19%	24%	17%		10%	18%	25%		14%	23%	23%
CFAP20	4%	22%	23%		10%	10%	16%		22%	8%	19%
CLK1	21%	21%	21%		22%	19%	23%		16%	19%	20%
CNBP	11%	23%	19%		14%	16%	22%		17%	18%	19%
CPSF3L	16%	21%	18%		15%	12%	21%		18%	15%	19%
CRELD1	19%	14%	18%		18%	16%	14%		21%	15%	18%
CSNK2B	18%	13%	13%		5%	9%	16%		9%	11%	20%
CUL7	15%	27%	28%		20%	25%	20%		19%	24%	30%
DBN1	14%	24%	20%		16%	19%	27%		16%	21%	28%
DCTN1	12%	18%	21%		13%	12%	23%		18%	20%	19%
DNAJC11	8%	15%	24%		10%	9%	24%		17%	27%	7%
DNAJC7	8%	19%	15%		8%	11%	18%		7%	17%	23%
DPF2	24%	21%	19%		17%	19%	19%		14%	22%	15%
EMC1	9%	12%	10%		8%	15%	24%		13%	14%	12%

FBXO9	**9%**	**24%**	**18%**		**15%**	**13%**	**16%**		**10%**	**21%**	**22%**
FERMT2	**12%**	**17%**	**15%**		**16%**	**17%**	**19%**		**11%**	**19%**	**17%**
FIBP	**21%**	**24%**	**20%**		**22%**	**24%**	**21%**		**27%**	**20%**	**28%**
GGNBP2	**13%**	**21%**	**24%**		**19%**	**21%**	**21%**		**10%**	**18%**	**19%**
GIT1	**17%**	**17%**	**14%**		**8%**	**23%**	**26%**		**12%**	**15%**	**21%**
GPAA1	**18%**	**18%**	**22%**		**13%**	**16%**	**23%**		**16%**	**21%**	**15%**
GPI	**6%**	**18%**	**18%**		**8%**	**21%**	**19%**		**6%**	**17%**	**14%**
HNRNPM	**16%**	**24%**	**23%**		**16%**	**22%**	**24%**		**16%**	**23%**	**24%**
HNRNPU	**22%**	**16%**	**21%**		**23%**	**15%**	**19%**		**19%**	**21%**	**13%**
ILF2	**14%**	**20%**	**20%**		**12%**	**24%**	**20%**		**5%**	**18%**	**19%**
KPNB1	**17%**	**14%**	**17%**		**16%**	**11%**	**18%**		**18%**	**18%**	**15%**
LOC101109495	**14%**	**21%**	**23%**		**20%**	**17%**	**21%**		**21%**	**23%**	**18%**
LOC101112480	**25%**	**22%**	**19%**		**25%**	**22%**	**21%**		**25%**	**20%**	**18%**
LPCAT4	**12%**	**14%**	**15%**		**18%**	**15%**	**18%**		**19%**	**11%**	**20%**
MAP4K4	**14%**	**25%**	**23%**		**18%**	**28%**	**28%**		**14%**	**12%**	**27%**
MAT2A	**12%**	**16%**	**10%**		**13%**	**10%**	**18%**		**14%**	**11%**	**15%**
MPRIP	**23%**	**14%**	**13%**		**27%**	**19%**	**12%**		**24%**	**16%**	**13%**
MTCH1	**7%**	**22%**	**20%**		**4%**	**23%**	**23%**		**8%**	**21%**	**24%**
NCOA4	**16%**	**19%**	**20%**		**3%**	**13%**	**24%**		**14%**	**24%**	**20%**
NDUFA2	**16%**	**14%**	**15%**		**16%**	**13%**	**11%**		**12%**	**19%**	**14%**
PAM	**21%**	**28%**	**25%**		**22%**	**27%**	**27%**		**23%**	**27%**	**25%**
PRKCSH	**17%**	**15%**	**16%**		**19%**	**18%**	**22%**		**22%**	**20%**	**16%**
PSMA4	**16%**	**20%**	**18%**		**15%**	**18%**	**23%**		**24%**	**14%**	**16%**
PSMD2	**14%**	**20%**	**14%**		**5%**	**20%**	**18%**		**7%**	**17%**	**19%**
PTOV1	**11%**	**19%**	**23%**		**15%**	**21%**	**20%**		**14%**	**20%**	**21%**
RAF1	**20%**	**23%**	**21%**		**7%**	**22%**	**23%**		**14%**	**17%**	**20%**
RBM5	**13%**	**16%**	**16%**		**11%**	**18%**	**20%**		**16%**	**17%**	**15%**
RFXANK	**16%**	**20%**	**19%**		**23%**	**12%**	**24%**		**13%**	**18%**	**18%**
RPN1	**18%**	**18%**	**27%**		**29%**	**25%**	**25%**		**21%**	**17%**	**21%**
SGK1	**19%**	**17%**	**22%**		**21%**	**21%**	**18%**		**18%**	**21%**	**16%**
SLC25A3	**9%**	**21%**	**21%**		**12%**	**20%**	**24%**		**16%**	**19%**	**25%**
SNF8	**17%**	**26%**	**22%**		**20%**	**17%**	**22%**		**21%**	**20%**	**23%**
SORT1	**15%**	**22%**	**22%**		**19%**	**14%**	**29%**		**19%**	**24%**	**18%**
TBCB	**11%**	**25%**	**24%**		**11%**	**24%**	**23%**		**13%**	**23%**	**26%**
TERF2	**16%**	**24%**	**18%**		**27%**	**20%**	**19%**		**18%**	**20%**	**16%**
TMX2	**12%**	**21%**	**26%**		**9%**	**23%**	**23%**		**10%**	**24%**	**26%**
TRMT2A	**18%**	**24%**	**15%**		**14%**	**9%**	**24%**		**14%**	**13%**	**21%**
UAP1	**10%**	**15%**	**17%**		**7%**	**16%**	**19%**		**17%**	**15%**	**20%**
VPS52	**10%**	**20%**	**10%**		**12%**	**12%**	**19%**		**14%**	**11%**	**18%**

Pink and blue: maternally and paternally expressed, respectively. Numbers: % of paternal allele expression [paternal allele reads/(paternal allele reads+ maternal allele reads)]. Genes in bold: known sheep imprinted genes.

Table S1.2. The iSNPs and the percentages of their paterntal allele expression in the 80 monoallelically expressed genes in each animal/tissue sample

https://www.tandfonline.com/doi/suppl/10.1080/15592294.2018.1503489?scroll=top

Table S2. Summary of imprinted genes in the sheep (21), mouse (186), human (112), cow (49), pig (25) and all 263 imprinted genes combined from five species

Among the 263, 119 genes are present in sheep genome Oar_v4.0.
https://www.tandfonline.com/doi/suppl/10.1080/15592294.2018.1503489?scroll=top

Table S3. The iSNPs and the percentages of their paternal allele expression for the 18 putative imprinted genes in each animal/tissue samples

https://www.tandfonline.com/doi/suppl/10.1080/15592294.2018.1503489?scroll=top

Table S4. Expression levels mean of known and putative imprinted genes in in sheep tissues of maternal nutrition groups

Maternal nutrition group	Known imprinted genes	Brain	Kidney	Lung		Putative imprinted genes	Brain	Kidney	Lung
Control	*BEGAIN*	86.41	16.76	8.08		*COPG2*	58.51	28.74	29.49
	CDKN1C	9.77	123.68	40.19		*GATM*	158.17	363.23	34.52
	DIO3	1.83	2.41	0.06		*DIRAS3*	520.62	21.31	3.06
	DLK1	1.13	756.23	59.13		*SLC22A18*	1.07	16.40	0.38
	GRB10	12.22	36.49	29.98		*PHLDA2*	19.36	253.60	0.19
	IGF2	23.61	1907.47	3404.81		*BLCAP*	305.11	93.72	89.84
	IGF2R	23.75	299.86	235.25		*WARS*	113.19	67.29	113.22
	MEST	32.11	111.10	74.17		*PLAGL1*	20.74	208.89	111.97
	PEG3	29.69	174.60	47.25		*PPP1R9A*	47.27	42.20	46.67
	RTL1	0.49	31.27	0.74		*KCNQ1*	2.08	11.39	5.45
						CASD1	22.98	20.28	14.05
						PON3	0.54	11.89	157.89
						INPP5F	419.06	19.75	31.61
Overfed	*BEGAIN*	93.49	14.61	10.41		*COPG2*	59.67	27.07	26.82
	CDKN1C	7.06	139.19	42.01		*GATM*	147.21	506.73	30.74
	DIO3	1.41	3.76	0.29		*DIRAS3*	412.49	21.35	2.37
	DLK1	0.12	721.70	94.27		*SLC22A18*	1.15	9.55	0.72
	GRB10	12.14	30.95	28.23		*PHLDA2*	0.44	130.65	8.28
	IGF2	38.26	2096.00	3074.34		*BLCAP*	308.53	88.44	89.03
	IGF2R	23.64	405.87	205.58		*WARS*	121.30	75.56	124.26
	MEST	27.94	136.66	86.21		*PLAGL1*	19.86	216.79	103.98
	PEG3	28.62	224.42	35.94		*PPP1R9A*	45.46	49.64	35.04
	RTL1	0.24	20.37	1.42		*KCNQ1*	2.51	11.02	4.80
						CASD1	22.11	20.79	12.91
						PON3	0.68	12.19	105.34
						INPP5F	334.57	19.57	30.29
Restricted	*BEGAIN*	54.53	19.67	9.59		*COPG2*	62.56	27.42	30.70
	CDKN1C	15.27	131.04	43.48		*GATM*	193.92	421.41	30.54
	DIO3	1.24	1.91	0.04		*DIRAS3*	407.41	32.33	1.28
	DLK1	0.43	750.71	55.69		*SLC22A18*	0.53	10.56	0.17
	GRB10	11.69	35.42	31.79		*PHLDA2*	0.47	206.26	1.31
	IGF2	5.22	1965.73	3054.94		*BLCAP*	265.86	94.72	92.80
	IGF2R	15.78	371.21	222.87		*WARS*	102.75	72.70	127.45
	MEST	30.87	110.79	80.57		*PLAGL1*	19.73	216.57	109.18
	PEG3	22.48	252.27	44.18		*PPP1R9A*	42.57	51.06	43.89
	RTL1	0.36	21.90	0.69		*KCNQ1*	1.76	9.86	4.08
						CASD1	19.60	21.08	14.46
						PON3	0.50	11.19	111.54
						INPP5F	299.25	20.70	33.22

TPM<1 is used as a cut-off for gene expression.
Genes highlighted are lowly expressed.

Table S5. RNA integrity number in each sample

Tissue	Treatment	Sample ID	RIN	260/280	Qubit RNA concentration (ng/ul)
Brain	Control	1	8.3	2.2	1176
		2	8.7	2.15	230
		3	7	2.23	85.8
		4	8.1	2.22	472
		5	8.8	2.14	1170
		6	7	2.14	576
		7	8	2.14	1158
	Restricted	1	8.3	2.19	724
		2	7.5	2.14	252
		3	8.4	2.13	103
		4	8.1	2.16	858
	Overfed	1	8.2	2.18	720
		2	7.4	2.19	220
		3	8.5	2.19	468
		4	9	2.18	1266
Lung	Control	1	9.5	2.18	796
		2	9.4	2.14	396
		3	9.4	2.18	510
		4	9	2.17	464
		5	10	2.14	573
		6	9.7	2.14	1860
		7	9.9	2.14	1920
	Restricted	1	8.2	2.16	1448
		2	8.9	2.14	422
		3	8.8	2.13	384
		4	9.4	2.12	342
	Overfed	1	9	2.17	988
		2	9.1	2.18	540
		3	9.3	2.19	488
		4	9.1	2.18	684
Kidney	Control	1	8.9	2.12	450
		2	7.3	2.15	1264
		3	9.3	2.08	736
		4	7.8	2.11	1160
		5	9.1	2.14	1470
		6	7.3	2.14	1092
		7	8.3	2.14	2226
	Restricted	1	8.8	2.04	2412
		2	9.1	2.1	1996
		3	7.5	2.18	1280
		4	9.3	2.16	330
	Overfed	1	9.2	2.1	494
		2	8.4	2.1	524
		3	8.9	2.15	648
		4	7.8	2.2	1224

Table S6. RNA sequencing and DNA sequencing mapping rate for unique aligned reads in two genomes

	Mapping_rate		
Sample name	**Input reads**	**Reference_genome**	**Alternative_genome**
RNA sequencing			
Brain_Con1	19,338,492	87.65%	87.55%
Brain_Con2	7,403,965	87.87%	87.91%
Brain_Con3	16,659,394	88.73%	88.74%
Brain_Con4	10,877,799	89.29%	89.41%
Brain_Con5	44,248,481	88.58%	88.69%
Brain_Con6	27,184,026	88.24%	88.33%
Brain_Con7	22,361,399	88.07%	88.15%
Brain_Over1	24,241,471	88.45%	88.55%
Brain_Over2	12,234,121	89.03%	89.05%
Brain_Over3	13,845,220	88.87%	88.96%
Brain_Over4	30,882,144	88.67%	88.78%
Brain_Res1	16,265,786	89.46%	89.52%
Brain_Res2	16,451,888	89.51%	89.53%
Brain_Res3	12,068,236	88.79%	88.86%
Brain_Res4	19,787,096	88.72%	88.81%
Kidney_Con1	5,309,507	88.85%	89.00%
Kidney_Con2	19,799,155	88.45%	88.50%
Kidney_Con3	22,380,911	88.85%	89.05%
Kidney_Con4	26,838,096	88.56%	88.66%
Kidney_Con5	27,727,956	88.54%	88.72%
Kidney_Con6	19,647,949	88.18%	88.26%
Kidney_Con7	22,924,014	88.14%	88.27%
Kidney_Over1	8,348,235	88.67%	88.84%
Kidney_Over2	23,979,270	88.55%	88.73%
Kidney_Over3	7,705,718	88.89%	89.06%
Kidney_Over4	19,777,286	88.60%	88.72%
Kidney_Res1	22,860,452	88.61%	88.77%
Kidney_Res2	20,851,640	88.32%	88.43%
Kidney_Res3	26,710,129	88.16%	88.34%
Kidney_Res4	5,475,073	88.95%	89.10%
Lung_Con1	18,685,815	88.06%	88.30%
Lung_Con2	22,413,568	87.68%	87.90%
Lung_Con3	20,516,820	87.74%	87.97%
Lung_Con4	26,061,352	87.92%	88.11%
Lung_Con5	29,341,237	87.68%	87.90%
Lung_Con6	33,475,352	87.16%	87.27%
Lung_Con7	27,083,308	87.76%	87.94%
Lung_Over1	67,688,330	87.19%	87.38%
Lung_Over2	24,310,426	88.87%	89.14%
Lung_Over3	15,834,344	88.24%	88.47%
Lung_Over4	33,703,648	87.30%	87.53%
Lung_Res1	28,273,422	87.79%	88.04%
Lung_Res2	37,304,508	87.51%	87.69%
Lung_Res3	14,983,923	88.03%	88.20%
Lung_Res4	15,457,570	88.02%	88.20%
DNA sequencing			
Ram_1	521,179,196	85.29%	85.14%
Ram_2	164,576,169	85.30%	85.17%
Ram_3	357,811,435	85.77%	85.68%
Ram_4	289,304,114	85.92%	85.83%

Table S7. RNA Sequencing mapping rates for multiple aligned reads

Fetus ID	Input reads	% Mapped Reads	Number of Mapped Reads
Brain_Con1	19,338,492	89%	17,261,538
Brain_Con2	7,403,965	90%	6,629,510
Brain_Con3	16,659,394	90%	15,055,094
Brain_Con4	10,877,799	91%	9,932,518
Brain_Con5	44,248,481	90%	40,040,450
Brain_Con6	27,184,026	90%	24,500,963
Brain_Con7	22,361,399	90%	20,089,481
Brain_Over1	24,241,471	91%	14,836,023
Brain_Over2	12,234,121	91%	14,979,444
Brain_Over3	13,845,220	91%	10,926,581
Brain_Over4	30,882,144	91%	17,921,173
Brain_Res1	16,265,786	90%	21,904,593
Brain_Res2	16,451,888	91%	11,086,560
Brain_Res3	12,068,236	91%	12,564,537
Brain_Res4	19,787,096	91%	27,966,870
Kidney_Con1	5,309,507	90%	16,897,583
Kidney_Con2	19,799,155	90%	20,199,107
Kidney_Con3	22,380,911	90%	18,491,810
Kidney_Con4	26,838,096	90%	23,499,521
Kidney_Con5	27,727,956	90%	26,421,784
Kidney_Con6	19,647,949	89%	29,926,965
Kidney_Con7	22,924,014	90%	24,366,852
Kidney_Over1	8,348,235	90%	25,508,281
Kidney_Over2	23,979,270	90%	33,525,561
Kidney_Over3	7,705,718	90%	13,539,473
Kidney_Over4	19,777,286	90%	13,964,369
Kidney_Res1	22,860,452	89%	60,526,905
Kidney_Res2	20,851,640	91%	22,129,781
Kidney_Res3	26,710,129	91%	14,345,916
Kidney_Res4	5,475,073	90%	30,242,283
Lung_Con1	18,685,815	91%	4,836,961
Lung_Con2	22,413,568	90%	17,858,838
Lung_Con3	20,516,820	91%	20,386,772
Lung_Con4	26,061,352	90%	24,242,852
Lung_Con5	29,341,237	91%	25,146,483
Lung_Con6	33,475,352	90%	17,692,978
Lung_Con7	27,083,308	90%	20,656,829
Lung_Over1	67,688,330	91%	7,591,885
Lung_Over2	24,310,426	91%	21,765,983
Lung_Over3	15,834,344	91%	7,026,844
Lung_Over4	33,703,648	91%	17,920,199
Lung_Res1	28,273,422	91%	20,732,144
Lung_Res2	37,304,508	90%	18,835,286
Lung_Res3	14,983,923	90%	24,124,589
Lung_Res4	15,457,570	91%	4,992,172

Table S8.1.DEG of monoallellically expressed genes in sheep fetal tissues of maternal nutrition

Comparisons	Tissue	Genes	Condition1 (TPM)	Condition2 (TPM)	Single Log2 FC	Confident Log2 FC
Con vs. Res	Brain	*LOC101112480*	12.241	21.36	0.80	1.23

Table S8.2. DEG of known mammlian imprinted genes in sheep fetal tissues of maternal nutrition. Red genes are imprinted genes in sheep

Comparisons	Tissue	Genes	Condition1 (TPM)	Condition2 (TPM)	Single Log2 FC	Confident Log2 FC
Con vs. Over	Brain	*KRT7*	4.35	1.58	-1.46	-1.39
		PHLDA2	19.36	0.44	-5.46	-1.71
	Kidney	*ADAM23*	2.10	5.83	1.48	2.69
		AOX1	13.25	3.10	-2.10	-1.39
		RBP5	18.10	13.30	-0.44	-1.08
		SGK2	17.48	13.63	-0.36	-1.04
		SLC22A18	16.40	9.63	-0.77	-1.24
	Lung	*PHLDA2*	0.21	8.22	5.29	6.58
		WT1	0.12	2.08	4.11	3.38
Con vs. Res	Brain	*AOX1*	2.82	0.71	-1.98	-1.82
		GALNT6	5.00	39.82	2.99	1.97
		GLIS3	10.16	4.48	-1.18	-1.04
		IGF2	16.45	5.19	-1.67	-2.07
		PHLDA2	19.36	0.47	-5.36	-6.32
		SGK2	4.52	36.38	3.01	1.47
		SLC22A2	1.14	0.23	-2.33	-2.28
		SMOC2	3.15	1.37	-1.20	-1.10
		TP73	2.66	0.39	-2.76	-2.63
		TSPAN32	1.16	2.25	0.96	1.02
	Kidney	*AOX1*	13.25	3.45	-1.94	-1.39
	Lung	*DIRAS3*	3.06	1.29	-1.24	-1.11
		PHLDA2	0.21	1.29	2.61	2.23

Red genes are imprinted genes in sheep

Table S9. Primers used for PCR and Sanger sequencing

Gene Name	Forward primer	Reverse primer	Product length	TM
CASD1	TGGCAGCAGACACAAGGGGTATCTT	TGCACTCTGCTTCAGTTTTCTTCAGT	449	55° C
COPG2	AGAAAGACATGCACAAGGACAGAC G	TCCTATAGCTACCAATGCCCCCACC	560	60° C
DIRAS3	ACCCAAACCACAGCACACAAGTCAG	CGACCATCGAAGATACCTACCGCCA	620	62° C
INPP5F	AACATAAACACATTGACTGGC	ACTGGTTCAACTGACAAAAAC	263	55° C
PLAGL1	GCATCCTACATCCCAGTTTCCACGC	ACAAGGGAAAGTGTGCTTCATCCGC	375	55° C
PPP1R9A	TGGTAATGCTAGTGCTTGCTGTTGT	AACATTGTCAACTGGTCATTGATCTAC A	307	55° C
SLC22A18	AGGAAGCCCTCTAGCCTCCAAAGTG	TCCAGTCCACTCGTGGGCAGTTAAG	650	63° C

Figure S1. Identification of informative SNPs (iSNPs).

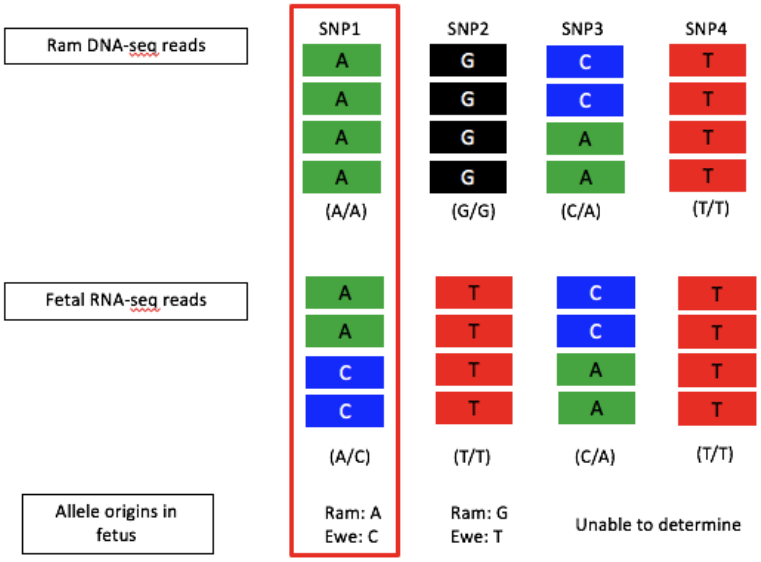

Four different types of SNP combination were observed and only SNP1 was considered informative because it is heterozygous in the fetus and homozygous in the ram. Others are either discordant or uninformative in the allele's parental origin.

Figure S2. Expression levels (TPM mean) of sheep imprinted genes in the brain, kidney, and lung tissue of day 135 fetal sheep from ewes fed a control diet.

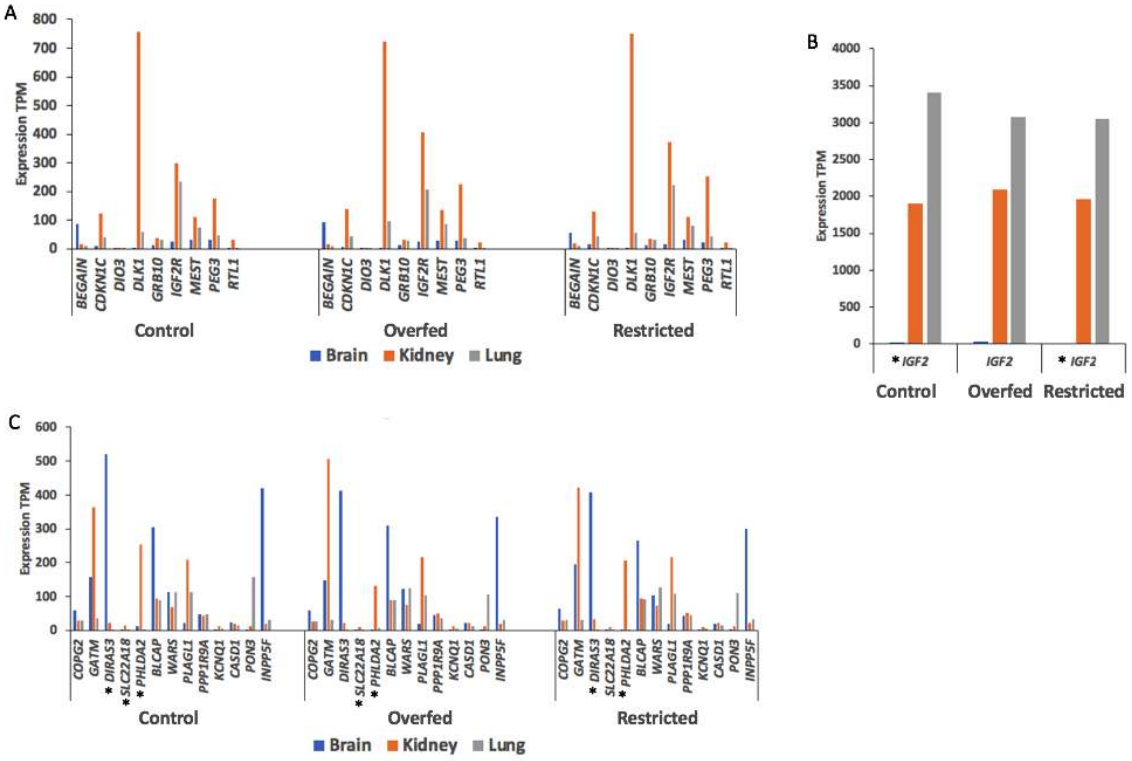

A-B.The 10 coding and previously known imprinted genes in the sheep genome. C. The 13 putative imprinted genes identified in our study. Blue: brain, orange: kidney, grey: lung. (*) Indicates genes are differentially expressed that present in Table2.

Chapter Three

Dosage Compensation of the X Chromosomes in Bovine Germline, Early Embryos and Somatic Tissues

(Under revision, Genome Biology and Evolution)

Duan J.E., Shi W., Jue N.K., Jiang Z., Kuo L., O'Neill R., Wolf E., Dong H., Zheng X., Chen J. & Tian X.C.

3.1. Abstract

Dosage compensation of the mammalian X chromosome (X) was proposed by Susumu Ohno as a mechanism wherein the inactivation of one X in females would lead to the doubling the expression of the other. This would resolve the dosage imbalance between eutherian females (XX) vs. male (XY) and between a single active X vs. autosome pairs (A). Expression ratio of X- and A-linked genes has been relatively well-studied in humans and mice, despite controversial results over the existence of up-regulation of X-linked genes. Here we report the first comprehensive test of Ohno's hypothesis in bovine pre-attachment embryos, germline and somatic tissues. Overall an incomplete dosage compensation ($0.5<X:A<1$) of expressed genes and an excess X dosage compensation ($X:A>1$) of ubiquitously expressed "dosage-sensitive" genes were seen. No significant differences in X:A ratios were observed between bovine female and male somatic tissues, further supporting Ohno's hypothesis. Interestingly, pre-implantation embryos manifested a unique pattern of X dosage compensation dynamics. Specifically, X dosage decreased after fertilization, indicating that the sperm brings in an inactive X to the matured oocyte. Subsequently, the activation of the bovine embryonic genome enhanced expression of X-linked genes and increased the X dosage. As a result, an excess compensation was exhibited from the 8-cell stage to the compact morula stage. The X dosage peaked at the 16-cell stage and stabilized after the blastocyst stage. Together, our findings confirm Ohno's hypothesis of X dosage compensation in the bovine and extend it by showing incomplete and over-compensation for expressed and "dosage-sensitive" genes, respectively.

Keywords Ohno's hypothesis; X dosage compensation; Pre-attachment embryos; Bovine

3.2. Introduction

Gene dosage is the number of copies of a given gene in cells of an organism and can be manifested by the amount of its products (Ercan, 2015). Maintenance of proper gene dosage is essential in functional cellular networks such as in embryogenesis, and fetus development. Aneuploidy such as monosomy or trisomy is an abnormal change in the dosage of chromosomes and is generally detrimental to the organism (Holtzman et al., 1992). For example, aneuploidy accounts for 46.3% of spontaneous abortions in humans (Hassold et al., 1980). Small changes in dosage of single genes can lead to many diseases (Hurles et al., 2008) and the onset of tumorigenesis (Gordon et al., 2012). However, monosomy of the X chromosome in mammalian males is well-tolerated, although over a thousand genes important for both sexes are located on X (Ercan, 2015). Susumu Ohno hypothesized that to prevent the deleterious effects of haploinsufficiency in males, a compensatory mechanism involving the doubling expression of X-linked genes must occur (Ohno et al., 1959). This, however, at the same time could cause a quadruple dosage of X in females. By transcriptionally silencing one of the two X chromosomes in females the dosage of the X chromosome between males and females is balanced (Veitia and Potier, 2015). Meanwhile, this also balances the gene dosage between sex chromosome and autosome pairs (A) in both sexes (Ohno, 1966).

Although X chromosome inactivation (XCI) has been observed in all mammalian species studied to date (Heard et al., 1997; Lyon, 1961; Ohno et al., 1959), dosage compensation by doubling the expression of X-linked genes has only been studied in very few species and is still heavily debated (Deng et al., 2011; He et al., 2011; Kharchenko et al., 2011; Nguyen and Disteche, 2006; Xiong et al., 2010). Dosage compensation is determined by calculating the ratio of averaged expression value of X-linked genes to that of the autosomes (X:A ratio). The ratio

X:A ≅ 1 indicates the doubling of X gene expression, while X:A of 0.5 rejects Ohno's hypothesis. Two previous microarray studies fully supported dosage compensation in both humans and mice (Gupta et al., 2006; Nguyen and Disteche, 2006). However, the first RNA sequencing (RNA-seq) study of humans and mice (Xiong et al., 2010) claimed that microarray-based expression was not suitable for comparing expression levels of different genes, and reported X:A of approximately 0.5 i.e. a lack of dosage compensation. Subsequently, the same RNA-seq data were re-analyzed with all low and non-expressed genes removed because such genes are enriched on X chromosomes and thus could skew the comparison. Results from such filtering verified the hypothesis (Deng et al., 2011; Kharchenko et al., 2011). Since then, Ohno's hypothesis has been tested with many different analysis approaches including comparing the ratio between the modern X to the proto XX using 1:1 orthologs between humans and chickens (Lin et al., 2012) or comparing only genes coding for large proteins as the "dosage-sensitive housekeeping genes" (Pessia et al., 2014). It has been found that different experimental platforms, analysis methods, and cutoff values all influenced the dosage compensation results. Thus, more questions than answers are presented on the evolution of dosage compensation of sex chromosomes (He and Zhang, 2016).

While debates persist over dosage compensation, XCI has been observed in all mammalian species studied to date (Okamoto et al., 2011). In the bovine, XCI was proposed by De La Fuente et al. (1999), and confirmed by Xue et al. (2002). In early bovine embryos imprinted XCI was observed at the morula stage (Ferreira et al. 2010) and random XCI occurred between the blastocyst and elongation stages (Bermejo-Alvarez et al., 2011). Although a recent study reported incomplete X dosage compensation in bovine fat, liver, muscle, and pituitary gland (Ka et al., 2016), further studies are needed for bovine early embryos and germ cells.

Here we report the first comprehensive test of Ohno's hypothesis in the compensatory upregulation of the X chromosome in bovine embryos, germline and a vast array of somatic tissues using seven RNA-seq datasets (three from bovine pre-attachment embryos and four from somatic tissues), including immature and mature oocytes, *in vivo* and *in vitro* embryos up to the blastocyst stage (days 1-7; day 0= standing estrus), conceptuses (embryos and associated extra-embryonic membranes) from day 7 to day 19, two adult female-specific tissues, eight adult female and male somatic tissues. Using median expression of the X:A ratio with its 95% bootstrap confidence intervals, we report incomplete compensatory up-regulation of expressed X-linked genes and complete dosage compensation of "dosage-sensitive" genes. Our data thus fully support Ohno's hypothesis in that the compensatory upregulation of X chromosome expression affects "dosage-sensitive" genes in bovine developing embryos, germline cells and female/male tissues.

3.3. Materials and Methods

3.3.1. Paralog analysis

To determine the unique or non-unique mapping strategy, we first calculated paralog enrichment on each bovine chromosome. Paralogs were identified on BioMart (Ensembl genome browser: http://useast.ensembl.org/biomart/; ensemble genes 85) and defined as genes with greater than 70% amino acid identity. This minimal cutoff for paralogs was a result of our pervious study, which determined that 70% was the best match of the BioMart search algorithm for the identification of X-linked multi-gene families (Jue et al., 2013). The total number of genes on each chromosome was calculated using bovine genome reference annotation UMD3.1 (http://useast.ensembl.org/Bos_taurus/Info/Annotation?redirect=no). Enrichment of paralogs gene number for each autosome was calculated by Fisher's exact test compare to that on X chromosome (Table 1).

3.3.2. RNA-seq datasets and read trimming

Raw FASTQ files were obtained from NCBI GEO database (Table 2). A total of seven datasets including 1) *in vivo* developed matured oocytes and 2-cell to blastocyst stage pre-implantation embryos (Jiang et al., 2014), 2) immature oocyte, *in vitro* developed matured oocytes, 4-cell, 8-cell, 16-cell, and blastocyst embryos (Graf et al., 2014), 3) conceptuses at days 7, 10, 13, 16, and 19 (embryos and associated extra-embryonic membranes) (Mamo et al., 2012), 4) female endometria and corpora lutea (CL) (Moore et al., 2016), 5) female somatic tissues of brain, liver, muscle and kidney (Chen et al., 2015), 6) male somatic tissues of fat, muscle, hypothalamus, duodenum, liver, lung and kidney (PRJEB6377), 7) female and male somatic tissues of fat, liver, muscle, and pituitary gland (Seo et al., 2016).

All RNA-seq raw reads were downloaded from NCBI using sratoolkit (version 2.5.0;

http://www.ncbi.nlm.nih.gov/Traces/sra/sra.cgi?view=toolkit_doc&f=std#s-2). The sequence read archive (sra) format files were converted to fastq format by fastq-dump (version 2.5.0; http://www.ncbi.nlm.nih.gov/Traces/sra/sra.cgi?view=toolkit_doc&f=fastq-dump). Quality-trimming and control were conducted as follows before mapping to the reference genome. Firstly, Trimmomatic (version 0.33; http://www.usadellab.org/cms/?page=trimmomatic) was applied to removing the universal sequencing adaptors of SOLiD and Illumina in respective datasets with a minimum Phred score of 20 and minimal length of 30bp. Subsequently, read quality was examined using FastQC (version 0.11.3; http://www.bioinformatics.babraham.ac.uk/projects/fastqc/). The summary of the numbers of reads in each sample after trimming is presented in supplementary table S1. The average number of read input for mapping across all samples is 22,814,027.

3.3.3. Mapping and transcript assembly

RNA-seq read mapping and transcript assembly were preformed based on the following pipeline. Trimmed RNA-seq reads were aligned to Ensemble bovine reference genome assembly UMD3.1.1 using Hisat2 version 2.0.5 aligner (Pertea et al., 2016). Transcript splice site detection was used and both unique and non-uniquely mapped reads were kept for the subsequent analysis. The percentages of non-uniquely mapped reads for each sample are summarized in supplementary table S1 and the averaged overall mapping rate was 83.5%. IsoEM version 1.1.5 (Nicolae et al., 2011b) was used to quantify gene expression to transcripts per kilobase million (TPM) using default parameters. For non-uniquely mapped reads, IsoEM assign fractions of the multiple aligned reads to each location using an expectation maximization algorithm (Nicolae et al., 2011b). Expressed genes were defined as expression level TPM >1. “Dosage-sensitive” genes were selected as ubiquitously expressed genes (TPM>1) throughout all somatic samples or

embryonic sample.

3.3.4. RNA-seq dataset overview

Matrices of gene expression TPM for the embryo (datasets 1-3) and somatic tissues (datasets 4-8) were processed separately in R to identify ubiquitous genes. Correlation plots and unsupervised hierarchical clustering were conducted in R for quality control and identification of biologically distinct subgroups. Outliers in the biological replicates were removed for the downstream analysis.

The chromosome-wide gene expression distributions were isolated by gene locations on each chromosome in all samples using $\log_2$-transformed TPM (TPM>1), the boxplots for the distribution were made in R.

3.3.5. GO analysis

Gene ontology enrichment analysis was performed in DAVID (Huang et al., 2009a) and 245 and 7,603 genes on the X and autosomes, respectively, were found as ubiquitous in the somatic tissue datasets. Similarly, 117 and 3,947 genes on the X and autosomes, respectively, were found as ubiquitous in the embryo datasets. The p-values in top 10 biological processes were plotted using plotly (https://plot.ly) in R. Pie charts for biological processes were generated as described by The Gene Ontology Consortium (2015).

3.3.6. X:A ratio calculation

When calculating the X:A ratio, we applied the pairwiseCI package in R (Schaarschmidt and Gerhard, 2015) to obtain a 95% confidence interval for the ratio of the median of X to the median of A as in a previous study (Sangrithi et al., 2017). It is based on 1,000 bootstrap replicates where sampling from the original data was done with replacement and stratified by the

group variables. Bootstrapping (Efron and Tibshirani, 1994) was used because it is simple to apply and does not require any distribution assumptions.

3.4. Results

3.4.1. Overview of the RNA-seq datasets and paralog analysis

We used seven bovine RNA-seq datasets, three embryonic and four somatic, generated by us (Jiang et al., 2014) and downloaded from NCBI (Table 2). In total, we have 40 samples including 19 embryos and 21 tissues from all datasets. Pearson correlation and unsupervised hierarchical clustering (supplementary fig. S1) show that replicates within each tissue or embryonic stage clustered closely to each other, suggesting even though the data were obtained from different studies, the data were replicable and reliable. Because we only compared the X:A ratio and gene expression within each dataset instead of across datasets, we were able to use the data from different studies and experimental platforms after data normalization.Paralogs are homologous genes within the same genome created by gene duplication (Gevers et al., 2004). This is one potential way to achieve X dosage compensation because X lacks a homolog in males (Jue et al., 2013). We found an approximately 1.4-fold increase in the percentage of paralogs (>70% amino acid identity (Jue et al., 2013)) on the bovine X chromosome (33%) compared to the genome averages (24%; Table 1). This enrichment is significantly higher (Table 1; $p < 0.05$ by Fisher's exact test) than to that of most chromosomes, with the exception of Chromosomes 15, 21, and 23 ($p = 0.97$, 0.10, and 0.61, respectively), suggesting the potential roles of paralogs in X dosage compensation. Such paralog enrichment on X has also been observed in humans (32% vs. 17%; 1.9-fold) and mice (51% vs. 35%; 1.5-fold) (Jue et al., 2013). This information demonstrated that unique mapping as performed in a previous RNA-seq study (Xiong et al., 2010) is not appropriate because many paralogs will be excluded from the analysis, and potentially skewing the X:A comparison. Thus, we applied the "non-unique" mapping strategy for reads mapping. Reads that aligned to multiple locations (such as paralog gene family) in the reference

genome or had alternative splice junctions were kept in all subsequent analysis. This resulted in a total of 959 X-linked and 20,316 autosomal protein coding genes.

Deng et al. (2011) suggested that the low and non-expression values in RNA-seq data may result from background noise of sequencing and read mapping. Inclusion of such values would be inappropriate and strongly influence the results. Furthermore, when we calculated the percentages of X-linked and autosomal genes with low transcript per million (TPM) values (Fig. 1A and supplementary table S2), we found that on the average the X chromosome has 11.7% more genes with TPM ≤1 than autosomes. Somatic tissues including endometrium, fat, liver and muscle had the most enrichment of lowly expressed X-linked genes (supplementary table S2). Therefore, we used a cutoff of TPM>1 as expressed genes to remove data bias. After this filtering, 468 X-linked genes and 12,288 autosomal genes on average were used for X:A ratio calculation. The numbers of expressed genes (TPM >1) on X chromosome or autosomes in each sample are listed in supplementary table S2.

3.4.2. Ranges of gene expression of all chromosomes

We then investigated the gene expression profiles of all chromosomes to determine whether the transcriptional outputs from X chromosome were comparable to those of each autosome pairs. We performed $\log_2$-transformation of TPM to to normalize the data distribution. The TPM distribution of X-linked genes was not significantly different from those of all autosome pairs in 11 out of 40 samples using all expressed genes, and 31 out of 40 samples using ubiquitously expressed genes ($p > 0.05$, by two-sided Kolmogorov-Smirnov test, Fig. 1B and supplementary table S3). Such distributions were also demonstrated by kernel density estimation (Fig. 1C). These observations demonstrate that regardless of the number of X chromosomes, the

expression levels of ubiquitously expressed genes on X were comparable to those of each autosome pair in all samples, suggesting dosage compensation.

3.4.3. X chromosome up-regulation in adult somatic tissues

To determine the X chromosome dosage compensation in adult cattle tissue, we analyzed RNA-seq datasets (Table 2) for two female-specific tissues, endometrium and corpus luteum, and other somatic tissues from both males and females including the brain (hypothalamus), liver, kidney, muscle, fat, pituitary gland, lung, and duodenum. Overall, the X:A ratios of these tissues were in the range of 0.5 to 1, suggesting up-regulation of the expression from the X chromosome, yet the dosage compensation is incomplete (Fig. 2A & 2B). Specifically, the liver gave the highest X:A ratio (1.01) in females and showed complete compensation, followed by the pituitary gland (0.91). These data suggest that the X chromosome expression was enriched for activities in these tissues. In contrast, fat, muscle, endometrium and the lung gave relatively low but incomplete compensation X:A ratios (0.64 - 0.72), indicating less X chromosome activities. Furthermore, we compared the X chromosome expression distribution between males and females in common somatic tissues and observed no significant difference ($p > 0.05$, by two-sided Kolmogorov-Smirnov test, supplementary table S4), except in muscle. The X:A ratio of common tissues between sexes was also not significantly different ($p = 0.45$, by paired t-test after log-transformation).

Although all somatic tissues we analyzed had up-regulated expression of X-linked genes which support Ohno's hypothesis, the confidence intervals of X:A ratios did not encompass 1 in most of the samples. As suggested in previous studies "dosage-sensitive" genes with housekeeping functions were more likely affected by dosage imbalance and were up-regulated (Pessia et al., 2012). When non-dosage-sensitive genes were included in the X:A calculation, the

X:A ratio were likely lower (Sangrithi et al., 2017). Therefore, we further selected ubiquitously expressed genes (TPM>1) throughout all somatic samples. Gene ontology analysis showed strong evidence that these ubiquitously expressed genes had housekeeping roles (supplementary fig. S2), such as translation, RNA transcription, protein transport, and cellular and metabolic process (supplementary fig. S2). A total of 245 and 7,603 genes on the X chromosome and autosomes, respectively, were included as ubiquitously expressed genes in the recalculation of the X:A ratios (Fig. 2C & 2D). The confidence intervals encompassed 1 and the medians were greater than 1 in most of the samples. Brain and its specific regions such as the pituitary gland and hypothalamus had the highest X:A ratios (1.20, 1.28, and 1.22, respectively), consistent with previous reports in other species (Deng et al., 2011; Nguyen and Disteche, 2006).

3.4.4. X chromosome up-regulation in immature and mature oocytes

Germinal vesicle stage (immature) oocytes are arrested at the diplotene stage of the first prophase of meiosis (Pro I) (Mehlmann, 2005), and contain a duplicated genome (XXXX:AAAA) and two active X chromosomes (Fukuda et al., 2015). The matured oocytes, on the other hand, are arrested at the second metaphase of meiosis (MII) (Li and Albertini, 2013) and are haploid (1N) although each homologous chromosome contains two sister chromatids/complements of DNA (2C; XX:AA). Our analysis included immature and both *in vivo* and *in vitro* matured oocytes (Graf et al., 2014; Jiang et al., 2014). First, we identified expressed genes (TPM>1) and ubiquitously expressed genes across all pre-implantation samples. Fewer expressed ubiquitous genes were found in these samples than in somatic tissues but similar gene ontology terms (supplementary fig. S3 & 4). A total of 117 X-linked and 3,947 autosomal genes were used as ubiquitous genes for X:A ratio calculation. Compared to expressed genes (TPM>1, X:A ≈0.75 Fig. 3C) , ubiquitously expressed genes had higher X:A ratios in immature and mature oocytes at

1 and 0.87, respectively (Fig. 3D). Taken together, our analyses reveal a higher X:A ratio for ubiquitous genes, and a balanced X to autosome expression in immature diploid oocytes and an incomplete balance in mature haploid oocytes.

3.4.5. X chromosome up-regulation in pre-implantation embryos

X inactivation and reactivation happen in cycles during early embryonic development. In mice, the zygote contains an inactive X from the sperm but three X chromosome reactivation events occur subsequently: 1) embryonic genomic activation (EGA) at 2-cell, 2) pluripotency establishment in inner cell mass (ICM) of blastocyst, and 3) primordial germ cell generation in the genital ridge (Ohhata and Wutz, 2013). Using the bovine X-linked monomine oxidase type A (*MAOA*), Ferreira et al. (2010) demonstrated that transcripts from both the maternal and paternal *MAOA* were present in embryos at the 4-, 8- to 16-cell, and blastocyst stages, while only the maternal transcripts were present in compact morula. These data revealed that XCI occurred in an imprinted fashion in the morula stage in the bovine and the paternal X was reactivated at the blastocyst stage. A more permanent random XCI was observed between the blastocyst and early elongation stages by analyzing seven X-linked genes in day14 embryos (Bermejo-Alvarez et al., 2011). However, the expression dynamics of an individual gene cannot represent the activity of the whole X chromosome, global transcript analysis will generate a more definitive conclusion on X inactivation-reactivation dynamics.

We therefore analyzed RNA-seq data from pre-attachment embryos. In *in vivo* produced pre-implantation embryos, we observed an incomplete dosage compensation ($0.5 < X:A < 1$) using expressed genes and an excess of compensation ($X:A > 1$) from the 8-cell to compact morula stages using ubiquitous genes (Fig. 3A & 3B). X dosage slightly decreased after fertilization, with the lowest X:A ratio seen at the 4-cell stage, indicating that the sperm brought

in an inactive X chromosome to the matured oocyte. The X:A ratio started to increase from the 4- to 8- cell stage, coincident with embryonic genome activation (EGA) for bovine *in vivo* embryos (Jiang et al., 2014), suggesting that EGA actives both paternal and maternal genome and has a more profound effect on the X chromosome. The increased X:A ratio exhibited excess compensation from the 8-cell to compact morula stage. A sharp decrease of X:A ratio was then observed between early (32-cell) and compact morula stages, corresponding to the first observed inactivation of the paternal X chromosome in bovine embryos. The X:A subsequently stabilized from days 7 to 19 of gestation, corresponding to random XCI between the blastocyst and early elongation stages.

Using expressed genes, *in vitro* produced bovine pre-implantation embryos present a similar X:A dynamics from fertilization to the 8-cell stage (Fig. 3C & 3D). However, no excess dosage compensation was observed using ubiquitous genes at any stage but the blastocyst, suggesting a deviation of X compensation from *in vivo* embryos. These observations are consistent with recent findings of aberrant X regulation in *in vitro* produced human and mouse embryos (Tan et al., 2016).

3.4.6. Effect of PAR and putative XCI-escaping genes on X upregulation

Pseudoautosomal regions (PARs) contain homologous genes between the X and Y chromosomes, and are important in homologous chromosome pairing and recombination during male meiosis (Das et al., 2009). A total of 20 PAR genes (Table S3) have been characterized in bovine, sheep, goats and other ruminants (Raudsepp and Chowdhary, 2015). Most PAR genes are known to escape XCI in humans (Helena Mangs and Morris, 2007). Moreover, approximately 15% and 3% of non-PAR X-linked genes in humans and mice, respectively, are known to escape XCI (Berletch et al., 2011). In the bovine, 55 such X-linked genes

(supplementary table S5) were classified as candidates that escape XCI (Ka et al., 2016). To tease out the effects of these bi-allelically expressed PAR genes and XCI-escaping genes, we plotted X:A ratios in the categories of "all genes", "expressed genes", "genes subjected to XCI (excluding PAR genes and putative XCI-escaping genes)" and "dosage-sensitive genes" (Fig. 4). The X:A ratios for "all genes" had the median value closer to 0.5, while the ratios for "expressed genes" were closer to 1. When we excluded PARs and putative XCI-escaping genes from "expressed genes", the outliers of extremely high X:A ratios disappeared, suggesting bi-allelically expressed X-linked genes did contribute to the high X:A ratios. Moreover, "dosage sensitive genes" maintained the highest X:A ratios (greater than 1), further confirming the hyperexpression nature of this subgroup of genes.

3.5. Discussion

In this study, we determined the X chromosome dosage profiles in 4 chromosome scenarios in the bovine. Immature oocytes represent diploid germline with duplicated genome/4 complements of DNA (XXXX:AAAA); mature oocyte represent haploid germline with duplicated genome/2 complements of DNA (XX:AA); bovine pre-implantation embryos at various stages represent the gradual change from two active X (XaXa:AA) to one inactive X chromosome (XaXi:AA); female and male somatic tissues contain diploid cells with one already inactivated X (XaXi:AA or XY:AA). Our analyses showed incomplete compensation ($0.5<X:A<1$) of X chromosome to autosome pairs in all scenarios for expressed genes (TPM>1) and excess compensation (X:A>1) for "dosage-sensitive" genes in somatic tissues and certain stages in early embryos. These findings suggest that X dosage up-regulation occurs in bovine germlines, pre-attachment embryos and somatic tissues analyzed here.

Our results in bovine are consistent with previous findings in other mammalian species using similar strategies of data filtering (Deng et al., 2011; Pessia et al., 2012). However, studies applying different threshold criteria on RNA-seq data generated conflicting results for mammalian X dosage compensation. Xiong et al. (2010) included genes with low and no expression and reported X:A ratio close to 0.5. Whereas many follow-up studies reanalyzing the same RNA-seq data after removing the "noise" concluded hyper-activation of X on expressed genes (Deng et al., 2011), especially dosage-sensitive ones (genes encoding protein-complex of seven or more members and having housekeeping roles) (Pessia et al., 2012). Thus, dosage compensation, unlike X chromosome inactivation, has been proposed to be a local process with hyper-expression by only dosage-sensitive genes (Pessia et al., 2014). In our study, we applied two gene selection methods in order to identify "dosage-sensitive" genes: expressed genes that

are TPM>1 and ubiquitous genes whose TPM's are >1 in all somatic samples or in all embryo samples. We found similar results as in humans and mice that incomplete dosage compensation was incomplete in most scenarios when expressed genes were used, while ubiquitous genes had a higher X dosage, implying that the expression of a group of X-linked bovine genes are collectively more than doubled. Furthermore, this level of up-regulation could not be globally applied to all genes on the X chromosome.

The previous study by Xiong et al (2010) filtered out reads that mapped to multiple locations of the genome and those that spanned splice junctions. Such elimination may generate biased X: A ratio as shown by Jue et al (2013) who analyzed how the X:A ratios could be changed by using different mapping parameters such as unique vs. non-unique mapping. It was concluded that "unique" mapping excluded reads that may be from paralog gene families. Because paralogs are enriched on the mammalian X chromosome and gene duplication is a way to achieve dosage compensation for haploinsufficient genes, excluding reads for paralogs could produce bias in the estimation of the X:A ratios. Therefore, we used the Hisat2 software that by default reports both uniquely and multi-mapped reads Hisat2 is known to have the highest correctly multi-mapped reads compared to other aligners (Kim et al., 2015).

Bovine female somatic tissues had a slightly higher X:A ratio than the same tissues of males. This difference, however, was not significantly different ($p = 0.45$). X chromosome expression distribution was also similar between sexes ($p > 0.05$). These demonstrated that the expression of the X chromosome is balanced between males and females although they have different numbers of the X chromosome. The slightly higher X:A ratio in females may be a result of genes that escape X chromosome inactivation (Couldrey et al., 2017). Although it is unclear

how many genes escape XCI in the bovine, a previous report documented a few X-linked genes escaping XCI in a mosaic fashion in the bovine (Yen et al., 2007).

The brain tissue had the highest X:A ratio compared to the other tissues, consistent with previous RNA-seq studies in several mammalian species (Deng et al., 2011; Nguyen and Disteche, 2006). This could be related to the fact that may genes related to brain functions, such as *MAOA*, are located on the X chromosome (Zechner et al., 2001). On the contrary, X dosage of other bovine somatic tissues including fat, liver, muscle, and the pituitary gland was previously determined as incompletely compensated (Ka et al., 2016), which is consistent with results in humans, mice and ours.

Germ cells and the developing embryos undergo drastic epigenetic changes. We observed balanced expression of the X chromosome with that of the autosomes in diploid immature oocytes and incomplete balance in haploid matured oocytes. These data are consistent with those by Fukuda et al who also showed higher dosage compensation of X chromosome in immature than matured oocytes in the human and mouse (Fukuda et al., 2015). However, X:A ratio slightly decreased after fertilization probably due to the sperm brings in some mRNAs of autosomal origin in addition to an inactive X (Huynh and Lee, 2003). Because early embryonic development is primarily dependent on stored maternal mRNAs and proteins which gradually degrade until embryonic genomic activation (EGA) (Memili and First, 2000), a consistent decrease and then increase of X:A before and after EGA, respectively, were observed. The timing of the changes in X:A in *in vivo* embryos, however, was one cell cycle earlier than their *in vitro* counterparts due to the timing difference between these two types of embryos, which are 4-8 and 8-16 cell stages, respectively (Graf et al., 2014; Jiang et al., 2014; Kues et al., 2008; Misirlioglu et al., 2006; Telford et al., 1990).

In conclusion, our study shows the up-regulation of X chromosome in four bovine genome scenarios, supporting a balanced expression between a single active X and autosome pairs. However, deviating from Ohno's theory, dosage compensation to rescue X haploinsufficiency appears to be an incomplete process for expressed genes but a complete process for "dosage-sensitive" genes. Removal of PAR genes and those putatively escape XCI eliminated the outliers of extremely high X:A ratios. In addition, the switch from imprinted XCI at the compact morula stage to random XCI at the blastocyst stage may happen so rapidly that the potential transient state of two active X chromosome could not be captured in the current dataset with limited time points. Whether a transient two active X state occurs or not during blastulation requires frequent sampling and further study. Lastly, no relative X expression difference was observed between bovine female and male somatic tissues, suggesting Ohno's hypothesis balanced the overall X between sexes.

Table 1. The enrichment of paralogs on each autosome compare to that on X chromosome

Chromosome	Total number of Genes	Number (%) of Paralogs	*P*-value	Chromosome	Total number of Genes	Number (%) of Paralogs	*P*-value
1	985	167 (17)	5.65e-18	16	710	129 (18)	6.56e-13
2	1,021	229 (22)	1.88e-08	17	665	149 (22)	6.55e-07
3	1,372	314 (23)	7.24e-09	18	1,236	207 (17)	1.20e-20
4	855	222 (26)	0.00031	19	1,347	303 (22)	2.13e-09
5	1,323	336 (25)	1.51e-05	20	384	91 (24)	0.00027
6	692	156 (23)	6.65e-07	21	731	221 (30)	0.10
7	1,396	377 (27)	0.00046	22	608	110 (18)	6.40e-12
8	829	230 (28)	0.0059	23	785	264 (34)	0.61
9	602	146 (24)	6.45e-05	24	347	98 (28)	0.049
10	1,074	316 (29)	0.033	25	766	102 (13)	7.22e-24
11	1,047	192 (18)	1.63e-15	26	437	82 (19)	5.63e-09
12	414	98 (24)	0.00018	27	274	73 (27)	0.022
13	850	185 (22)	1.31e-08	28	355	78 (22)	3.08e-05
14	571	135 (24)	2.76e-05	29	705	186 (26)	0.0012
15	1,050	387 (37)	0.97	X	1,128	374 (33)	
Genome Average	819	199 (24)	1.46e-05				

Table 2. The raw FASTQ files generated by us and downloaded from NCBI GEO database

	Tissue Type (replicates)	Breed/subspecies	Number of samples	Library type	BioProject ID	Reference
1	*In vivo* MII oocytes and embryos: 2-, 4-, 8-, 16-, 32-cell, CM, and BL (n=2)	Holstein	8	Single-read SOLiD	PRJNA254699	Jiang et al., 2014
2	*In vitro* GV & MII oocytes and embryos: 4-, 8-, 16-cell, and BL (n=3)	German Simmental (♀) and Brahman (♂) cross	6	Single-read Illumina	PRJNA228235	Graf et al., 2014
3	*In vivo* Conceptuses: Day 7 (n=6), 10 (n=7), 13 (n=5), 16 (n=5), 19 (n=5)	Charolais and Limousin cross	5	Single-read Illumina	PRJNA243569	Mamo et al., 2012
4	Female specific tissue: endometria (n=12), corpora lutea (n=14)	Holstein	2	Paired-end Illumina	PRJNA298914	Moore et al., 2016
5	Female somatic tissues: brain, liver, muscle and kidney (n=4)	*Bos indicus*×*Bos taurus*	4	Single-read Illumina	PRJNA268096	Chen et al., 2015
6	Male somatic tissues: fat, muscle, hypothalamus, duodenum, liver, lung and kidney (pools of 7-14 animals)	*Bos taurus*	7	Paired-end Illumina	PRJEB6377	PRJEB6377, 2014
7	Female and male somatic tissues: fat, liver, muscle, and pituitary gland (n=5)	Hanwoo (Korean cattle)	8	Paired-end Illumina	PRJNA273164	Seo et al., 2016

Figure 1 Expression ranges of genes on the X and autosome pairs in the bovine.

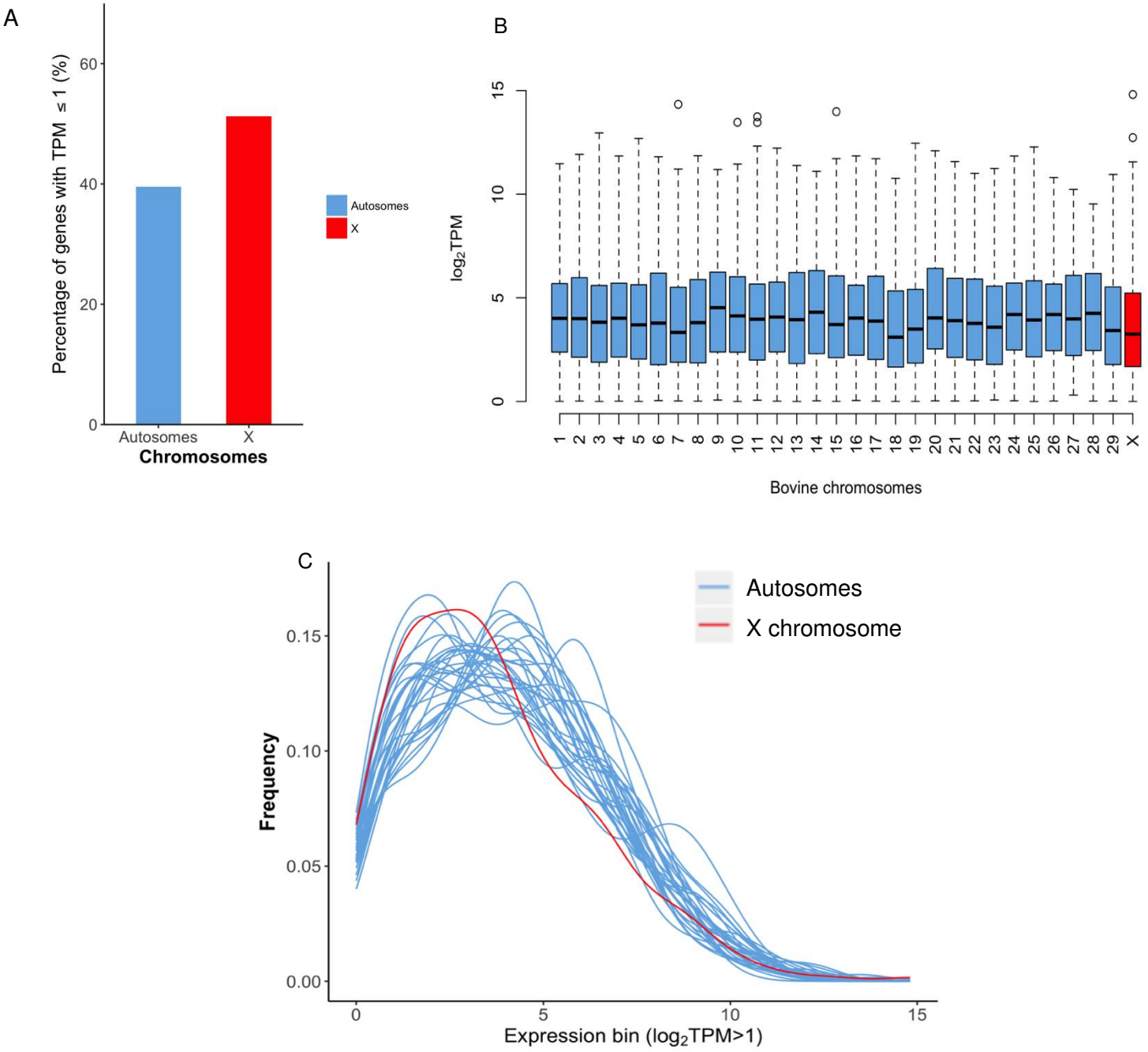

(A) the averaged percentages of lowly expressed genes (TPM<1) on the X and autosomes in all samples, (B) A representative (*in vivo* matured oocytes) box-plot showing that the range and median expression levels of X-linked genes (red) (TPM > 1) were similar to those of each autosome pairs (blue) in the bovine, (C) A representative (*in vivo* matured oocyte) Kernel density plot showing that the distribution of X-linked gene (red) expression (TPM > 1) was similar to those of each autosome pairs (blue) in the bovine

Figure 2 Median X:A ratios with 95% confidence intervals of bovine female (A, B) and male (C, D) somatic tissues.

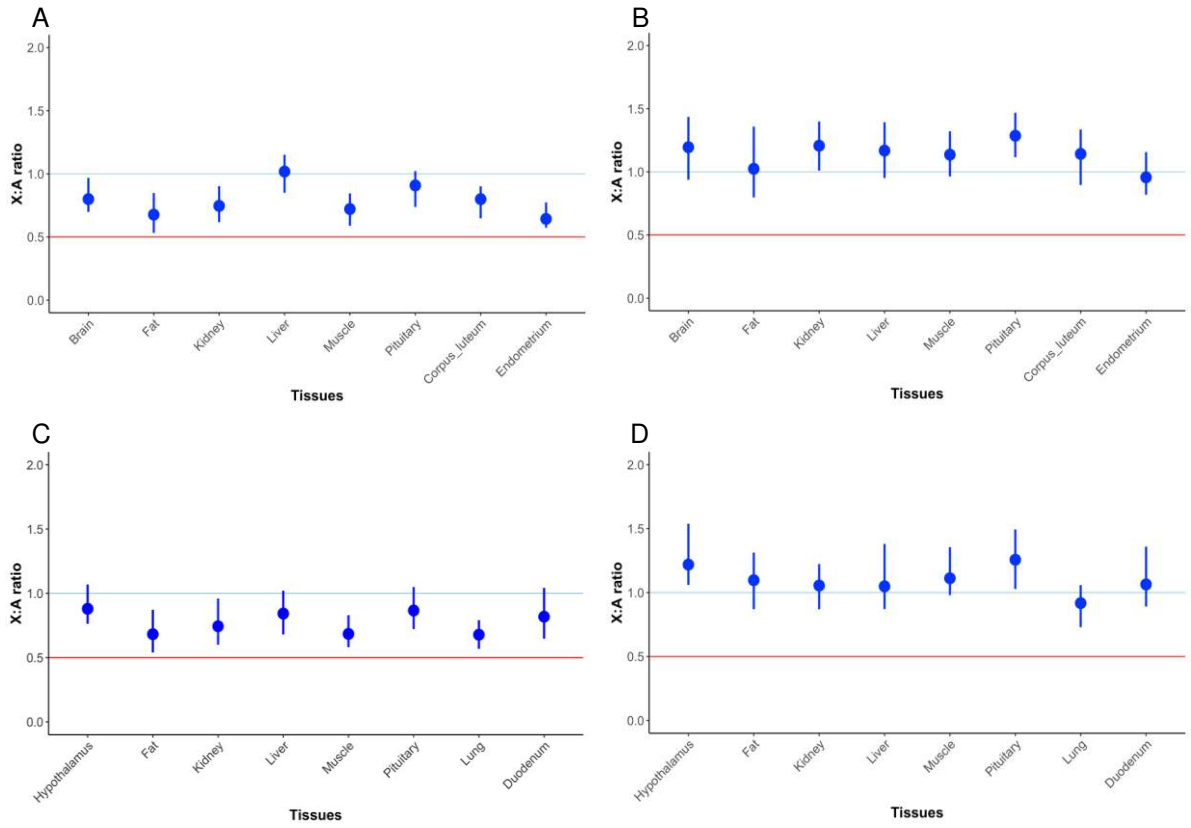

The X:A ratios were calculated using expressed (TPM > 1) genes (A, C) and ubiquitously expressed (TPM > 1 and present in all somatic datasets; B, D) genes. Blue line: X:A=1, complete dosage compensation; Red line: X:A=0.5, no dosage compensation

Figure 3 Median X:A ratios with 95% confidence intervals of bovine *in vivo* (A, B) and *in vitro* (C, D) produced oocytes and pre- and post-implantation embryos.

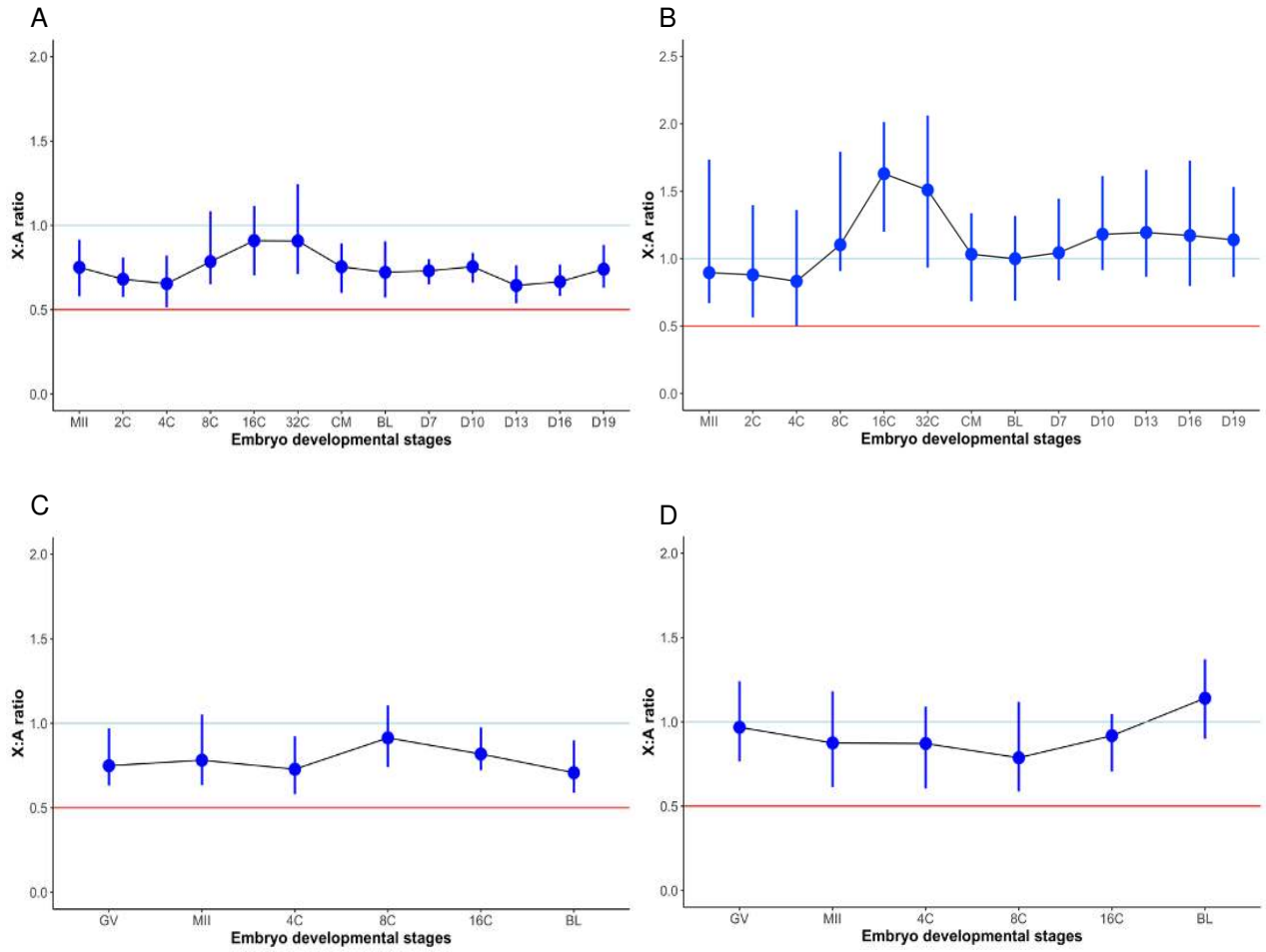

The X:A ratios were calculated using expressed (TPM > 1) genes (A, C) and ubiquitously expressed (TPM > 1 and present in all embryo datasets; B, D). GV=germinal vesicle, MII: metaphase of second meiosis, CM=compact morula, BL=blastocyst. Blue line: X:A=1, complete dosage compensation; Red line: X:A=0.5, no dosage compensation

Figure 4 Boxplot of the X:A medians for all datasets.

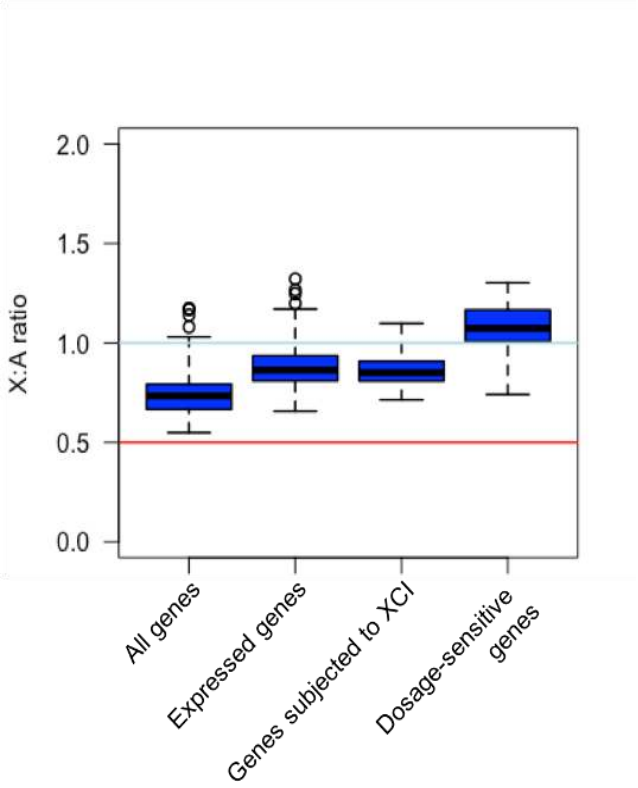

Genes were categorized in “all genes”, “expressed (TPM > 1) genes”, “genes subjected to XCI (excluding PAR genes and putative XCI-escaping genes)” and “dosage-sensitive (ubiquitously expressed) genes”. Blue line: X:A=1, complete dosage compensation; Red line: X:A=0.5, no dosage compensation

3.6. Supplementary information

Table S1. The numbers of reads after trimming and the percentages of multiple-mapped reads for each sample

Dataset and sample ID	reads after trimming	mapping rate	note
PRJNA254699			
vivo_MII_1	13,344,621	67.94%	
vivo_MII_2	18,617,919	75.05%	
vivo_2C_1	14,956,109	55.95%	
vivo_2C_2	17,338,409	59.86%	
vivo_4C_1	15,023,254	59.58%	
vivo_4C_2	17,197,154	59.64%	
vivo_8C_1	15,783,933	69.73%	
vivo_8C_2	14,502,762	71.51%	
vivo_16C_1	13,396,684	64.66%	
vivo_16C_2	10,060,614	60.97%	
vivo_32C_1	10,032,365	69.07%	
vivo_32C_2	12,974,794	69.63%	
vivo_CM_1	12,589,309	65.50%	
vivo_CM_2	15,390,895	68.73%	
vivo_BL_1	14,067,130	68.06%	
vivo_BL_2	9,150,958	64.80%	
PRJNA228235			
vitro_GV_1	12,435,200	86.06%	
vitro_GV_2	18,497,510	86.05%	
vitro_GV_3	17,285,535	89.25%	
vitro_MII_1	16,015,797	83.46%	
vitro_MII_2	22,751,494	79.96%	
vitro_MII_3	17,124,799	88.56%	
vitro_4C_1	22,296,494	88.42%	
vitro_4C_2	27,796,793	77.10%	
vitro_4C_3	10,396,440	87.35%	
vitro_8C_1	27,893,112	87.97%	
vitro_8C_2	25,488,457	83.21%	
vitro_8C_3	18,606,472	85.83%	
vitro_16C_1	19,025,171	85.27%	
vitro_16C_2	9,019,897	82.69%	
vitro_16C_3	17,900,332	88.01%	
vitro_BL_1	57,889,754	88.59%	
vitro_BL_2	34,653,160	72.19%	
vitro_BL_3	35,436,710	87.67%	
PRJNA243569			
vivo_D7_1	23,635,335	59.57%	
vivo_D7_2	24,040,750	58.01%	
vivo_D7_3	23,940,535	64.70%	
vivo_D7_4	25,478,230	14.15%	
vivo_D7_5	24,569,767	61.13%	
vivo_D7_6	22,747,482	40.04%	
vivo_D10_1	15,816,819	64.35%	

vivo_D10_2	23,320,839	17.44%	
vivo_D10_3	21,782,930	37.38%	
vivo_D10_4	25,132,063	66.69%	
vivo_D10_5	24,890,896	69.17%	
vivo_D10_6	25,740,652	41.76%	
vivo_D10_7	24,112,411	46.97%	
vivo_D13_1	23,247,754	87.40%	
vivo_D13_2	21,782,930	37.38%	
vivo_D13_3	21,779,998	79.40%	
vivo_D13_4	23,191,573	79.47%	
vivo_D13_5	21,182,412	80.76%	
vivo_D16_1	20,971,194	65.07%	
vivo_D16_2	12,156,512	80.09%	
vivo_D16_3	23,247,754	87.40%	
vivo_D16_4	21,182,412	80.76%	
vivo_D16_5	13,861,219	57.12%	
vivo_D19_1	23,643,876	90.74%	
vivo_D19_2	23,320,839	17.44%	
vivo_D19_3	23,191,573	79.47%	
vivo_D19_4	23,643,876	90.74%	
vivo_D19_5	21,779,998	79.40%	
PRJNA298914			
endometrium_1	16,651,250	82.77%	
endometrium_2	18,827,510	90.34%	
endometrium_3	13,845,319	91.11%	
endometrium_4	15,951,167	89.57%	
endometrium_5	22,393,957	93.39%	
endometrium_6	16,362,983	93.67%	
endometrium_7	17,348,883	93.21%	
endometrium_8	18,445,197	92.69%	
endometrium_9	19,283,243	93.14%	
endometrium_10	18,939,982	93.70%	
endometrium_11	20,759,413	93.37%	
endometrium_12	17,542,556	93.01%	
endometrium_13	20,884,795	91.55%	
endometrium_14	23,021,723	93.55%	
corpus luteum_1	23,265,821	94.14%	
corpus luteum_2	24,500,079	94.16%	
corpus luteum_3	17,189,314	93.58%	
corpus luteum_4	24,116,581	94.33%	
corpus luteum_5	17,455,310	94.18%	
corpus luteum_6	21,176,305	94.04%	
corpus luteum_7	17,183,335	94.33%	
corpus luteum_8	16,333,836	93.81%	
corpus luteum_9	16,040,727	94.36%	
corpus luteum_10	22,241,217	94.24%	
corpus luteum_11	15,914,273	94.02%	
corpus luteum_12	15,020,472	94.04%	
PRJNA268096			
female_brain_1	35,348,846	97.06%	

female_brain_2	53,329,221	91.48%	
female_brain_3	41,368,457	97.14%	
female_brain_4	42,597,403	97.21%	
female_liver_1	44,445,152	97.66%	
female_liver_2	63,210,755	91.46%	
female_liver_3	42,200,070	97.57%	
female_liver_4	43,889,675	97.68%	
female_muscle_1	31,582,057	97.03%	
female_muscle_2	40,896,874	91.86%	
female_muscle_3	33,407,493	97.06%	
female_muscle_4	29,430,409	97.08%	
female_kidney_1	40,922,470	96.71%	
female_kidney_2	51,224,824	96.10%	
female_kidney_3	49,478,093	96.56%	
female_kidney_4	47,980,505	96.22%	
PRJEB6377			
male_fat	36,590,829	93.08%	
male_duodenum	50,036,922	89.50%	
male_hypothalamus	26,696,424	94.86%	
male_kidney	25,051,316	83.25%	
male_liver	29,568,966	89.11%	
male_lung	22,596,488	93.81%	
male_muscle	28,739,583	80.97%	
PRJNA273164			
female_fat1	24,789,261	96.28%	
female_fat2	20,825,485	91.31%	
female_fat3	19,286,633	96.04%	
female_fat4	22,796,156	95.36%	
female_fat5	17,233,202	89.12%	
female_liver1	25,533,421	96.30%	
female_liver2	19,424,452	95.88%	
female_liver3	22,086,390	96.40%	
female_liver4	17,088,005	97.31%	
female_liver5	18,335,813	97.64%	
female_muscle1	18,338,844	95.17%	
female_muscle2	24,154,490	95.26%	
female_muscle3	19,760,958	96.66%	
female_muscle4	22,434,484	96.68%	
female_muscle5	19,985,126	96.90%	
female_pituitary1	19,748,641	94.48%	
female_pituitary2	22,093,652	94.24%	
female_pituitary3	20,713,183	94.13%	
female_pituitary4	16,399,117	95.88%	
female_pituitary5	19,140,730	95.70%	
male_fat1	15,218,534	97.14%	
male_fat2	24,642,148	90.46%	
male_fat3	15,553,433	96.55%	
male_fat4	15,996,788	96.99%	
male_fat5	22,929,105	92.65%	
male_liver1	16,491,043	97.33%	

male_liver2	12,611,921	84.10%	
male_liver3	15,841,117	97.48%	
male_liver4	31,342,847	95.63%	
male_liver5	24,835,352	96.81%	
male_muscle1	16,509,891	97.35%	
male_muscle2	26,746,481	89.31%	
male_muscle3	21,491,187	0.07%	discarded
male_muscle4	14,941,149	97.56%	
male_muscle5	18,804,572	96.32%	
male_pituitary1	15,953,420	96.22%	
male_pituitary2	26,312,948	88.73%	
male_pituitary3	17,196,868	95.81%	
male_pituitary4	30,868,150	95.64%	
male_pituitary5	19,610,395	94.78%	
average for all samples	**23,004,544**	**83.4%**	

Table S2. The numbers of lowly expressed genes (TPM≤1) on the X chromosome and autosomes in each sample

Dataset and sample ID	Total X-linked genes 959		Total autosome genes 20,316		values low to high		
	X-linked gene counts (TPM ≤ 1)	Percentage (%)	Autosome gene counts (TPM ≤ 1)	Percentage (%)	Percentage deviations (X%-A%)	X-linked genes (TPM>1)	Autosome (TPM>1)
PRJNA254699							
vivo_MII_1	598	62.4%	10,914	53.7%	8.6%	361	9,402
vivo_MII_2	657	68.5%	12,299	60.5%	8.0%	302	8,017
vivo_2C_1	571	59.5%	10,065	49.5%	10.0%	388	10,251
vivo_2C_2	557	58.1%	9,711	47.8%	10.3%	402	10,605
vivo_4C_1	520	54.2%	9,496	46.7%	7.5%	439	10,820
vivo_4C_2	551	57.5%	9,703	47.8%	9.7%	408	10,613
vivo_8C_1	589	61.4%	10,782	53.1%	8.3%	370	9,534
vivo_8C_2	586	61.1%	10,357	51.0%	10.1%	373	9,959
vivo_16C_1	521	54.3%	10,388	51.1%	3.2%	438	9,928
vivo_16C_2	527	55.0%	10,156	50.0%	5.0%	432	10,160
vivo_32C_1	567	59.1%	11,064	54.5%	4.7%	392	9,252
vivo_32C_2	554	57.8%	10,553	51.9%	5.8%	405	9,763
vivo_CM_2	596	62.1%	11,465	56.4%	5.7%	363	8,851
vivo_CM_1	622	64.9%	10,473	51.6%	13.3%	337	9,843
vivo_BL_1	630	65.7%	10,396	51.2%	14.5%	329	9,920
vivo_BL_2	616	64.2%	10,147	49.9%	14.3%	343	10,169
PRJNA228235							
vitro_GV_1	515	53.7%	8,636	42.5%	11.2%	444	11,680
vitro_GV_2	519	54.1%	8,928	43.9%	10.2%	440	11,388
vitro_GV_3	505	52.7%	8,834	43.5%	9.2%	454	11,482
vitro_MII_1	532	55.5%	9,254	45.6%	9.9%	427	11,062
vitro_MII_2	512	53.4%	9,018	44.4%	9.0%	447	11,298
vitro_MII_3	528	55.1%	9,466	46.6%	8.5%	431	10,850
vitro_4C_1	534	55.7%	9,146	45.0%	10.7%	425	11,170
vitro_4C_2	541	56.4%	9,484	46.7%	9.7%	418	10,832
vitro_4C_3	536	55.9%	9,276	45.7%	10.2%	423	11,040
vitro_8C_1	486	50.7%	8,916	43.9%	6.8%	473	11,400
vitro_8C_2	563	58.7%	10,133	49.9%	8.8%	396	10,183
vitro_8C_3	450	46.9%	8,291	40.8%	6.1%	509	12,025
vitro_16C_1	558	58.2%	10,565	52.0%	6.2%	401	9,751

vitro_16C_2	484	50.5%	9,078	44.7%	5.8%	475	11,238
vitro_16C_3	426	44.4%	8,465	41.7%	2.8%	533	11,851
vitro_BL_1	466	48.6%	9,110	44.8%	3.8%	493	11,206
vitro_BL_2	425	44.3%	8,417	41.4%	2.9%	534	11,899
vitro_BL_3	421	43.9%	8,264	40.7%	3.2%	538	12,052
PRJNA243569							
vivo_D7_1	272	28.4%	4,344	21.4%	7.0%	687	15,972
vivo_D7_2	371	38.7%	6,143	30.2%	8.4%	588	14,173
vivo_D7_3	440	45.9%	7,084	34.9%	11.0%	519	13,232
vivo_D7_4	443	46.2%	7,450	36.7%	9.5%	516	12,866
vivo_D7_5	469	48.9%	7,529	37.1%	11.8%	490	12,787
vivo_D7_6	424	44.2%	6,703	33.0%	11.2%	535	13,613
vivo_D10_1	410	42.8%	6,676	32.9%	9.9%	549	13,640
vivo_D10_2	547	57.0%	8,747	43.1%	14.0%	412	11,569
vivo_D10_3	522	54.4%	8,569	42.2%	12.3%	437	11,747
vivo_D10_4	454	47.3%	7,141	35.1%	12.2%	505	13,175
vivo_D10_5	465	48.5%	7,231	35.6%	12.9%	494	13,085
vivo_D10_6	415	43.3%	5,661	27.9%	15.4%	544	14,655
vivo_D10_7	434	45.3%	7,182	35.4%	9.9%	525	13,134
vivo_D13_1	428	44.6%	6,946	34.2%	10.4%	531	13,370
vivo_D13_2	522	54.4%	8,568	42.2%	12.3%	437	11,748
vivo_D13_3	489	51.0%	7,679	37.8%	13.2%	470	12,637
vivo_D13_4	486	50.7%	7,639	37.6%	13.1%	473	12,677
vivo_D13_5	351	36.6%	4,431	21.8%	14.8%	608	15,885
vivo_D16_1	367	38.3%	5,333	26.3%	12.0%	592	14,983
vivo_D16_2	409	42.6%	6,451	31.8%	10.9%	550	13,865
vivo_D16_3	428	44.6%	6,947	34.2%	10.4%	531	13,369
vivo_D16_4	350	36.5%	4,435	21.8%	14.7%	609	15,881
vivo_D16_5	352	36.7%	5,533	27.2%	9.5%	607	14,783
vivo_D19_1	527	55.0%	8,673	42.7%	12.3%	432	11,643
vivo_D19_2	547	57.0%	8,744	43.0%	14.0%	412	11,572
vivo_D19_3	486	50.7%	7,638	37.6%	13.1%	473	12,678
vivo_D19_4	527	55.0%	8,674	42.7%	12.3%	432	11,642
vivo_D19_5	489	51.0%	7,679	37.8%	13.2%	470	12,637
PRJNA298914							
endometrium_1	487	50.8%	7,262	35.7%	15.0%	472	13,054

endometrium_2	480	50.1%	7,302	35.9%	14.1%	479	13,014
endometrium_3	486	50.7%	7,229	35.6%	15.1%	473	13,087
endometrium_4	482	50.3%	7,191	35.4%	14.9%	477	13,125
endometrium_5	472	49.2%	7,273	35.8%	13.4%	487	13,043
endometrium_6	481	50.2%	7,228	35.6%	14.6%	478	13,088
endometrium_7	474	49.4%	7,213	35.5%	13.9%	485	13,103
endometrium_8	470	49.0%	7,075	34.8%	14.2%	489	13,241
endometrium_9	483	50.4%	7,131	35.1%	15.3%	476	13,185
endometrium_10	484	50.5%	7,414	36.5%	14.0%	475	12,902
endometrium_11	479	49.9%	7,262	35.7%	14.2%	480	13,054
endometrium_12	472	49.2%	7,257	35.7%	13.5%	487	13,059
endometrium_13	498	51.9%	7,430	36.6%	15.4%	461	12,886
endometrium_14	488	50.9%	7,333	36.1%	14.8%	471	12,983
corpus luteum_1	460	48.0%	7,584	37.3%	10.6%	499	12,732
corpus luteum_2	470	49.0%	7,471	36.8%	12.2%	489	12,845
corpus luteum_3	509	53.1%	7,964	39.2%	13.9%	450	12,352
corpus luteum_4	468	48.8%	7,694	37.9%	10.9%	491	12,622
corpus luteum_5	470	49.0%	7,556	37.2%	11.8%	489	12,760
corpus luteum_6	491	51.2%	8,195	40.3%	10.9%	468	12,121
corpus luteum_7	504	52.6%	8,173	40.2%	12.3%	455	12,143
corpus luteum_8	487	50.8%	8,114	39.9%	10.8%	472	12,202
corpus luteum_9	506	52.8%	8,290	40.8%	12.0%	453	12,026
corpus luteum_10	499	52.0%	8,220	40.5%	11.6%	460	12,096
corpus luteum_11	510	53.2%	8,228	40.5%	12.7%	449	12,088
corpus luteum_12	496	51.7%	8,014	39.4%	12.3%	463	12,302
PRJNA268096							
female_brain_1	370	38.6%	5,977	29.4%	9.2%	589	14,339
female_brain_2	370	38.6%	5,830	28.7%	9.9%	589	14,486
female_brain_3	407	42.4%	6,711	33.0%	9.4%	552	13,605
female_brain_4	392	40.9%	6,332	31.2%	9.7%	567	13,984
female_liver_1	523	54.5%	8,155	40.1%	14.4%	436	12,161
female_liver_2	518	54.0%	7,897	38.9%	15.1%	441	12,419
female_liver_3	522	54.4%	8,159	40.2%	14.3%	437	12,157
female_liver_4	526	54.8%	8,238	40.5%	14.3%	433	12,078
female_muscle_1	431	44.9%	7,488	36.9%	8.1%	528	12,828
female_muscle_2	399	41.6%	6,890	33.9%	7.7%	560	13,426

female_muscle_3	427	44.5%	7,457	36.7%	7.8%	532	12,859
female_muscle_4	420	43.8%	7,293	35.9%	7.9%	539	13,023
female_kidney_1	395	41.2%	6,295	31.0%	10.2%	564	14,021
female_kidney_2	400	41.7%	6,410	31.6%	10.2%	559	13,906
female_kidney_3	415	43.3%	6,505	32.0%	11.3%	544	13,811
female_kidney_4	407	42.4%	6,504	32.0%	10.4%	552	13,812
PRJEB6377							
male_fat	450	46.9%	6,799	33.5%	13.5%	509	13,517
male_duodenum	582	60.7%	9,611	47.3%	13.4%	377	10,705
male_hypothalamus	374	39.0%	5,970	29.4%	9.6%	585	14,346
male_kidney	485	50.6%	7,113	35.0%	15.6%	474	13,203
male_lung	456	47.5%	6,494	32.0%	15.6%	503	13,822
male_muscle	525	54.7%	7,783	38.3%	16.4%	434	12,533
male_liver	556	58.0%	8,711	42.9%	15.1%	403	11,605
PRJNA273164							
female_fat1	472	49.2%	7,144	35.2%	14.1%	487	13,172
female_fat2	535	55.8%	7,925	39.0%	16.8%	424	12,391
female_fat3	537	56.0%	8,176	40.2%	15.8%	422	12,140
female_fat4	514	53.6%	7,534	37.1%	16.5%	445	12,782
female_fat5	479	49.9%	7,536	37.1%	12.9%	480	12,780
female_liver1	522	54.4%	7,794	38.4%	16.1%	437	12,522
female_liver2	520	54.2%	7,730	38.0%	16.2%	439	12,586
female_liver3	529	55.2%	8,179	40.3%	14.9%	430	12,137
female_liver4	567	59.1%	8,846	43.5%	15.6%	392	11,470
female_liver5	589	61.4%	9,414	46.3%	15.1%	370	10,902
female_muscle1	517	53.9%	8,377	41.2%	12.7%	442	11,939
female_muscle2	521	54.3%	8,120	40.0%	14.4%	438	12,196
female_muscle3	518	54.0%	8,513	41.9%	12.1%	441	11,803
female_muscle4	561	58.5%	9,069	44.6%	13.9%	398	11,247
female_muscle5	549	57.2%	8,984	44.2%	13.0%	410	11,332
female_pituitary1	422	44.0%	6,582	32.4%	11.6%	537	13,734
female_pituitary2	436	45.5%	6,809	33.5%	11.9%	523	13,507
female_pituitary3	425	44.3%	6,859	33.8%	10.6%	534	13,457
female_pituitary4	464	48.4%	7,439	36.6%	11.8%	495	12,877
female_pituitary5	467	48.7%	7,437	36.6%	12.1%	492	12,879
male_fat1	521	54.3%	8,104	39.9%	14.4%	438	12,212

male_fat2	508	53.0%	7,893	38.9%	14.1%	451	12,423
male_fat3	501	52.2%	7,902	38.9%	13.3%	458	12,414
male_fat4	495	51.6%	7,820	38.5%	13.1%	464	12,496
male_fat5	591	61.6%	9,473	46.6%	15.0%	368	10,843
male_liver1	562	58.6%	8,964	44.1%	14.5%	397	11,352
male_liver2	534	55.7%	8,378	41.2%	14.4%	425	11,938
male_liver3	574	59.9%	9,322	45.9%	14.0%	385	10,994
male_liver4	540	56.3%	8,250	40.6%	15.7%	419	12,066
male_liver5	548	57.1%	8,508	41.9%	15.3%	411	11,808
male_muscle1	550	57.4%	9,117	44.9%	12.5%	409	11,199
male_muscle2	560	58.4%	9,249	45.5%	12.9%	399	11,067
male_muscle4	536	55.9%	8,727	43.0%	12.9%	423	11,589
male_muscle5	542	56.5%	8,819	43.4%	13.1%	417	11,497
male_pituitary1	456	47.5%	7,382	36.3%	11.2%	503	12,934
male_pituitary2	447	46.6%	7,182	35.4%	11.3%	512	13,134
male_pituitary3	466	48.6%	7,574	37.3%	11.3%	493	12,742
male_pituitary4	477	49.7%	7,697	37.9%	11.9%	482	12,619
male_pituitary5	414	43.2%	6,364	31.3%	11.8%	545	13,952
PRJNA229443							
contl_placenta	512	53.4%	7,761	38.2%	15.2%	447	12,555
scnt_placenta	548	57.1%	8,546	42.1%	15.1%	411	11,770

Table S3. TPM distribution of X and autosomes expression difference in each sample

Sample	Expressed genes *P*-value	Ubiquitously expressed genes *P*-value
PRJNA254699		
00C_vivo	0.035	0.48
2C_vivo	8.53E-06	0.012
4C_vivo	6.31E-05	0.044
8C_vivo	0.18	0.25
16C_vivo	0.74	0.0076
32C_vivo	0.63	0.10
CM_vivo	0.029	0.98
BL_vivo	0.0028	0.68
PRJNA228235		
GOC_vitro	0.063	0.94
MOC_vitro	0.094	0.36
4C_vitro	0.03	0.26
8C_vitro	0.0064	0.36
16C_vitro	0.079	0.16
BL_vitro	0.0029	0.19
PRJNA243569		
D7_vivo	0	0.61
D10_vivo	2.60E-07	0.16
D13_vivo	1.00E-07	0.20
D16_vivo	6.00E-07	0.26
D19_vivo	0.00026	0.15
PRJNA298914		
CL	7.95E-05	0.25
EM	5.50E-07	0.88
PRJNA268096		
female_brain	0.0017	0.021
female_kidney	8.35E-05	0.04
female_liver	0.43	0.16
female_muscle	2.84E-06	0.10
PRJEB6377		
male_adipose	6.46E-05	0.52
male_duodenum	0.05	0.91
male_hypothalamus	0.052	0.018
male_kidney	0.00048	0.40
male_lung	8.68E-06	0.16
male_liver	0	0
male_muscle	0	0
PRJNA273164		
female_fat	6.54E-06	0.29
female_liver	0.19	0.25
female_muscle	1.18E-05	0.19
female_pituitary	0.04	0.0039
male_fat	2.56E-05	0.25
male_liver	0.11	0.56
male_muscle	2.00E-05	0.33
male_pituitary	0.0067	0.0069

green highlighed P-value greater than 0.05 for no significant difference between X and autosomes

Table S4. TPM distribution of X chromosome difference of common tissues between males and females

Common tissue type	*P*-value
Brain	0.55
Fat	0.15
Kidney	0.32
Liver	0.32
Muscle	0.044
Pituitary	0.18

Table S5.1. X-linked genes in PAR

PPP2R3B
SLC25A6
IL3RA
CSF2RA
ASMTL
CRLF2
PRKX
MXRA5
ARSH
ARSE
GYG2
CD99
ZBED1
GPR143
TBL1X
ANOS1
PNPLA4
NLGN4
ARSD
ARSF

Table S5.2. Candidate XCI escapee genes

ARR3
ASB11
ATP2B3
CA5B
CD99
CHM
CNKSR2
CYBB
DDX3Y
DGAT2L6
DMD
DRP2
EBP
EIF1AY
EIF2S3
FIGF
GATA1
GPC3
GRPR
HMGB3
IL13RA2
KDM6A
LOC513911
MAGEH1
MAOB
MED12
MIR3431
MOSPD1
NLGN3
OFD1Y
PHEX
PORCN
PRR32
PSMD10
RAB39B
RBM3
RENBP
SH3KBP1
SLC6A14
SMARCA1
SRPX
SUV39H1
TBL1X
TENM1
TLR7
TLR8
USP27X
USP9Y
VSIG4
XIAP
XIST
XPNPEP2
ZCCHC12
ZFX
ZMYM3

Figure S1. Correlation plots and unsupervised hierarchical clustering of RNA-seq datasets for somatic (A) and embryo tissues (B).

A

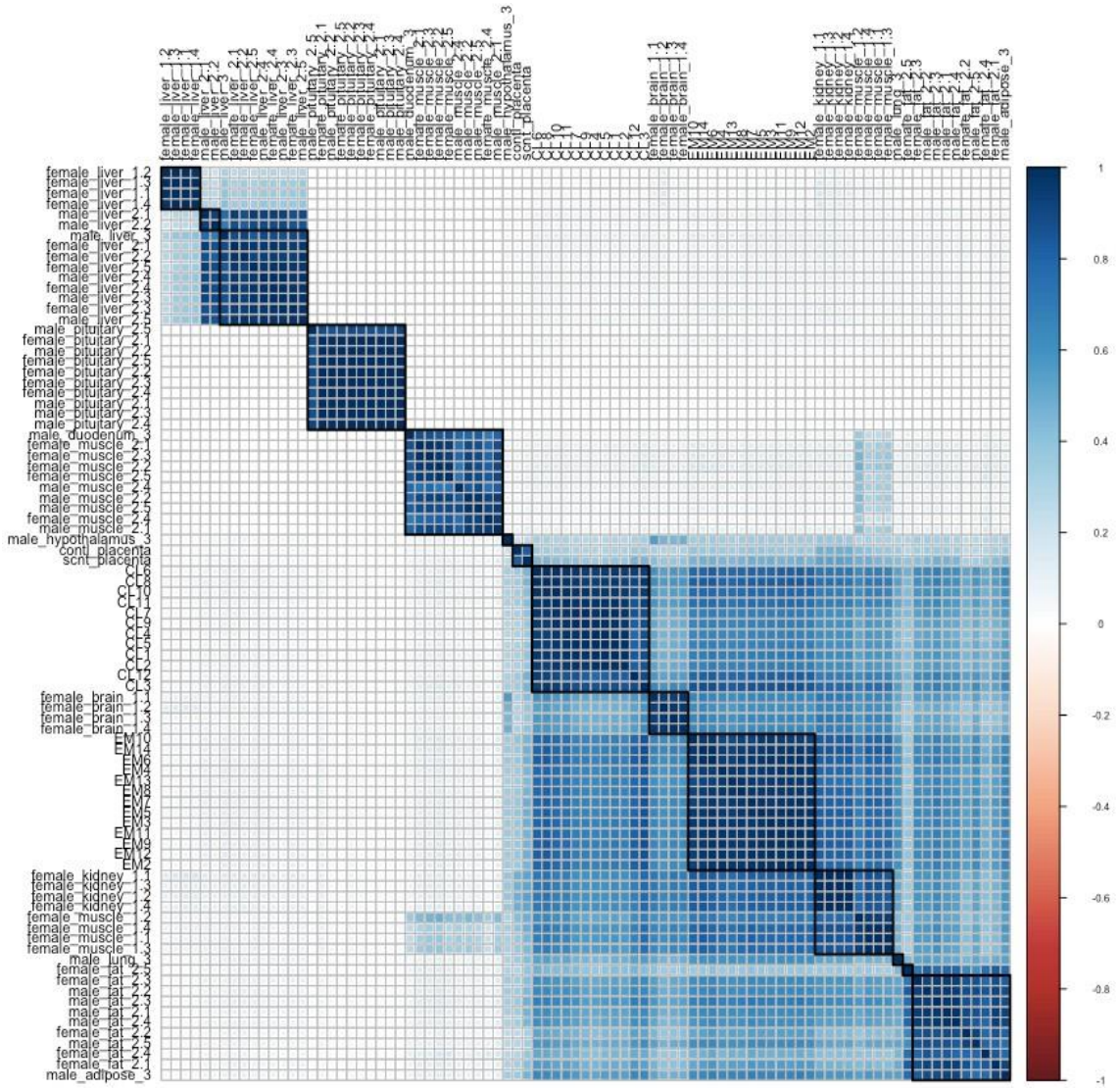

A

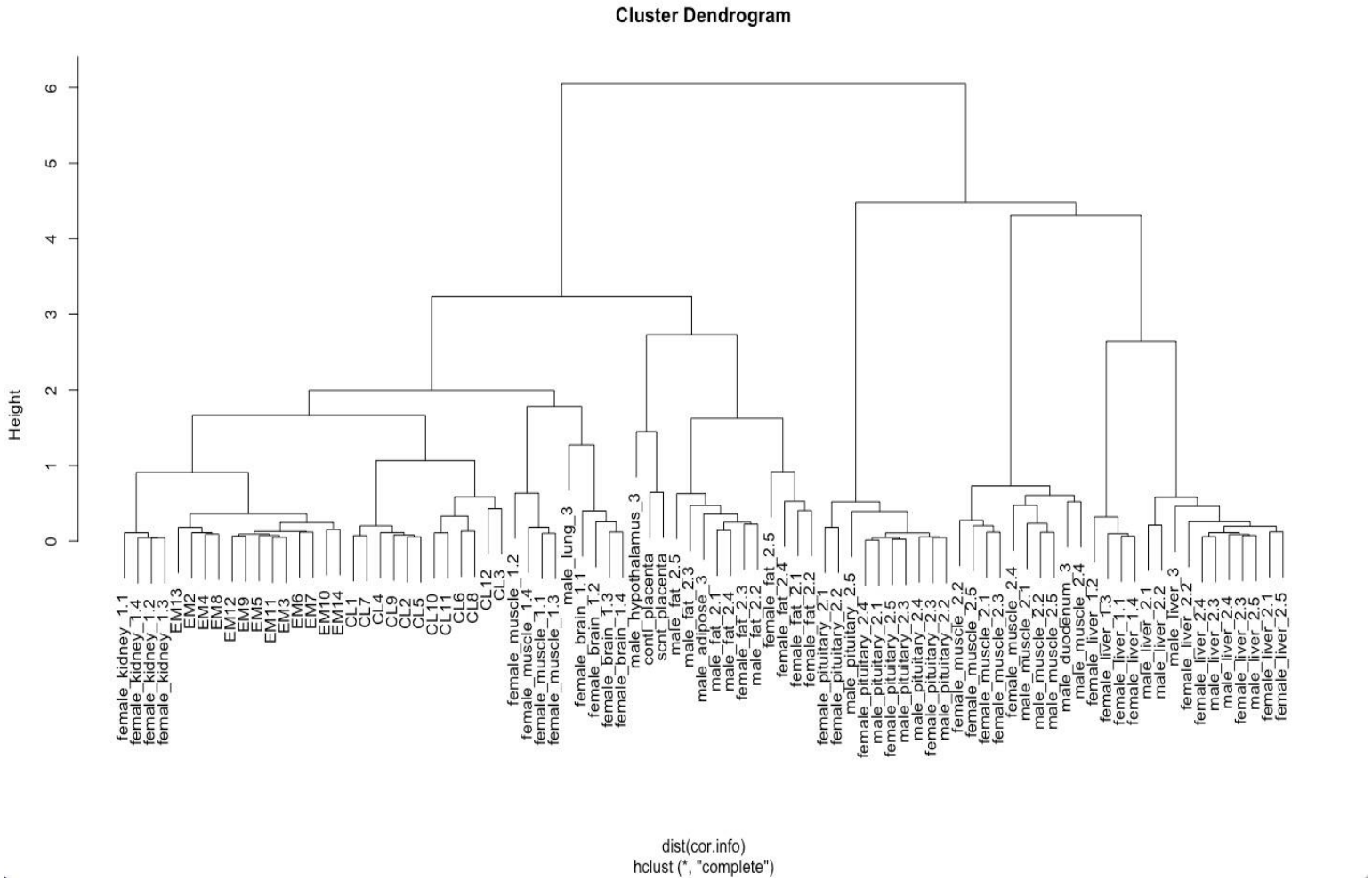

The color spectrum in correlation plots ranges from blue to red, indicating high to low correlations between sample replicates. Hierarchical Clustering was conducted with all genes. EM= endometrium, CL=corpus luteum, GV=germinal vesicle, MII= metaphase of second meiosis, CM=compact morula, BL=blastocyst

B

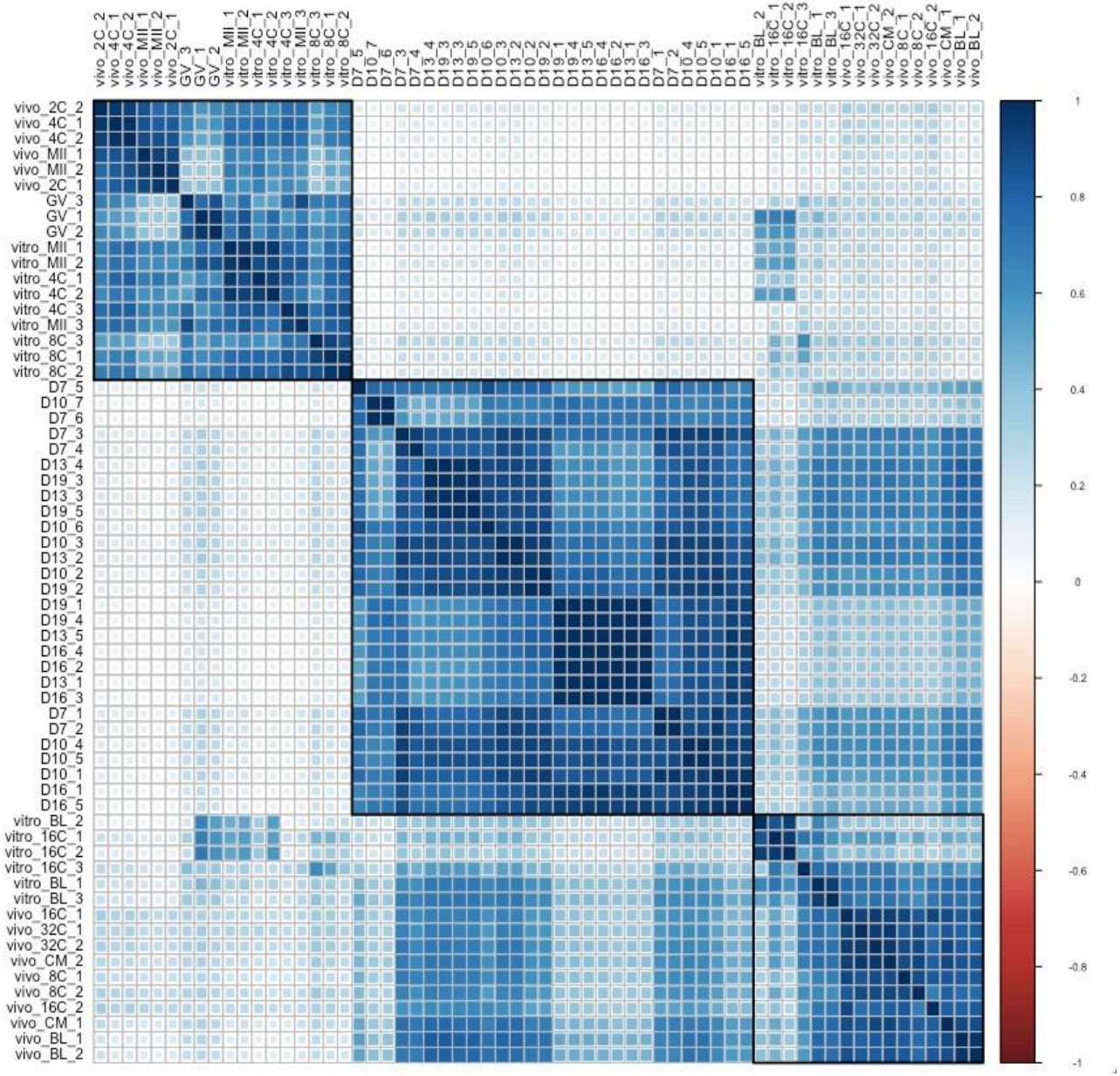
vivo_2C_2
vivo_4C_1
vivo_4C_2
vivo_MII_1
vivo_MII_2
vivo_2C_1
GV_3
GV_1
GV_2
vitro_MII_1
vitro_MII_2
vitro_4C_1
vitro_4C_2
vitro_4C_3
vitro_MII_3
vitro_8C_3
vitro_8C_1
vitro_8C_2
D7_5
D10_7
D7_6
D7_3
D7_4
D13_4
D19_3
D13_3
D19_5
D10_6
D10_3
D13_2
D10_2
D19_2
D19_1
D19_4
D13_5
D16_4
D16_2
D13_1
D16_3
D7_1
D7_2
D10_4
D10_5
D10_1
D16_1
D16_5
vitro_BL_2
vitro_16C_1
vitro_16C_2
vitro_16C_3
vitro_BL_1
vitro_BL_3
vivo_16C_1
vivo_32C_1
vivo_32C_2
vivo_CM_2
vivo_8C_1
vivo_8C_2
vivo_16C_2
vivo_CM_1
vivo_BL_1
vivo_BL_2
1
0.8
0.6
0.4
0.2
0
-0.2
-0.4
-0.6
-0.8
-1

B

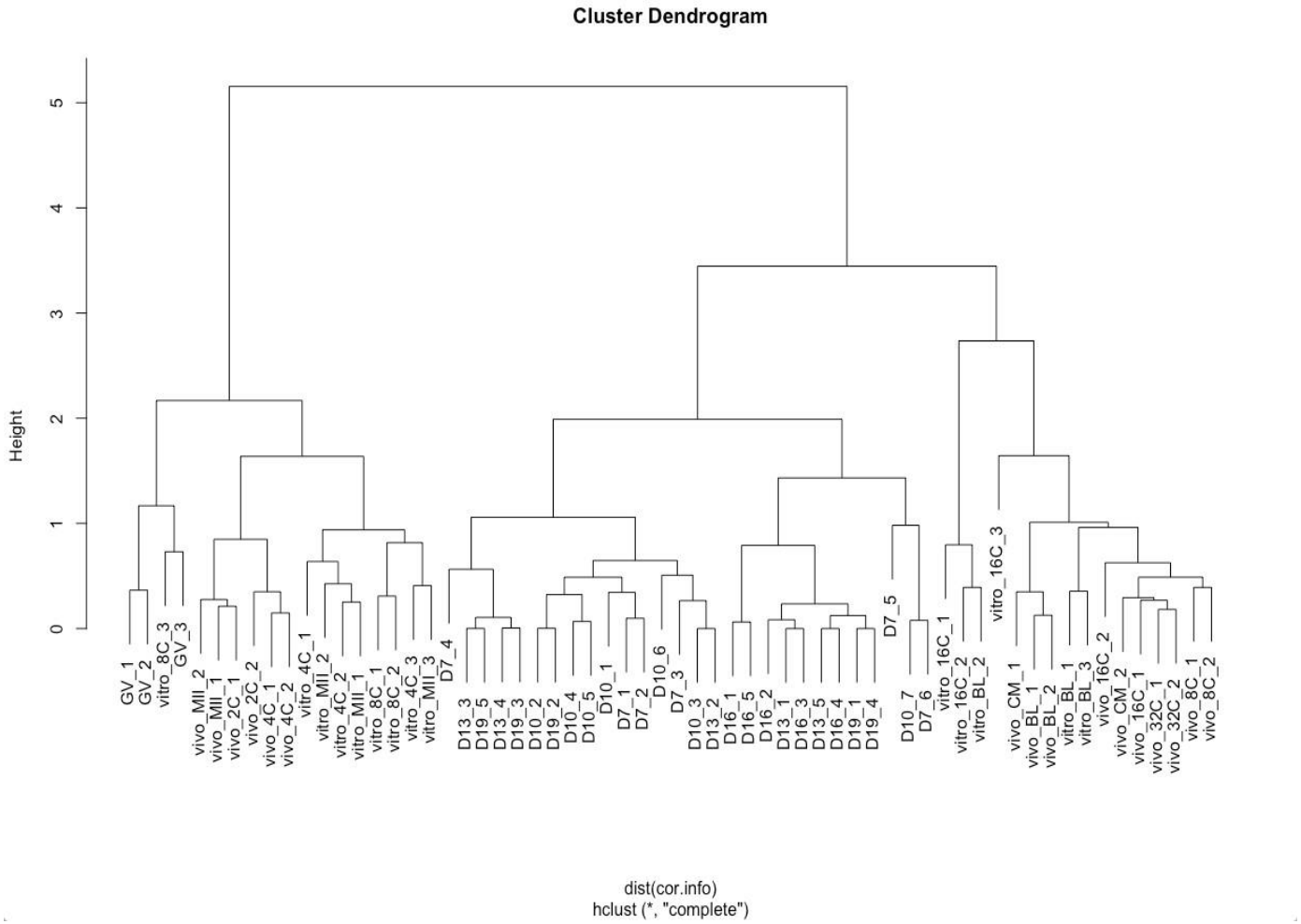

The color spectrum in correlation plots ranges from blue to red, indicating high to low correlations between sample replicates. Hierarchical Clustering was conducted with all genes. EM= endometrium, CL=corpus luteum, GV=germinal vesicle, MII= metaphase of second meiosis, CM=compact morula, BL=blastocyst

Figure S2. Gene ontology enrichment analysis of ubiquitously expressed genes in somatic tissue datasets

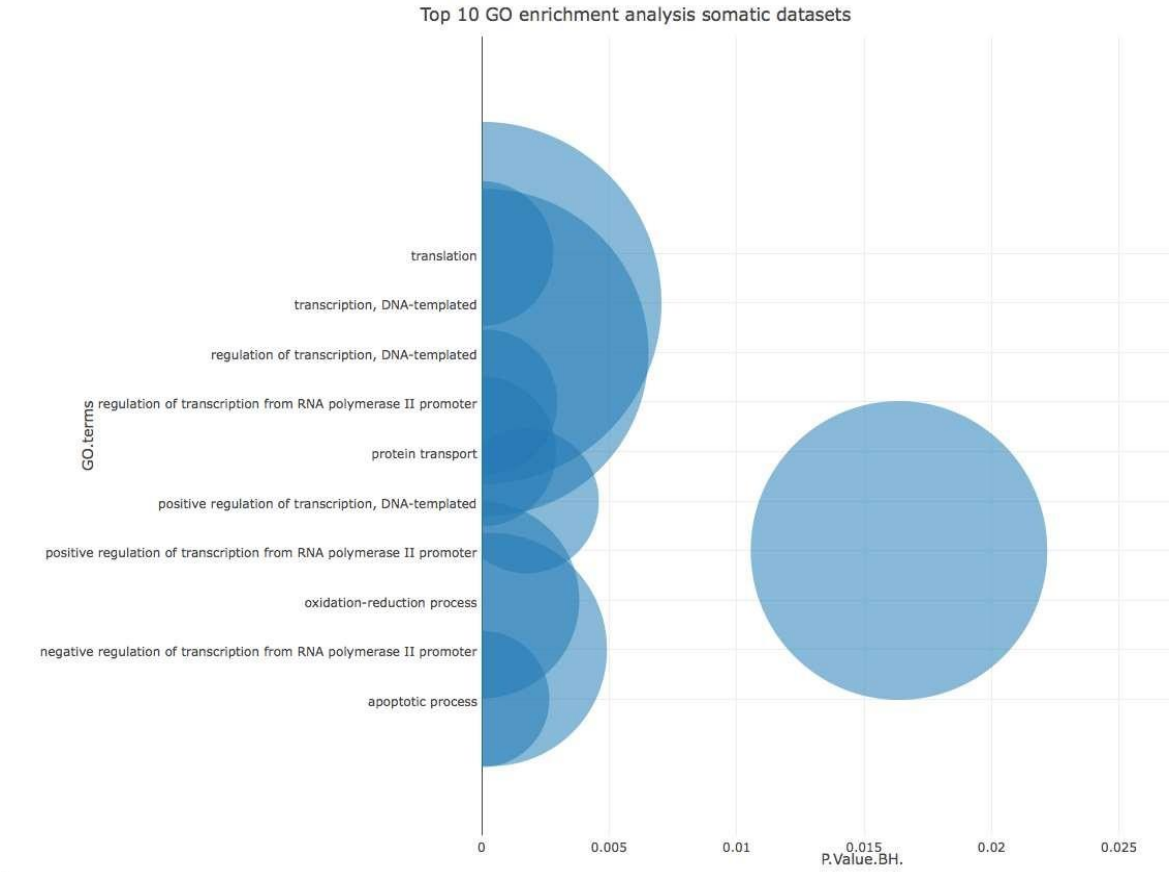

(A) GO analysis of 245 genes on X chromosomes and 7,603 genes on autosomes as ubiquitous in the somatic tissue datasets. Plotted are top ten biological processes with their p-values (X-axis)

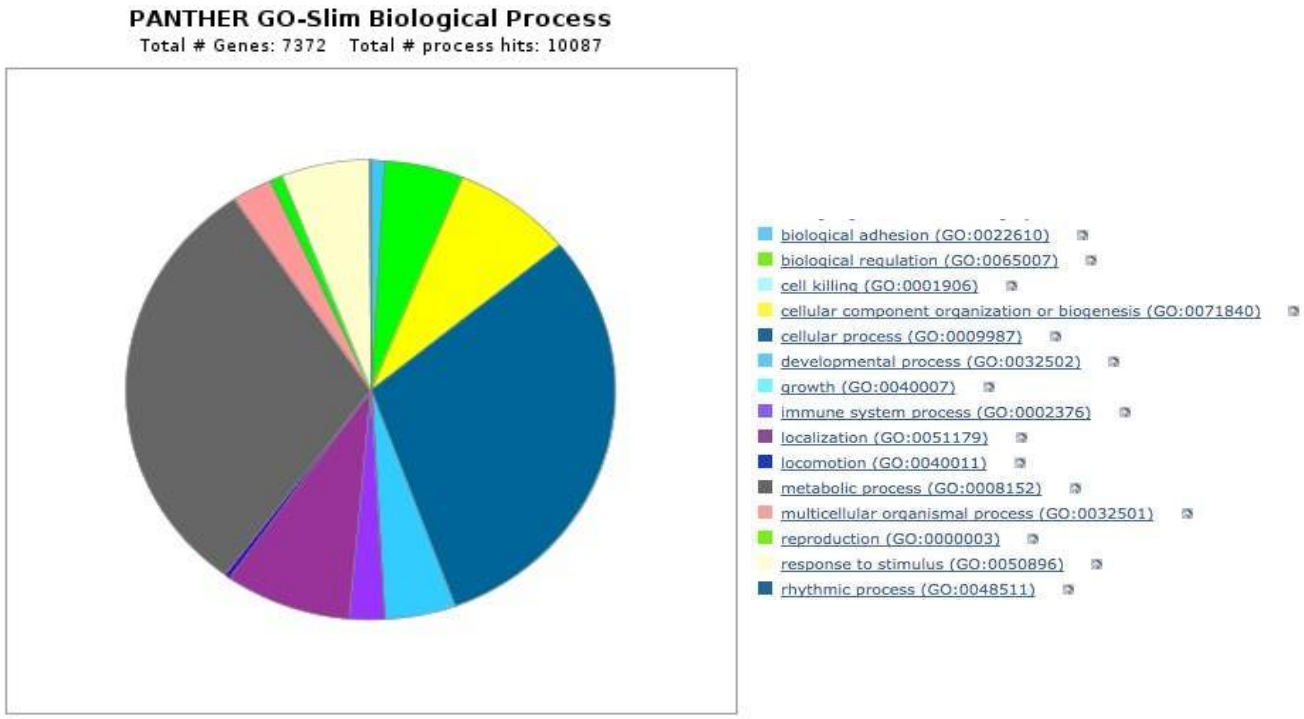

(B): Pie chart for biological process was generated in The Gene Ontology Consortium

Figure S3. Gene ontology enrichment analysis of ubiquitously expressed genes in embryo datasets

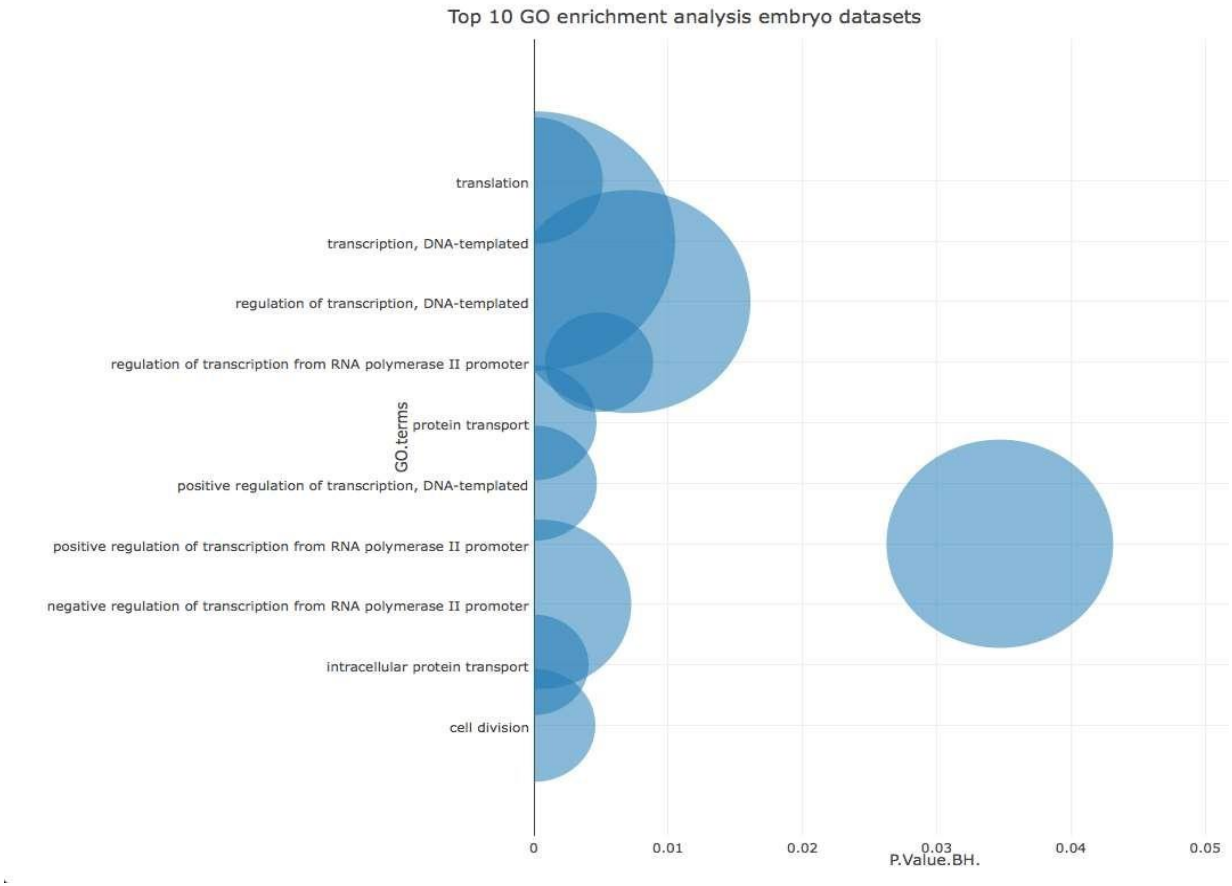

(A) GO analysis of the 117 genes on X chromosome and 3,947 genes on autosomes as ubiquitous in the embryo datasets. Plotted are top ten biological processes with their p-values (X-axis)

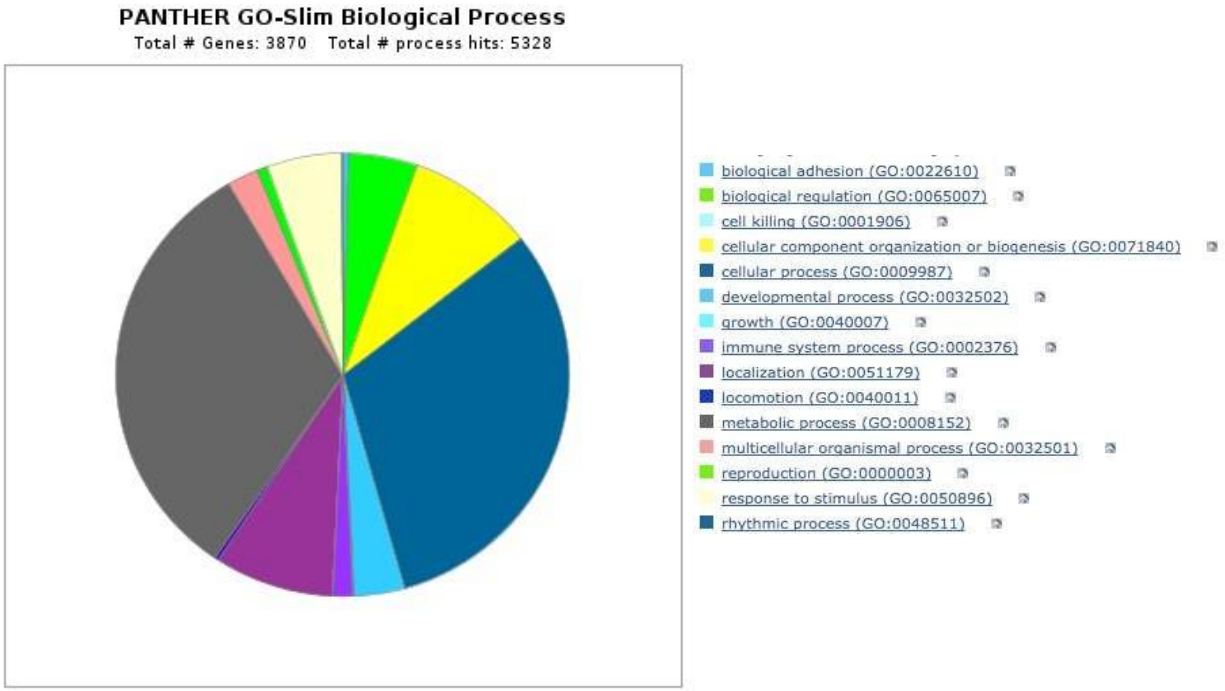

(B) Pie chart for biological process was generated in The Gene Ontology Consortium

Figure S4. Common ubiquitously expressed genes between somatics and embryonic tissues

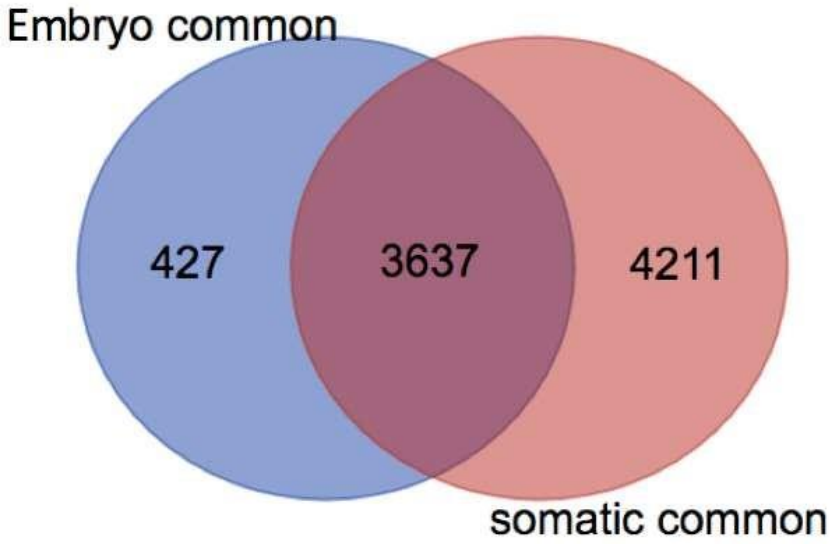

Chapter Four

Methylome Dynamics of Bovine Gametes and *In Vivo* Early Embryos

Duan J.E., Jiang Z., Alqahtani F., Mandoiu I., Dong H., Zheng X., Marjani S.L., Chen J. & Tian X.C.

4.1. Abstract

Dynamic changes in DNA methylation are crucial in the process of early mammalian embryogenesis. Global DNA methylation studies in the bovine, however, remain mostly at the immunostaining level. We adopted the single-cell whole genome bisulfite sequencing (scWGBS) method to characterize stage-specific genome-wide DNA methylation in bovine sperm, immature oocytes, oocytes matured *in vivo* and *in vitro*, as well as *in vivo* developed embryos at the 2-, 4-, 8- and 16-cell stages. We found that the major wave of genome-wide DNA demethylation was complete by the 8-cell stage when *de novo* methylation became prominent. Sperm and oocytes were differentially methylated in numerous regions (DMRs), largely intergenic, suggesting that these noncoding regions may play important roles in gamete specification. DMRs were also identified between *in vivo* and *in vitro* matured oocytes, demonstrating environmental effects on epigenetic modifications. Moreover, virtually no (less than 1.5%) DNA methylation was found in mitochondrial DNA. Finally, by using RNA-seq data generated from embryos at the same developmental stages, we revealed a weak inverse correlation between gene expression and promoter methylation. These data provide insights into the critical features of the methylome of bovine embryos, and serve as an important reference for embryos produced by assisted reproduction, such as *in vitro* fertilization and cloning, and a model for the epigenetic dynamics that occur in human early embryos.

Keywords: DNA methylation; Gametes, Single early embryo; WGBS; Bovine

4.2. Introduction

Cytosine methylation plays essential roles in mammalian development, including transposon silencing, cell differentiation, genomic imprinting, and X chromosome inactivation (Hackett and Surani, 2013). DNA methylation is relatively stable in differentiated somatic cells, but highly dynamic during primordial germ cell development and pre-implantation embryogenesis (Saadeh and Schulz, 2014). Embryonic DNA methylation reprogramming requires genome-wide DNA demethylation, which erases the epigenetic marks of the parental genomes, as well as rapid *de novo* methylation to establish the epigenetic state of the early embryo (Seisenberger et al., 2012). With the recent advancement of the methylation high-throughput sequencing technology, many methylome studies have been conducted on mammalian pre-implantation embryos (Gao et al., 2017; Guo et al., 2014; Jiang et al., 2018; Smith et al., 2012; Zhu et al., 2018). In the mouse, reduced representation bisulfite sequencing (RRBS) revealed rapid genome-wide demethylation in zygotes (Smith et al., 2012). In primates (Guo et al., 2014; Gao et al., 2017; Zhu et al., 2018), however, this major demethylation event did not occur until the 2-cell stage. Contrary to observations generated by immunostaining, which showed the highest DNA methylation in mouse blastocysts (Dean et al., 2001), the lowest DNA methylation levels were found at the blastocyst stage, despite that fact that *de novo* methylation had been initiated earlier than this stage (Smith et al., 2012).

In bovine embryos, many studies have been conducted on the global methylation dynamics by immunostaining of 5mC (Dean et al., 2001; Beaujean et al., 2004; Park et al., 2007) and one by DNA methylation array with a finite numbers of probes (Salilew-Wondim et al., 2015). While immunostaining provides important overall methylation dynamics, it does not provide specific sequence information of the methylated/de-methylated regions. We were the

first to report methylome dynamics at the single-base resolution in bovine *in vivo* pre-implantation embryos using RRBS (Jiang et al., 2018). However, RRBS preferentially selects CpG-rich regions, such as CpG islands, while CpG shores are usually under-represented (Doherty and Couldrey, 2014). These shore regions are known to play important roles in tissue differentiation (Doi et al., 2009). Recently, the development of single-cell whole genome bisulfite sequencing (scWGBS-seq) allowed for the reliable and affordable revelation of all potentially CpG sites in a single oocyte or embryo (Smallwood et al., 2014).

Cattle are one of the most economically valuable livestock species (Woolliams, 1996), and we have found that bovine embryos share more similarities with humans than mice in gene expression profiles and developmental timing (Jiang et al., 2014). The understanding of the methylome dynamics during bovine *in vivo* pre-implantation embryogenesis will provide the gold standard reference that can lead to improvements in assisted reproductive technologies and provide evolutionary insights across species. Importantly, bovine embryos serve as a great model for understanding human development where *in vivo* embryos are not available for research studies.

4.3. Methods

4.3.1. Collection of bovine single gametes and embryos

Frozen bovine sperm from a Holstein bull with proven fertility were thawed and washed using PureCeption gradient solution to remove somatic cell contaminations. After serial dilutions, three aliquots of approximately 20 sperm each were snap frozen and stored at -80°C until library preparation.

Ovarian stimulation and oocyte retrieval from Holsten cows (n=10) was performed as previously described (Hayakawa et al., 2009; Jiang et al., 2014, 2018). Briefly, superovulation was achieved using five doses of intramuscular injections of FSH beginning five days after insertion of a Controlled Intra-vaginal Drug Release (CIDR) device. Two doses of prostaglandin F2 alpha were given along with the last two FSH treatments, followed by CIDR removal. Standing estrus (Day 0) was seen approximately 48h post-prostaglandin injection. GnRH was then administered at estrus exhibition. Each cow was inseminated 12- and 24-hours post-standing heat. Donor cows were sacrificed at 30 hours and 2-4 days after estrus to collect *in vivo* matured oocytes and 2- to 16-cell embryos by oviductal flushing, respectively. Cumulus-oocyte complexes were collected from slaughterhouse ovaries for GV oocytes. BO-IVM medium (IVF Bioscience) was used for oocyte *in vitro* maturation. This was conducted in four-well dishes for 24 hours at 38.5 °C with 5% CO_2. The stage of oocytes and embryos was then examined under light microscopy and only Grade 1 embryos by standards of the International Embryo Technology Society were selected for further study.

All single oocytes and embryos were washed with D-PBS containing 1 mg/ml polyvinylpyrrolidone (PBS-PVP) and transferred into 50 µl droplets of 0.1% protease to remove the zona pellucida. Single oocytes and embryos were rinsed three times in PBS-PVP, and the

absence of contaminating cells was confirmed, they then were snap frozen with minimal medium and stored at -80°C until library preparation.

4.3.2. Preparation of WBGS libraries

We obtained pools of 20 sperm (n=3), single germinal vesicle (GV) oocytes (n=4), single *in vivo* matured oocytes (n=6), single *in vitro* matured oocytes (n=6) and single embryos at the 2-cell (n=4), 4-cell (n=5), 8-cell (n=4) and 16-cell (n=3) stages (**Table S1)**. We followed the protocol of single-cell WGBS library preparation by Smallwood et al. (2014) to prepare the single oocyte/embryo WGBS libraries. Briefly, sperm cells or a single oocyte/embryo were seeded into lysis buffer with 20 mg/ml of protease and 10% Trition-X 100. Genomic DNA was released after incubation at 50 °C for 3 hours, followed by 75 °C for 30 minutes to inactivate the protease. Bisulfite treatment to convert unmethylated cytosines to uracils was conducted by using the MethylCode Bisulfite Conversion Kit (Thermo Fisher). The synthesis of complementary strands was repeated five times with Biotinylated random primer Bio-P5-N9 (Biotin-CTACACGACGCTCTTCCGATCTNNNNNNNNN). This allowed for the maximizing of the tagged DNA strands and the generation of multiple copies of each fragment. The second strands were synthesized using another random primer, P7-N9 (AGACGTGTGCTCTTCCGATCTNNNNNNNNN). Final libraries were prepared after 12 cycles of PCR amplification using Illunima Universal PCR primer and indexed primer (NEBNext Multiplex Oligos for Illumina, New England BioLabs). Agencourt Ampure beads were used to purify the amplified libraries. The quality and quantity of the libraries were determined using high-sensitivity DNA chips on the Agilent Bioanalyzer, and KAPA Library Quantification Kits (KAPA Biosystems). Single-cell indexed libraries were pooled and sequenced on Illumina HiSeq4000 platform with 150 bp paired-end reads. The raw FASTQ files

are available at Gene Expression Omnibus (GEO) (www.ncbi.nlm.nih.gov/geo) under accession number GSE121758.

4.3.3. Reads filtering and mapping

After the sequencing adapters were removed by TrimGalore-0.4.3 (Krueger, 2017) using the parameters of quality score higher than 20 and length greater than 36, reads that contained a total number of 15 Ns were removed. FastQC (Andrews, 2010) was used to assess the read quality. Further, 12 bp low quality reads at the 5' end of both pairs were also removed. Trimmed sequences were mapped to the bovine genome UMD3.1.1 using Bismark - v.0.18.1(Krueger and Andrews, 2011), with parameters: --non_directional, --score_min L,0,-0.6, --un. This resulted in 11.8 million reads uniquely mapped with a mapping efficiency of 9.3% (**Table S1**). This is higher than the average mapping efficiency (1.4%) of mouse single oocytes subjected to the same protocol (Smallwood et al., 2014). After mapping, we removed duplicates and non-converted reads using deduplicate_bismark and filter_non_conversion, respectively (Krueger and Andrews, 2011). There were on average 4 million reads per sample for downstream analysis (**Table S1**).

4.3.4. Quantification of methylation level and CpG density

Using Bismark Methylation Extractor (Krueger and Andrews, 2011), methylation coverage for every single C was extracted and read coverage files were generated. When calculating the methylation level of each CpG site, the read coverage files of cytosine in CpG context were used. The DNA methylation level of each CpG site was calculated using count_methylated ("C" reads) divided by sum of count_methylated and count_unmethylated ("C" + "T" or total read counts). The numbers of CpG sites with 1X, 5X or 10X total read counts of each stage were summarized in **Table S1**. The processed CpG coverage files are available in

GSE121758. Data visualization and analysis were preformed using custom R and Java scripts and SeqMonk (Andrews, 2007).

To facilitate the comparison of methylation levels across samples, we applied the consecutive genomic window method to bin the bovine genome (Zhu et al., 2018). Briefly, we first filtered out CpGs that had total read counts of less than 5. Then, we bound the genome to 300-bp tiles. Only tiles that contained greater than three CpG sites were kept. Tiles from replicate samples of the same developmental stage were combined to increase the coverage (**Figure 2A**). The numbers of captured 300-bp tiles in each stage are summarized in **Figure S1E**. We also identified the common 300-bp tiles among all samples as commonly methylated. Uniquely methylated tiles were then obtained for each sample. DNA methylation of each sample was calculated by averaging the 300-bp tiles' methylation. Moreover, we calculated the CpG density as described by Guo et al., 2014. We determined the total number of all CpG sites located within 150 bp upstream and 150 bp downstream of each CpG site. Then the CpG density of every 300-bp tile was determined as the average of all CpG sites within this 300-bp tile.

4.3.6. Pairwise comparison of methylation changes and gamete-specific DMRs

Using Bedtools (Quinlan and Hall, 2010), we identified the common 300-bp tiles between consecutive stages and between male and female gametes. We followed the previous study (Guo et al., 2014) to classify changing tiles as those with methylation differences greater than 40% and significantly different by Fisher's exact test (P-value ≤0.05, FDR ≤0.05), while the remaining tiles were defined as stable tiles. Increasing/decreasing tiles between consecutive stages were used to define DNA methylation increases or decreases. Differentially methylated regions (DMRs) were defined as common 300-bp tiles between two types of gametes/stages that had methylation levels ≥ 75% in one stage/type and ≤ 25% in another, and significantly different

by Fisher's exact test (P-value ≤0.05, FDR ≤0.05). Hyper- and hypo-methylated tiles were those with DNA methylation levels ≥ 75% and ≤ 25%, respectively.

4.3.7. Genomic feature annotation

Genomic features, including promoters (1,000 bp upstream of Transcription Start Sites; TSS), exons, introns, CpG islands (CGIs), intergenic, long interspersed nuclear elements (LINEs), short interspersed nuclear elements (SINEs), and long terminal repeats (LTRs) were downloaded from University of California, Santa Cruz (UCSC) genome browser (bovine genome UMD3.1.1).

4.3.8. Gene Ontology (GO) analysis

GO analysis of genes annotated from DMRs was performed using DAVID (https://david.ncifcrf.gov, Huang et al., 2009a, 2009b). Biological processes with a P-value ≤0.05 were determined to be statistically significant.

4.3.9. Gene expression analysis

We downloaded RNA-seq data of bovine sperm (Lesch et al., 2016), GV oocytes, *in vitro* matured oocytes (Graf et al., 2014), and *in vivo* matured oocytes and embryos (Jiang et al., 2014). Raw reads were trimmed by Trimmomatic (Bolger et al., 2014) and aligned to bovine reference genome assembly UMD3.1.1 using Hisat2 version 2.0.5 aligner (Pertea et al., 2016). IsoEM version 1.1.5 (Nicolae et al., 2011) was used to quantify gene expression to fragment per kilobase million (FPKM) using default parameters. Transcripts that annotated to LINEs, SINEs, and LTRs were determined by Bedtools (Quinlan and Hall, 2010). Spearman correlation coefficients between log2 transformed gene expression levels and DNA methylation levels of promoter, gene body, exon, intron, CGIs, LINEs, SINEs, and LTRs were calculated and plotted

in R (R Core Team, 2014).

4.4. Results and Discussion

4.4.1. Profiles of the WGBS libraries of bovine gametes and embryos

Using scWGBS, we analyzed a total of 35 samples of sperm, GV, *in vivo* and *in vitro* matured oocytes and cleavage stage *in vivo* developed embryos. The bisulfite conversion efficiency was more than 97% in each sample (**Table S1**). Pearson correlations indicated higher reproducibility within stages than between stages (**Figure S1A**). Captured CpGs broadly spread across each chromosome (**Figure S1B-C**). Two distinct profiles of methylation were observed: 1) highly methylated sperm and 2) lowly methylated oocytes and embryos (**Figure S1C**). However, virtually no (less than 1.5%) DNA methylation was found in mitochondrial DNA (**Figure S1B-C**); this is in agreement with findings in humans (Hong et al., 2013; Liu et al., 2016) and mice (Mechta et al., 2017).

In single oocytes and embryos, an average of 9 million reads uniquely mapped to the bovine genome assembly, UMD3.1.1, with an averaged 9.3% mapping rate (**Table S1**). This is higher than the average mapping efficiency (1.4%) of mouse single oocytes subjected to the same protocol (Smallwood et al., 2014). After removing duplicated and non-bisulfite converted reads, an average of 4 million reads per sample remained for downstream analysis (**Table S1**). We obtained an average of 1.8 million and 116, 655 CpG dinucleotides at 1X and 10X read counts, respectively (**Table S1**). In sperm samples, the average mapped reads (40 million), mapping rates (25.3%), unique reads (35.6 million) and the numbers of CpGs with 1X and 10X read counts (12 million and 608,253) were much higher than those of the single oocytes and embryos.

4.4.2. Unique features of methylome dynamics in bovine gametes and pre-implantation embryos

A circus plot was generated to display CpG methylation levels within 300-bp tiles across all 30 bovine chromosomes (**Figure S1D**). The number of total 300-bp tiles in each stage is summarized in **Figure S1E**. Two distinct methylation patterns were found: methylation in sperm was much higher (72.5%; **Figure 1A**) than oocytes (29.0% - 31.3%) and embryos (15.3% - 32.1%, **Figure 1A and Figure S1D**). These changes are caused by the global demethylation in the early bovine embryos. After fertilization, CpG methylation in gametes (72.5% in sperm and ~30% in oocyte; **Figure 1A**) decreased rapidly and reached the first low point at the 2-cell stage (25.0%; **Figure 1A**). Subsequently, a slight increase in DNA methylation was observed at the 4-cell stage (26.7%; **Figure 1A**). As development progressed, a further and major overall demethylation occurred reaching the lowest point at the 8-cell stage (15.3%; **Figure 1A**) and coinciding with onset of major embryonic genome activation (Misirlioglu et al., 2006; Graf et al., 2014; Jiang et al., 2014). A doubling of DNA methylation was then seen at the 16-cell stage (32.1%; **Figure 1A**). The timing of this major event of *de novo* methylation was consistent with our previous finding using RRBS (Jiang et al., 2018), as well as with the results generated by immunostaining (Dean et al., 2001; Dobbs et al., 2013; O'Doherty et al., 2015).

Of note, the three types of oocytes studied were all different in their DNA methylation levels. Although the global methylation of *in vivo* matured oocytes (31.6%) was only about 2% higher than that of the GV oocytes (29.7%), this change occurred to the haploid genome in a relatively short time and may not be minimal. Our data provides the molecular basis for the observation reported by Kono et al. (1996) that the maturation process involves addition of DNA methylation in mouse oocytes. Moreover, a small but noticeable difference in methylation levels

was also seen between *in vitro* (29.0%) and *in vivo* matured oocytes. This difference suggests aberrant DNA methylation during *in vitro* maturation. *In vitro* maturation, fertilization, and culture has been linked to abnormal embryo development (Smith et al., 2005) and large offspring syndrome (Young et al., 1998).

Interestingly, the methylation levels of non-CpG (CpH) sites showed an opposite demethylation-remethylation patterns and remained mostly at low levels (**Figure 1B and Figure S1F**). For example, non-CpG methylation peaked at the 8-cell stage and was the lowest in sperm, a reverse pattern to that of CpG methylation. Although non-CpG methylation has been reported to be enriched in oocytes (Tomizawa et al., 2011) and pluripotent stem cells, its functions, if any, remain poorly understood. Our result showed that non-CpG methylation peaked when high expression of pluripotency genes and embryonic genome activation occurred in bovine pre-implantation embryos (Jiang et al., 2014), suggesting an active regulatory role of non-CpG methylation on pluripotent gene expression.

4.4.3. Potential mechanisms for the methylome dynamics

To better understand the mechanisms of the DNA methylation dynamics, we analyzed the RNA-seq data of bovine gametes and embryos (Graf et al., 2014; Jiang et al., 2014; Lesch et al., 2016) for genes that encode DNA methylcytosine dioxygenases (*TET1, TET2*, and *TET3*) and DNA methyltransferases (*DNMT1, DNMT3A, DNMT3B* and *DNMTL*). The dioxygenases (Huang et al., 2014), *TET3* and *TET2,* were highly enriched in oocytes and 2-cell stage embryos, and their levels started to fade away at the 4-cell stage (**Figure 1C**), indicating a *TET*-mediated active DNA demethylation event immediately after fertilization (Wu and Zhang, 2017). Interestingly, expression of the other TET hydroxylase family member, *TET1,* was first seen at 4-cell stage and peaked at the 16-cell stage (**Figure 1C**), corresponding to its known function of

promoting the pluripotency of the inner cell mass (ICM) in the blastocyst (Seisenberger et al., 2013). On the other hand, the expression level of transcripts for *DNMT1*, the methylation maintenance enzyme (Goyal et al., 2006) was highest in *in vivo* matured oocytes, reduced gradually after fertilization, and reached the lowest level at the 8-cell stage (**Figure 1C**). This may be why the overall methylation levels of matured oocytes and the first two cleavage embryos did not dramatically decline until the 8-cell stage since bisulfite treatment cannot distinguish between 5-methylcytosine and the product of TET activity, 5-hydroxymethylcytosine. Transcripts for the *de novo* methyltransferase *DNMT3A* (Cheng and Blumenthal, 2011), and the cooperative homology, *DNMT3L* (Hata et al., 2002), were low until the 16-cell stage (**Figure 1C**), when we observed a doubling of DNA methylation levels. Another gene in the *DNMT3* family, *DNMT3B,* had an expression pattern similar to that of *DNMT1*, and may be important for *de novo* methylation at earlier stages (Liao et al., 2015). Taken together, the expression dynamics of methyltransferases is closed related to the dynamics of methylome in bovine oocytes and early embryos, and active demethylation by members of the TET family may be involved throughout early embryo development as opposed to the zygotic stage in the mouse (Iqbal et al., 2011).

4.4.4. Genomic regions of dynamic methylation changes

To determine the specific genomic regions that underwent dynamic methylation changes, we analyzed the methylation levels of promoters, exons, introns, CGIs, and intergenic regions of all annotated bovine genes (**Figure 1D**). We found that promoters and CGIs were consistently lowly methylated across all developmental stages, an observation similar to those found in other species (Guo et al., 2014). Interestingly, exons were hypermethylated (methylation level $\geq$ 75%) in sperm, but hypomethylated in oocytes and cleavage stage embryos. Methylation levels in exons had a minor increase at the 2-cell stage, but surged remarkably between the 8- and 16-cell

stages. On the other hand, changes in introns and intergenic regions closely resembled the whole genome dynamics (**Figure 1D**). In summary, the patterns of methylation dynamics in promoters and CGIs, which make up less than 1% of the genome, did not follow those of the whole genome and stayed in a hypomethylated state (methylation level $\leq$ 25%). These data suggest that the global methylation changes mainly reflects those of non-coding regions, such as intergenic regions and introns. Regulatory regions, such as promoters and CGIs, as well as coding regions (exons) have their own specific pattern of fluctuations.

We further examined DNA methylation along the gene body and 15 kb up and down stream of all annotated bovine genes (**Figure 1E**). A valley in methylation levels was observed around the TSS of all genes, coinciding with the predominantly unmethylated promoters. Methylation gradually increased from TSS to TES and slightly decreased after TES in all stages. This pattern was repeatedly observed in all examined gametes and developmental stages (**Figure 1E**) and was also seen in our RRBS study (Jiang et al., 2018). This suggests that DNA methylation may be used as a marker for gene TSS and TES boundaries (Naumann et al., 2009) in addition to its role in gene expression regulation. It also indicates a regulatory role of gene body methylation in transcription activation (Zilberman, 2017).

4.4.5. CpG density and methylome dynamics

To determine whether CpG density affects DNA demethylation and remethylation patterns, we plotted the DNA methylation levels of 300-bp tiles against their CpG density in all samples (**Figure 2A**). Genome regions were categorized into high (80%-100%), intermediate (20%-40%, 40%-60%, and 60%-80%), and low (0-20%) methylation levels (**Figure 2B**) and the correlation to CpG density for each was plotted in **Figure 2C-E**. Sperm exhibited a strong negative correlation (r=-0.97) between CpG density and methylation levels: regions of low CpG

density had high methylation, while those with relatively high CpG density had low-to-intermediate methylation (**Figure 2A**). Surprisingly, such a negative correlation in sperm had also been reported previously in differentiated somatic cells, likely because both cell types are highly methylated (Smith et al., 2012). However, among the other samples, only the 16-cell stage embryos had some trend of negative correlation (**Figure 2A**). Despite the negative correlation of CpG density and methylation levels, tiles with high CpG density, such as those in CGIs, were still more methylated in sperm and the 16-cell stage than in the other cleavage stages. The high overall levels of methylation of the sperm was the result of containing more than 60% of highly methylated tiles, while oocytes and cleavage embryos only had less than 20% of such tiles (**Figure 2B**). In addition, previous studies have also found that about 70% of promoter regions and CGIs that had high CpG densities remained predominantly unmethylated (Xie et al., 2013; Guo et al., 2014; Takahashi et al., 2017), corresponding to the reverse correlation between CpG density and CpG methylation level observed in our results.

4.4.6. Correlation between dynamics of transcriptomes and methylomes

Using RNA-seq data of bovine sperm (Lesch et al., 2016), GV oocytes, oocytes matured *in vitro* (Graf et al., 2014) and *in vivo* as well as cleavage stage embryos (Jiang et al., 2014), we observed weak negative correlations, ranging from -0.30 in sperm to -0.18 in the *in vivo* matured oocyte, between methylation levels of promoters and expression of the corresponding genes (**Figure S2A**). There were very weak negative correlations (in the range of -0.21 to -0.11) between the methylation and expression of the regions within gene body, exon, intron, and CGI. (**Figure S2B**). The correlation between methylation levels of the repetitive elements and the expression of the corresponding transcripts, however, was positive, ranging from 0.14 to 0.18 (**Figure S2B**). A previous study in mouse embryos also reported similar observations (Papin et

al., 2017). (**Figure S2C**). While both LINEs and SINEs, but not LTRs, underwent drastic de-methylation from gametes to 8-cell stage, their overall RNA expression remained at relative low but constant levels (FPKM< 40) throughout development, indicating the repression of repetitive element expression was possibly exerted through other mechanisms (Reik, 2007).

4.4.7. Commonly and uniquely methylated regions

A total of 14,939 tiles of 300 bp were found across all samples and termed commonly methylated. Their distribution along the 30 bovine chromosomes is illustrated in circos plots (**Figure 3A**). These tiles were characterized by low GC content, low CGI density and low gene density (**Figure 3B**). Specifically, 86% of these tiles were located in non-coding regions (intergenic and introns), 3% in CGIs, and 11% in repetitive regions such as LINEs (2%), SINEs (1%) and LTRs (8%). Because commonly methylated introns are the only regions that can lead to examination of functional genes in this group of tiles, we looked at their Gene Ontology (GO) terms and found that were enriched for involvement in cell differentiation and migration, signal transduction, protein localization and metabolic processes (**Figure 3B** and **Table S2**). Many of these were house-keeping genes suggesting the importance of consistent expression during early development. Interestingly, commonly methylated tiles exhibited a very similar dynamic pattern of methylation changes to that of the global pattern in oocytes and embryos, but not in sperm (**Figure 3C**). This difference suggests that the sperm and oocytes/embryos are differentially methylated even in the intergenic regions. After fertilization, the embryos appeared to maintain a pattern more similar to the oocytes than the sperm. Also, of note, commonly methylated tiles only have an methylation level of 19.4% in sperm, compared to the global methylation at an overall level of 72.5%, suggesting that these tiles although mainly intergenic, possibly resisted global demethylation.

Within commonly methylated regions, tiles that were hypermethylated in a specific stage and their GO categories are represented by heatmaps (**Figure 3D**). In the sperm, these tiles were enriched in genes of muscle contraction regulation, as well as oocyte development and differentiation (**Figure 3D and Table S3**), corresponding to the need for their repression. On the other hand, hypermethylated tiles in *in vivo* matured oocytes were involved in more GO terms than GV and *in vitro* matured oocytes (**Table S3**). A common GO term for hypermethylated tiles among the three types of oocytes was response to oxygen-containing compound (**Figure 3D and Table S3**). Oxygen stress in *in vitro* culture could generate excessive cytotoxic reactive oxygen species (ROS) and affect the viability of gametes (Park et al., 2005). The hypermethylation of these genes in oocytes is consistent with better quality when oocytes are matured in low oxygen conditions; perhaps the hypermethylation of these genes hampers the oocytes' ability to adapt to artificial culture environments (Waldenström et al., 2009). Additionally, the hypermethylated regions in 8- or 16-cell embryos were mostly hypermethylated in other stages (**Figure 3D)**, suggesting these regions either resisted demethylation or regained their methylation during the *de novo* process.

We next analyzed the uniquely methylated regions in each sample (**Figure S3A**). Sperm had the highest number tiles (276,190), followed by the 16-cell embryos (31,628), with the least in *in vivo* matured oocytes (877). Those in sperm (**Figure S3B**) were enriched in intergenic (30%) and repetitive regions (31%), including 16% in SINES, 12% in LINEs and 3% in LTR, while only 1% fell in the promoter regions. The GO terms of genes represented by these tiles were immune and inflammatory responses, G-protein receptor signaling pathway, and cell adhesion (**Figure S3B**). Uniquely methylated regions in oocytes and embryos were also enriched in intergenic and repetitive regions (**Figure S3C**). The changes in the methylation levels of these

tiles in oocytes and embryos (**Figure S3D**) closely resembled the commonly methylated regions (**Figure 3C**) and global changes in methylation. However, sperm uniquely methylated regions (95% of the total tiles) were hypermethylated; while, sperm commonly methylated region (5% of the total tiles) were hypomethylated, indicating that the sperm uniquely methylated regions were likely targets of methylation erasure and re-establishment during embryonic development.

4.4.8. Pairwise comparisons of methylomes at consecutive stages of development

Overall, the methylation of the majority tiles (77.6% on average of each stage) were stable (differences ≤ 40%) during development (**Figure 4A**), indicating that methylome dynamic changes occurred in a small number of regions of the genome. Of the two transitions that had the most changing tiles (**Figure 4A**), a large portion (84.7%) showed decrease in methylation from sperm to 2-cell; while, 78.7% of tiles increased methylation from 8- to 16-cell. A total of 951 genes were represented by the differentially methylated tiles (**Figure S3E**) between the 8- and 16-cell stages, with 256 and 695 hypermethylated at the 8- and 16-cell stage, respectively (**Figure S3E**). Genes hypermethylated at the 8-cell stage were categorized into the GO terms of: actin cytoskeleton reorganization, negative regulation of transcription and cell adhesion; whereas, those associated with intracellular protein transport, cell migration and DNA-template transcription were hypermethylated at the 16-cell stage (**Figure S3E and Table S4**). Moreover, we have found four differentially expressed genes between 8- and 16-cell stage: *ELOVL5, DEK, CAD,* and *KIAA1191* had DMRs (**Table S5**). The negatively correlation between gene expression and DNA methylation was expected.

4.4.9. Characteristics of DMRs between different types of gametes

We plotted heatmaps of DMRs from six comparisons: between sperm and any one of the three types of oocytes (**Figure S4A-C**), and between any two of the three oocyte types (**Figure**

S4D-F). The greatest number of DMRs and corresponding genes were found between sperm and *in vitro* matured oocytes (6,211), while the least were between GV and *in vivo* matured oocytes (755) (**Figure 4B**). Large numbers of DMRs (801) were also found between *in vivo* and *in vitro* matured oocytes. Between sperm and *in vivo* matured oocytes, 1,200 DMRs were highly methylated in *in vivo* matured oocytes (**Figure 4C**) and 1,453 were highly methylated in sperm (**Figure 4C**). These DMRs may represent parent-of-origin specific epigenetic modifications. Most of them, however, were distributed in intergenic regions. A high percentage of DMRs were LTRs (oocyte: 12%; sperm: 3%) and SINEs (oocyte: 2%; sperm: 6%), respectively. More highly methylated DMRs in sperm were in exons (sperm: 8%; oocyte: 3%) and CGIs (sperm: 13%; oocyte: 8%) than those in oocytes.

We then profiled the dynamic changes of DMRs that were highly methylated in one type of gametes during pre-implantation development (**Figure 4D**, upper left panel). Only DMRs that are located in the commonly methylated regions could be included across all samples. DMRs among the different types of oocytes were mostly intermediately methylated (25-75%). Interestingly, the majority of DMRs that were highly methylated in *in vivo* matured oocytes had intermediate methylation in both GV oocytes and *in vitro* matured oocytes, indicating that the *in vitro* environment failed to establish proper DNA methylation in these regions during the maturation process. Previous studies also demonstrated the suboptimal *in vitro* culture altered the DNA methylation landscape in bovine embryos (Salilew-Wondim et al., 2015). Furthermore, changes in DMRs that were hypermethylated in *in vivo* matured oocytes (**Figure 4D** upper left panel), resembled the global methylome dynamics during pre-implantation development. In contrast, DMRs hypermethylated in sperm (**Figure 4D** upper right panel) had relatively high methylation in the 2-cell stage compared to those hypermethylated in oocytes.

Additionally, we identified 1,063 and 9,310 tiles that were either hypermethylated or hypomethylated in both sperm and *in vivo* matured oocytes (**Figure 4D** bottom left panel). The hypomethylated tiles were not further de-methylated in pre-implantation embryos, but increased their methylation at the 16-cell stage (**Figure 4D** bottom right panel). However, tiles that were hypermethylated in both gametes and localized in mostly intergenic regions became largely hypomethylated during subsequent development with minimal methylation levels reached at the 8-cell stage (**Figure 4D**).

The Gene Ontology of annotated genes encompassing all DMRs from the six comparisons were summarized in **Table S6.** Interestingly, only one common GO term, cell adhesion, was found in DMRs that were hypermethylated in sperm while hypomethylated in the three types of oocytes (**Figure S4A-C**). A previous methylome study (Perrier et al., 2018) compared bull sperm to somatic tissues, and also found the GO terms of cell adhesion in methylated region of sperm, along with migration and fertilization, which are essential functions of sperm. In the DMR comparison between *in vivo* and *in vitro* matured oocytes, genes in positive regulation of endosome, cellular component organization, and cytoplasmic transport were hypermethylated in *in vivo* matured oocytes, while those related to urogenital and reproductive system development and cell development were hypermethylated in *in vitro* matured oocytes. Our results provide candidate genes that were differentially methylated due to the suboptimal *in vitro* culture. These genes could be potential targets for the optimization of *in vitro* maturation and fertilization. Additionally, we analyzed the gene DMR with corresponded gene expression levels in the six comparisons (**Table S7**). Interestingly, genes with multiple DMRs, such as *RNF122* in the comparison between GV and *in vivo* MII, showed the region specific DMR patterns along the gene body, i.e. some DMRs were hypermethylated in GV while

others were hypermethylated in *in vivo* MII, and the gene expression regulation difference could through complicate mechanisms.

4.4.10. Methylation of the X chromosomes and imprinted genes

In the mouse, the sperm carries an inactive X chromosome which is quickly reactivated after fertilization (Goto and Monk, 1998). We found that the bovine gametes also had differentially methylated X chromosomes with the one in sperm much more methylated than the one in matured oocytes. After fertilization, the overall DNA demethylation pattern of the X chromosome in the sperm closely resembled that of the whole genome (**Figure 5A-B**), suggesting reactivation of the paternal X chromosome. This is consistent with the observation that expression of the X-linked *MaoA* gene was detected from both parental X chromosomes until the morula stage when XCI was first observed (Ferreira et al. 2010). Interestingly, the methylation level of X chromosome in sperm was about 10% lower than that of the entire sperm genome (**Figure 5B**), which was also observed in our RRBS study (Jiang et al., 2018) and in a monkey WGBS study (Gao et al., 2017). This is likely a result of more X-linked hypomethylated tiles on the X chromosome than the whole genome (Figure S1D).

The expression of the X-linked *XIST* gene is essential for initiation of XCI in the mouse embryos (Kalantry et al., 2009). In males, *XIST* is expressed in testes to coat the sex body that forms during male meiotic sex chromosome inactivation (MSCI) (Turner, 2007). In our data, the CpG site in *XIST* gene was not well cover in every sample (**Figure 5A & Figure S5**). We could still observe that in sperm *XIST* gene was relatively lowly methylated compare to other regions of the X (**Figure 5A & Figure S5**). Using expression data from Lesch et al (2016) and Jiang et al. (2014), we found that *XIST* was absent in the sperm, but its transcription was initiated at the 2-cell stage (**Figure 5C**)**,** supporting the previous data by De La Fuente et al., (1999). The major

elevation of *XIST* expression was observed between the 4- to 8- cell stage, when embryonic genome activation occurs, and peaked at morula stage, this is likely because XCI will be established soon (**Figure 5C**), which was first reported by Xue et al. (2002) in the bovine.

Genome imprinting is a phenomenon of gene expression in a parent-of-origin specific manner (Pfeifer, 2000) and can be regulated by differential epigenetic marks on gametes (Plasschaert and Bartolomei, 2014). Unlike the whole genome, which undergoes a drastic reprogramming after fertilization, genomic imprinted genes retain their germline differentially methylated regions (gDMRs) through the demethylation process in a parent-of-origin specific manner (Sanz et al., 2010; Stewart et al., 2016). To date, 53 imprinted genes have been identified in the bovine (Chen et al., 2016), of which 34 are annotated in the current genome and analyzed in our study.

We first characterized genes for which the imprinted control regions (ICR) (Pervjakova et al., 2016) are known regulatory gDMRs. The ICRs for imprinted genes *PEG3* (Kim et al., 2007) and *H19* (Robbins et al., 2012) (**Figure 5D**) are located at the first exon (Kim et al., 2007) and 3kb upstream of the *H19* promoter (Hansmann et al., 2011; Robbins et al., 2012), respectively. In bovine gametes and early embryos, the methylation of these ICRs in gametes corresponded to their parent-of-origin expression, for example, paternally expressed (Kim et al., 2007) gene *PEG3* was hypomethylated in sperm at its ICR and hypermethylation in oocytes, and the methylation was maintained at around 50% up to the 16-cell stage (**Figure 5D**), as expected.

Interestingly, we observed two distinct patterns of gamete-specific methylation for bovine imprinted genes. The first pattern included 20 genes, 9 paternally and 11 maternally expressed, whose methylation along the gene body negatively correlated with their reported allelic expression, as expected. For example, the paternally expressed gene *SGCE* was

hypomethylated in sperm and hypermethylated in *in vivo* matured oocytes, while the maternally expressed gene *IGF2R* was hypomethylated in oocytes and hypermethylated in sperm. In the second pattern which included 14 genes, 8 paternally and 6 maternally expressed, a positive correlation of gene body methylation and the known allelic expression pattern was seen (**Figure 5E**). For instance, the paternally expressed genes, *BEGAIN*, *IGF2*, and *RTL1,* were hypermethylated in the gene bodies in sperm and hypomethylated in oocytes, while the maternal expressed *OOEP* and *PHLDA2* were hypermethylated in oocytes in their gene bodies. Our RRBS study (Jiang et al., 2018) of bovine embryos also reported similar findings. The disagreement between methylation and expression patterns could be due to the involvement of other epigenetic mechanisms as well as the fact that the gene body may not contain the imprinting control region. The expression heatmap (**Figure 5E**) showed that the majority of paternally expressed genes had high expression levels in sperm, while a significant number of the maternally expressed genes had high expression in GV oocytes.

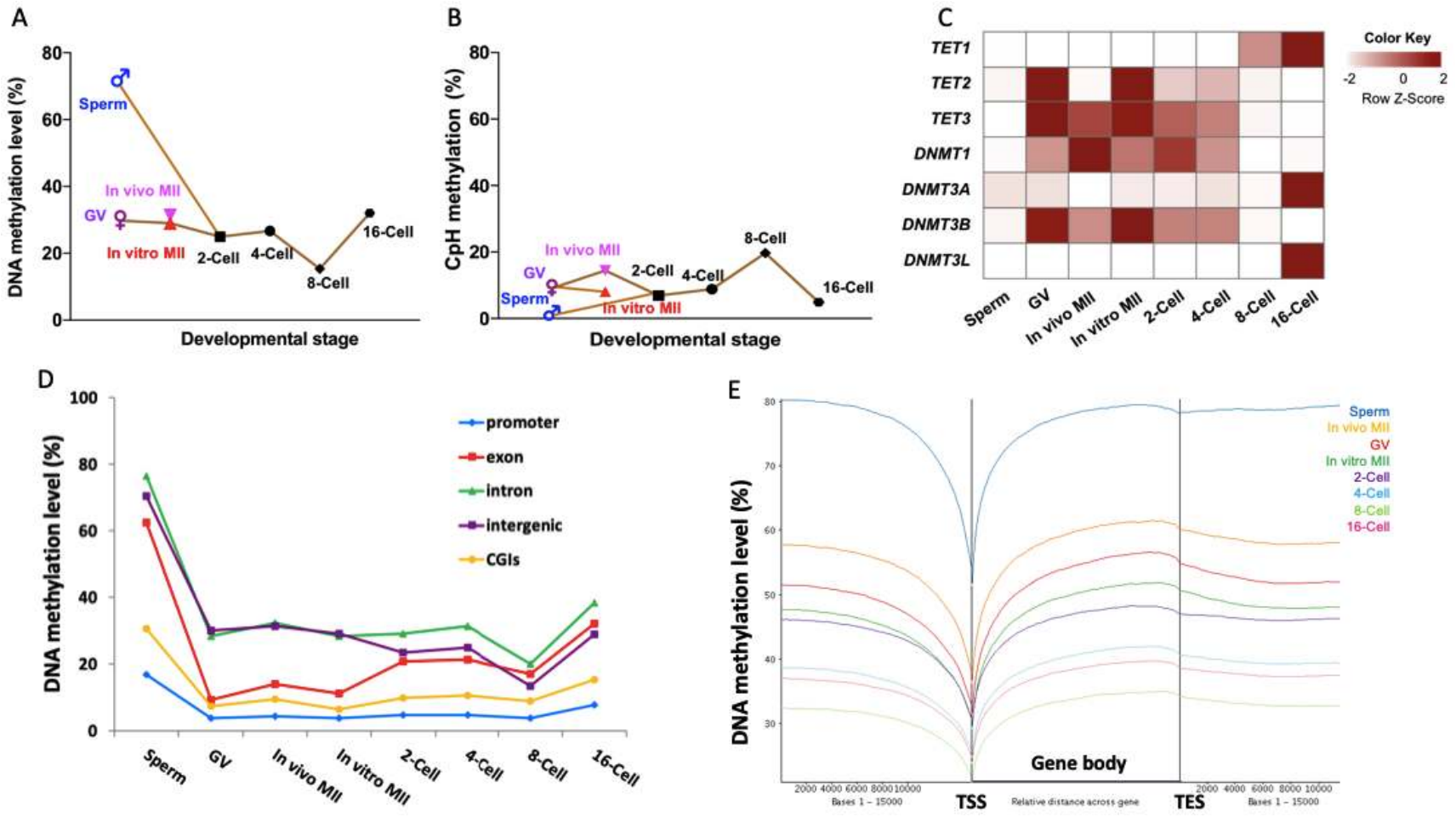

Figure 1. Methylome dynamics during bovine pre-implantation embryonic development.
Line chart of averaged levels of CpG (A) and CpH (B) methylation across stages**.** Heatmap (C) of fragment per kilobase million (FPKM) expressions of *DNMT* and *TET* gene families in bovine early embryos**.** Line chart (D) of the average DNA methylation levels of annotated genomic features across stages. Trend plot (E) of averaged DNA methylation levels along the gene bodies (from transcription start sites (TSS) to transcription end sites (TES)) and 15,000 base pairs (bp) up- and down-stream of the gene body. GV: germinal vesicle oocytes; MII: matured oocytes.

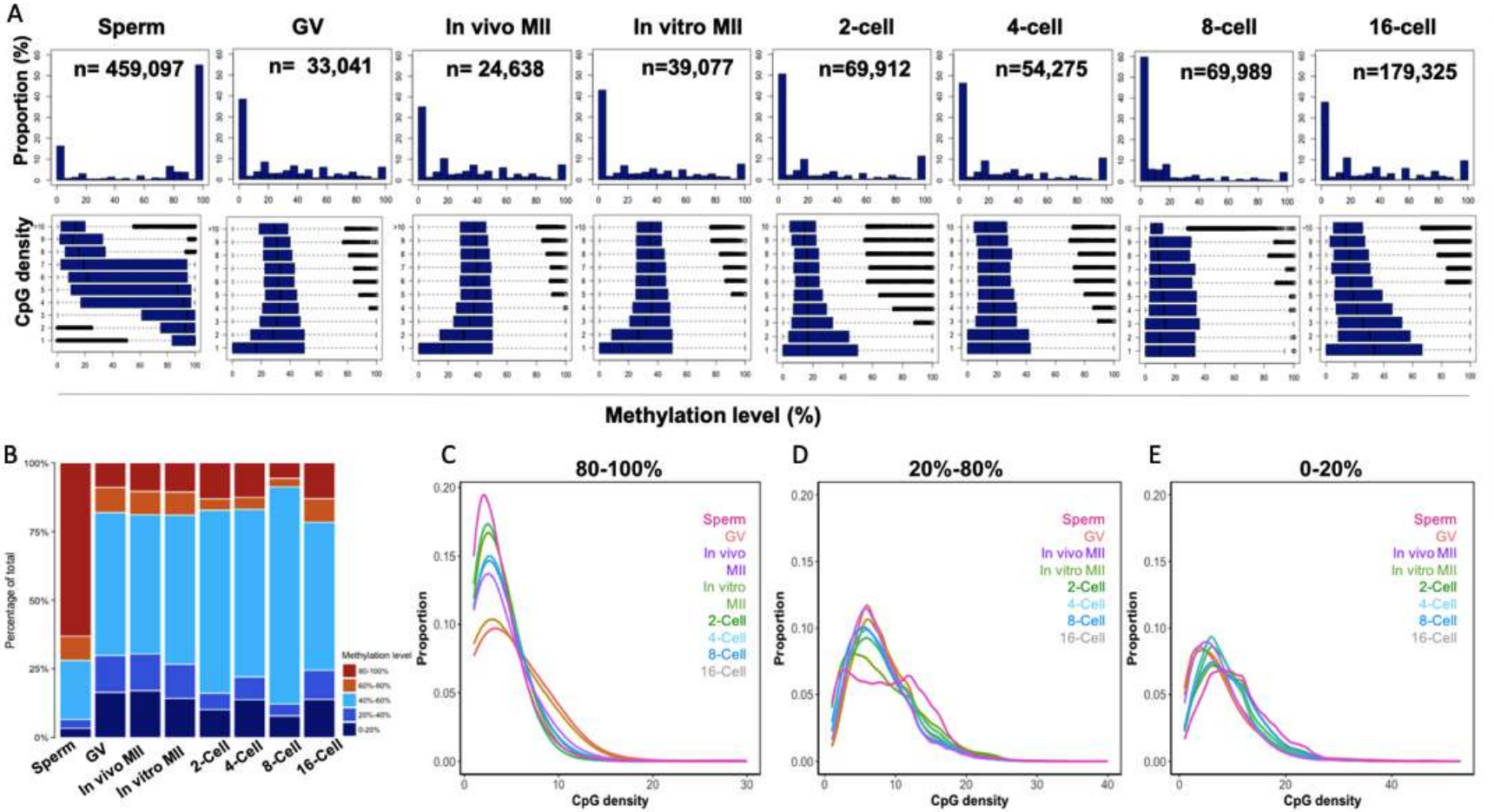

Figure 2. CpG density and the methylome dynamics of bovine gametes and pre-implantation embryos.
Histogram (A) of the percentages of 300-bp tiles with different DNA methylation levels at each development stage (upper panels). Box plots of methylation levels across different CpG densities at each stage (bottom panels). Stack bar plot (B) of the percentages of tiles with high (80%-100%), intermediate (60%-80%; 40%-60%, 20-40%), and low (0-20%) methylation levels. The distribution of high (C), intermediate (D) and low (E) methylation tiles against CpG densities at each stage. GV: germinal vesicle oocytes; MII: matured oocytes.

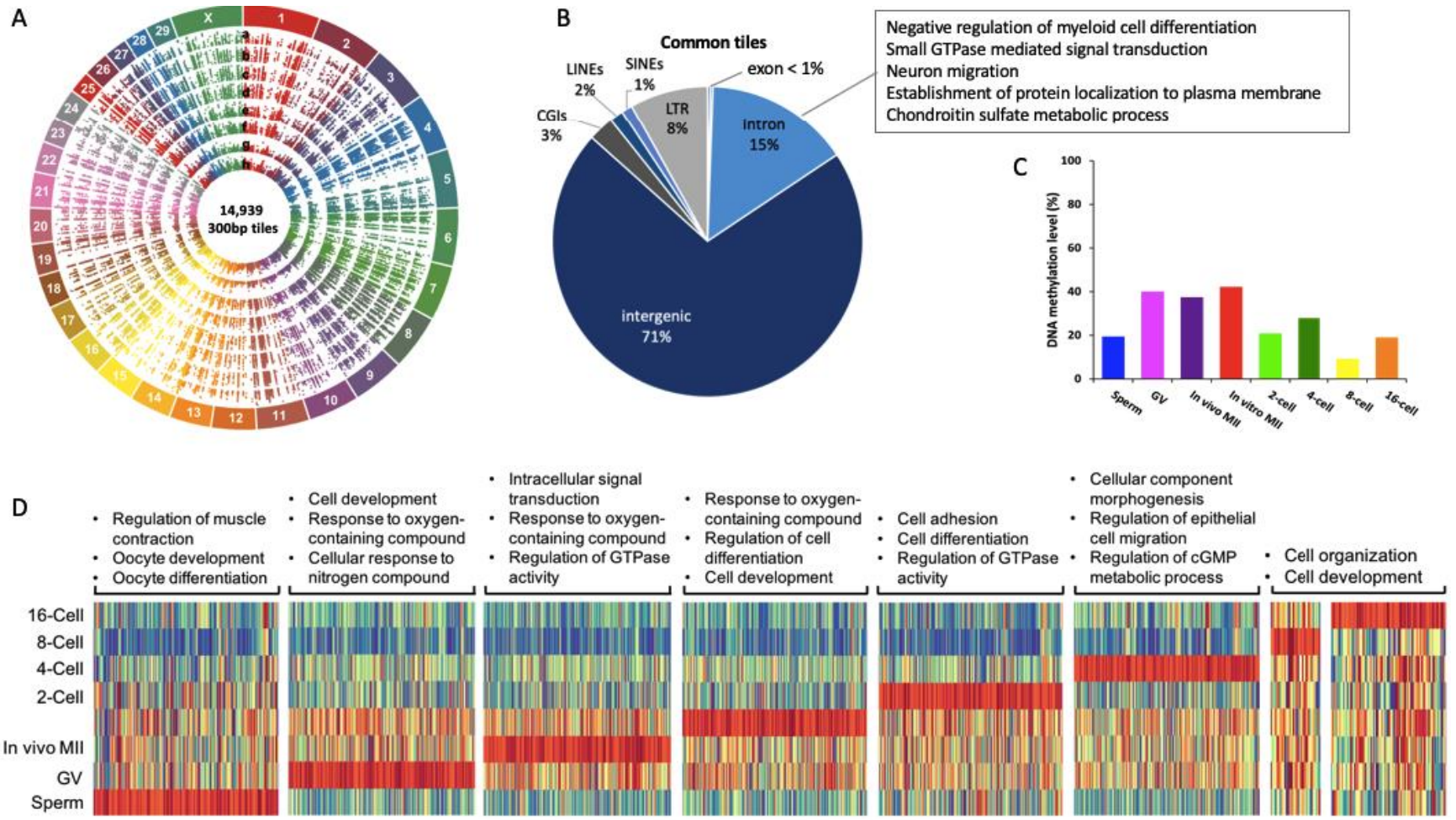

Figure 3. Commonly and uniquely methylated regions in bovine gametes and pre-implantation embryos.
Circos plot (A) visualization of 14,939 commonly methylated 300-bp tiles among all samples. a. sperm, b. GV, c. *in vivo* MII, d. *in vitro* MII, e. 2-cell, f. 4-cell, g. 8-cell, h. 16-cell. Pie plot (B) of the distribution of commonly methylated tiles in genomic regions and their associated GO term representatives. Bar plot (C) of averaged DNA methylation levels across stages. Heatmap (D) of enrichment of hypermethylated regions in each stage and associated GO term representatives. GV: germinal vesicle oocytes; MII: matured oocytes. Green: hypomethylation, red: hypermethylation.

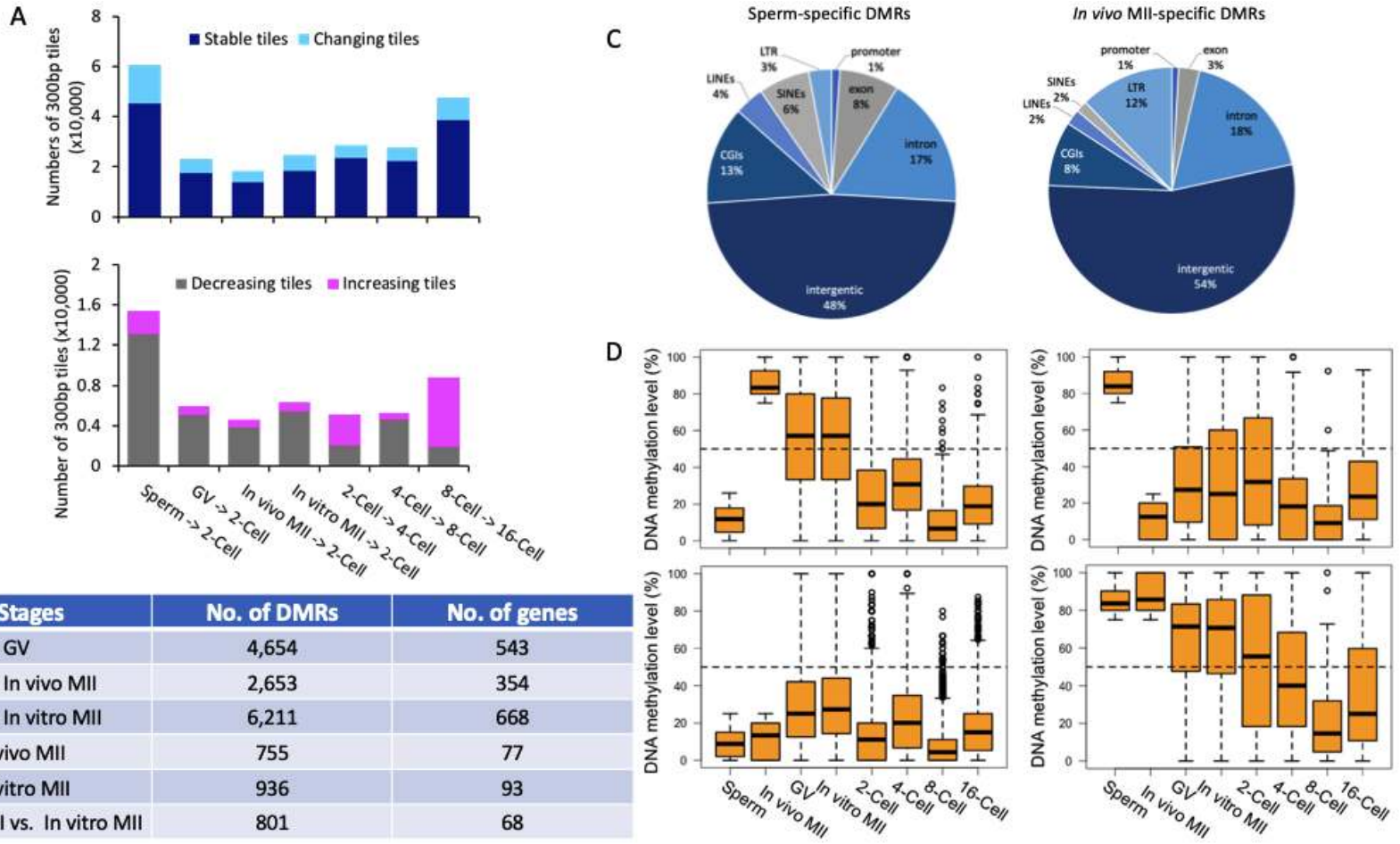

B

Stages	No. of DMRs	No. of genes
Sperm vs. GV	4,654	543
Sperm vs. In vivo MII	2,653	354
Sperm vs. In vitro MII	6,211	668
GV vs. In vivo MII	755	77
GV vs. In vitro MII	936	93
In vivo MII vs. In vitro MII	801	68

Figure 4. Pairwise comparisons of methylomes between consecutive development stagesand DMRs in gametes.
Histogram (A) of the numbers of stable (dark blue) and changing (sky blue) tiles between consecutive stages. Histogram of the numbers of decreasing (gray) and increasing (pink) tiles between consecutive stages. The numbers (B) of DMRs and corresponding genes between gametes of different types. Pie plots (C) of the distribution of *in vivo* MII- and sperm-specific DMRs in annotated genomic regions. Box plots (D) of DNA methylation levels of oocyte- (upper left) or sperm- (upper right) specific DMRs in gametes and early embryos, as well as distributions of tiles hypomethylated (≤25%; bottom left) and hypermethylated (≥75%; bottom right) tiles in both gametes in each development stage. GV: germinal vesicle oocytes; MII: matured oocytes.

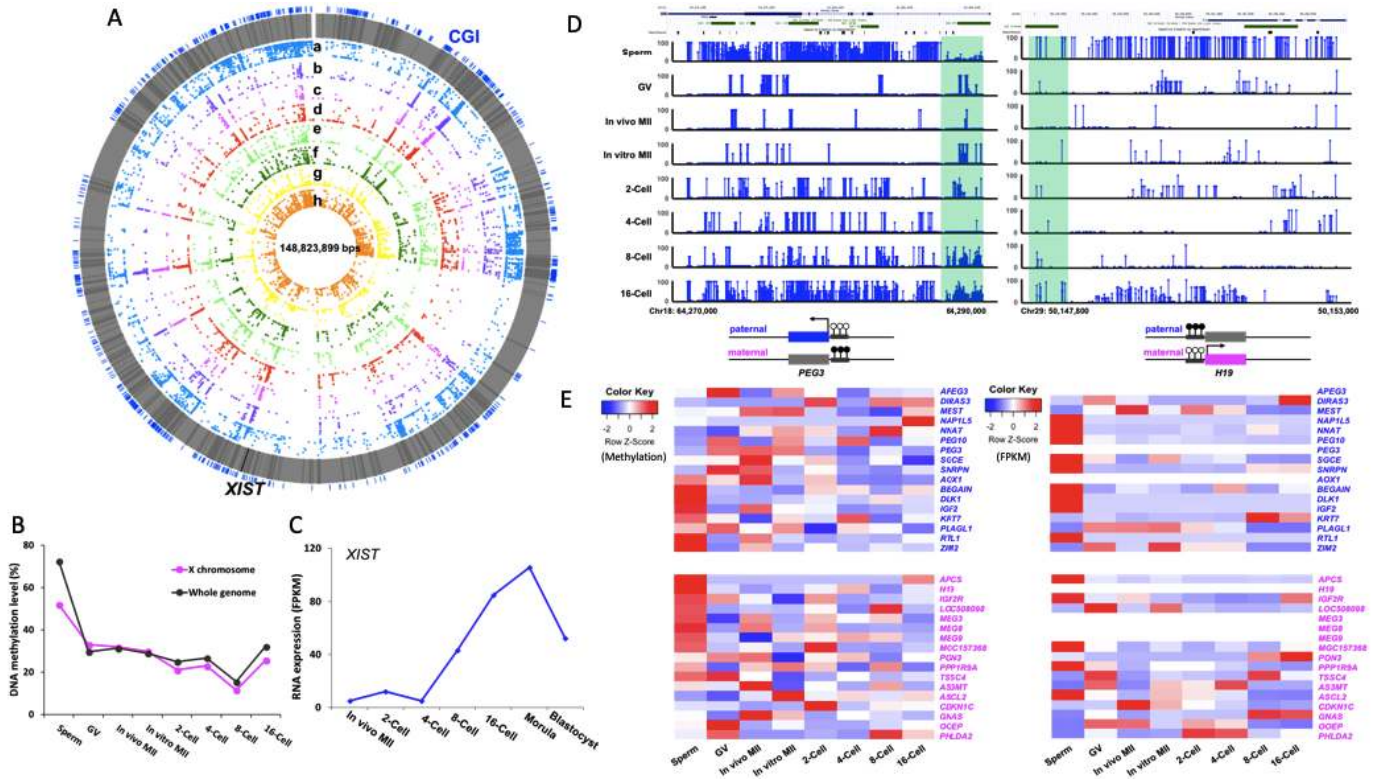

Figure 5. Methylation of the X chromosome and imprinted genes in bovine gametes and pre-implantation embryos.
Circos plot (A) visualization of the methylation dynamics of genomic region of the X chromosome. All genes are in gray lines, Xist gene is in black line. CGIs are in blue lines. a. sperm, b. GV, c. *in vivo* MII, d. *in vitro* MII, e. 2-cell, f. 4-cell, g. 8-cell, h. 16-cell. Line plot (B) showing the DNA methylation dynamics of the X chromosome followed the global pattern of methylation changes. Line chart (C) of fragment per kilobase million (FPKM) expressions levels of *XIST* in bovine early embryos. Visualization of (D) imprinted control regions (ICR) of *PEG3* and *H19*. Heatmap of (E) of the methylation and expression levels (FPKM) of 34 imprinted genes in pre-implantation embryos. GV: germinal vesicle oocytes; MII: matured oocytes. Blue text: paternally expressed genes, pink text: maternally expressed genes, Color key for heatmap: blue, hypomethylation and low expression, red, hypermethylation and high expression.

4.5. Supplementary information

Table S1. Summary of WGBS library mapping and data processing

Stages	No. of Total Sequencing Reads	No. of Mapped Reads	Mapping Rates	Duplicated reads (rates)	Non-converted reads	Remained reads	Total Unique CpG Sites (1X) Across Stages	Total Unique CpG Sites (5X) Across Stages	Total Unique CpG Sites (10X) Across Stages	Bisulfite Conversion Rates
Sperm_1	161,216,442	39,681,472	24.6%	4686722 (11.8%)	260,312	34,469,772	12,993,162	1,653,714	608,253	98.13%
Sperm_2	211,319,602	53,205,362	25.2%	6488800 (12.2%)	345,993	46,018,888				98.78%
Sperm_3	115,697,874	30,044,218	26.0%	2685134 (8.9%)	209,614	26,937,100				98.20%
GV_1	65,016,220	11,138,582	17.1%	4351074 (39.1%)	590,462	5,605,132	1,288,230	199,922	83,160	98.60%
GV_2	92,984,096	9,846,682	10.6%	5163658 (52.5%)	398,547	3,884,834				98.55%
GV_3	118,194,368	16,944,488	14.3%	11235552 (66.3)	435,246	4,836,406				98.49%
GV_4	107,145,508	7,368,766	6.9%	2635962 (35.8)	286,843	4,158,022				98.60%
In vivo_MII_1	85,538,162	5,131,986	6.0%	2184726 (42.6%)	279,052	2,388,694	486,489	63,628	23,081	98.51%
In vivo_MII_2	121,845,464	14,076,078	11.6%	9129286 (64.9%)	489,460	3,966,146				98.54%
In vivo_MII_3	88,260,850	4,711,248	5.3%	2683234 (57.0%)	88,736	1,849,790				98.59%
In vivo_MII_4	100,727,086	3,998,724	4.0%	1808178 (45.2%)	155,908	1,878,188				98.46%
In vivo_MII_5	5,365,330	311,090	5.8%	16750 (5.4%)	24,940	244,444				98.90%
In vivo_MII_6	83,411,048	2,481,584	3.0%	1503746(60.4%)	180,699	616,102				98.51%
In vitro_MII_1	50,214,588	4,595,662	9.2%	2776720 (60.4%)	65,986	1,686,930	775,917	146,750	67,363	95.48%
In vitro_MII_2	55,528,252	11,645,192	21.0%	7370920 (63.3%)	265,776	3,741,820				96.28%
In vitro_MII_3	58,002,506	6,542,116	11.3%	5137740 (78.5%)	136,798	1,130,062				97.00%
In vitro_MII_4	54,537,430	702,602	1.3%	299796 (42.7%)	24,107	354,532				97.72%
In vitro_MII_5	90,523,956	6,039,752	6.7%	1558380 (25.8%)	401,697	3,677,436				97.30%
In vitro_MII_6	114,323,238	5,606,912	4.9%	1775736 (31.7%)	413,647	3,003,244				98.18%
2-Cell_1	129,875,908	7,163,764	5.5%	3579644 (50.0%)	160,494	3,262,596	1,716,507	267,711	113,416	98.37%
2-Cell_2	164,502,830	9,436,404	5.7%	5080396 (53.8%)	226,277	3,902,624				98.40%
2-Cell_3	91,770,914	17,880,216	19.5%	5201486 (29.1%)	514,479	11,648,538				98.46%
2-Cell_4	70,534,008	1,289,856	1.8%	349382 (27.1%)	62,024	816,282				98.47%
4-Cell_1	97,778,054	5,066,414	5.2%	2952796 (58.3%)	207,742	1,697,262	1,253,797	189,680	76,240	98.29%
4-Cell_2	81,628,404	15,646,310	19.2%	8706226 (55.7%)	230,536	6,477,846				98.41%
4-Cell_3	111,193,874	13,843,092	12.4%	5416762 (39.1%)	344,497	7,736,016				98.34%
4-Cell_4	102,385,078	2,225,868	2.2%	580404 (26.1%)	80,738	1,483,814				98.22%
4-Cell_5	110,694,850	3,642,164	3.3%	1129354 (31.0%)	91,131	2,330,144				98.64%
8-Cell_1	112,311,296	20,399,528	18.2%	6952396 (34.1%)	982,604	11,480,484	1,405,250	239,397	109,682	98.36%
8-Cell_2	94,629,426	4,341,724	4.6%	1847986 (42.6%)	240,195	2,012,882				98.22%
8-Cell_3	90,751,254	2,211,738	2.4%	818182 (37.0%)	410,908	571,472				98.44%
8-Cell_4	97,579,526	3,754,886	3.8%	937256 (25.0%)	62,678	2,691,994				98.53%
16-Cell_1	106,037,758	18,636,794	17.6%	6276054 (33.7%)	235,637	11,887,768	5,791,048	799,933	343,641	98.33%
16-Cell_2	104,228,166	23,488,986	22.5%	7677668 32.7%)	392,183	15,025,234				98.40%
16-Cell_3	197,773,964	29,686,398	15.0%	6293204 (21.2%)	1,653,919	20,083,406				98.45%

Table S2. Gene Ontology (GO) terms for genes with commonly methylated introns among all samples

Term	Count	%	P-value	Genes
GO:0045638~negative regulation of myeloid cell differentiation	3	1.78	0.0083	PTK2B, MEIS1, CTR9
GO:0007264~small GTPase mediated signal transduction	6	3.55	0.0297	PLCE1, RALGPS1, RAB37, DOCK9, RHOBTB2, RGL1
GO:0001764~neuron migration	4	2.37	0.0366	GPM6A, PRKG1, GFRA3, KIRREL3
GO:0090002~establishment of protein localization to plasma membrane	3	1.78	0.0369	CAV3, TNFRSF1A, TMEM150A
GO:0030204~chondroitin sulfate metabolic process	2	1.18	0.0427	B3GAT2, B3GAT1

Table S3.1. Gene Ontology (GO) terms for hypermethylated genes in sperm

Term	Count	%	P-value	Genes
GO:0060047~heart contraction	3	14.29	0.0083	CAV3, RPS6KA2, PDE5A
GO:0003015~heart process	3	14.29	0.0086	CAV3, RPS6KA2, PDE5A
GO:0010611~regulation of cardiac muscle hypertrophy	2	9.52	0.0219	CAV3, PDE5A
GO:0014743~regulation of muscle hypertrophy	2	9.52	0.0230	CAV3, PDE5A
GO:0003300~cardiac muscle hypertrophy	2	9.52	0.0370	CAV3, PDE5A
GO:0043502~regulation of muscle adaptation	2	9.52	0.0381	CAV3, PDE5A
GO:0014897~striated muscle hypertrophy	2	9.52	0.0392	CAV3, PDE5A
GO:0008015~blood circulation	3	14.29	0.0392	CAV3, RPS6KA2, PDE5A
GO:0003013~circulatory system process	3	14.29	0.0402	CAV3, RPS6KA2, PDE5A
GO:0014896~muscle hypertrophy	2	9.52	0.0402	CAV3, PDE5A
GO:0048599~oocyte development	2	9.52	0.0434	RPS6KA2, PDE5A
GO:0055117~regulation of cardiac muscle contraction	2	9.52	0.0445	CAV3, PDE5A
GO:0009994~oocyte differentiation	2	9.52	0.0477	RPS6KA2, PDE5A

Table S3.2. Gene Ontology (GO) terms for hypermethylated genes in GV

Term	Count	%	P-value	Genes
GO:1901700~response to oxygen-containing compound	12	15.58	0.0005	PIK3CG, DNMT3A, TNFRSF1A, SLC38A9, PTK2B, TNFRSF10D, MET, ATP1A1, NFKB1, MSN, CTNNA1, PLCB1
GO:0045822~negative regulation of heart contraction	3	3.90	0.0016	PDE5A, ADRA1A, ATP1A1
GO:1901701~cellular response to oxygen-containing compound	9	11.69	0.0021	PIK3CG, DNMT3A, SLC38A9, PTK2B, MET, NFKB1, MSN, CTNNA1, PLCB1
GO:1903523~negative regulation of blood circulation	3	3.90	0.0041	PDE5A, ADRA1A, ATP1A1
GO:0007610~behavior	7	9.09	0.0083	GRIA1, FBXL20, PREX2, PLCB1, MEIS1, KIRREL3, EPHB2
GO:0048468~cell development	14	18.18	0.0113	PREX2, MET, TTPA, CTNNA1, MEIS1, EPHB2, RNF8, TNFRSF1A, GPM6A, PTK2B, PDE5A, UNC5D, MSN, KIRREL3
GO:1901699~cellular response to nitrogen compound	6	7.79	0.0119	PIK3CG, DNMT3A, SLC38A9, NFKB1, CTNNA1, PLCB1
GO:0001885~endothelial cell development	3	3.90	0.0150	TNFRSF1A, MET, MSN
GO:0060284~regulation of cell development	8	10.39	0.0155	TNFRSF1A, PTK2B, PDE5A, TTPA, UNC5D, CTNNA1, MEIS1, EPHB2
GO:0051865~protein autoubiquitination	3	3.90	0.0193	RNF8, UHRF2, ASB4
GO:0006942~regulation of striated muscle contraction	3	3.90	0.0215	PDE5A, ADRA1A, ATP1A1
GO:0000902~cell morphogenesis	10	12.99	0.0232	MKLN1, GPM6A, PTK2B, PREX2, MET, UNC5D, LRGUK, MSN, KIRREL3, EPHB2
GO:0071417~cellular response to organonitrogen compound	5	6.49	0.0265	PIK3CG, DNMT3A, SLC38A9, NFKB1, CTNNA1
GO:0009967~positive regulation of signal transduction	10	12.99	0.0265	PIK3CG, TNFRSF1A, SLC38A9, PTK2B, PDE5A, ADRA1A, NFKB1, CTNNA1, PLCB1, ADAMTS3
GO:0048584~positive regulation of response to stimulus	12	15.58	0.0268	RNF8, PIK3CG, TNFRSF1A, SLC38A9, PTK2B, PDE5A, MET, ADRA1A, NFKB1, CTNNA1, PLCB1, ADAMTS3
GO:0032989~cellular component morphogenesis	10	12.99	0.0332	MKLN1, GPM6A, PTK2B, PREX2, MET, UNC5D, LRGUK, MSN, KIRREL3, EPHB2
GO:0044708~single-organism behavior	5	6.49	0.0332	GRIA1, FBXL20, PREX2, PLCB1, EPHB2
GO:0045446~endothelial cell differentiation	3	3.90	0.0344	TNFRSF1A, MET, MSN
GO:0071407~cellular response to organic cyclic compound	5	6.49	0.0390	PIK3CG, ATP1A1, NFKB1, MSN, CTNNA1
GO:0051241~negative regulation of multicellular organismal process	8	10.39	0.0392	PTK2B, PDE5A, ADRA1A, ATP1A1, NFKB1, CTNNA1, MEIS1, EPHB2
GO:0033993~response to lipid	6	7.79	0.0399	TNFRSF1A, PTK2B, TNFRSF10D, ATP1A1, NFKB1, MSN
GO:0010647~positive regulation of cell communication	10	12.99	0.0402	PIK3CG, TNFRSF1A, SLC38A9, PTK2B, PDE5A, ADRA1A, NFKB1, CTNNA1, PLCB1, ADAMTS3
GO:0023056~positive regulation of signaling	10	12.99	0.0415	PIK3CG, TNFRSF1A, SLC38A9, PTK2B, PDE5A, ADRA1A, NFKB1, CTNNA1, PLCB1, ADAMTS3
GO:0007416~synapse assembly	3	3.90	0.0423	GPM6A, KIRREL3, EPHB2
GO:0003158~endothelium development	3	3.90	0.0454	TNFRSF1A, MET, MSN
GO:0040011~locomotion	10	12.99	0.0480	GPM6A, PTK2B, MET, UNC5D, MSN, CTNNA1, PLCB1, GFRA3, KIRREL3, EPHB2

Table S3.3. Gene Ontology (GO) terms for hypermethylated genes in in vivo MII

Term	Count	%	P-value	Genes
GO:0045822~negative regulation of heart contraction	3	4.92	0.0010	PDE5A, ADRA1A, ATP1A1
GO:0051674~localization of cell	11	18.03	0.0011	PTPRK, GPM6A, MET, PTPN23, UNC5D, MSN, CTNNA1, PRKG1, PLCB1, GFRA3, KIRREL3
GO:0048870~cell motility	11	18.03	0.0011	PTPRK, GPM6A, MET, PTPN23, UNC5D, MSN, CTNNA1, PRKG1, PLCB1, GFRA3, KIRREL3
GO:1901701~cellular response to oxygen-containing compound	8	13.11	0.0018	PIK3CG, PTPRK, SLC38A9, MET, NFKB1, MSN, CTNNA1, PLCB1
GO:0016477~cell migration	10	16.39	0.0018	PTPRK, GPM6A, MET, PTPN23, UNC5D, MSN, PRKG1, PLCB1, GFRA3, KIRREL3
GO:1903523~negative regulation of blood circulation	3	4.92	0.0024	PDE5A, ADRA1A, ATP1A1
GO:0040011~locomotion	11	18.03	0.0028	PTPRK, GPM6A, MET, PTPN23, UNC5D, MSN, CTNNA1, PRKG1, PLCB1, GFRA3, KIRREL3
GO:0006937~regulation of muscle contraction	4	6.56	0.0034	PDE5A, ADRA1A, ATP1A1, PRKG1
GO:1901700~response to oxygen-containing compound	9	14.75	0.0041	PIK3CG, PTPRK, SLC38A9, MET, ATP1A1, NFKB1, MSN, CTNNA1, PLCB1
GO:0001764~neuron migration	4	6.56	0.0047	GPM6A, PRKG1, GFRA3, KIRREL3
GO:0090257~regulation of muscle system process	4	6.56	0.0065	PDE5A, ADRA1A, ATP1A1, PRKG1
GO:0006928~movement of cell or subcellular component	11	18.03	0.0066	PTPRK, GPM6A, MET, PTPN23, UNC5D, MSN, CTNNA1, PRKG1, PLCB1, GFRA3, KIRREL3
GO:0035556~intracellular signal transduction	14	22.95	0.0069	PIK3CG, SLC38A9, DOCK9, NFKB1, PRKG1, ARFGEF1, RGL1, RAB37, PDE5A, ADRA1A, RGS7, PLCB1, ASB4, LCP2
GO:2000145~regulation of cell motility	7	11.48	0.0084	PTPRK, MET, PTPN23, UNC5D, MSN, CTNNA1, PLCB1
GO:0098609~cell-cell adhesion	8	13.11	0.0089	METAP1, PDE5A, PTPN23, UNC5D, MSN, CTNNA1, PRKG1, KIRREL3
GO:0043087~regulation of GTPase activity	5	8.20	0.0092	ASAP1, RGS7, PRKG1, PLCB1, ARFGEF1
GO:0051241~negative regulation of multicellular organismal process	8	13.11	0.0100	PDE5A, PTPN23, ASAP1, ADRA1A, ATP1A1, NFKB1, CTNNA1, PRKG1
GO:0040012~regulation of locomotion	7	11.48	0.0104	PTPRK, MET, PTPN23, UNC5D, MSN, CTNNA1, PLCB1
GO:0048584~positive regulation of response to stimulus	11	18.03	0.0105	PIK3CG, SLC38A9, PDE5A, MET, ADRA1A, NFKB1, CTNNA1, PLCB1, ADAMTS3, ARFGEF1, LCP2
GO:0051270~regulation of cellular component movement	7	11.48	0.0117	PTPRK, MET, PTPN23, UNC5D, MSN, CTNNA1, PLCB1
GO:0043085~positive regulation of catalytic activity	8	13.11	0.0125	PIK3CG, PDE5A, ASAP1, RGS7, WRN, PLCB1, ARFGEF1, LCP2
GO:0006942~regulation of striated muscle contraction	3	4.92	0.0129	PDE5A, ADRA1A, ATP1A1
GO:0071407~cellular response to organic cyclic compound	5	8.20	0.0161	PIK3CG, ATP1A1, NFKB1, MSN, CTNNA1
GO:2000146~negative regulation of cell motility	4	6.56	0.0173	PTPRK, PTPN23, CTNNA1, PLCB1
GO:2000643~positive regulation of early endosome to late endosome transport	2	3.28	0.0198	PTPN23, MSN
GO:1901699~cellular response to nitrogen compound	5	8.20	0.0203	PIK3CG, SLC38A9, NFKB1, CTNNA1, PLCB1

GO:0007155~cell adhesion	9	14.75	0.0214	PTPRK, METAP1, PDE5A, PTPN23, UNC5D, MSN, CTNNA1, PRKG1, KIRREL3
GO:0022610~biological adhesion	9	14.75	0.0219	PTPRK, METAP1, PDE5A, PTPN23, UNC5D, MSN, CTNNA1, PRKG1, KIRREL3
GO:1903651~positive regulation of cytoplasmic transport	2	3.28	0.0230	PTPN23, MSN
GO:0050790~regulation of catalytic activity	10	16.39	0.0249	PIK3CG, PDE5A, ASAP1, RGS7, NFKB1, WRN, PRKG1, PLCB1, ARFGEF1, LCP2
GO:0006936~muscle contraction	4	6.56	0.0251	PDE5A, ADRA1A, ATP1A1, PRKG1
GO:0040013~negative regulation of locomotion	4	6.56	0.0254	PTPRK, PTPN23, CTNNA1, PLCB1
GO:0051271~negative regulation of cellular component movement	4	6.56	0.0254	PTPRK, PTPN23, CTNNA1, PLCB1
GO:0030334~regulation of cell migration	6	9.84	0.0267	PTPRK, MET, PTPN23, UNC5D, MSN, PLCB1
GO:0043547~positive regulation of GTPase activity	4	6.56	0.0293	ASAP1, RGS7, PLCB1, ARFGEF1
GO:1903337~positive regulation of vacuolar transport	2	3.28	0.0328	PTPN23, MSN
GO:2000641~regulation of early endosome to late endosome transport	2	3.28	0.0328	PTPN23, MSN
GO:0010560~positive regulation of glycoprotein biosynthetic process	2	3.28	0.0360	PLCB1, ARFGEF1
GO:1903649~regulation of cytoplasmic transport	2	3.28	0.0360	PTPN23, MSN
GO:0051345~positive regulation of hydrolase activity	5	8.20	0.0384	ASAP1, RGS7, WRN, PLCB1, ARFGEF1
GO:0000902~cell morphogenesis	8	13.11	0.0389	GPM6A, MET, PTPN23, ASAP1, UNC5D, LRGUK, MSN, KIRREL3
GO:0003012~muscle system process	4	6.56	0.0398	PDE5A, ADRA1A, ATP1A1, PRKG1
GO:1903020~positive regulation of glycoprotein metabolic process	2	3.28	0.0424	PLCB1, ARFGEF1
GO:0044093~positive regulation of molecular function	8	13.11	0.0432	PIK3CG, PDE5A, ASAP1, RGS7, WRN, PLCB1, ARFGEF1, LCP2
GO:0009967~positive regulation of signal transduction	8	13.11	0.0434	PIK3CG, SLC38A9, PDE5A, ADRA1A, NFKB1, CTNNA1, PLCB1, ADAMTS3
GO:0006941~striated muscle contraction	3	4.92	0.0443	PDE5A, ADRA1A, ATP1A1

Table S3.4. Gene Ontology (GO) terms for hypermethylated genes in in vitro MII

Term	Count	%	P-value	Genes
GO:0007610~behavior	7	9.72	0.0040	GRIA1, FBXL20, PREX2, PLCB1, MEIS1, KIRREL3, EPHB2
GO:1901700~response to oxygen-containing compound	9	12.50	0.0089	TNFRSF1A, SLC38A9, TNFRSF10D, MET, ATP1A1, NFKB1, MSN, CTNNA1, PLCB1
GO:0001885~endothelial cell development	3	4.17	0.0114	TNFRSF1A, MET, MSN
GO:0044708~single-organism behavior	5	6.94	0.0207	GRIA1, FBXL20, PREX2, PLCB1, EPHB2
GO:0040011~locomotion	10	13.89	0.0207	LAMA4, MET, UNC5D, MSN, CTNNA1, PRKG1, PLCB1, GFRA3, KIRREL3, EPHB2
GO:0048468~cell development	12	16.67	0.0221	TNFRSF1A, PREX2, PDE5A, MET, TTPA, UNC5D, MSN, CTNNA1, PRKG1, MEIS1, KIRREL3, EPHB2
GO:0060284~regulation of cell development	7	9.72	0.0252	TNFRSF1A, PDE5A, TTPA, UNC5D, CTNNA1, MEIS1, EPHB2
GO:0045595~regulation of cell differentiation	10	13.89	0.0254	RBFOX1, TNFRSF1A, PDE5A, TTPA, UNC5D, CTNNA1, PLCB1, MEIS1, ASB4, EPHB2
GO:0045446~endothelial cell differentiation	3	4.17	0.0263	TNFRSF1A, MET, MSN
GO:0048870~cell motility	9	12.50	0.0270	LAMA4, MET, UNC5D, MSN, CTNNA1, PRKG1, PLCB1, GFRA3, KIRREL3
GO:0051674~localization of cell	9	12.50	0.0270	LAMA4, MET, UNC5D, MSN, CTNNA1, PRKG1, PLCB1, GFRA3, KIRREL3
GO:0003158~endothelium development	3	4.17	0.0348	TNFRSF1A, MET, MSN
GO:0006928~movement of cell or subcellular component	10	13.89	0.0403	LAMA4, MET, UNC5D, MSN, CTNNA1, PRKG1, PLCB1, GFRA3, KIRREL3, EPHB2
GO:0007399~nervous system development	11	15.28	0.0443	RBFOX1, PREX2, UNC5D, CTNNA1, PRKG1, PLCB1, MEIS1, PLPPR1, GFRA3, KIRREL3, EPHB2
GO:0006937~regulation of muscle contraction	3	4.17	0.0460	PDE5A, ATP1A1, PRKG1
GO:0010721~negative regulation of cell development	4	5.56	0.0471	TTPA, CTNNA1, MEIS1, EPHB2
GO:1901701~cellular response to oxygen-containing compound	6	8.33	0.0497	SLC38A9, MET, NFKB1, MSN, CTNNA1, PLCB1

Table S3.5. Function for hypermethylated genes in 2-cell stage

ASAP1	This gene encodes an ADP-ribosylation factor (ARF) GTPase-activating protein.
HS6ST2	Heparan sulfate proteoglycans are ubiquitous components of the cell surface, extracellular matrix, and basement membranes, and interact with various ligands to influence cell growth, differentiation, adhesion, and migration.

Table S3.6. Gene Ontology (GO) terms for hypermethylated genes in 4-cell stage

Term	Count	%	P-value	Genes
GO:0000902~cell morphogenesis	6	19.35	0.0174	MKLN1, PTK2B, MET, PTPN23, LRGUK, KIRREL3
GO:0010632~regulation of epithelial cell migration	3	9.68	0.0181	PTK2B, MET, PTPN23
GO:0032989~cellular component morphogenesis	6	19.35	0.0223	MKLN1, PTK2B, MET, PTPN23, LRGUK, KIRREL3
GO:0030823~regulation of cGMP metabolic process	2	6.45	0.0273	PTK2B, PDE5A
GO:0044248~cellular catabolic process	6	19.35	0.0296	PTK2B, ENPP3, PDE5A, PTPN23, SKIV2L2, RNF122
GO:0010631~epithelial cell migration	3	9.68	0.0324	PTK2B, MET, PTPN23
GO:0090132~epithelium migration	3	9.68	0.0331	PTK2B, MET, PTPN23
GO:0090130~tissue migration	3	9.68	0.0351	PTK2B, MET, PTPN23
GO:0034655~nucleobase-containing compound catabolic process	3	9.68	0.0402	ENPP3, PDE5A, SKIV2L2
GO:0046068~cGMP metabolic process	2	6.45	0.0492	PTK2B, PDE5A
GO:0046700~heterocycle catabolic process	3	9.68	0.0499	ENPP3, PDE5A, SKIV2L2

Table S3.7. Function for hypermethylated genes in 8-cell stage

KIRREL3	The protein encoded by this gene is a synaptic cell adhesion molecule
MACROD2	Deacetylase involved in removing ADP-ribose from mono-ADP-ribosylated proteins.
RGL1	Negative regulator of GA responses, member of GRAS family of transcription factors

Table S3.8. Gene Ontology (GO) terms for hypermethylated genes in 16-cell stage

Term	Count	%	P-value	Genes
GO:0007416~synapse assembly	2	18.18	0.0435	KIRREL3, EPHB2
GO:0050808~synapse organization	2	18.18	0.0853	KIRREL3, EPHB2
GO:0021537~telencephalon development	2	18.18	0.0940	KIRREL3, EPHB2

Table S4.1. GO terms for DMRs between the 8- and 16-cell embryos that are hypermethylated in the 8-cell embryos

Term	Count	%	PValue	Genes
GO:0031532~actin cytoskeleton reorganization	4	1.50	0.023	MICALL2, FLNA, PARVB, INSRR
GO:0000122~negative regulation of transcription from RNA polymerase II promoter	13	4.89	0.024	EGR1, EHMT1, FOXJ1, TP53, MBD3, SUFU, CHD8, PHF19, ATN1, RARA, TBL1X, HDAC7, SUDS3
GO:2000824~negative regulation of androgen receptor activity	2	0.75	0.030	FOXH1, HEYL
GO:0007059~chromosome segregation	4	1.50	0.031	CIAO1, PPP2R1A, NAA60, CDK5RAP2
GO:0051306~mitotic sister chromatid separation	2	0.75	0.044	PPP2R1A, DIS3L2
GO:0001578~microtubule bundle formation	3	1.13	0.046	GAS2L2, CDK5RAP2, NCKAP5L
GO:0007155~cell adhesion	7	2.63	0.046	PRKCA, LGALS3BP, STAB1, TTYH1, NINJ2, PARVB, CTNNA2
GO:0050896~response to stimulus	3	1.13	0.053	CNGB1, SCNN1B, VSX1
GO:0006468~protein phosphorylation	6	2.26	0.055	PRKCA, SCYL1, LIMK2, COQ8A, RARA, ILF3
GO:2001046~positive regulation of integrin-mediated signaling pathway	2	0.75	0.073	LIMS2, FLNA
GO:0090267~positive regulation of mitotic cell cycle spindle assembly checkpoint	2	0.75	0.073	DYNC1LI1, PCID2
GO:0006915~apoptotic process	7	2.63	0.086	PRKCA, TP53, BAD, TRAF7, BRAT1, SUDS3, PEG3

Table S4.2. GO terms of DMRs between 8 vs. 16-cell that hypermethylated in 16-cell

Term	Count	%	PValue	Genes
GO:0006886~intracellular protein transport	18	2.55	0.0010	VPS18, STX1A, SYNDIG1, AP1B1, SNX8, SNX17, NAPB, TSNARE1, TBC1D22A, TBC1D16, CTTN, SGSM1, TOM1L2, SGSM3, TBC1D14, GRTP1, TBC1D13, GGA3
GO:0031338~regulation of vesicle fusion	7	0.99	0.0022	TBC1D16, SGSM1, SGSM3, TBC1D14, TBC1D13, GRTP1, TBC1D22A
GO:0031175~neuron projection development	10	1.41	0.0031	NCAM1, MICALL2, EFHD1, STMN3, RASGRF1, RAB35, CAMSAP1, CAMSAP3, CAPZB, MICALL1
GO:0090630~activation of GTPase activity	9	1.27	0.0038	TBC1D16, SGSM1, SGSM3, RASGRF1, TBC1D14, TBC1D13, GRTP1, TBC1D22A, AKT2
GO:0040011~locomotion	4	0.57	0.0051	ATP2B2, JPH3, SPNS2, WDR1
GO:0007613~memory	7	0.99	0.0060	JPH3, DRD1, B4GALT2, CRTC1, TH, DBH, SORCS3
GO:0008283~cell proliferation	14	1.98	0.0080	GNAT1, PTPN6, HRAS, BYSL, RHBDF1, CSPG4, PRKDC, TACC3, BRAT1, RASGRF1, BOK, ASCC3, ERCC1, CUL1
GO:0016477~cell migration	12	1.70	0.0107	FGFR4, NDE1, PTPRF, PTK6, FSCN1, RHBDF1, CSPG4, LIMD1, TNK2, EPHB3, CD63, BRAT1
GO:2001046~positive regulation of integrin-mediated signaling pathway	3	0.42	0.0161	LIMS2, CD63, FLNA
GO:0008286~insulin receptor signaling pathway	6	0.85	0.0204	SLC2A8, PDK2, BAIAP2L2, BAIAP2, AKT2, PIK3R2
GO:0006351~transcription, DNA-templated	37	5.23	0.0210	PTOV1, ZNF18, MED22, ZNF75D, KCNIP3, PCGF3, RAX2, HSF1, SMARCB1, SND1, AGO2, ZNF444, LIMD1, TCEA2, ALX4, TFDP1, NFATC1, CTBP2, TFPT, L3MBTL2, WDR5, RXRA, TBX4, RXRG, PRKCB, UHRF1, BRMS1, ZNF692, ASCC3, RFX2, MAD2L2, PUF60, HDAC7, NR5A1, SMARCA4, ZIM2, PEG3
GO:0036010~protein localization to endosome	3	0.42	0.0236	TOLLIP, RAB35, MICALL1
GO:0007601~visual perception	10	1.41	0.0274	PDE6B, RAX2, CDHR1, TH, CACNB2, RGS9, CNGB1, GPR179, CRX, GUCY2D
GO:0030198~extracellular matrix organization	8	1.13	0.0289	SMOC2, FBLN1, ELF3, ADAMTSL2, COL27A1, POMT1, ELN, EMILIN1
GO:0010976~positive regulation of neuron projection development	6	0.85	0.0302	FGFR1, RET, PTK6, CAMK2B, RAPGEF1, MARK2
GO:0007043~cell-cell junction assembly	3	0.42	0.0321	FSCN1, TRPV4, HDAC7
GO:0031115~negative regulation of microtubule polymerization	3	0.42	0.0321	TBCD, MAPRE1, CAPZB
GO:0048227~plasma membrane to endosome transport	3	0.42	0.0321	SGSM3, RAB5C, RAB35
GO:0006897~endocytosis	9	1.27	0.0350	MARCH2, HRAS, ATP9B, SNX8, RBSN, TNK2, EHD2, MICALL1, EPN2
GO:0007257~activation of JUN kinase activity	4	0.57	0.0375	DAB2IP, MAP4K2, MAPK8IP3, AXIN1
GO:0016485~protein processing	7	0.99	0.0392	NCSTN, ATG4B, RHBDF1, F7, PCSK7, NRDC, CPZ
GO:0070527~platelet aggregation	5	0.71	0.0393	ACTB, PTPN6, FERMT3, CSRP1, FLNA
GO:2000146~negative regulation of cell motility	3	0.42	0.0416	FBLN1, SLC9A3R1, PIN1

Table S5. Differentially expressed genes between 8- and 16- cell stage with DMRs

Genes hypermethylated in 8-cell stage

	RNA Seq gene expression					WGBS methylation level			
Gene Name	8-cell	16-cell	Fold Change	log2 of Fold Change	P Value	8-cell	16-cell	P Value	q Value
ELOVL5	13.48	80.03	5.94	2.57	0.03	100	12	6.45E-11	8.25E-10
DEK	18.39	81.61	4.44	2.15	0.03	85	0	1.66E-16	5.93E-15

Genes hypermethylated in 16-cell stage

	RNA Seq gene expression					WGBS methylation level			
Gene Name	8-cell	16-cell	Fold Change	log2 of Fold Change	P Value	8-cell	16-cell	P Value	q Value
CAD	16.74	0.00	- Inf	NA	0.02	0	100	2.22E-19	9.29E-18
KIAA1191	85.57	8.51	0.10	-3.33	0.00	0	100	2.22E-19	9.29E-18

Table S6.1. GO terms for DMRs between sperm and GV oocytes

Hypermethylated genes in sperm				
Term	**Count**	**%**	**P-value**	**Genes**
GO:0007166~cell surface receptor signaling pathway	13	3.10	0.0003	EDN3, TSPAN4, ADCYAP1R1, PTH1R, CD151, GCGR, VIPR2, TSPAN11, CRHR1, TNFRSF1A, TSPAN32, ADGRB1, ADGRA1
GO:0006836~neurotransmitter transport	5	1.19	0.0005	SLC6A9, CPLX1, SLC6A12, SLC6A13, SLC6A6
GO:0009607~response to biotic stimulus	4	0.95	0.0018	IFITM1, IFITM2, IFITM3
GO:0007612~learning	5	1.19	0.0050	SLC8A3, JPH4, JPH3, SORCS3, EPHB2
GO:0030322~stabilization of membrane potential	4	0.95	0.0056	KCNN4, KCNK9, KCNK7, KCNK5
GO:0071805~potassium ion transmembrane transport	6	1.43	0.0061	HPN, KCNK9, KCNK7, SLC9A3, KCNK5, KCNIP3
GO:0007155~cell adhesion	11	2.63	0.0075	COL18A1, ISLR, LGALS3BP, TNXB, PTPRF, TTYH1, ITGAD, THBS2, SSPO, LRFN3, PARVB
GO:0043406~positive regulation of MAP kinase activity	5	1.19	0.0087	NOX4, FGFR1, EDN3, PDE5A, PIK3R6
GO:0007601~visual perception	8	1.91	0.0099	PDE6B, LAMB2, CABP4, COL1A1, OLFM2, RHO, GUCY2D, GRK1
GO:0045332~phospholipid translocation	3	0.72	0.0106	KCNN4, ATP9B, ATP8A2
GO:0043206~extracellular fibril organization	3	0.72	0.0106	TNXB, LTBP2, ADAMTS2
GO:0051601~exocyst localization	3	0.72	0.0106	EXOC3L4, EXOC3L1, TNFAIP2
GO:0042130~negative regulation of T cell proliferation	4	0.95	0.0123	MAD1L1, IL2RA, PDE5A, PLA2G2F
GO:0016337~single organismal cell-cell adhesion	6	1.43	0.0129	TNXB, LIMS2, COL13A1, PKP3, TTYH1, NTN1
GO:0043085~positive regulation of catalytic activity	4	0.95	0.0221	NCF1, DCP1B, BCL2, SFTPB
GO:0006887~exocytosis	5	1.19	0.0221	EXOC3L4, CPLX1, EXOC3L1, VAMP2, TNFAIP2
GO:0030198~extracellular matrix organization	6	1.43	0.0251	COL18A1, SMOC2, TNXB, ADAMTSL2, COL27A1, EMILIN1
GO:0022898~regulation of transmembrane transporter activity	2	0.48	0.0462	INS, BCL2
GO:0007193~adenylate cyclase-inhibiting G-protein coupled receptor signaling pathway	4	0.95	0.0477	ADCY1, GNAI2, OPRL1, GPR37L1
Hypermethylated in GV oocytes				
Term	**Count**	**%**	**P-value**	**Genes**
GO:0034613~cellular protein localization	4	2.70	0.0019	ARMCX3, CTNNA1, AXIN2, CD63
GO:0030097~hemopoiesis	3	2.03	0.0252	ADD2, KIRREL3, CDK13
GO:0007275~multicellular organism development	5	3.38	0.0476	TNFRSF1A, CDX1, TNFRSF10D, SUFU, FGF4
GO:2000643~positive regulation of early endosome to late endosome transport	2	1.35	0.0485	PTPN23, MSN

Table S6.2 GO terms for DMRs between sperm vs. *in vivo* MII

Hypermethylated in sperm				
Term	Count	%	P-value	Genes
GO:0007155~cell adhesion	11	4.38	0.0002	COL18A1, ISLR, NCAM1, TNXB, PTPRF, TTYH1, NINJ2, EPHB4, THBS2, SSPO, ITGA2B
GO:0001508~action potential	3	1.20	0.0067	KCNB1, CHRNB4, CHRNA4
GO:0007275~multicellular organism development	8	3.19	0.0089	SPEM1, TRIM54, TNFRSF10D, RTL1, COLEC11, ALX4, SUFU, QRICH1
GO:0016337~single organismal cell-cell adhesion	5	1.99	0.0101	TNXB, LIMS2, PKP1, PKP3, TTYH1
GO:0007626~locomotory behavior	5	1.99	0.0147	CHRNB4, APBA2, CHRNA4, DBH, OLFM2
GO:0035094~response to nicotine	3	1.20	0.0234	CHRNB4, CHRNA4, CHRNG
GO:0098655~cation transmembrane transport	3	1.20	0.0261	CHRNB4, CHRNA4, CHRNG
GO:0006508~proteolysis	7	2.79	0.0377	F10, CAPN5, HTRA1, CPQ, ST14, RHBDF1, DPP6
GO:1903038~negative regulation of leukocyte cell-cell adhesion	2	0.80	0.0417	PPARA, ASS1
GO:0043588~skin development	3	1.20	0.0480	RYR1, ADAMTS2, SUFU
Hypermethylated in in vivo MII				
Term	Count	%	P-value	Genes
GO:0071354~cellular response to interleukin-6	3	2.59	0.0011	SBNO2, RELA, NFKB1
GO:0034097~response to cytokine	3	2.59	0.0105	RELA, BCL2, NFKB1
GO:0030282~bone mineralization	3	2.59	0.0105	SBNO2, GPC3, PHEX
GO:2000630~positive regulation of miRNA metabolic process	2	1.72	0.0194	RELA, NFKB1
GO:0006898~receptor-mediated endocytosis	3	2.59	0.0253	CUBN, ENPP3, AMN
GO:0071316~cellular response to nicotine	2	1.72	0.0258	RELA, NFKB1
GO:0007613~memory	3	2.59	0.0279	CHRNB2, PLCB1, SORCS3
GO:0051963~regulation of synapse assembly	2	1.72	0.0321	CHRNB2, GHSR
GO:0038061~NIK/NF-kappaB signaling	2	1.72	0.0321	RELA, NFKB1
GO:0071375~cellular response to peptide hormone stimulus	2	1.72	0.0384	RELA, NFKB1
GO:2000643~positive regulation of early endosome to late endosome transport	2	1.72	0.0384	PTPN23, MSN
GO:0001778~plasma membrane repair	2	1.72	0.0447	DYSF, MYOF
GO:0022612~gland morphogenesis	2	1.72	0.0447	BCL2, MSN

Table S6.3 GO terms for DMRs between sperm vs. *in vitro* MII

Hypermethylated in sperm				
Term	Count	%	P-value	Genes
GO:1904322~cellular response to forskolin	4	0.72	0.0010	ADCY3, ADCY1, ADCY5, EFNA5
GO:0030198~extracellular matrix organization	9	1.61	0.0019	COL18A1, CSGALNACT1, SMOC2, TNXB, ADAMTSL2, COL27A1, ELN, VWA1, EMILIN1
GO:0043542~endothelial cell migration	5	0.90	0.0027	PAXIP1, PTP4A3, PECAM1, NOS3, LOXL2
GO:0002062~chondrocyte differentiation	6	1.08	0.0037	FGFR1, WNT5B, PTH1R, GLI2, RUNX1, RUNX3
GO:0007193~adenylate cyclase-inhibiting G-protein coupled receptor signaling pathway	6	1.08	0.0049	ADCY3, ADCY1, OPRL1, ADCY5, PSAPL1, GPR37L1
GO:0002159~desmosome assembly	3	0.54	0.0059	JUP, PRKCA, PKP3
GO:0019933~cAMP-mediated signaling	5	0.90	0.0089	ADCY3, ADCY1, PDE2A, ADCY5, GHRHR
GO:0002076~osteoblast development	4	0.72	0.0091	ACHE, PTH1R, LIMD1, GLI2
GO:0022400~regulation of rhodopsin mediated signaling pathway	4	0.72	0.0091	PRKCA, RGS9, RHO, GRK1
GO:0006816~calcium ion transport	6	1.08	0.0096	CACNA1G, CHRNA4, ITPR3, CAMK2A, RAMP1, CDH23
GO:0016337~single organismal cell-cell adhesion	7	1.25	0.0122	ARVCF, TNXB, LIMS2, PKP1, PKP3, TTYH1, NTN1
GO:0006814~sodium ion transport	5	0.90	0.0131	SLC13A5, ATP4B, SLC12A3, SLC13A3, SLC5A10
GO:0090630~activation of GTPase activity	7	1.25	0.0131	TBC1D16, TBC1D10C, FOXJ1, RASGRF1, TBC1D14, EVI5L, TBC1D22A
GO:0007601~visual perception	9	1.61	0.0166	UNC119, AIPL1, LAMB2, TH, CABP4, RGS9, RHO, GUCY2D, GRK1
GO:0048469~cell maturation	5	0.90	0.0184	FGFR1, SOX10, GATA2, PTH1R, GHRHR
GO:0043117~positive regulation of vascular permeability	3	0.54	0.0193	PDE2A, PTP4A3, TRPV4
GO:0051601~exocyst localization	3	0.54	0.0193	EXOC3L4, EXOC3L1, TNFAIP2
GO:0045835~negative regulation of meiotic nuclear division	3	0.54	0.0193	OSM, LIF, RPS6KA2
GO:0007626~locomotory behavior	7	1.25	0.0202	ATP2B2, ADCY5, TH, APBA2, CHRNA4, DBH, CDH23
GO:0031338~regulation of vesicle fusion	5	0.90	0.0204	TBC1D16, TBC1D10C, TBC1D14, EVI5L, TBC1D22A
GO:0007155~cell adhesion	12	2.15	0.0236	COL18A1, ISLR, NCAM1, PRKCA, VWF, ACHE, TNXB, FLOT2, PECAM1, TTYH1, THBS2, SSPO
GO:0055085~transmembrane transport	9	1.61	0.0250	SLC13A5, SLC22A18, SLC16A6, SLC25A47, SLC22A6, SLC13A3, SLC25A45, SLC5A10, SLC43A3
GO:0007189~adenylate cyclase-activating G-protein coupled receptor signaling pathway	5	0.90	0.0273	ADCY3, ADCY1, ADCY5, PTH1R, GHRHR
GO:0001525~angiogenesis	10	1.79	0.0285	COL18A1, PRKCA, FGFR1, PECAM1, NOS3, MMP2, RAMP1, VASH1, EPHB2, ANGPTL4
GO:0007219~Notch signaling pathway	7	1.25	0.0311	KRT19, PTP4A3, GMDS, MAML2, AGXT, ZNF423, ANGPTL4
GO:0045746~negative regulation of Notch signaling pathway	4	0.72	0.0320	GATA2, PEAR1, DLK1, NEURL1
GO:0007204~positive regulation of cytosolic calcium ion concentration	6	1.08	0.0354	GNA15, GALR1, OPRL1, ADCY5, TRPV4, CACNA1A
GO:0060349~bone morphogenesis	4	0.72	0.0360	T, ACP5, IFITM5, ACTN3
GO:0007613~memory	5	0.90	0.0383	CRTC1, TH, DBH, ITPR3, SORCS3
GO:0048266~behavioral response to pain	3	0.54	0.0389	OSM, VWA1, CACNA1A
GO:1901379~regulation of potassium ion transmembrane transport	3	0.54	0.0389	DPP6, KCNIP1, KCNIP3
GO:0007416~synapse assembly	4	0.72	0.0402	CEL, NRXN2, CACNA1A, KIRREL3
GO:0042511~positive regulation of tyrosine phosphorylation of Stat1 protein	3	0.54	0.0465	LIF, FGFR3, HPX
GO:0007422~peripheral nervous system development	3	0.54	0.0465	OSM, SOX10, ERBB2
GO:0045651~positive regulation of macrophage differentiation	3	0.54	0.0465	LIF, PRKCA, IL34
GO:0035987~endodermal cell differentiation	4	0.72	0.0493	LAMB3, COL6A1, ITGB2, MMP2
Hypermethylated in in vitro MII				
Term	Count	%	P-value	Genes
GO:0006898~receptor-mediated endocytosis	4	2.84	0.0027	CD163L1, CUBN, ENPP3, SCARA5
GO:0001764~neuron migration	4	2.84	0.0242	BARHL1, PRKG1, GFRA3, KIRREL3

GO:1902259~regulation of delayed rectifier potassium channel activity	2	1.42	0.0292	KCNS1, VAMP2
GO:0072112~glomerular visceral epithelial cell differentiation	2	1.42	0.0292	FOXC2, KLF15
GO:0042058~regulation of epidermal growth factor receptor signaling pathway	2	1.42	0.0364	MVB12A, RHBDF1

Table S6.4 GO terms for DMRs between GV vs. *in vivo* MII

Hypermethylated in GV				
Term	Count	%	P-value	Genes
GO:1901700~response to oxygen-containing compound	8	15.38	0.0036	EGR1, TNFRSF1A, PFKL, PTK2B, TNFRSF10D, MET, MSN, CTNNA1
GO:0001885~endothelial cell development	3	5.77	0.0055	TNFRSF1A, MET, MSN
GO:0098609~cell-cell adhesion	7	13.46	0.0094	EGR1, PDE5A, UNC5D, MSN, CTNNA1, EBI3, KIRREL3
GO:0045446~endothelial cell differentiation	3	5.77	0.0129	TNFRSF1A, MET, MSN
GO:0010646~regulation of cell communication	12	23.08	0.0147	EGR1, TNFRSF1A, MAGI3, PFKL, GRIA1, PTK2B, PREX2, PDE5A, MGLL, CTNNA1, ADAMTS3, SUFU
GO:0023051~regulation of signaling	12	23.08	0.0159	EGR1, TNFRSF1A, MAGI3, PFKL, GRIA1, PTK2B, PREX2, PDE5A, MGLL, CTNNA1, ADAMTS3, SUFU
GO:0007155~cell adhesion	8	15.38	0.0166	EGR1, PTK2B, PDE5A, UNC5D, MSN, CTNNA1, EBI3, KIRREL3
GO:0022610~biological adhesion	8	15.38	0.0170	EGR1, PTK2B, PDE5A, UNC5D, MSN, CTNNA1, EBI3, KIRREL3
GO:0003158~endothelium development	3	5.77	0.0172	TNFRSF1A, MET, MSN
GO:1904018~positive regulation of vasculature development	3	5.77	0.0305	EGR1, PTK2B, ASB4
GO:0071480~cellular response to gamma radiation	2	3.85	0.0306	EGR1, WRN
GO:0048468~cell development	9	17.31	0.0347	TNFRSF1A, PTK2B, PREX2, PDE5A, MET, UNC5D, MSN, CTNNA1, KIRREL3
GO:0000902~cell morphogenesis	7	13.46	0.0357	PTK2B, PREX2, MET, UNC5D, LRGUK, MSN, KIRREL3
GO:0043067~regulation of programmed cell death	7	13.46	0.0374	EGR1, TNFRSF1A, PTK2B, TNFRSF10D, MET, WRN, CTNNA1
GO:0048699~generation of neurons	7	13.46	0.0381	PTK2B, PREX2, UNC5D, CTNNA1, DBN1, SUFU, KIRREL3
GO:0042787~protein ubiquitination involved in ubiquitin-dependent protein catabolic process	3	5.77	0.0431	PTK2B, RNF122, SUFU
GO:0030823~regulation of cGMP metabolic process	2	3.85	0.0431	PTK2B, PDE5A
GO:2000058~regulation of protein ubiquitination involved in ubiquitin-dependent protein catabolic process	2	3.85	0.0431	PTK2B, SUFU
GO:0007163~establishment or maintenance of cell polarity	3	5.77	0.0437	PTK2B, MSN, CTNNA1
GO:0032989~cellular component morphogenesis	7	13.46	0.0464	PTK2B, PREX2, MET, UNC5D, LRGUK, MSN, KIRREL3
GO:0010941~regulation of cell death	7	13.46	0.0467	EGR1, TNFRSF1A, PTK2B, TNFRSF10D, MET, WRN, CTNNA1
GO:1901701~cellular response to oxygen-containing compound	5	9.62	0.0477	EGR1, PTK2B, MET, MSN, CTNNA1
GO:2000145~regulation of cell motility	5	9.62	0.0488	PTK2B, MET, UNC5D, MSN, CTNNA1
Hypermethylated in in vivo MII				
Term	Count	%	P-value	Genes
GO:0016192~vesicle-mediated transport	6	13.95	0.0289	CUBN, CALY, ENPP3, PTPN23, LOXL4, TNFAIP2
GO:0006897~endocytosis	4	9.30	0.0319	CUBN, CALY, ENPP3, LOXL4
GO:0006898~receptor-mediated endocytosis	3	6.98	0.0344	CUBN, ENPP3, LOXL4

Table S6.5 GO terms for DMRs between GV vs. *in vitro* MII

Hypermethylated in GV				
Term	Count	%	P-value	Genes
GO:1901700~response to oxygen-containing compound	12	0.12	0.0001	TNFRSF1A, RET, SLC38A9, PTK2B, TNFRSF10D, RPS6KA2, MET, PRDX2, NFKB1, CTNNA1, SPON2, PLCB1
GO:1901701~cellular response to oxygen-containing compound	10	0.10	0.0001	RET, SLC38A9, PTK2B, RPS6KA2, MET, PRDX2, NFKB1, CTNNA1, SPON2, PLCB1
GO:0046068~cGMP metabolic process	3	0.03	0.0060	ATP2B2, PTK2B, PDE5A
GO:0010646~regulation of cell communication	16	0.16	0.0094	KLK6, RET, MAGI3, RALGPS1, SLC38A9, NFKB1, CTNNA1, ATP2B2, TNFRSF1A, GRIA1, PTK2B, PDE5A, MNT, MGLL, DEPTOR, PLCB1
GO:0043067~regulation of programmed cell death	10	0.10	0.0100	TNFRSF1A, PTK2B, BOK, TNFRSF10D, RPS6KA2, MET, MNT, DEPTOR, PRDX2, CTNNA1
GO:0023051~regulation of signaling	16	0.16	0.0103	KLK6, RET, MAGI3, RALGPS1, SLC38A9, NFKB1, CTNNA1, ATP2B2, TNFRSF1A, GRIA1, PTK2B, PDE5A, MNT, MGLL, DEPTOR, PLCB1
GO:0010941~regulation of cell death	10	0.10	0.0139	TNFRSF1A, PTK2B, BOK, TNFRSF10D, RPS6KA2, MET, MNT, DEPTOR, PRDX2, CTNNA1
GO:2000145~regulation of cell motility	7	0.07	0.0151	RET, PTK2B, MET, PTPN23, UNC5D, CTNNA1, PLCB1
GO:0040012~regulation of locomotion	7	0.07	0.0187	RET, PTK2B, MET, PTPN23, UNC5D, CTNNA1, PLCB1
GO:0008219~cell death	11	0.11	0.0202	KLK6, TNFRSF1A, PTK2B, BOK, TNFRSF10D, RPS6KA2, MET, MNT, DEPTOR, PRDX2, CTNNA1
GO:0040011~locomotion	10	0.10	0.0207	ATP2B2, RET, PTK2B, MET, PTPN23, UNC5D, CTNNA1, PLCB1, GFRA3, KIRREL3
GO:0051270~regulation of cellular component movement	7	0.07	0.0208	RET, PTK2B, MET, PTPN23, UNC5D, CTNNA1, PLCB1
GO:0033993~response to lipid	6	0.06	0.0230	TNFRSF1A, RET, PTK2B, TNFRSF10D, NFKB1, SPON2
GO:0007166~cell surface receptor signaling pathway	13	0.13	0.0237	TNFRSF1A, RET, CPE, PTK2B, BOK, TNFRSF10D, CD82, MET, NFKB1, CTNNA1, ADGRB1, PLCB1, FAM83G
GO:0009966~regulation of signal transduction	14	0.14	0.0241	KLK6, RET, MAGI3, RALGPS1, SLC38A9, NFKB1, CTNNA1, TNFRSF1A, PTK2B, PDE5A, MNT, MGLL, DEPTOR, PLCB1
GO:0048870~cell motility	9	0.09	0.0270	RET, PTK2B, MET, PTPN23, UNC5D, CTNNA1, PLCB1, GFRA3, KIRREL3
GO:0042981~regulation of apoptotic process	9	0.09	0.0270	TNFRSF1A, PTK2B, BOK, TNFRSF10D, RPS6KA2, MNT, DEPTOR, PRDX2, CTNNA1
GO:0051674~localization of cell	9	0.09	0.0270	RET, PTK2B, MET, PTPN23, UNC5D, CTNNA1, PLCB1, GFRA3, KIRREL3
GO:0097190~apoptotic signaling pathway	6	0.06	0.0279	TNFRSF1A, BOK, TNFRSF10D, MNT, DEPTOR, CTNNA1
GO:0032496~response to lipopolysaccharide	4	0.04	0.0302	TNFRSF1A, TNFRSF10D, NFKB1, SPON2
GO:0097191~extrinsic apoptotic signaling pathway	4	0.04	0.0311	TNFRSF1A, BOK, TNFRSF10D, CTNNA1
GO:0012501~programmed cell death	10	0.10	0.0364	TNFRSF1A, PTK2B, BOK, TNFRSF10D, RPS6KA2, MET, MNT, DEPTOR, PRDX2, CTNNA1
GO:0002237~response to molecule of bacterial origin	4	0.04	0.0370	TNFRSF1A, TNFRSF10D, NFKB1, SPON2
GO:0006928~movement of cell or subcellular component	10	0.10	0.0403	TNNT2, RET, PTK2B, MET, PTPN23, UNC5D, CTNNA1, PLCB1, GFRA3, KIRREL3
GO:0016477~cell migration	8	0.08	0.0418	RET, PTK2B, MET, PTPN23, UNC5D, PLCB1, GFRA3, KIRREL3
GO:0007155~cell adhesion	9	0.09	0.0420	RET, PKP1, PTK2B, PDE5A, PTPN23, UNC5D, CTNNA1, THBS2, KIRREL3
GO:0070887~cellular response to chemical stimulus	12	0.12	0.0422	TNFRSF1A, RET, SLC38A9, PTK2B, RPS6KA2, MET, PRDX2, NFKB1, CTNNA1, SPON2, PLCB1, FAM83G
GO:0030334~regulation of cell migration	6	0.06	0.0428	RET, PTK2B, MET, PTPN23, UNC5D, PLCB1
GO:0022610~biological adhesion	9	0.09	0.0430	RET, PKP1, PTK2B, PDE5A, PTPN23, UNC5D, CTNNA1, THBS2, KIRREL3
GO:0035556~intracellular signal transduction	13	0.13	0.0446	TNFRSF1A, MAGI3, RET, RALGPS1, SLC38A9, RAB37, PTK2B, BOK, RPS6KA2, PDE5A, DEPTOR, NFKB1, PLCB1
GO:0071229~cellular response to acid chemical	3	0.03	0.0470	RET, SLC38A9, PTK2B
GO:0055065~metal ion homeostasis	5	0.05	0.0477	ATP2B2, CNNM4, ATP2B3, PTK2B, SCNN1A
GO:0009612~response to mechanical stimulus	3	0.03	0.0488	TNFRSF1A, ATP2B2, NFKB1
Hypermethylated in in vitro MII				
Term	Count	%	P-value	Genes
GO:0006898~receptor-mediated endocytosis	4	9.30	0.0059	RAMP3, LGALS3BP, CUBN, ENPP3

GO:0032835~glomerulus development	3	6.98	0.0062	FOXC2, KLF15, KIRREL3
GO:0006897~endocytosis	5	11.63	0.0111	RAMP3, LGALS3BP, CUBN, CALY, ENPP3
GO:0007610~behavior	5	11.63	0.0182	NRXN2, FBXL20, CHRNA4, SORCS3, KIRREL3
GO:0001764~neuron migration	3	6.98	0.0270	PRKG1, GFRA3, KIRREL3
GO:0072006~nephron development	3	6.98	0.0305	FOXC2, KLF15, KIRREL3
GO:0061318~renal filtration cell differentiation	2	4.65	0.0322	FOXC2, KLF15
GO:0072112~glomerular visceral epithelial cell differentiation	2	4.65	0.0322	FOXC2, KLF15
GO:0044708~single-organism behavior	4	9.30	0.0324	NRXN2, FBXL20, CHRNA4, SORCS3
GO:0072311~glomerular epithelial cell differentiation	2	4.65	0.0346	FOXC2, KLF15
GO:0003013~circulatory system process	4	9.30	0.0360	RAMP3, PDE5A, FOXC2, PRKG1
GO:0072010~glomerular epithelium development	2	4.65	0.0370	FOXC2, KLF15
GO:0045932~negative regulation of muscle contraction	2	4.65	0.0394	PDE5A, PRKG1
GO:0090075~relaxation of muscle	2	4.65	0.0419	PDE5A, PRKG1

Table S6.6 GO terms for DMRs between *in vivo* MII vs. *in vitro* MII

Hypermethylated in in vivo MII				
Term	Count	%	P-value	Genes
GO:2000643~positive regulation of early endosome to late endosome transport	2	4.55	0.0141	PTPN23, MSN
GO:0051128~regulation of cellular component organization	10	22.73	0.0154	FGFR1, PHLDB1, RPS6KA2, ARHGEF19, PTPN23, MSN, LMOD1, BIN1, ZW10, OPRD1
GO:1903651~positive regulation of cytoplasmic transport	2	4.55	0.0164	PTPN23, MSN
GO:1903337~positive regulation of vacuolar transport	2	4.55	0.0234	PTPN23, MSN
GO:2000641~regulation of early endosome to late endosome transport	2	4.55	0.0234	PTPN23, MSN
GO:1903649~regulation of cytoplasmic transport	2	4.55	0.0257	PTPN23, MSN
GO:1903335~regulation of vacuolar transport	2	4.55	0.0417	PTPN23, MSN
Hypermethylated in in vitro MII				
Term	Count	%	P-value	Genes
GO:0098609~cell-cell adhesion	7	17.5	0.0051	EGR1, PDE5A, TTYH1, RARA, MSN, CTNNA1, KIRREL3
GO:0032835~glomerulus development	3	7.5	0.0051	EGR1, KLF15, KIRREL3
GO:0016337~single organismal cell-cell adhesion	6	15	0.0075	EGR1, PDE5A, TTYH1, RARA, MSN, CTNNA1
GO:0007155~cell adhesion	8	20	0.0085	EGR1, PDE5A, TTYH1, RARA, MSN, CTNNA1, SSPO, KIRREL3
GO:0022610~biological adhesion	8	20	0.0087	EGR1, PDE5A, TTYH1, RARA, MSN, CTNNA1, SSPO, KIRREL3
GO:0098602~single organism cell adhesion	6	15	0.0106	EGR1, PDE5A, TTYH1, RARA, MSN, CTNNA1
GO:0001822~kidney development	4	10	0.0110	EGR1, RARA, KLF15, KIRREL3
GO:0072001~renal system development	4	10	0.0134	EGR1, RARA, KLF15, KIRREL3
GO:0001655~urogenital system development	4	10	0.0193	EGR1, RARA, KLF15, KIRREL3
GO:0048609~multicellular organismal reproductive process	5	12.5	0.0202	EGR1, OSBP2, PDE5A, RARA, LRGUK
GO:0032504~multicellular organism reproduction	5	12.5	0.0212	EGR1, OSBP2, PDE5A, RARA, LRGUK
GO:0072006~nephron development	3	7.5	0.0256	EGR1, KLF15, KIRREL3
GO:0044702~single organism reproductive process	6	15	0.0341	EGR1, OSBP2, PDE5A, TTPA, RARA, LRGUK
GO:0022414~reproductive process	6	15	0.0446	EGR1, OSBP2, PDE5A, TTPA, RARA, LRGUK
GO:0000003~reproduction	6	15	0.0450	EGR1, OSBP2, PDE5A, TTPA, RARA, LRGUK
GO:0048468~cell development	8	20	0.0496	OSBP2, PREX2, PDE5A, TTPA, RARA, MSN, CTNNA1, KIRREL3

Table S7.1 Gene expression for DMRs between sperm and GV oocytes

Gene expression in DMRs from GV vs. Sperm							
Gene	**Chr**	**GV_me**	**Sperm_me**	**p-value**	**q-value**	**GV expression**	**Spmer expression**
PFKL	AC_000158.1	0	100	2.22E-19	3.30E-18	0.888	0.197475
PLCL2	AC_000158.1	0	100	2.22E-19	3.30E-18	11.425	45.9542
NYNRIN	AC_000167.1	0	80	1.24E-15	1.32E-14	0.287	3.66222
JPH4	AC_000167.1	0	100	2.22E-19	3.30E-18	0.095	7.74329
KATNBL1	AC_000167.1	76	0	6.99E-15	7.30E-14	17.392	19.9724
SAMD4A	AC_000167.1	0	83	3.95E-16	4.80E-15	0.229	92.4821
SLC8A3	AC_000167.1	0	100	2.22E-19	3.30E-18	0.035	0.271869
MERTK	AC_000168.1	80	0	1.24E-15	1.32E-14	1.856	4.29607
SEMA4C	AC_000168.1	0	100	2.22E-19	3.30E-18	0.174	2.54157
SEMA4C	AC_000168.1	0	100	2.22E-19	3.30E-18	0.174	2.54157
FHL2	AC_000168.1	0	100	2.22E-19	3.30E-18	4.781	8.26512
DYSF	AC_000168.1	75	0	1.25E-14	1.28E-13	0.372	2.59209
DYSF	AC_000168.1	100	7	2.90E-13	2.83E-12	0.372	2.59209
DYSF	AC_000168.1	80	20	6.94E-06	2.81E-05	0.372	2.59209
ADD2	AC_000168.1	80	0	1.24E-15	1.32E-14	2.157	0.106467
CAMKMT	AC_000168.1	100	5	1.69E-14	1.73E-13	1.742	13.4428
EMILIN1	AC_000168.1	0	100	2.22E-19	3.30E-18	0.121	2.56389
OTOF	AC_000168.1	0	100	2.22E-19	3.30E-18	0.074	0.0557878
DNMT3A	AC_000168.1	80	16	7.24E-07	3.49E-06	2.959	2.73006
NOL10	AC_000168.1	0	100	2.22E-19	3.30E-18	20.124	20.8117
RALGPS1	AC_000168.1	80	0	1.24E-15	1.32E-14	2.175	23.5689
RALGPS1	AC_000168.1	80	18	2.38E-06	1.04E-05	2.175	23.5689
ENG	AC_000168.1	0	80	1.24E-15	1.32E-14	0.13	5.34783
AIF1L	AC_000168.1	0	100	2.22E-19	3.30E-18	0.079	2.89621
NTNG2	AC_000168.1	0	100	2.22E-19	3.30E-18	0.108	0.683614
AK8	AC_000168.1	0	80	1.24E-15	1.32E-14	0.377	44.5611
GFI1B	AC_000168.1	0	100	2.22E-19	3.30E-18	2.411	0.0413428
GFI1B	AC_000168.1	0	100	2.22E-19	3.30E-18	2.411	0.0413428
RALGDS	AC_000168.1	85	0	1.66E-16	2.20E-15	10.95	7.0163
INPP5E	AC_000168.1	0	100	2.22E-19	3.30E-18	0.551	8.13702
AGPAT2	AC_000168.1	12	80	4.35E-08	2.36E-07	0.54	9.63912
SARDH	AC_000168.1	9	100	3.27E-12	2.95E-11	0.083	0.12003
SARDH	AC_000168.1	0	100	2.22E-19	3.30E-18	0.083	0.12003
SARDH	AC_000168.1	0	100	2.22E-19	3.30E-18	0.083	0.12003
TPRN	AC_000168.1	0	100	2.22E-19	3.30E-18	0.548	1.47106
TPRN	AC_000168.1	0	83	3.95E-16	4.80E-15	0.548	1.47106
RXRA	AC_000168.1	0	100	2.22E-19	3.30E-18	1.763	0.201091
IFITM2	AC_000168.1	0	90	1.66E-17	2.40E-16	0.997	80.6682

PCDH17	AC_000169.1	83	0	3.95E-16	4.80E-15	0.277	1.29798
ARL11	AC_000169.1	11	100	2.69E-11	2.18E-10	0.41	0.261074
MYCBP2	AC_000169.1	75	8	7.09E-09	4.60E-08	11.59	14.5207
DOCK9	AC_000169.1	93	10	9.09E-11	7.03E-10	21.342	5.15748
DOCK9	AC_000169.1	88	18	2.56E-07	1.29E-06	21.342	5.15748
RAB20	AC_000169.1	0	100	2.22E-19	3.30E-18	0.13	0.975288
RASA3	AC_000169.1	0	100	2.22E-19	3.30E-18	0.065	1.43627
RASA3	AC_000169.1	0	100	2.22E-19	3.30E-18	0.065	1.43627
RASA3	AC_000169.1	0	100	2.22E-19	3.30E-18	0.065	1.43627
RASA3	AC_000169.1	0	100	2.22E-19	3.30E-18	0.065	1.43627
RASA3	AC_000169.1	0	100	2.22E-19	3.30E-18	0.065	1.43627
RASA3	AC_000169.1	0	100	2.22E-19	3.30E-18	0.065	1.43627
RASA3	AC_000169.1	0	100	2.22E-19	3.30E-18	0.065	1.43627
PLCB1	AC_000170.1	85	21	3.15E-06	1.36E-05	2.134	1.56312
PLCB1	AC_000170.1	80	10	8.02E-09	5.15E-08	2.134	1.56312
PLCB1	AC_000170.1	90	25	5.95E-06	2.48E-05	2.134	1.56312
PLCB1	AC_000170.1	100	2	5.84E-17	8.25E-16	2.134	1.56312
PLCB1	AC_000170.1	93	21	3.73E-07	1.86E-06	2.134	1.56312
SFMBT2	AC_000170.1	0	83	3.95E-16	4.80E-15	1.462	4.04179
PFKFB3	AC_000170.1	0	100	2.22E-19	3.30E-18	1.697	6.93267
IL2RA	AC_000170.1	0	100	2.22E-19	3.30E-18	5.055	0.169466
CUBN	AC_000170.1	100	0	2.22E-19	3.30E-18	0.254	4.77637
DIP2C	AC_000170.1	0	100	2.22E-19	3.30E-18	0.766	12.4809
TCEA2	AC_000170.1	20	100	2.92E-08	1.72E-07	0.957	36.3719
SAMD10	AC_000170.1	0	100	2.22E-19	3.30E-18	0.05	0.151801
TRIB3	AC_000170.1	0	80	1.24E-15	1.32E-14	0.076	0.121916
NECAB3	AC_000170.1	0	100	2.22E-19	3.30E-18	0.096	3.25575
NECAB3	AC_000170.1	83	0	3.95E-16	4.80E-15	0.096	3.25575
CHMP4B	AC_000170.1	80	5	3.50E-11	2.77E-10	10.25	17.6036
KCNB1	AC_000170.1	0	100	2.22E-19	3.30E-18	0.011	0.595133
BCAS4	AC_000170.1	0	100	2.22E-19	3.30E-18	2.562	1.27598
BCAS4	AC_000170.1	0	100	2.22E-19	3.30E-18	2.562	1.27598
SLC39A4	AC_000171.1	0	100	2.22E-19	3.30E-18	0.143	0.49789
DGAT1	AC_000171.1	100	0	2.22E-19	3.30E-18	5.034	9.26291
NRBP2	AC_000171.1	0	75	1.25E-14	1.28E-13	0.015	0.416031
VAMP2	AC_000171.1	0	83	3.95E-16	4.80E-15	8.347	5.04003
VAMP2	AC_000171.1	0	100	2.22E-19	3.30E-18	8.347	5.04003
VAMP2	AC_000171.1	0	100	2.22E-19	3.30E-18	8.347	5.04003
VAMP2	AC_000171.1	0	100	2.22E-19	3.30E-18	8.347	5.04003
VAMP2	AC_000171.1	0	93	5.27E-18	7.78E-17	8.347	5.04003
VAMP2	AC_000171.1	0	100	2.22E-19	3.30E-18	8.347	5.04003
VAMP2	AC_000171.1	0	100	2.22E-19	3.30E-18	8.347	5.04003
VAMP2	AC_000171.1	0	100	2.22E-19	3.30E-18	8.347	5.04003
ARC	AC_000171.1	20	100	2.92E-08	1.72E-07	0.173	0.0375706
TSNARE1	AC_000171.1	0	100	2.22E-19	3.30E-18	1.913	0.00898524

TSNARE1	AC_000171.1	0	100	2.22E-19	3.30E-18	1.913	0.00898524
TSNARE1	AC_000171.1	0	100	2.22E-19	3.30E-18	1.913	0.00898524
TSNARE1	AC_000171.1	0	80	1.24E-15	1.32E-14	1.913	0.00898524
TRAPPC9	AC_000171.1	0	100	2.22E-19	3.30E-18	2.403	10.3207
ASAP1	AC_000171.1	0	100	2.22E-19	3.30E-18	39.817	4.84221
ASAP1	AC_000171.1	10	90	2.77E-10	2.09E-09	39.817	4.84221
TTPA	AC_000171.1	76	11	6.43E-08	3.45E-07	0.139	1.44846
PREX2	AC_000171.1	100	10	8.84E-12	7.26E-11	0.157	1.02787
PREX2	AC_000171.1	76	15	1.29E-06	5.88E-06	0.157	1.02787
PREX2	AC_000171.1	80	21	1.20E-05	4.73E-05	0.157	1.02787
DEPTOR	AC_000171.1	100	11	2.69E-11	2.18E-10	4.076	0.937093
DEPTOR	AC_000171.1	80	11	2.08E-08	1.27E-07	4.076	0.937093
ALKBH8	AC_000172.1	16	75	3.16E-06	1.36E-05	3.047	3.89821
PDE2A	AC_000172.1	0	85	1.66E-16	2.20E-15	0.039	2.68373
PDE2A	AC_000172.1	0	85	1.66E-16	2.20E-15	0.039	2.68373
ARRB1	AC_000172.1	80	0	1.24E-15	1.32E-14	0.907	0.862835
ZNF408	AC_000172.1	16	100	1.86E-09	1.25E-08	1.262	1.9867
MYBPC3	AC_000172.1	0	100	2.22E-19	3.30E-18	0.01	0.272787
RGS7	AC_000173.1	80	11	2.08E-08	1.27E-07	1.014	0.674704
RGS7	AC_000173.1	82	15	1.98E-07	1.01E-06	1.014	0.674704
LAD1	AC_000173.1	20	100	2.92E-08	1.72E-07	3.584	0.0617539
CSRP1	AC_000173.1	0	100	2.22E-19	3.30E-18	0.036	22.8617
ACAP3	AC_000173.1	20	100	2.92E-08	1.72E-07	0.299	0.365091
PLXNA2	AC_000173.1	0	100	2.22E-19	3.30E-18	0.033	2.16689
CPE	AC_000174.1	75	20	2.62E-05	9.81E-05	5.305	7.84652
CUX2	AC_000174.1	80	0	1.24E-15	1.32E-14	45.73	0.223335
ACADS	AC_000174.1	100	0	2.22E-19	3.30E-18	3.249	3.73854
SGSM1	AC_000174.1	100	0	2.22E-19	3.30E-18	0.268	1.15444
EMID1	AC_000174.1	0	100	2.22E-19	3.30E-18	1.867	1.45839
EMID1	AC_000174.1	0	100	2.22E-19	3.30E-18	1.867	1.45839
EMID1	AC_000174.1	0	100	2.22E-19	3.30E-18	1.867	1.45839
OSBP2	AC_000174.1	10	100	8.84E-12	7.26E-11	1.183	14.0231
SUSD2	AC_000174.1	0	100	2.22E-19	3.30E-18	0.012	0.533469
GGT5	AC_000174.1	20	100	2.92E-08	1.72E-07	1.886	0.631976
GGT5	AC_000174.1	20	100	2.92E-08	1.72E-07	1.886	0.631976
GGT1	AC_000174.1	0	100	2.22E-19	3.30E-18	0.027	0.665504
GGT1	AC_000174.1	0	100	2.22E-19	3.30E-18	0.027	0.665504
SLC7A4	AC_000174.1	0	100	2.22E-19	3.30E-18	0.019	0.587754
GNB1L	AC_000174.1	16	80	7.24E-07	3.49E-06	2.053	0.53128
TXNRD2	AC_000174.1	0	100	2.22E-19	3.30E-18	1.364	0.0301001
TXNRD2	AC_000174.1	0	100	2.22E-19	3.30E-18	1.364	0.0301001
CTRB1	AC_000175.1	0	80	1.24E-15	1.32E-14	0.338	2.03802
SLC7A5	AC_000175.1	20	100	2.92E-08	1.72E-07	0.103	22.6674
SLC22A31	AC_000175.1	100	12	6.45E-11	5.03E-10	1.469	1.63851
ZNF423	AC_000175.1	0	100	2.22E-19	3.30E-18	0.009	1.49701

ZNF423	AC_000175.1	0	100	2.22E-19	3.30E-18	0.009	1.49701
ZNF423	AC_000175.1	0	88	3.94E-17	5.58E-16	0.009	1.49701
EXOC3L1	AC_000175.1	0	100	2.22E-19	3.30E-18	1.545	1.44007
PEPD	AC_000175.1	0	100	2.22E-19	3.30E-18	0.057	3.74324
PEPD	AC_000175.1	0	100	2.22E-19	3.30E-18	0.057	3.74324
PEPD	AC_000175.1	0	100	2.22E-19	3.30E-18	0.057	3.74324
GPI	AC_000175.1	16	85	1.60E-07	8.31E-07	115.286	52.6938
FXYD1	AC_000175.1	0	83	3.95E-16	4.80E-15	0.387	5.61115
LRFN3	AC_000175.1	0	83	3.95E-16	4.80E-15	0.489	0.822277
C18H19orf47	AC_000175.1	0	85	1.66E-16	2.20E-15	6.111	1.74616
KCNN4	AC_000175.1	0	100	2.22E-19	3.30E-18	9.122	0.0324022
KLC3	AC_000175.1	20	90	4.80E-07	2.36E-06	2.236	0.6625
KDELR1	AC_000175.1	100	0	2.22E-19	3.30E-18	12	15.9696
FCGRT	AC_000175.1	0	88	3.94E-17	5.58E-16	3.272	0.128583
NLRP12	AC_000175.1	100	0	2.22E-19	3.30E-18	0.013	0.0885662
FIZ1	AC_000175.1	100	0	2.22E-19	3.30E-18	0.675	0.0353889
TTYH1	AC_000175.1	0	100	2.22E-19	3.30E-18	0.927	53.4688
TMC4	AC_000175.1	80	0	1.24E-15	1.32E-14	11.065	0.246617
ZIM2	AC_000175.1	0	100	2.22E-19	3.30E-18	33.988	0.068638
MSI2	AC_000176.1	0	81	9.35E-16	1.13E-14	1.261	3.4265
MSI2	AC_000176.1	0	100	2.22E-19	3.30E-18	1.261	3.4265
RNF43	AC_000176.1	0	100	2.22E-19	3.30E-18	2.151	0.584618
GAS2L2	AC_000176.1	0	100	2.22E-19	3.30E-18	0.351	0.147563
GAS2L2	AC_000176.1	0	100	2.22E-19	3.30E-18	0.351	0.147563
MNT	AC_000176.1	100	0	2.22E-19	3.30E-18	4.813	1.52517
P2RX1	AC_000176.1	0	100	2.22E-19	3.30E-18	30.979	0.134512
SLC35G6	AC_000176.1	0	100	2.22E-19	3.30E-18	0.381	14.2108
GUCY2D	AC_000176.1	16	100	1.86E-09	1.25E-08	0.207	0.0841453
PER1	AC_000176.1	0	80	1.24E-15	1.32E-14	21.299	7.59761
CCDC42	AC_000176.1	0	100	2.22E-19	3.30E-18	32.208	25.8806
NTN1	AC_000176.1	0	100	2.22E-19	3.30E-18	2.205	0.550449
SGCA	AC_000176.1	0	83	3.95E-16	4.80E-15	0.551	4.48E-05
RPL19	AC_000176.1	77	23	5.94E-05	2.11E-04	1281.436	133.855
FBXL20	AC_000176.1	100	14	3.79E-10	2.81E-09	29.104	6.7384
GRB7	AC_000176.1	0	100	2.22E-19	3.30E-18	0.587	0.375847
HDAC5	AC_000176.1	0	100	2.22E-19	3.30E-18	0.54	7.63568
PLCD3	AC_000176.1	0	81	9.35E-16	1.13E-14	2.178	1.43795
CRHR1	AC_000176.1	0	83	3.95E-16	4.80E-15	0.075	3.05045
RBFOX3	AC_000176.1	0	100	2.22E-19	3.30E-18	0.287	0.0541617
RBFOX3	AC_000176.1	0	100	2.22E-19	3.30E-18	0.287	0.0541617
RBFOX3	AC_000176.1	0	100	2.22E-19	3.30E-18	0.287	0.0541617
LGALS3BP	AC_000176.1	0	100	2.22E-19	3.30E-18	0.158	12.465
LGALS3BP	AC_000176.1	0	100	2.22E-19	3.30E-18	0.158	12.465
LGALS3BP	AC_000176.1	0	100	2.22E-19	3.30E-18	0.158	12.465
SEC14L1	AC_000176.1	0	80	1.24E-15	1.32E-14	18.812	31.2194

ST6GALNAC2	AC_000176.1	0	100	2.22E-19	3.30E-18	2.707	23.0638
RAB37	AC_000176.1	80	0	1.24E-15	1.32E-14	5.424	0.531397
RAB37	AC_000176.1	80	10	8.02E-09	5.15E-08	5.424	0.531397
RAB37	AC_000176.1	83	0	3.95E-16	4.80E-15	5.424	0.531397
RAB37	AC_000176.1	87	7	3.08E-11	2.44E-10	5.424	0.531397
RAB37	AC_000176.1	83	15	1.57E-07	8.18E-07	5.424	0.531397
RAB37	AC_000176.1	80	20	6.94E-06	2.81E-05	5.424	0.531397
RAB37	AC_000176.1	85	25	2.09E-05	7.94E-05	5.424	0.531397
TTYH2	AC_000176.1	0	100	2.22E-19	3.30E-18	0.025	2.69215
ABCA9	AC_000176.1	0	100	2.22E-19	3.30E-18	0.128	1.46739
AXIN2	AC_000176.1	100	0	2.22E-19	3.30E-18	2.486	0.321127
LIMS2	AC_000159.1	0	100	2.22E-19	3.30E-18	0.017	12.1793
LIMS2	AC_000159.1	0	100	2.22E-19	3.30E-18	0.017	12.1793
TFCP2L1	AC_000159.1	0	100	2.22E-19	3.30E-18	0.096	1.95606
4-Mar	AC_000159.1	100	0	2.22E-19	3.30E-18	0.525	0.0251621
TNS1	AC_000159.1	0	100	2.22E-19	3.30E-18	0.613	8.80054
TNS1	AC_000159.1	0	100	2.22E-19	3.30E-18	0.613	8.80054
TNS1	AC_000159.1	0	100	2.22E-19	3.30E-18	0.613	8.80054
DNPEP	AC_000159.1	80	0	1.24E-15	1.32E-14	13.277	88.9103
SLC4A3	AC_000159.1	0	100	2.22E-19	3.30E-18	0.187	1.40557
SLC4A3	AC_000159.1	0	100	2.22E-19	3.30E-18	0.187	1.40557
ZCCHC17	AC_000159.1	0	100	2.22E-19	3.30E-18	16.436	38.4618
CD164L2	AC_000159.1	0	75	1.25E-14	1.28E-13	37.44	4.59861
EPHB2	AC_000159.1	0	100	2.22E-19	3.30E-18	0.013	0.528627
EPHB2	AC_000159.1	0	100	2.22E-19	3.30E-18	0.013	0.528627
EPHB2	AC_000159.1	20	100	2.92E-08	1.72E-07	0.013	0.528627
EPHB2	AC_000159.1	0	100	2.22E-19	3.30E-18	0.013	0.528627
EPHB2	AC_000159.1	0	100	2.22E-19	3.30E-18	0.013	0.528627
PADI4	AC_000159.1	0	100	2.22E-19	3.30E-18	0.019	0.107179
PADI4	AC_000159.1	20	100	2.92E-08	1.72E-07	0.019	0.107179
PADI1	AC_000159.1	0	100	2.22E-19	3.30E-18	0.565	0.00684407
ZNF366	AC_000177.1	80	0	1.24E-15	1.32E-14	1.066	0.245052
SLC38A9	AC_000177.1	80	5	3.50E-11	2.77E-10	23.88	12.0679
SLC38A9	AC_000177.1	83	13	3.69E-08	2.13E-07	23.88	12.0679
BRD9	AC_000177.1	0	100	2.22E-19	3.30E-18	8.891	7.39757
SLC9A3	AC_000177.1	0	100	2.22E-19	3.30E-18	0.741	0.282475
ST8SIA2	AC_000178.1	20	100	2.92E-08	1.72E-07	0.686	2.57432
MRPS11	AC_000178.1	100	16	1.86E-09	1.25E-08	24.469	1.91452
ARNT2	AC_000178.1	0	100	2.22E-19	3.30E-18	2.224	2.29686
ACSBG1	AC_000178.1	0	100	2.22E-19	3.30E-18	0.042	11.0506
ISL2	AC_000178.1	100	0	2.22E-19	3.30E-18	7.716	0.0596224
FRMD5	AC_000178.1	91	6	1.77E-12	1.63E-11	8.882	0.203298
FRMD5	AC_000178.1	100	21	5.72E-08	3.07E-07	8.882	0.203298
FRMD5	AC_000178.1	75	12	2.23E-07	1.13E-06	8.882	0.203298
FRMD5	AC_000178.1	76	23	7.24E-05	2.54E-04	8.882	0.203298

FRMD5	AC_000178.1	100	0	2.22E-19	3.30E-18	8.882	0.203298
FRMD5	AC_000178.1	80	16	7.24E-07	3.49E-06	8.882	0.203298
FRMD5	AC_000178.1	80	11	2.08E-08	1.27E-07	8.882	0.203298
EXOC3L4	AC_000178.1	0	80	1.24E-15	1.32E-14	0.433	0.202865
EXOC3L4	AC_000178.1	16	80	7.24E-07	3.49E-06	0.433	0.202865
TNFAIP2	AC_000178.1	0	100	2.22E-19	3.30E-18	0.091	3.27001
TNFAIP2	AC_000178.1	0	100	2.22E-19	3.30E-18	0.091	3.27001
TNFAIP2	AC_000178.1	14	100	3.79E-10	2.81E-09	0.091	3.27001
TNFAIP2	AC_000178.1	14	100	3.79E-10	2.81E-09	0.091	3.27001
TNFAIP2	AC_000178.1	20	100	2.92E-08	1.72E-07	0.091	3.27001
ADSSL1	AC_000178.1	0	100	2.22E-19	3.30E-18	0.028	14.3029
ADSSL1	AC_000178.1	0	100	2.22E-19	3.30E-18	0.028	14.3029
ADSSL1	AC_000178.1	0	100	2.22E-19	3.30E-18	0.028	14.3029
ADSSL1	AC_000178.1	0	90	1.66E-17	2.40E-16	0.028	14.3029
VILL	AC_000179.1	0	100	2.22E-19	3.30E-18	0.021	3.56041
SYNPR	AC_000179.1	80	22	1.84E-05	7.05E-05	1.72	0.493366
SYNPR	AC_000179.1	80	4	7.32E-12	6.05E-11	1.72	0.493366
ERC2	AC_000179.1	80	0	1.24E-15	1.32E-14	5.638	0.399069
SFMBT1	AC_000179.1	16	80	7.24E-07	3.49E-06	9.88	17.3451
GNAI2	AC_000179.1	0	85	1.66E-16	2.20E-15	11.738	62.7405
APEH	AC_000179.1	100	0	2.22E-19	3.30E-18	2.519	12.0954
LAMB2	AC_000179.1	0	100	2.22E-19	3.30E-18	0.113	0.0489692
LAMB2	AC_000179.1	0	83	3.95E-16	4.80E-15	0.113	0.0489692
H1FOO	AC_000179.1	0	100	2.22E-19	3.30E-18	638.647	1.64813
RHO	AC_000179.1	0	100	2.22E-19	3.30E-18	0.538	0.102191
RHO	AC_000179.1	0	100	2.22E-19	3.30E-18	0.538	0.102191
SLC6A6	AC_000179.1	0	100	2.22E-19	3.30E-18	0.189	8.29457
NUP210	AC_000179.1	0	100	2.22E-19	3.30E-18	0.119	2.69E-06
NUP210	AC_000179.1	12	100	6.45E-11	5.03E-10	0.119	2.69E-06
NUP210	AC_000179.1	100	16	1.86E-09	1.25E-08	0.119	2.69E-06
NUP210	AC_000179.1	0	100	2.22E-19	3.30E-18	0.119	2.69E-06
EEFSEC	AC_000179.1	0	100	2.22E-19	3.30E-18	1.196	3.16696
EEFSEC	AC_000179.1	0	100	2.22E-19	3.30E-18	1.196	3.16696
EEFSEC	AC_000179.1	0	83	3.95E-16	4.80E-15	1.196	3.16696
EEFSEC	AC_000179.1	0	100	2.22E-19	3.30E-18	1.196	3.16696
MGLL	AC_000179.1	0	100	2.22E-19	3.30E-18	0.776	4.96885
MGLL	AC_000179.1	0	88	3.94E-17	5.58E-16	0.776	4.96885
MGLL	AC_000179.1	0	100	2.22E-19	3.30E-18	0.776	4.96885
MGLL	AC_000179.1	0	100	2.22E-19	3.30E-18	0.776	4.96885
MGLL	AC_000179.1	0	100	2.22E-19	3.30E-18	0.776	4.96885
MGLL	AC_000179.1	0	100	2.22E-19	3.30E-18	0.776	4.96885
MGLL	AC_000179.1	0	100	2.22E-19	3.30E-18	0.776	4.96885
MGLL	AC_000179.1	0	100	2.22E-19	3.30E-18	0.776	4.96885
MGLL	AC_000179.1	0	80	1.24E-15	1.32E-14	0.776	4.96885
CHCHD6	AC_000179.1	20	100	2.92E-08	1.72E-07	1.991	0.0769569

ALDH1L1	AC_000179.1	0	100	2.22E-19	3.30E-18	0.018	0.125084
MAPK13	AC_000180.1	16	100	1.86E-09	1.25E-08	0.124	1.2245
RNF8	AC_000180.1	80	15	4.06E-07	2.01E-06	173.175	24.6931
MRPL2	AC_000180.1	100	0	2.22E-19	3.30E-18	63.72	25.8689
HIST1H1C	AC_000180.1	80	12	4.35E-08	2.36E-07	168.516	0.347191
MAK	AC_000180.1	85	0	1.66E-16	2.20E-15	1.998	20.5848
TUBB2B	AC_000180.1	0	100	2.22E-19	3.30E-18	4.438	2.88E-07
GMDS	AC_000180.1	0	100	2.22E-19	3.30E-18	1.846	29.0845
GMDS	AC_000180.1	0	100	2.22E-19	3.30E-18	1.846	29.0845
GMDS	AC_000180.1	20	87	1.14E-06	5.21E-06	1.846	29.0845
GMDS	AC_000180.1	0	100	2.22E-19	3.30E-18	1.846	29.0845
GMDS	AC_000180.1	0	100	2.22E-19	3.30E-18	1.846	29.0845
GMDS	AC_000180.1	0	100	2.22E-19	3.30E-18	1.846	29.0845
PARD6G	AC_000181.1	0	100	2.22E-19	3.30E-18	0.18	0.705794
ATP9B	AC_000181.1	0	100	2.22E-19	3.30E-18	1.054	20.9405
CELF4	AC_000181.1	0	100	2.22E-19	3.30E-18	0.892	0.498227
KCTD1	AC_000181.1	100	10	8.84E-12	7.26E-11	3.893	2.85029
ST8SIA5	AC_000181.1	100	0	2.22E-19	3.30E-18	0.098	0.267697
ST8SIA5	AC_000181.1	0	100	2.22E-19	3.30E-18	0.098	0.267697
BCL2	AC_000181.1	0	100	2.22E-19	3.30E-18	0.742	2.29554
BCL2	AC_000181.1	0	100	2.22E-19	3.30E-18	0.742	2.29554
PDIA2	AC_000182.1	0	100	2.22E-19	3.30E-18	0.193	0.0197089
PDIA2	AC_000182.1	0	100	2.22E-19	3.30E-18	0.193	0.0197089
AXIN1	AC_000182.1	0	87	7.02E-17	9.70E-16	8.127	2.99307
FBXL16	AC_000182.1	100	20	2.92E-08	1.72E-07	0.915	0.756621
FBXL16	AC_000182.1	20	83	3.33E-06	1.43E-05	0.915	0.756621
MAPK8IP3	AC_000182.1	0	100	2.22E-19	3.30E-18	3.017	2.75834
TBL3	AC_000182.1	0	83	3.95E-16	4.80E-15	1.21	9.98598
DNAH3	AC_000182.1	100	20	2.92E-08	1.72E-07	0.334	6.18503
QPRT	AC_000182.1	0	80	1.24E-15	1.32E-14	0.074	1.49625
NCF1	AC_000182.1	0	100	2.22E-19	3.30E-18	0.347	0.120512
GTF2IRD1	AC_000182.1	0	100	2.22E-19	3.30E-18	0.277	1.03709
GTF2IRD1	AC_000182.1	0	100	2.22E-19	3.30E-18	0.277	1.03709
POLR2J	AC_000182.1	0	87	7.02E-17	9.70E-16	939.48	5.48768
LRWD1	AC_000182.1	0	100	2.22E-19	3.30E-18	1.981	9.38676
COL26A1	AC_000182.1	0	100	2.22E-19	3.30E-18	0.01	0.355506
COL26A1	AC_000182.1	0	100	2.22E-19	3.30E-18	0.01	0.355506
TRIM56	AC_000182.1	0	85	1.66E-16	2.20E-15	0.004	0.267774
TMEM130	AC_000182.1	0	100	2.22E-19	3.30E-18	0.151	0.498274
CARD11	AC_000182.1	0	100	2.22E-19	3.30E-18	0.036	0.584971
LFNG	AC_000182.1	0	100	2.22E-19	3.30E-18	1.155	2.2758
LFNG	AC_000182.1	0	100	2.22E-19	3.30E-18	1.155	2.2758
LFNG	AC_000182.1	0	100	2.22E-19	3.30E-18	1.155	2.2758
LFNG	AC_000182.1	0	100	2.22E-19	3.30E-18	1.155	2.2758
MAD1L1	AC_000182.1	0	100	2.22E-19	3.30E-18	0.594	2.44948

MAD1L1	AC_000182.1	0	100	2.22E-19	3.30E-18	0.594	2.44948
MAD1L1	AC_000182.1	0	100	2.22E-19	3.30E-18	0.594	2.44948
MAD1L1	AC_000182.1	0	87	7.02E-17	9.70E-16	0.594	2.44948
TMEM184A	AC_000182.1	0	100	2.22E-19	3.30E-18	0.062	0.466166
TMEM184A	AC_000182.1	0	100	2.22E-19	3.30E-18	0.062	0.466166
TMEM184A	AC_000182.1	0	100	2.22E-19	3.30E-18	0.062	0.466166
MICALL2	AC_000182.1	0	100	2.22E-19	3.30E-18	0.551	0.182125
MICALL2	AC_000182.1	0	100	2.22E-19	3.30E-18	0.551	0.182125
MICALL2	AC_000182.1	0	100	2.22E-19	3.30E-18	0.551	0.182125
MICALL2	AC_000182.1	20	100	2.92E-08	1.72E-07	0.551	0.182125
MICALL2	AC_000182.1	20	80	6.94E-06	2.81E-05	0.551	0.182125
ADAP1	AC_000182.1	0	100	2.22E-19	3.30E-18	28.765	0.734833
ADAP1	AC_000182.1	0	100	2.22E-19	3.30E-18	28.765	0.734833
ADAP1	AC_000182.1	0	83	3.95E-16	4.80E-15	28.765	0.734833
MYOF	AC_000183.1	100	9	3.27E-12	2.95E-11	6.025	12.114
CRTAC1	AC_000183.1	0	100	2.22E-19	3.30E-18	0.289	0.0517082
CRTAC1	AC_000183.1	0	100	2.22E-19	3.30E-18	0.289	0.0517082
LOXL4	AC_000183.1	0	100	2.22E-19	3.30E-18	0.014	0.144052
SUFU	AC_000183.1	0	100	2.22E-19	3.30E-18	2.698	3.82115
SUFU	AC_000183.1	20	100	2.92E-08	1.72E-07	2.698	3.82115
SUFU	AC_000183.1	75	6	8.00E-10	5.54E-09	2.698	3.82115
SUFU	AC_000183.1	0	100	2.22E-19	3.30E-18	2.698	3.82115
SORCS3	AC_000183.1	0	100	2.22E-19	3.30E-18	8.191	20.632
SORCS3	AC_000183.1	20	88	8.27E-07	3.96E-06	8.191	20.632
SORCS3	AC_000183.1	0	100	2.22E-19	3.30E-18	8.191	20.632
SORCS3	AC_000183.1	0	100	2.22E-19	3.30E-18	8.191	20.632
SORCS3	AC_000183.1	0	83	3.95E-16	4.80E-15	8.191	20.632
SORCS3	AC_000183.1	0	100	2.22E-19	3.30E-18	8.191	20.632
SORCS3	AC_000183.1	0	85	1.66E-16	2.20E-15	8.191	20.632
SORCS3	AC_000183.1	0	80	1.24E-15	1.32E-14	8.191	20.632
SORCS3	AC_000183.1	0	100	2.22E-19	3.30E-18	8.191	20.632
SORCS3	AC_000183.1	0	80	1.24E-15	1.32E-14	8.191	20.632
CTBP2	AC_000183.1	0	100	2.22E-19	3.30E-18	21.969	0.0139396
PTPRE	AC_000183.1	0	100	2.22E-19	3.30E-18	1.274	1.64891
IRF2	AC_000184.1	0	100	2.22E-19	3.30E-18	0.511	4.58319
CFAP97	AC_000184.1	80	0	1.24E-15	1.32E-14	20.386	67.3662
WRN	AC_000184.1	88	0	3.94E-17	5.58E-16	10.07	8.79611
WRN	AC_000184.1	80	0	1.24E-15	1.32E-14	10.07	8.79611
WRN	AC_000184.1	75	0	1.25E-14	1.28E-13	10.07	8.79611
WRN	AC_000184.1	100	5	1.69E-14	1.73E-13	10.07	8.79611
WRN	AC_000184.1	100	0	2.22E-19	3.30E-18	10.07	8.79611
WRN	AC_000184.1	83	0	3.95E-16	4.80E-15	10.07	8.79611
WRN	AC_000184.1	83	0	3.95E-16	4.80E-15	10.07	8.79611
WRN	AC_000184.1	80	0	1.24E-15	1.32E-14	10.07	8.79611
WRN	AC_000184.1	80	0	1.24E-15	1.32E-14	10.07	8.79611

WRN	AC_000184.1	100	4	2.93E-15	3.09E-14	10.07	8.79611
WRN	AC_000184.1	78	0	2.95E-15	3.11E-14	10.07	8.79611
WRN	AC_000184.1	100	7	2.90E-13	2.83E-12	10.07	8.79611
WRN	AC_000184.1	91	6	1.77E-12	1.63E-11	10.07	8.79611
WRN	AC_000184.1	100	9	3.27E-12	2.95E-11	10.07	8.79611
WRN	AC_000184.1	100	13	1.74E-10	1.32E-09	10.07	8.79611
WRN	AC_000184.1	87	10	8.39E-10	5.80E-09	10.07	8.79611
WRN	AC_000184.1	81	14	1.53E-07	7.97E-07	10.07	8.79611
WRN	AC_000184.1	87	18	3.61E-07	1.80E-06	10.07	8.79611
WRN	AC_000184.1	85	18	5.63E-07	2.75E-06	10.07	8.79611
WRN	AC_000184.1	83	17	5.72E-07	2.80E-06	10.07	8.79611
WRN	AC_000184.1	100	0	2.22E-19	3.30E-18	10.07	8.79611
WRN	AC_000184.1	100	0	2.22E-19	3.30E-18	10.07	8.79611
WRN	AC_000184.1	83	0	3.95E-16	4.80E-15	10.07	8.79611
WRN	AC_000184.1	81	0	9.35E-16	1.13E-14	10.07	8.79611
WRN	AC_000184.1	80	0	1.24E-15	1.32E-14	10.07	8.79611
WRN	AC_000184.1	80	0	1.24E-15	1.32E-14	10.07	8.79611
WRN	AC_000184.1	80	2	2.15E-13	2.12E-12	10.07	8.79611
WRN	AC_000184.1	100	13	1.74E-10	1.32E-09	10.07	8.79611
WRN	AC_000184.1	89	12	2.24E-09	1.50E-08	10.07	8.79611
WRN	AC_000184.1	89	13	5.59E-09	3.66E-08	10.07	8.79611
WRN	AC_000184.1	100	20	2.92E-08	1.72E-07	10.07	8.79611
WRN	AC_000184.1	80	12	4.35E-08	2.36E-07	10.07	8.79611
WRN	AC_000184.1	90	19	2.52E-07	1.28E-06	10.07	8.79611
WRN	AC_000184.1	76	13	2.97E-07	1.49E-06	10.07	8.79611
WRN	AC_000184.1	88	25	1.06E-05	4.21E-05	10.07	8.79611
WRN	AC_000184.1	93	0	5.27E-18	7.78E-17	10.07	8.79611
WRN	AC_000184.1	82	0	5.25E-16	6.39E-15	10.07	8.79611
WRN	AC_000184.1	97	7	7.91E-13	7.35E-12	10.07	8.79611
WRN	AC_000184.1	85	7	6.35E-11	4.99E-10	10.07	8.79611
WRN	AC_000184.1	100	12	6.45E-11	5.03E-10	10.07	8.79611
WRN	AC_000184.1	75	5	2.05E-10	1.55E-09	10.07	8.79611
WRN	AC_000184.1	100	16	1.86E-09	1.25E-08	10.07	8.79611
WRN	AC_000184.1	87	12	5.03E-09	3.30E-08	10.07	8.79611
WRN	AC_000184.1	100	20	2.92E-08	1.72E-07	10.07	8.79611
WRN	AC_000184.1	83	22	9.08E-06	3.65E-05	10.07	8.79611
RNF122	AC_000184.1	80	7	4.23E-10	3.12E-09	9.872	10.1717
RNF122	AC_000184.1	100	20	2.92E-08	1.72E-07	9.872	10.1717
RNF122	AC_000184.1	83	22	9.08E-06	3.65E-05	9.872	10.1717
RNF122	AC_000184.1	0	100	2.22E-19	3.30E-18	9.872	10.1717
RNF122	AC_000184.1	80	0	1.24E-15	1.32E-14	9.872	10.1717
RNF122	AC_000184.1	75	14	9.09E-07	4.25E-06	9.872	10.1717
RNF122	AC_000184.1	100	0	2.22E-19	3.30E-18	9.872	10.1717
RNF122	AC_000184.1	83	0	3.95E-16	4.80E-15	9.872	10.1717
RNF122	AC_000184.1	80	3	1.61E-12	1.48E-11	9.872	10.1717

RNF122	AC_000184.1	80	0	1.24E-15	1.32E-14	9.872	10.1717
RNF122	AC_000184.1	80	0	1.24E-15	1.32E-14	9.872	10.1717
RNF122	AC_000184.1	100	20	2.92E-08	1.72E-07	9.872	10.1717
RNF122	AC_000184.1	20	91	3.85E-07	1.92E-06	9.872	10.1717
RNF122	AC_000184.1	75	25	2.10E-04	6.57E-04	9.872	10.1717
RNF122	AC_000184.1	75	25	2.10E-04	6.57E-04	9.872	10.1717
RNF122	AC_000184.1	100	14	3.79E-10	2.81E-09	9.872	10.1717
RNF122	AC_000184.1	90	25	6.49E-06	2.70E-05	9.872	10.1717
RNF122	AC_000184.1	100	0	2.22E-19	3.30E-18	9.872	10.1717
RNF122	AC_000184.1	80	0	1.24E-15	1.32E-14	9.872	10.1717
RNF122	AC_000184.1	100	7	2.90E-13	2.83E-12	9.872	10.1717
RNF122	AC_000184.1	80	11	2.08E-08	1.27E-07	9.872	10.1717
RNF122	AC_000184.1	80	13	1.01E-07	5.30E-07	9.872	10.1717
RNF122	AC_000184.1	83	20	3.33E-06	1.43E-05	9.872	10.1717
RNF122	AC_000184.1	100	0	2.22E-19	3.30E-18	9.872	10.1717
RNF122	AC_000184.1	0	80	1.24E-15	1.32E-14	9.872	10.1717
RNF122	AC_000184.1	80	6	1.16E-10	8.91E-10	9.872	10.1717
RNF122	AC_000184.1	80	20	6.94E-06	2.81E-05	9.872	10.1717
RNF122	AC_000184.1	77	22	3.69E-05	1.34E-04	9.872	10.1717
RNF122	AC_000184.1	100	9	3.27E-12	2.95E-11	9.872	10.1717
RNF122	AC_000184.1	80	12	4.35E-08	2.36E-07	9.872	10.1717
RNF122	AC_000184.1	88	25	1.06E-05	4.21E-05	9.872	10.1717
RNF122	AC_000184.1	85	13	1.98E-08	1.21E-07	9.872	10.1717
RNF122	AC_000184.1	80	11	2.08E-08	1.27E-07	9.872	10.1717
RNF122	AC_000184.1	80	11	2.08E-08	1.27E-07	9.872	10.1717
RNF122	AC_000184.1	80	16	7.24E-07	3.49E-06	9.872	10.1717
RNF122	AC_000184.1	83	18	1.10E-06	5.02E-06	9.872	10.1717
RNF122	AC_000184.1	0	85	1.66E-16	2.20E-15	9.872	10.1717
RNF122	AC_000184.1	81	20	5.62E-06	2.36E-05	9.872	10.1717
RNF122	AC_000184.1	80	25	7.02E-05	2.46E-04	9.872	10.1717
RNF122	AC_000184.1	80	25	7.02E-05	2.46E-04	9.872	10.1717
RNF122	AC_000184.1	83	11	7.24E-09	4.69E-08	9.872	10.1717
RNF122	AC_000184.1	80	16	7.24E-07	3.49E-06	9.872	10.1717
RNF122	AC_000184.1	0	100	2.22E-19	3.30E-18	9.872	10.1717
RNF122	AC_000184.1	0	78	2.95E-15	3.11E-14	9.872	10.1717
RNF122	AC_000184.1	80	4	7.32E-12	6.05E-11	9.872	10.1717
RNF122	AC_000184.1	85	9	5.67E-10	3.93E-09	9.872	10.1717
RNF122	AC_000184.1	75	14	9.09E-07	4.25E-06	9.872	10.1717
RNF122	AC_000184.1	0	83	3.95E-16	4.80E-15	9.872	10.1717
RNF122	AC_000184.1	80	0	1.24E-15	1.32E-14	9.872	10.1717
RNF122	AC_000184.1	80	16	7.24E-07	3.49E-06	9.872	10.1717
RNF122	AC_000184.1	100	0	2.22E-19	3.30E-18	9.872	10.1717
RNF122	AC_000184.1	78	4	1.58E-11	1.30E-10	9.872	10.1717
RNF122	AC_000184.1	75	9	1.70E-08	1.05E-07	9.872	10.1717
RNF122	AC_000184.1	80	16	7.24E-07	3.49E-06	9.872	10.1717

RNF122	AC_000184.1	100	14	3.79E-10	2.81E-09	9.872	10.1717
RNF122	AC_000184.1	80	9	3.43E-09	2.27E-08	9.872	10.1717
RNF122	AC_000184.1	80	10	8.02E-09	5.15E-08	9.872	10.1717
RNF122	AC_000184.1	80	15	4.06E-07	2.01E-06	9.872	10.1717
RNF122	AC_000184.1	80	15	4.06E-07	2.01E-06	9.872	10.1717
RNF122	AC_000184.1	77	16	1.60E-06	7.23E-06	9.872	10.1717
RNF122	AC_000184.1	20	84	2.42E-06	1.06E-05	9.872	10.1717
RNF122	AC_000184.1	80	4	7.32E-12	6.05E-11	9.872	10.1717
RNF122	AC_000184.1	88	0	3.94E-17	5.58E-16	9.872	10.1717
RNF122	AC_000184.1	85	0	1.66E-16	2.20E-15	9.872	10.1717
RNF122	AC_000184.1	10	75	4.51E-08	2.45E-07	9.872	10.1717
RNF122	AC_000184.1	80	18	2.38E-06	1.04E-05	9.872	10.1717
RNF122	AC_000184.1	78	0	2.95E-15	3.11E-14	9.872	10.1717
RNF122	AC_000184.1	100	7	2.90E-13	2.83E-12	9.872	10.1717
RNF122	AC_000184.1	80	18	2.38E-06	1.04E-05	9.872	10.1717
RNF122	AC_000184.1	0	80	1.24E-15	1.32E-14	9.872	10.1717
RNF122	AC_000184.1	0	75	1.25E-14	1.28E-13	9.872	10.1717
RNF122	AC_000184.1	100	15	9.23E-10	6.36E-09	9.872	10.1717
RNF122	AC_000184.1	90	12	1.75E-09	1.20E-08	9.872	10.1717
RNF122	AC_000184.1	75	11	9.55E-08	5.06E-07	9.872	10.1717
RNF122	AC_000184.1	80	0	1.24E-15	1.32E-14	9.872	10.1717
RNF122	AC_000184.1	80	9	3.43E-09	2.27E-08	9.872	10.1717
RNF122	AC_000184.1	75	23	9.52E-05	3.26E-04	9.872	10.1717
RNF122	AC_000184.1	90	0	1.66E-17	2.40E-16	9.872	10.1717
RNF122	AC_000184.1	83	0	3.95E-16	4.80E-15	9.872	10.1717
RNF122	AC_000184.1	80	4	7.32E-12	6.05E-11	9.872	10.1717
RNF122	AC_000184.1	100	20	2.92E-08	1.72E-07	9.872	10.1717
RNF122	AC_000184.1	85	17	3.24E-07	1.62E-06	9.872	10.1717
RNF122	AC_000184.1	75	15	1.62E-06	7.31E-06	9.872	10.1717
RNF122	AC_000184.1	80	19	4.34E-06	1.85E-05	9.872	10.1717
RNF122	AC_000184.1	83	21	5.30E-06	2.22E-05	9.872	10.1717
RNF122	AC_000184.1	83	0	3.95E-16	4.80E-15	9.872	10.1717
RNF122	AC_000184.1	83	4	2.57E-12	2.35E-11	9.872	10.1717
RNF122	AC_000184.1	88	18	2.56E-07	1.29E-06	9.872	10.1717
RNF122	AC_000184.1	85	0	1.66E-16	2.20E-15	9.872	10.1717
RNF122	AC_000184.1	85	10	1.65E-09	1.12E-08	9.872	10.1717
RNF122	AC_000184.1	100	25	5.20E-07	2.55E-06	9.872	10.1717
RNF122	AC_000184.1	92	24	2.34E-06	1.03E-05	9.872	10.1717
RNF122	AC_000184.1	80	4	7.32E-12	6.05E-11	9.872	10.1717
RNF122	AC_000184.1	88	16	7.03E-08	3.76E-07	9.872	10.1717
RNF122	AC_000184.1	75	25	2.10E-04	6.57E-04	9.872	10.1717
RNF122	AC_000184.1	80	16	7.24E-07	3.49E-06	9.872	10.1717
RNF122	AC_000184.1	100	0	2.22E-19	3.30E-18	9.872	10.1717
UNC5D	AC_000184.1	100	1	5.75E-18	8.47E-17	9.564	0.293699
UNC5D	AC_000184.1	100	5	1.69E-14	1.73E-13	9.564	0.293699

UNC5D	AC_000184.1	100	15	9.23E-10	6.36E-09	9.564	0.293699
UNC5D	AC_000184.1	97	15	2.19E-09	1.47E-08	9.564	0.293699
UNC5D	AC_000184.1	100	17	4.16E-09	2.74E-08	9.564	0.293699
UNC5D	AC_000184.1	88	18	2.56E-07	1.29E-06	9.564	0.293699
UNC5D	AC_000184.1	100	24	2.94E-07	1.48E-06	9.564	0.293699
UNC5D	AC_000184.1	100	24	2.94E-07	1.48E-06	9.564	0.293699
FGFR1	AC_000184.1	0	100	2.22E-19	3.30E-18	1.222	4.27163
FGFR1	AC_000184.1	0	100	2.22E-19	3.30E-18	1.222	4.27163
SFRP1	AC_000184.1	0	75	1.25E-14	1.28E-13	4.191	0.563249
ARV1	AC_000185.1	100	0	2.22E-19	3.30E-18	6.677	41.2131
SYT15	AC_000185.1	0	83	3.95E-16	4.80E-15	0.017	0.0270671
ROBO4	AC_000186.1	0	100	2.22E-19	3.30E-18	0.264	1.91423
ST14	AC_000186.1	0	83	3.95E-16	4.80E-15	0.066	0.233181
FADS2	AC_000186.1	0	100	2.22E-19	3.30E-18	0.051	34.409
FADS2	AC_000186.1	0	100	2.22E-19	3.30E-18	0.051	34.409
MACROD1	AC_000186.1	0	80	1.24E-15	1.32E-14	5.449	8.30819
MACROD1	AC_000186.1	0	100	2.22E-19	3.30E-18	5.449	8.30819
MACROD1	AC_000186.1	0	100	2.22E-19	3.30E-18	5.449	8.30819
MACROD1	AC_000186.1	0	83	3.95E-16	4.80E-15	5.449	8.30819
MACROD1	AC_000186.1	0	80	1.24E-15	1.32E-14	5.449	8.30819
MACROD1	AC_000186.1	0	80	1.24E-15	1.32E-14	5.449	8.30819
MACROD1	AC_000186.1	0	100	2.22E-19	3.30E-18	5.449	8.30819
NRXN2	AC_000186.1	0	100	2.22E-19	3.30E-18	0.23	4.57515
LTBP3	AC_000186.1	80	0	1.24E-15	1.32E-14	0.2	4.5186
KCNK7	AC_000186.1	0	100	2.22E-19	3.30E-18	5.012	0.153702
KCNK7	AC_000186.1	0	100	2.22E-19	3.30E-18	5.012	0.153702
MAP3K11	AC_000186.1	20	100	2.92E-08	1.72E-07	3.373	1.86971
KLC2	AC_000186.1	75	0	1.25E-14	1.28E-13	0.59	19.3057
ALDH3B1	AC_000186.1	0	80	1.24E-15	1.32E-14	0.14	1.67588
GAL	AC_000186.1	0	100	2.22E-19	3.30E-18	0.129	0.502274
ANO1	AC_000186.1	0	100	2.22E-19	3.30E-18	0.03	52.6666
ANO1	AC_000186.1	0	100	2.22E-19	3.30E-18	0.03	52.6666
ANO1	AC_000186.1	0	100	2.22E-19	3.30E-18	0.03	52.6666
TSPAN4	AC_000186.1	0	100	2.22E-19	3.30E-18	0.216	2.43992
CD151	AC_000186.1	0	100	2.22E-19	3.30E-18	5.355	2.44507
PKP3	AC_000186.1	0	100	2.22E-19	3.30E-18	0.108	0.0558369
IFITM3	AC_000186.1	0	100	2.22E-19	3.30E-18	0.745	19.5725
IFITM3	AC_000186.1	0	100	2.22E-19	3.30E-18	0.745	19.5725
IGSF9	AC_000160.1	0	83	3.95E-16	4.80E-15	0.148	0.376391
IGSF9	AC_000160.1	0	100	2.22E-19	3.30E-18	0.148	0.376391
IGSF9	AC_000160.1	0	80	1.24E-15	1.32E-14	0.148	0.376391
MUC1	AC_000160.1	0	88	3.94E-17	5.58E-16	0.529	0.33369
PHGDH	AC_000160.1	0	100	2.22E-19	3.30E-18	0.183	8.71506
ATP1A1	AC_000160.1	85	11	3.76E-09	2.48E-08	68.749	148.908
ATP1A1	AC_000160.1	88	18	2.56E-07	1.29E-06	68.749	148.908

TRIM33	AC_000160.1	100	14	3.79E-10	2.81E-09	64.699	18.3993
MYBPHL	AC_000160.1	0	100	2.22E-19	3.30E-18	0.121	0.238176
SLC44A5	AC_000160.1	80	0	1.24E-15	1.32E-14	15.46	7.84819
LRP8	AC_000160.1	0	100	2.22E-19	3.30E-18	0.404	27.1152
ERI3	AC_000160.1	0	100	2.22E-19	3.30E-18	16.469	8.40504
ERI3	AC_000160.1	0	100	2.22E-19	3.30E-18	16.469	8.40504
SLC6A9	AC_000160.1	25	100	5.20E-07	2.55E-06	0.4	0.408613
SLC6A9	AC_000160.1	25	100	5.20E-07	2.55E-06	0.4	0.408613
PTPRF	AC_000160.1	0	83	3.95E-16	4.80E-15	1.055	4.93606
PTPRF	AC_000160.1	11	100	2.69E-11	2.18E-10	1.055	4.93606
PTPRF	AC_000160.1	0	100	2.22E-19	3.30E-18	1.055	4.93606
PTPRF	AC_000160.1	0	100	2.22E-19	3.30E-18	1.055	4.93606
YBX1	AC_000160.1	100	0	2.22E-19	3.30E-18	167.373	136.83
SCLY	AC_000160.1	0	85	1.66E-16	2.20E-15	5.341	1.3474
HES6	AC_000160.1	100	20	2.92E-08	1.72E-07	0.019	1.23965
PPP1R7	AC_000160.1	100	11	2.69E-11	2.18E-10	1.141	49.8063
THAP4	AC_000160.1	100	9	3.27E-12	2.95E-11	11.392	3.32E-10
THAP4	AC_000160.1	0	80	1.24E-15	1.32E-14	11.392	3.32E-10
PDCD1	AC_000160.1	0	100	2.22E-19	3.30E-18	0.018	0.19741
GRB10	AC_000161.1	0	100	2.22E-19	3.30E-18	1.866	0.612057
ZPBP	AC_000161.1	0	87	7.02E-17	9.70E-16	10.6	139.982
ASB4	AC_000161.1	100	2	5.84E-17	8.25E-16	0.292	2.29124
ASB4	AC_000161.1	90	4	1.49E-13	1.47E-12	0.292	2.29124
ASB4	AC_000161.1	100	10	8.84E-12	7.26E-11	0.292	2.29124
ASB4	AC_000161.1	83	6	3.47E-11	2.75E-10	0.292	2.29124
ASB4	AC_000161.1	75	4	5.64E-11	4.44E-10	0.292	2.29124
ASB4	AC_000161.1	92	18	8.16E-08	4.36E-07	0.292	2.29124
KIAA1324L	AC_000161.1	85	11	3.76E-09	2.48E-08	14.742	26.3772
KIAA1324L	AC_000161.1	80	15	4.06E-07	2.01E-06	14.742	26.3772
KIAA1324L	AC_000161.1	75	17	5.30E-06	2.22E-05	14.742	26.3772
KIAA1324L	AC_000161.1	80	0	1.24E-15	1.32E-14	14.742	26.3772
LHFPL3	AC_000161.1	77	0	5.26E-15	5.50E-14	88.447	0.712787
LHFPL3	AC_000161.1	80	12	4.35E-08	2.36E-07	88.447	0.712787
LHFPL3	AC_000161.1	14	83	8.33E-08	4.44E-07	88.447	0.712787
LHFPL3	AC_000161.1	76	22	4.90E-05	1.77E-04	88.447	0.712787
PIK3CG	AC_000161.1	100	9	3.27E-12	2.95E-11	0.008	2.34793
MET	AC_000161.1	100	17	4.16E-09	2.74E-08	0.14	3.35075
MET	AC_000161.1	93	15	7.59E-09	4.91E-08	0.14	3.35075
MET	AC_000161.1	80	11	2.08E-08	1.27E-07	0.14	3.35075
MET	AC_000161.1	87	18	3.61E-07	1.80E-06	0.14	3.35075
HOXA3	AC_000161.1	100	0	2.22E-19	3.30E-18	7.99	0.576763
GTPBP10	AC_000161.1	0	100	2.22E-19	3.30E-18	36.996	16.8739
GTPBP10	AC_000161.1	83	0	3.95E-16	4.80E-15	36.996	16.8739
GTPBP10	AC_000161.1	0	100	2.22E-19	3.30E-18	36.996	16.8739
ADCY1	AC_000161.1	0	90	1.66E-17	2.40E-16	0.047	2.7462

CAMK2B	AC_000161.1	0	100	2.22E-19	3.30E-18	0.723	0.127235
CAMK2B	AC_000161.1	0	100	2.22E-19	3.30E-18	0.723	0.127235
CAMK2B	AC_000161.1	12	100	6.45E-11	5.03E-10	0.723	0.127235
CAMK2B	AC_000161.1	0	100	2.22E-19	3.30E-18	0.723	0.127235
CAMK2B	AC_000161.1	0	100	2.22E-19	3.30E-18	0.723	0.127235
CDK13	AC_000161.1	100	4	2.93E-15	3.09E-14	20.688	15.9006
CDK13	AC_000161.1	100	8	9.20E-13	8.52E-12	20.688	15.9006
CDK13	AC_000161.1	80	11	2.08E-08	1.27E-07	20.688	15.9006
CDK13	AC_000161.1	81	15	2.83E-07	1.43E-06	20.688	15.9006
CDK13	AC_000161.1	100	4	2.93E-15	3.09E-14	20.688	15.9006
CDK13	AC_000161.1	100	8	9.20E-13	8.52E-12	20.688	15.9006
CDK13	AC_000161.1	80	11	2.08E-08	1.27E-07	20.688	15.9006
CDK13	AC_000161.1	81	15	2.83E-07	1.43E-06	20.688	15.9006
FLNC	AC_000161.1	0	100	2.22E-19	3.30E-18	25.289	0.616482
SMO	AC_000161.1	16	100	1.86E-09	1.25E-08	0.345	4.28726
COPG2	AC_000161.1	100	0	2.22E-19	3.30E-18	81.719	38.8886
MKLN1	AC_000161.1	80	20	6.94E-06	2.81E-05	122.779	54.2709
LRGUK	AC_000161.1	83	10	3.22E-09	2.14E-08	2.844	4.2307
LRGUK	AC_000161.1	80	0	1.24E-15	1.32E-14	2.844	4.2307
LRGUK	AC_000161.1	100	16	1.86E-09	1.25E-08	2.844	4.2307
LRGUK	AC_000161.1	100	25	5.20E-07	2.55E-06	2.844	4.2307
LRGUK	AC_000161.1	80	16	7.24E-07	3.49E-06	2.844	4.2307
LRGUK	AC_000161.1	83	20	3.33E-06	1.43E-05	2.844	4.2307
LRGUK	AC_000161.1	85	0	1.66E-16	2.20E-15	2.844	4.2307
LRGUK	AC_000161.1	0	75	1.25E-14	1.28E-13	2.844	4.2307
LRGUK	AC_000161.1	75	0	1.25E-14	1.28E-13	2.844	4.2307
LRGUK	AC_000161.1	77	11	5.04E-08	2.73E-07	2.844	4.2307
LRGUK	AC_000161.1	80	14	1.93E-07	9.80E-07	2.844	4.2307
LRGUK	AC_000161.1	90	20	4.80E-07	2.36E-06	2.844	4.2307
LRGUK	AC_000161.1	75	16	3.16E-06	1.36E-05	2.844	4.2307
LRGUK	AC_000161.1	80	8	1.14E-09	7.86E-09	2.844	4.2307
LRGUK	AC_000161.1	100	19	1.64E-08	1.02E-07	2.844	4.2307
LRGUK	AC_000161.1	77	22	3.69E-05	1.34E-04	2.844	4.2307
SLC13A4	AC_000161.1	0	100	2.22E-19	3.30E-18	0.01	0.0585892
UBN2	AC_000161.1	92	10	1.40E-10	1.07E-09	55.015	3.21039
UBN2	AC_000161.1	77	0	5.26E-15	5.50E-14	55.015	3.21039
UBN2	AC_000161.1	84	2	4.19E-14	4.26E-13	55.015	3.21039
UBN2	AC_000161.1	96	10	3.54E-11	2.80E-10	55.015	3.21039
UBN2	AC_000161.1	76	5	1.27E-10	9.69E-10	55.015	3.21039
UBN2	AC_000161.1	100	16	1.86E-09	1.25E-08	55.015	3.21039
UBN2	AC_000161.1	83	21	5.30E-06	2.22E-05	55.015	3.21039
UBN2	AC_000161.1	80	7	4.23E-10	3.12E-09	55.015	3.21039
UBN2	AC_000161.1	84	12	1.22E-08	7.78E-08	55.015	3.21039
UBN2	AC_000161.1	80	12	4.35E-08	2.36E-07	55.015	3.21039
SSPO	AC_000161.1	0	80	1.24E-15	1.32E-14	0.002	6.73901

SSPO	AC_000161.1	20	100	2.92E-08	1.72E-07	0.002	6.73901
LRRC61	AC_000161.1	0	100	2.22E-19	3.30E-18	0.447	0.902497
ASIC3	AC_000161.1	0	100	2.22E-19	3.30E-18	0.247	0.0670749
CDK5	AC_000161.1	0	80	1.24E-15	1.32E-14	117.235	3.36212
TMUB1	AC_000161.1	12	100	6.45E-11	5.03E-10	3.563	0.833155
GALNTL5	AC_000161.1	100	14	3.79E-10	2.81E-09	0.18	0.229288
SP7	AC_000162.1	0	100	2.22E-19	3.30E-18	0.01	0.0416708
SPRYD3	AC_000162.1	80	0	1.24E-15	1.32E-14	1.286	10.0505
NR4A1	AC_000162.1	0	100	2.22E-19	3.30E-18	27.527	59.1168
ENDOU	AC_000162.1	0	80	1.24E-15	1.32E-14	0.548	0.858649
CD63	AC_000162.1	100	0	2.22E-19	3.30E-18	121.698	43.8496
ITPR2	AC_000162.1	100	14	3.79E-10	2.81E-09	2.054	0.00624904
CHD4	AC_000162.1	100	20	2.92E-08	1.72E-07	21.262	32.8897
TNFRSF1A	AC_000162.1	80	0	1.24E-15	1.32E-14	0.315	15.1137
TNFRSF1A	AC_000162.1	0	100	2.22E-19	3.30E-18	0.315	15.1137
SCNN1A	AC_000162.1	80	0	1.24E-15	1.32E-14	4.3	1.35987
TSPAN11	AC_000162.1	0	100	2.22E-19	3.30E-18	0.029	0.189952
DCP1B	AC_000162.1	25	100	5.20E-07	2.55E-06	0.063	13.4787
3-Sep	AC_000162.1	0	100	2.22E-19	3.30E-18	18.311	6.71972
PARVB	AC_000162.1	0	100	2.22E-19	3.30E-18	0.016	0.260424
PARVB	AC_000162.1	0	85	1.66E-16	2.20E-15	0.016	0.260424
PARVB	AC_000162.1	0	83	3.95E-16	4.80E-15	0.016	0.260424
PARVB	AC_000162.1	0	100	2.22E-19	3.30E-18	0.016	0.260424
TTC38	AC_000162.1	0	100	2.22E-19	3.30E-18	0.036	1.79398
TBC1D22A	AC_000162.1	0	100	2.22E-19	3.30E-18	0.875	8.54892
TBC1D22A	AC_000162.1	0	100	2.22E-19	3.30E-18	0.875	8.54892
TBC1D22A	AC_000162.1	0	100	2.22E-19	3.30E-18	0.875	8.54892
HDAC10	AC_000162.1	0	100	2.22E-19	3.30E-18	3.22	3.73E-07
MAPK12	AC_000162.1	0	87	7.02E-17	9.70E-16	0.075	0.340854
MAPK12	AC_000162.1	0	85	1.66E-16	2.20E-15	0.075	0.340854
PDE5A	AC_000163.1	100	13	1.74E-10	1.32E-09	20.575	14.8399
PDE5A	AC_000163.1	12	80	4.35E-08	2.36E-07	20.575	14.8399
PDE5A	AC_000163.1	83	20	3.33E-06	1.43E-05	20.575	14.8399
PDE5A	AC_000163.1	25	79	8.51E-05	2.97E-04	20.575	14.8399
PDE5A	AC_000163.1	80	7	4.23E-10	3.12E-09	20.575	14.8399
PDE5A	AC_000163.1	90	15	1.78E-08	1.10E-07	20.575	14.8399
PDE5A	AC_000163.1	90	22	1.43E-06	6.46E-06	20.575	14.8399
PDE5A	AC_000163.1	83	8	4.40E-10	3.24E-09	20.575	14.8399
NFKB1	AC_000163.1	80	0	1.24E-15	1.32E-14	5.368	2.82109
NFKB1	AC_000163.1	83	3	4.30E-13	4.19E-12	5.368	2.82109
NFKB1	AC_000163.1	83	25	3.36E-05	1.23E-04	5.368	2.82109
ADAMTS3	AC_000163.1	81	0	9.35E-16	1.13E-14	0.48	0.815374
ADAMTS3	AC_000163.1	100	13	1.74E-10	1.32E-09	0.48	0.815374
ADAMTS3	AC_000163.1	93	13	1.56E-09	1.07E-08	0.48	0.815374
ADAMTS3	AC_000163.1	87	11	1.94E-09	1.31E-08	0.48	0.815374

ADAMTS3	AC_000163.1	75	8	7.09E-09	4.60E-08	0.48	0.815374
ADAMTS3	AC_000163.1	85	13	1.98E-08	1.21E-07	0.48	0.815374
ADAMTS3	AC_000163.1	90	20	4.80E-07	2.36E-06	0.48	0.815374
ADAMTS3	AC_000163.1	100	0	2.22E-19	3.30E-18	0.48	0.815374
ADAMTS3	AC_000163.1	83	0	3.95E-16	4.80E-15	0.48	0.815374
ADAMTS3	AC_000163.1	76	2	1.10E-12	1.02E-11	0.48	0.815374
ADAMTS3	AC_000163.1	87	7	3.08E-11	2.44E-10	0.48	0.815374
ADAMTS3	AC_000163.1	80	7	3.48E-10	2.61E-09	0.48	0.815374
ADAMTS3	AC_000163.1	94	12	4.73E-10	3.48E-09	0.48	0.815374
ADAMTS3	AC_000163.1	100	16	1.86E-09	1.25E-08	0.48	0.815374
ADAMTS3	AC_000163.1	87	15	4.73E-08	2.57E-07	0.48	0.815374
ADAMTS3	AC_000163.1	77	11	5.04E-08	2.73E-07	0.48	0.815374
ADAMTS3	AC_000163.1	76	13	2.97E-07	1.49E-06	0.48	0.815374
ADAMTS3	AC_000163.1	82	16	4.07E-07	2.02E-06	0.48	0.815374
ADAMTS3	AC_000163.1	100	25	5.20E-07	2.55E-06	0.48	0.815374
ADAMTS3	AC_000163.1	75	16	3.16E-06	1.36E-05	0.48	0.815374
ADAMTS3	AC_000163.1	80	6	1.16E-10	8.91E-10	0.48	0.815374
SH3BP2	AC_000163.1	0	100	2.22E-19	3.30E-18	0.027	1.04775
TNIP2	AC_000163.1	0	100	2.22E-19	3.30E-18	1.456	0.0316418
TNIP2	AC_000163.1	0	100	2.22E-19	3.30E-18	1.456	0.0316418
TNIP2	AC_000163.1	0	100	2.22E-19	3.30E-18	1.456	0.0316418
PCGF3	AC_000163.1	0	100	2.22E-19	3.30E-18	18.068	4.38092
GAK	AC_000163.1	0	100	2.22E-19	3.30E-18	5.639	47.1206
CD38	AC_000163.1	100	0	2.22E-19	3.30E-18	0.024	0.885186
ADAMTS2	AC_000164.1	0	100	2.22E-19	3.30E-18	0.317	1.22682
EPS15L1	AC_000164.1	0	100	2.22E-19	3.30E-18	80.258	1.85987
KANK2	AC_000164.1	0	100	2.22E-19	3.30E-18	1.231	2.5804
ACP5	AC_000164.1	0	100	2.22E-19	3.30E-18	0.11	4.61674
LRRC8E	AC_000164.1	0	100	2.22E-19	3.30E-18	12.207	0.158038
VAV1	AC_000164.1	0	80	1.24E-15	1.32E-14	0.209	5.27356
C3	AC_000164.1	0	100	2.22E-19	3.30E-18	0.049	1.40461
C3	AC_000164.1	0	100	2.22E-19	3.30E-18	0.049	1.40461
GNA15	AC_000164.1	0	100	2.22E-19	3.30E-18	0.135	0.126829
SLC12A2	AC_000164.1	100	0	2.22E-19	3.30E-18	22.906	23.0761
CLTB	AC_000164.1	0	100	2.22E-19	3.30E-18	4.821	1.73103
DBN1	AC_000164.1	100	0	2.22E-19	3.30E-18	5.413	15.3577
C7H19orf24	AC_000164.1	100	0	2.22E-19	3.30E-18	4.371	1.72247
CTNNA1	AC_000164.1	85	17	3.24E-07	1.62E-06	282.447	29.6623
CTNNA1	AC_000164.1	80	20	6.94E-06	2.81E-05	282.447	29.6623
PCDH1	AC_000164.1	0	100	2.22E-19	3.30E-18	2.623	1.2975
GRIA1	AC_000164.1	81	22	1.37E-05	5.36E-05	0.245	0.551824
GLRX	AC_000164.1	0	80	1.24E-15	1.32E-14	53.395	4.6074
UHRF2	AC_000165.1	80	5	3.50E-11	2.77E-10	405.262	6.3504
UHRF2	AC_000165.1	83	12	1.81E-08	1.11E-07	405.262	6.3504
HR	AC_000165.1	0	100	2.22E-19	3.30E-18	0.059	0.110229

HR	AC_000165.1	0	85	1.66E-16	2.20E-15	0.059	0.110229
PDLIM2	AC_000165.1	14	100	3.79E-10	2.81E-09	24.276	1.36257
RHOBTB2	AC_000165.1	16	100	1.86E-09	1.25E-08	0.079	1.10532
RHOBTB2	AC_000165.1	0	100	2.22E-19	3.30E-18	0.079	1.10532
CHMP7	AC_000165.1	25	92	3.96E-06	1.69E-05	26.863	22.6218
SEMA4D	AC_000165.1	100	0	2.22E-19	3.30E-18	4.448	1.15805
TMEM246	AC_000165.1	86	20	1.42E-06	6.42E-06	0.276	0.61765
COL27A1	AC_000165.1	0	100	2.22E-19	3.30E-18	0.064	1.08769
COL27A1	AC_000165.1	0	100	2.22E-19	3.30E-18	0.064	1.08769
TNC	AC_000165.1	100	20	2.92E-08	1.72E-07	0.397	9.43E-06
GSN	AC_000165.1	0	100	2.22E-19	3.30E-18	0.032	26.6831
GSN	AC_000165.1	0	100	2.22E-19	3.30E-18	0.032	26.6831
GSN	AC_000165.1	5	100	1.69E-14	1.73E-13	0.032	26.6831
GSN	AC_000165.1	0	100	2.22E-19	3.30E-18	0.032	26.6831
GSN	AC_000165.1	5	100	1.69E-14	1.73E-13	0.032	26.6831
ASCC3	AC_000166.1	100	14	3.79E-10	2.81E-09	31.562	6.19346
ASCC3	AC_000166.1	87	21	1.86E-06	8.35E-06	31.562	6.19346
ASCC3	AC_000166.1	83	24	2.27E-05	8.60E-05	31.562	6.19346
ASCC3	AC_000166.1	100	17	4.16E-09	2.74E-08	31.562	6.19346
MAP3K5	AC_000166.1	0	100	2.22E-19	3.30E-18	0.694	3.75012
MAP3K5	AC_000166.1	0	100	2.22E-19	3.30E-18	0.694	3.75012
UTRN	AC_000166.1	0	83	3.95E-16	4.80E-15	15.018	6.83952
AGPAT4	AC_000166.1	0	100	2.22E-19	3.30E-18	0.047	0.391436
RPS6KA2	AC_000166.1	0	87	7.02E-17	9.70E-16	0.203	1.24944
RPS6KA2	AC_000166.1	0	100	2.22E-19	3.30E-18	0.203	1.24944
RPS6KA2	AC_000166.1	0	100	2.22E-19	3.30E-18	0.203	1.24944
RPS6KA2	AC_000166.1	0	100	2.22E-19	3.30E-18	0.203	1.24944
RPS6KA2	AC_000166.1	0	83	3.95E-16	4.80E-15	0.203	1.24944
RPS6KA2	AC_000166.1	0	100	2.22E-19	3.30E-18	0.203	1.24944
RPS6KA2	AC_000166.1	3	77	4.67E-12	4.20E-11	0.203	1.24944
RPS6KA2	AC_000166.1	0	100	2.22E-19	3.30E-18	0.203	1.24944
THBS2	AC_000166.1	0	100	2.22E-19	3.30E-18	0.046	1.91925
THBS2	AC_000166.1	0	100	2.22E-19	3.30E-18	0.046	1.91925
THBS2	AC_000166.1	0	100	2.22E-19	3.30E-18	0.046	1.91925
THBS2	AC_000166.1	100	0	2.22E-19	3.30E-18	0.046	1.91925
THBS2	AC_000166.1	0	100	2.22E-19	3.30E-18	0.046	1.91925
THBS2	AC_000166.1	20	100	2.92E-08	1.72E-07	0.046	1.91925
THBS2	AC_000166.1	0	100	2.22E-19	3.30E-18	0.046	1.91925
ZNF75D	AC_000187.1	81	4	5.58E-12	5.00E-11	109.846	66.9043
ZNF75D	AC_000187.1	14	100	3.79E-10	2.81E-09	109.846	66.9043
ZNF75D	AC_000187.1	0	100	2.22E-19	3.30E-18	109.846	66.9043
ZNF75D	AC_000187.1	7	100	2.90E-13	2.83E-12	109.846	66.9043
FLNA	AC_000187.1	0	100	2.22E-19	3.30E-18	0.091	2.68062
ARMCX3	AC_000187.1	100	0	2.22E-19	3.30E-18	0.119	22.8209
MAGED4B	AC_000187.1	0	80	1.24E-15	1.32E-14	0.253	28.9642

MSN	AC_000187.1	77	9	8.67E-09	5.57E-08	42.143	9.52565
MSN	AC_000187.1	81	12	2.94E-08	1.73E-07	42.143	9.52565
MSN	AC_000187.1	81	16	5.78E-07	2.83E-06	42.143	9.52565
MOSPD2	AC_000187.1	16	85	1.60E-07	8.31E-07	23.626	6.82811

Table S7.2 Gene expression for DMRs between sperm vs. *in vivo* MII

Gene expression in DMRs from in vivo MII vs. Sperm							
Gene	**Chr**	**In vivo MII_me**	**Sperm_me**	**p-value**	**q-value**	**In vivo MII expression**	**Spmer expression**
KCNJ15	AC_000158.1	0	100	2.22E-19	4.69E-18	0.053	0.289892
DNAJC17	AC_000167.1	0	83	3.95E-16	6.84E-15	50.793	3.12752
ITPKA	AC_000167.1	100	0	2.22E-19	4.69E-18	0.015	1.33639
DYSF	AC_000168.1	83	7	1.31E-10	1.29E-09	0.004	2.59209
CAMKMT	AC_000168.1	100	5	1.69E-14	2.45E-13	0.25	13.4428
OSR1	AC_000168.1	0	100	2.22E-19	4.69E-18	0.157	3.88409
OSR1	AC_000168.1	0	100	2.22E-19	4.69E-18	0.157	3.88409
NAIF1	AC_000168.1	0	100	2.22E-19	4.69E-18	0.538	0.59891
ASS1	AC_000168.1	0	100	2.22E-19	4.69E-18	0.739	2.18424
ASS1	AC_000168.1	0	100	2.22E-19	4.69E-18	0.739	2.18424
ASS1	AC_000168.1	0	100	2.22E-19	4.69E-18	0.739	2.18424
INPP5E	AC_000168.1	0	100	2.22E-19	4.69E-18	0.252	8.13702
INPP5E	AC_000168.1	0	100	2.22E-19	4.69E-18	0.252	8.13702
TPT1	AC_000169.1	100	0	2.22E-19	4.69E-18	201.573	216.619
RNF6	AC_000169.1	100	20	2.92E-08	2.12E-07	2.473	106.775
DOCK9	AC_000169.1	80	11	2.08E-08	1.55E-07	11.036	5.15748
RAB20	AC_000169.1	0	100	2.22E-19	4.69E-18	0.142	0.975288
TFDP1	AC_000169.1	20	92	2.77E-07	1.65E-06	8.96	7.1083
RASA3	AC_000169.1	0	100	2.22E-19	4.69E-18	0.565	1.43627
RASA3	AC_000169.1	0	100	2.22E-19	4.69E-18	0.565	1.43627
RASA3	AC_000169.1	0	100	2.22E-19	4.69E-18	0.565	1.43627
RASA3	AC_000169.1	0	85	1.66E-16	3.11E-15	0.565	1.43627
PLCB1	AC_000170.1	75	10	4.51E-08	2.95E-07	0.06	1.56312
PLCB1	AC_000170.1	91	2	2.71E-15	4.07E-14	0.06	1.56312
PLCB1	AC_000170.1	88	21	1.50E-06	7.92E-06	0.06	1.56312
PFKP	AC_000170.1	0	100	2.22E-19	4.69E-18	0.048	30.7787
RBM38	AC_000170.1	0	100	2.22E-19	4.69E-18	102.274	3.80514
CHMP4B	AC_000170.1	80	5	3.50E-11	3.63E-10	8.831	17.6036
PPP1R16B	AC_000170.1	0	100	2.22E-19	4.69E-18	0.004	1.50396
KCNB1	AC_000170.1	0	100	2.22E-19	4.69E-18	0.022	0.595133
NRBP2	AC_000171.1	0	100	2.22E-19	4.69E-18	0.205	0.416031
VAMP2	AC_000171.1	0	100	2.22E-19	4.69E-18	0.552	5.04003
ASAP1	AC_000171.1	20	95	1.27E-07	8.00E-07	6.048	4.84221
CPQ	AC_000171.1	0	100	2.22E-19	4.69E-18	0.857	65.1425

CPQ	AC_000171.1	0	100	2.22E-19	4.69E-18	0.857	65.1425
NCAM1	AC_000172.1	0	100	2.22E-19	4.69E-18	0.014	7.27085
NCAM1	AC_000172.1	0	100	2.22E-19	4.69E-18	0.014	7.27085
PHLDB1	AC_000172.1	100	0	2.22E-19	4.69E-18	0.203	2.4146
BCL9L	AC_000172.1	0	100	2.22E-19	4.69E-18	0.078	2.06981
APBB1	AC_000172.1	0	100	2.22E-19	4.69E-18	0.036	2.96761
ARHGEF17	AC_000172.1	0	83	3.95E-16	6.84E-15	0.029	2.78951
SLCO2B1	AC_000172.1	0	100	2.22E-19	4.69E-18	0.014	2.77052
CAPN5	AC_000172.1	0	100	2.22E-19	4.69E-18	0.013	2.56793
EXT2	AC_000172.1	0	80	1.24E-15	1.87E-14	48.201	9.74457
IKBKE	AC_000173.1	14	92	4.81E-09	3.93E-08	0.036	0.151946
RGL1	AC_000173.1	76	22	4.90E-05	1.99E-04	5.433	32.4076
LAMB3	AC_000173.1	100	0	2.22E-19	4.69E-18	0.007	0.36457
AP1B1	AC_000174.1	0	100	2.22E-19	4.69E-18	2.302	31.4239
OSBP2	AC_000174.1	0	80	1.24E-15	1.87E-14	0.035	14.0231
OSBP2	AC_000174.1	0	100	2.22E-19	4.69E-18	0.035	14.0231
OSBP2	AC_000174.1	0	100	2.22E-19	4.69E-18	0.035	14.0231
SMTN	AC_000174.1	0	100	2.22E-19	4.69E-18	0.011	3.96868
SMTN	AC_000174.1	0	80	1.24E-15	1.87E-14	0.011	3.96868
GNB1L	AC_000174.1	0	100	2.22E-19	4.69E-18	0.027	0.53128
ZNF423	AC_000175.1	0	75	1.25E-14	1.81E-13	0.225	1.49701
ZNF423	AC_000175.1	0	100	2.22E-19	4.69E-18	0.225	1.49701
ZNF423	AC_000175.1	0	100	2.22E-19	4.69E-18	0.225	1.49701
ZNF423	AC_000175.1	0	100	2.22E-19	4.69E-18	0.225	1.49701
LIPE	AC_000175.1	0	80	1.24E-15	1.87E-14	11.61	8.02781
IRGQ	AC_000175.1	100	0	2.22E-19	4.69E-18	0.214	1.15819
TRAPPC6A	AC_000175.1	0	80	1.24E-15	1.87E-14	0.017	0.966851
KLC3	AC_000175.1	14	90	8.99E-09	7.07E-08	0.15	0.6625
IGLON5	AC_000175.1	0	85	1.66E-16	3.11E-15	0.078	14.9143
TTYH1	AC_000175.1	0	83	3.95E-16	6.84E-15	0.017	53.4688
TTYH1	AC_000175.1	0	100	2.22E-19	4.69E-18	0.017	53.4688
ZIM2	AC_000175.1	80	0	1.24E-15	1.87E-14	9.323	0.068638
IGF2BP1	AC_000176.1	0	100	2.22E-19	4.69E-18	0.137	1.60696
COPZ2	AC_000176.1	0	100	2.22E-19	4.69E-18	0.879	3.59874
COPZ2	AC_000176.1	0	100	2.22E-19	4.69E-18	0.879	3.59874
RPL19	AC_000176.1	80	0	1.24E-15	1.87E-14	27.609	133.855
FBXL20	AC_000176.1	100	16	1.86E-09	1.56E-08	52.768	6.7384
FBXL20	AC_000176.1	100	10	8.84E-12	9.63E-11	52.768	6.7384
ITGA2B	AC_000176.1	16	100	1.86E-09	1.56E-08	0.052	0.65249
MRC2	AC_000176.1	0	87	7.02E-17	1.38E-15	0.04	0.917673

RBFOX3	AC_000176.1	0	83	3.95E-16	6.84E-15	0.664	0.0541617
RAB37	AC_000176.1	0	100	2.22E-19	4.69E-18	0.14	0.531397
RAB37	AC_000176.1	100	11	2.69E-11	2.88E-10	0.14	0.531397
RAB37	AC_000176.1	80	6	1.16E-10	1.15E-09	0.14	0.531397
RAB37	AC_000176.1	20	87	1.14E-06	6.08E-06	0.14	0.531397
SLC39A11	AC_000176.1	0	100	2.22E-19	4.69E-18	2.317	10.2451
SLC39A11	AC_000176.1	0	100	2.22E-19	4.69E-18	2.317	10.2451
SLC39A11	AC_000176.1	0	80	1.24E-15	1.87E-14	2.317	10.2451
AXIN2	AC_000176.1	0	100	2.22E-19	4.69E-18	2.758	0.321127
FAM168B	AC_000159.1	0	100	2.22E-19	4.69E-18	34.317	15.9093
AGPS	AC_000159.1	100	0	2.22E-19	4.69E-18	71.586	20.5211
CERS6	AC_000159.1	75	15	1.62E-06	8.53E-06	0.031	2.91735
TMEM177	AC_000159.1	0	100	2.22E-19	4.69E-18	0.039	1.3049
INO80D	AC_000159.1	16	83	2.86E-07	1.71E-06	2.769	1.99658
UNC80	AC_000159.1	90	22	1.43E-06	7.53E-06	0.064	1.09951
SPEG	AC_000159.1	100	20	2.92E-08	2.12E-07	4.833	0.286045
OBSL1	AC_000159.1	0	100	2.22E-19	4.69E-18	0.014	1.48814
PHC2	AC_000159.1	0	100	2.22E-19	4.69E-18	8.287	29.4464
TRIM62	AC_000159.1	100	0	2.22E-19	4.69E-18	0.037	1.09498
EPHB2	AC_000159.1	0	83	3.95E-16	6.84E-15	0.22	0.528627
ALPL	AC_000159.1	100	0	2.22E-19	4.69E-18	0.059	1.66984
PADI4	AC_000159.1	0	100	2.22E-19	4.69E-18	0.022	0.107179
PADI4	AC_000159.1	0	100	2.22E-19	4.69E-18	0.022	0.107179
PADI4	AC_000159.1	0	100	2.22E-19	4.69E-18	0.022	0.107179
SLC38A9	AC_000177.1	80	4	7.32E-12	8.01E-11	10.109	12.0679
MRPS11	AC_000178.1	100	15	9.23E-10	8.02E-09	1.443	1.91452
MRPS11	AC_000178.1	100	23	1.80E-07	1.10E-06	1.443	1.91452
MRPS11	AC_000178.1	87	21	1.86E-06	9.75E-06	1.443	1.91452
ARNT2	AC_000178.1	0	83	3.95E-16	6.84E-15	0.972	2.29686
FRMD5	AC_000178.1	100	6	6.67E-14	9.52E-13	3.842	0.203298
FRMD5	AC_000178.1	80	12	4.35E-08	2.85E-07	3.842	0.203298
FRMD5	AC_000178.1	75	23	9.52E-05	3.61E-04	3.842	0.203298
FRMD5	AC_000178.1	80	0	1.24E-15	1.87E-14	3.842	0.203298
FRMD5	AC_000178.1	83	16	3.25E-07	1.92E-06	3.842	0.203298
FRMD5	AC_000178.1	83	14	8.33E-08	5.33E-07	3.842	0.203298
BEGAIN	AC_000178.1	20	91	3.85E-07	2.27E-06	0.046	0.239427
AMN	AC_000178.1	80	25	7.02E-05	2.74E-04	0.036	0.179502
C21H14orf180	AC_000178.1	0	100	2.22E-19	4.69E-18	0.011	0.0973423
C21H14orf180	AC_000178.1	0	100	2.22E-19	4.69E-18	0.011	0.0973423
C21H14orf180	AC_000178.1	0	94	2.96E-18	6.21E-17	0.011	0.0973423

SLC4A7	AC_000179.1	80	23	3.02E-05	1.25E-04	11.245	12.9901
SCN5A	AC_000179.1	0	83	3.95E-16	6.84E-15	0.75	0.949517
SCN5A	AC_000179.1	0	100	2.22E-19	4.69E-18	0.75	0.949517
BRPF1	AC_000179.1	0	100	2.22E-19	4.69E-18	1.437	2.63067
SUMF1	AC_000179.1	16	100	1.86E-09	1.56E-08	7.417	11.0717
SYNPR	AC_000179.1	100	20	2.92E-08	2.12E-07	3.006	0.493366
SYNPR	AC_000179.1	87	21	1.86E-06	9.75E-06	3.006	0.493366
ERC2	AC_000179.1	75	16	3.16E-06	1.58E-05	1.022	0.399069
DUSP7	AC_000179.1	80	0	1.24E-15	1.87E-14	15.385	1.07444
QRICH1	AC_000179.1	0	100	2.22E-19	4.69E-18	14.186	20.7372
NUP210	AC_000179.1	0	100	2.22E-19	4.69E-18	0.161	2.69E-06
NUP210	AC_000179.1	0	100	2.22E-19	4.69E-18	0.161	2.69E-06
EEFSEC	AC_000179.1	0	100	2.22E-19	4.69E-18	0.028	3.16696
MGLL	AC_000179.1	0	100	2.22E-19	4.69E-18	0.045	4.96885
MGLL	AC_000179.1	0	100	2.22E-19	4.69E-18	0.045	4.96885
MGLL	AC_000179.1	0	100	2.22E-19	4.69E-18	0.045	4.96885
MGLL	AC_000179.1	0	100	2.22E-19	4.69E-18	0.045	4.96885
MGLL	AC_000179.1	0	100	2.22E-19	4.69E-18	0.045	4.96885
MGLL	AC_000179.1	0	100	2.22E-19	4.69E-18	0.045	4.96885
MGLL	AC_000179.1	0	83	3.95E-16	6.84E-15	0.045	4.96885
NRM	AC_000180.1	0	100	2.22E-19	4.69E-18	0.581	0.0629649
ATP9B	AC_000181.1	0	83	3.95E-16	6.84E-15	0.513	20.9405
FHOD3	AC_000181.1	100	14	3.79E-10	3.60E-09	6.035	3.32774
BCL2	AC_000181.1	83	16	2.86E-07	1.71E-06	0.091	2.29554
RHBDF1	AC_000182.1	0	100	2.22E-19	4.69E-18	0.628	1.15272
RABEP2	AC_000182.1	100	0	2.22E-19	4.69E-18	1.15	3.18206
ATXN2L	AC_000182.1	0	80	1.24E-15	1.87E-14	14.898	142.313
YPEL3	AC_000182.1	0	100	2.22E-19	4.69E-18	10.012	12.0849
TBC1D10B	AC_000182.1	0	100	2.22E-19	4.69E-18	0.371	9.56179
ELN	AC_000182.1	0	100	2.22E-19	4.69E-18	5.444	89.7002
TRIM50	AC_000182.1	0	100	2.22E-19	4.69E-18	0.231	0.36161
EPHB4	AC_000182.1	0	100	2.22E-19	4.69E-18	0.2	2.07076
SLC29A4	AC_000182.1	100	14	3.79E-10	3.60E-09	0.407	0.192267
MAD1L1	AC_000182.1	20	100	2.92E-08	2.12E-07	0.132	2.44948
INTS1	AC_000182.1	100	0	2.22E-19	4.69E-18	0.031	16.9102
C25H7orf50	AC_000182.1	0	83	3.95E-16	6.84E-15	1.179	3.55481
GPR146	AC_000182.1	0	83	3.95E-16	6.84E-15	1.013	1.0669
PRKG1	AC_000183.1	87	7	3.08E-11	3.21E-10	34.973	2.01529
MYOF	AC_000183.1	100	9	3.27E-12	3.99E-11	0.805	12.114
SUFU	AC_000183.1	0	87	7.02E-17	1.38E-15	1.731	3.82115

SUFU	AC_000183.1	0	100	2.22E-19	4.69E-18	1.731	3.82115
SORCS3	AC_000183.1	0	100	2.22E-19	4.69E-18	2.896	20.632
SORCS3	AC_000183.1	0	100	2.22E-19	4.69E-18	2.896	20.632
SORCS3	AC_000183.1	0	100	2.22E-19	4.69E-18	2.896	20.632
SORCS3	AC_000183.1	100	0	2.22E-19	4.69E-18	2.896	20.632
SORCS3	AC_000183.1	100	12	6.45E-11	6.57E-10	2.896	20.632
SORCS3	AC_000183.1	0	100	2.22E-19	4.69E-18	2.896	20.632
HTRA1	AC_000183.1	0	100	2.22E-19	4.69E-18	0.013	34.0764
WRN	AC_000184.1	85	0	1.66E-16	3.11E-15	1.63	8.79611
WRN	AC_000184.1	80	0	1.24E-15	1.87E-14	1.63	8.79611
WRN	AC_000184.1	75	0	1.25E-14	1.81E-13	1.63	8.79611
WRN	AC_000184.1	100	5	1.69E-14	2.45E-13	1.63	8.79611
WRN	AC_000184.1	100	15	9.23E-10	8.02E-09	1.63	8.79611
WRN	AC_000184.1	100	18	7.85E-09	6.23E-08	1.63	8.79611
WRN	AC_000184.1	80	10	8.02E-09	6.31E-08	1.63	8.79611
WRN	AC_000184.1	100	0	2.22E-19	4.69E-18	1.63	8.79611
WRN	AC_000184.1	90	0	1.66E-17	3.40E-16	1.63	8.79611
WRN	AC_000184.1	88	0	3.94E-17	7.96E-16	1.63	8.79611
WRN	AC_000184.1	85	0	1.66E-16	3.11E-15	1.63	8.79611
WRN	AC_000184.1	80	0	1.24E-15	1.87E-14	1.63	8.79611
WRN	AC_000184.1	100	4	2.93E-15	4.38E-14	1.63	8.79611
WRN	AC_000184.1	76	0	6.99E-15	1.04E-13	1.63	8.79611
WRN	AC_000184.1	80	3	1.61E-12	2.01E-11	1.63	8.79611
WRN	AC_000184.1	94	17	2.51E-08	1.86E-07	1.63	8.79611
WRN	AC_000184.1	88	18	2.56E-07	1.53E-06	1.63	8.79611
WRN	AC_000184.1	100	0	2.22E-19	4.69E-18	1.63	8.79611
WRN	AC_000184.1	100	0	2.22E-19	4.69E-18	1.63	8.79611
WRN	AC_000184.1	93	0	5.27E-18	1.10E-16	1.63	8.79611
WRN	AC_000184.1	83	3	4.30E-13	5.86E-12	1.63	8.79611
WRN	AC_000184.1	96	12	2.44E-10	2.37E-09	1.63	8.79611
WRN	AC_000184.1	95	13	8.16E-10	7.14E-09	1.63	8.79611
WRN	AC_000184.1	88	13	7.12E-09	5.68E-08	1.63	8.79611
WRN	AC_000184.1	83	12	1.81E-08	1.36E-07	1.63	8.79611
WRN	AC_000184.1	100	20	2.92E-08	2.12E-07	1.63	8.79611
WRN	AC_000184.1	90	19	2.83E-07	1.69E-06	1.63	8.79611
WRN	AC_000184.1	100	25	5.20E-07	2.99E-06	1.63	8.79611
WRN	AC_000184.1	97	0	9.38E-19	1.97E-17	1.63	8.79611
WRN	AC_000184.1	95	3	3.52E-15	5.26E-14	1.63	8.79611
WRN	AC_000184.1	100	5	1.69E-14	2.45E-13	1.63	8.79611
WRN	AC_000184.1	97	7	7.91E-13	1.01E-11	1.63	8.79611

WRN	AC_000184.1	88	7	1.93E-11	2.08E-10	1.63	8.79611
WRN	AC_000184.1	86	12	6.41E-09	5.18E-08	1.63	8.79611
WRN	AC_000184.1	100	20	2.92E-08	2.12E-07	1.63	8.79611
WRN	AC_000184.1	85	16	1.81E-07	1.10E-06	1.63	8.79611
RNF122	AC_000184.1	0	83	3.95E-16	6.84E-15	2.269	10.1717
RNF122	AC_000184.1	75	14	9.09E-07	4.97E-06	2.269	10.1717
RNF122	AC_000184.1	88	22	2.41E-06	1.24E-05	2.269	10.1717
RNF122	AC_000184.1	83	5	1.01E-11	1.10E-10	2.269	10.1717
RNF122	AC_000184.1	87	11	1.94E-09	1.63E-08	2.269	10.1717
RNF122	AC_000184.1	100	0	2.22E-19	4.69E-18	2.269	10.1717
RNF122	AC_000184.1	80	5	3.50E-11	3.63E-10	2.269	10.1717
RNF122	AC_000184.1	14	100	3.79E-10	3.60E-09	2.269	10.1717
RNF122	AC_000184.1	88	25	9.72E-06	4.45E-05	2.269	10.1717
RNF122	AC_000184.1	83	12	1.81E-08	1.36E-07	2.269	10.1717
RNF122	AC_000184.1	20	87	1.14E-06	6.08E-06	2.269	10.1717
RNF122	AC_000184.1	100	14	3.79E-10	3.60E-09	2.269	10.1717
RNF122	AC_000184.1	0	87	7.02E-17	1.38E-15	2.269	10.1717
RNF122	AC_000184.1	80	0	1.24E-15	1.87E-14	2.269	10.1717
RNF122	AC_000184.1	80	0	1.24E-15	1.87E-14	2.269	10.1717
RNF122	AC_000184.1	80	10	8.02E-09	6.31E-08	2.269	10.1717
RNF122	AC_000184.1	11	80	2.08E-08	1.55E-07	2.269	10.1717
RNF122	AC_000184.1	100	22	9.72E-08	6.15E-07	2.269	10.1717
RNF122	AC_000184.1	20	80	6.94E-06	3.22E-05	2.269	10.1717
RNF122	AC_000184.1	100	25	5.20E-07	2.99E-06	2.269	10.1717
RNF122	AC_000184.1	80	18	2.38E-06	1.22E-05	2.269	10.1717
RNF122	AC_000184.1	80	18	2.38E-06	1.22E-05	2.269	10.1717
RNF122	AC_000184.1	83	13	3.69E-08	2.57E-07	2.269	10.1717
RNF122	AC_000184.1	83	10	2.71E-09	2.26E-08	2.269	10.1717
RNF122	AC_000184.1	85	20	1.96E-06	1.02E-05	2.269	10.1717
RNF122	AC_000184.1	100	10	8.84E-12	9.63E-11	2.269	10.1717
RNF122	AC_000184.1	16	100	1.86E-09	1.56E-08	2.269	10.1717
RNF122	AC_000184.1	83	20	3.33E-06	1.65E-05	2.269	10.1717
RNF122	AC_000184.1	100	8	9.20E-13	1.16E-11	2.269	10.1717
RNF122	AC_000184.1	75	16	3.16E-06	1.58E-05	2.269	10.1717
RNF122	AC_000184.1	80	8	1.14E-09	9.88E-09	2.269	10.1717
RNF122	AC_000184.1	80	20	6.94E-06	3.22E-05	2.269	10.1717
RNF122	AC_000184.1	10	85	1.65E-09	1.41E-08	2.269	10.1717
RNF122	AC_000184.1	80	10	8.02E-09	6.31E-08	2.269	10.1717
RNF122	AC_000184.1	20	78	1.17E-05	5.25E-05	2.269	10.1717
RNF122	AC_000184.1	100	12	6.45E-11	6.57E-10	2.269	10.1717

RNF122	AC_000184.1	83	14	8.33E-08	5.33E-07	2.269	10.1717
RNF122	AC_000184.1	80	14	1.93E-07	1.16E-06	2.269	10.1717
RNF122	AC_000184.1	90	11	7.82E-10	6.86E-09	2.269	10.1717
RNF122	AC_000184.1	100	16	1.86E-09	1.56E-08	2.269	10.1717
RNF122	AC_000184.1	85	22	5.47E-06	2.64E-05	2.269	10.1717
RNF122	AC_000184.1	100	0	2.22E-19	4.69E-18	2.269	10.1717
RNF122	AC_000184.1	80	4	7.32E-12	8.01E-11	2.269	10.1717
RNF122	AC_000184.1	84	16	2.28E-07	1.37E-06	2.269	10.1717
RNF122	AC_000184.1	0	84	2.22E-16	4.13E-15	2.269	10.1717
RNF122	AC_000184.1	80	0	1.24E-15	1.87E-14	2.269	10.1717
RNF122	AC_000184.1	75	0	1.25E-14	1.81E-13	2.269	10.1717
RNF122	AC_000184.1	100	0	2.22E-19	4.69E-18	2.269	10.1717
RNF122	AC_000184.1	100	0	2.22E-19	4.69E-18	2.269	10.1717
RNF122	AC_000184.1	90	0	1.66E-17	3.40E-16	2.269	10.1717
RNF122	AC_000184.1	90	0	1.66E-17	3.40E-16	2.269	10.1717
RNF122	AC_000184.1	100	8	9.20E-13	1.16E-11	2.269	10.1717
RNF122	AC_000184.1	80	11	2.08E-08	1.55E-07	2.269	10.1717
RNF122	AC_000184.1	100	24	2.94E-07	1.75E-06	2.269	10.1717
RNF122	AC_000184.1	21	75	3.99E-05	1.63E-04	2.269	10.1717
RNF122	AC_000184.1	75	7	2.27E-09	1.90E-08	2.269	10.1717
RNF122	AC_000184.1	80	11	2.08E-08	1.55E-07	2.269	10.1717
RNF122	AC_000184.1	85	11	3.76E-09	3.11E-08	2.269	10.1717
RNF122	AC_000184.1	80	23	3.02E-05	1.25E-04	2.269	10.1717
RNF122	AC_000184.1	85	5	4.73E-12	5.76E-11	2.269	10.1717
RNF122	AC_000184.1	100	9	3.27E-12	3.99E-11	2.269	10.1717
RNF122	AC_000184.1	25	85	2.09E-05	9.03E-05	2.269	10.1717
RNF122	AC_000184.1	80	0	1.24E-15	1.87E-14	2.269	10.1717
RNF122	AC_000184.1	80	14	1.93E-07	1.16E-06	2.269	10.1717
RNF122	AC_000184.1	83	17	5.72E-07	3.28E-06	2.269	10.1717
RNF122	AC_000184.1	100	16	1.86E-09	1.56E-08	2.269	10.1717
RNF122	AC_000184.1	16	75	3.16E-06	1.58E-05	2.269	10.1717
RNF122	AC_000184.1	80	10	8.02E-09	6.31E-08	2.269	10.1717
RNF122	AC_000184.1	75	10	4.51E-08	2.95E-07	2.269	10.1717
RNF122	AC_000184.1	75	12	2.23E-07	1.34E-06	2.269	10.1717
RNF122	AC_000184.1	100	25	5.20E-07	2.99E-06	2.269	10.1717
RNF122	AC_000184.1	76	24	1.14E-04	4.26E-04	2.269	10.1717
UNC5D	AC_000184.1	100	5	1.69E-14	2.45E-13	3.119	0.293699
UNC5D	AC_000184.1	95	15	4.09E-09	3.37E-08	3.119	0.293699
UNC5D	AC_000184.1	97	18	2.03E-08	1.52E-07	3.119	0.293699
LDB3	AC_000185.1	0	100	2.22E-19	4.69E-18	0.931	0.28762

FADS2	AC_000186.1	0	100	2.22E-19	4.69E-18	0.01	34.409
FADS2	AC_000186.1	16	100	1.86E-09	1.56E-08	0.01	34.409
MACROD1	AC_000186.1	0	100	2.22E-19	4.69E-18	0.955	8.30819
MACROD1	AC_000186.1	0	100	2.22E-19	4.69E-18	0.955	8.30819
MACROD1	AC_000186.1	0	80	1.24E-15	1.87E-14	0.955	8.30819
MACROD1	AC_000186.1	0	100	2.22E-19	4.69E-18	0.955	8.30819
NRXN2	AC_000186.1	0	100	2.22E-19	4.69E-18	0.016	4.57515
VPS51	AC_000186.1	100	0	2.22E-19	4.69E-18	0.408	16.563
RELA	AC_000186.1	100	0	2.22E-19	4.69E-18	40.482	15.7251
ANO1	AC_000186.1	12	100	6.45E-11	6.57E-10	0.227	52.6666
ANO1	AC_000186.1	0	100	2.22E-19	4.69E-18	0.227	52.6666
NADSYN1	AC_000186.1	0	85	1.66E-16	3.11E-15	0.047	1.3615
CARS	AC_000186.1	20	97	7.26E-08	4.66E-07	0.776	12.83
PHRF1	AC_000186.1	0	83	3.95E-16	6.84E-15	1.394	0.489806
CHRNB2	AC_000160.1	100	0	2.22E-19	4.69E-18	10.768	0.0575072
CELF3	AC_000160.1	20	80	6.94E-06	3.22E-05	0.124	0.743221
ATP1A1	AC_000160.1	100	11	2.69E-11	2.88E-10	24.236	148.908
ATP1A1	AC_000160.1	93	18	5.75E-08	3.72E-07	24.236	148.908
RNF220	AC_000160.1	0	100	2.22E-19	4.69E-18	8.801	0.0276694
PTPRF	AC_000160.1	0	87	7.02E-17	1.38E-15	3.076	4.93606
GRIK3	AC_000160.1	0	100	2.22E-19	4.69E-18	0.01	0.0418562
SH3BP4	AC_000160.1	20	100	2.92E-08	2.12E-07	0.189	5.17138
PER2	AC_000160.1	0	80	1.24E-15	1.87E-14	0.539	2.68266
KIAA1324L	AC_000161.1	83	14	8.33E-08	5.33E-07	3.943	26.3772
KIAA1324L	AC_000161.1	80	18	2.38E-06	1.22E-05	3.943	26.3772
MET	AC_000161.1	85	11	3.76E-09	3.11E-08	0.156	3.35075
MET	AC_000161.1	80	15	4.06E-07	2.38E-06	0.156	3.35075
MET	AC_000161.1	83	17	5.72E-07	3.28E-06	0.156	3.35075
ADCY1	AC_000161.1	0	100	2.22E-19	4.69E-18	0.016	2.7462
ADCY1	AC_000161.1	0	100	2.22E-19	4.69E-18	0.016	2.7462
ADCY1	AC_000161.1	0	100	2.22E-19	4.69E-18	0.016	2.7462
CDK13	AC_000161.1	88	3	5.16E-14	7.39E-13	4.127	15.9006
CDK13	AC_000161.1	88	15	3.75E-08	2.57E-07	4.127	15.9006
CDK13	AC_000161.1	88	3	5.16E-14	7.39E-13	4.127	15.9006
CDK13	AC_000161.1	88	15	3.75E-08	2.57E-07	4.127	15.9006
LRGUK	AC_000161.1	80	6	1.16E-10	1.15E-09	0.074	4.2307
LRGUK	AC_000161.1	100	20	2.92E-08	2.12E-07	0.074	4.2307
LRGUK	AC_000161.1	76	14	6.34E-07	3.63E-06	0.074	4.2307
LRGUK	AC_000161.1	100	6	6.67E-14	9.52E-13	0.074	4.2307
LRGUK	AC_000161.1	100	7	2.90E-13	3.97E-12	0.074	4.2307

LRGUK	AC_000161.1	100	12	6.45E-11	6.57E-10	0.074	4.2307
LRGUK	AC_000161.1	87	20	1.14E-06	6.08E-06	0.074	4.2307
LRGUK	AC_000161.1	16	75	3.16E-06	1.58E-05	0.074	4.2307
UBN2	AC_000161.1	100	0	2.22E-19	4.69E-18	3.553	3.21039
UBN2	AC_000161.1	100	2	5.84E-17	1.18E-15	3.553	3.21039
UBN2	AC_000161.1	90	5	6.30E-13	8.01E-12	3.553	3.21039
UBN2	AC_000161.1	100	10	8.84E-12	9.63E-11	3.553	3.21039
UBN2	AC_000161.1	80	7	4.23E-10	3.99E-09	3.553	3.21039
UBN2	AC_000161.1	100	21	5.72E-08	3.70E-07	3.553	3.21039
UBN2	AC_000161.1	92	12	9.13E-10	7.97E-09	3.553	3.21039
RHEBL1	AC_000162.1	100	0	2.22E-19	4.69E-18	63.627	0.755525
GLS2	AC_000162.1	0	100	2.22E-19	4.69E-18	85.077	0.903068
NABP2	AC_000162.1	100	0	2.22E-19	4.69E-18	11.492	4.72175
IKZF4	AC_000162.1	0	100	2.22E-19	4.69E-18	0.166	2.6742
ITPR2	AC_000162.1	75	6	8.00E-10	7.01E-09	1.345	0.00624904
PHB2	AC_000162.1	0	100	2.22E-19	4.69E-18	10.422	6.06531
PIANP	AC_000162.1	20	100	2.92E-08	2.12E-07	0.108	0.763825
PPARA	AC_000162.1	0	85	1.66E-16	3.11E-15	0.821	1.65248
HDAC10	AC_000162.1	0	100	2.22E-19	4.69E-18	0.076	3.73E-07
PDE5A	AC_000163.1	80	14	1.93E-07	1.16E-06	6.356	14.8399
PDE5A	AC_000163.1	83	20	3.33E-06	1.65E-05	6.356	14.8399
PDE5A	AC_000163.1	100	0	2.22E-19	4.69E-18	6.356	14.8399
PDE5A	AC_000163.1	80	10	8.02E-09	6.31E-08	6.356	14.8399
PDE5A	AC_000163.1	80	12	4.35E-08	2.85E-07	6.356	14.8399
PDE5A	AC_000163.1	80	0	1.24E-15	1.87E-14	6.356	14.8399
PDE5A	AC_000163.1	100	23	1.80E-07	1.10E-06	6.356	14.8399
NFKB1	AC_000163.1	80	3	1.61E-12	2.01E-11	10.451	2.82109
NFKB1	AC_000163.1	100	12	6.45E-11	6.57E-10	10.451	2.82109
NFKB1	AC_000163.1	90	11	7.82E-10	6.86E-09	10.451	2.82109
METAP1	AC_000163.1	80	13	1.01E-07	6.33E-07	11.068	9.01996
ADAMTS3	AC_000163.1	100	0	2.22E-19	4.69E-18	0.026	0.815374
ADAMTS3	AC_000163.1	100	8	9.20E-13	1.16E-11	0.026	0.815374
ADAMTS3	AC_000163.1	95	13	8.16E-10	7.14E-09	0.026	0.815374
ADAMTS3	AC_000163.1	87	11	1.94E-09	1.63E-08	0.026	0.815374
ADAMTS3	AC_000163.1	80	13	1.01E-07	6.33E-07	0.026	0.815374
ADAMTS3	AC_000163.1	100	2	5.84E-17	1.18E-15	0.026	0.815374
ADAMTS3	AC_000163.1	75	0	1.25E-14	1.81E-13	0.026	0.815374
ADAMTS3	AC_000163.1	80	7	3.48E-10	3.35E-09	0.026	0.815374
ADAMTS3	AC_000163.1	100	15	9.23E-10	8.02E-09	0.026	0.815374
ADAMTS3	AC_000163.1	80	13	1.01E-07	6.33E-07	0.026	0.815374

ADAMTS3	AC_000163.1	80	16	7.24E-07	4.12E-06	0.026	0.815374
ADAMTS3	AC_000163.1	85	25	2.09E-05	9.03E-05	0.026	0.815374
ADAMTS3	AC_000163.1	75	6	8.00E-10	7.01E-09	0.026	0.815374
TNIP2	AC_000163.1	0	100	2.22E-19	4.69E-18	2.49	0.0316418
TNIP2	AC_000163.1	0	100	2.22E-19	4.69E-18	2.49	0.0316418
TNIP2	AC_000163.1	0	100	2.22E-19	4.69E-18	2.49	0.0316418
TNIP2	AC_000163.1	0	100	2.22E-19	4.69E-18	2.49	0.0316418
TNIP2	AC_000163.1	14	100	3.79E-10	3.60E-09	2.49	0.0316418
CCDC96	AC_000163.1	100	0	2.22E-19	4.69E-18	0.013	66.6834
CCDC96	AC_000163.1	85	0	1.66E-16	3.11E-15	0.013	66.6834
ADAMTS2	AC_000164.1	0	100	2.22E-19	4.69E-18	0.066	1.22682
ADAMTS2	AC_000164.1	0	100	2.22E-19	4.69E-18	0.066	1.22682
KANK2	AC_000164.1	0	100	2.22E-19	4.69E-18	4.933	2.5804
KANK2	AC_000164.1	0	100	2.22E-19	4.69E-18	4.933	2.5804
C3	AC_000164.1	100	0	2.22E-19	4.69E-18	0.018	1.40461
ZBTB7A	AC_000164.1	100	20	2.92E-08	2.12E-07	0.081	1.57111
PDLIM4	AC_000164.1	16	100	1.86E-09	1.56E-08	0.175	4.14576
SBNO2	AC_000164.1	100	0	2.22E-19	4.69E-18	0.183	2.25867
GFRA3	AC_000164.1	83	18	1.10E-06	5.87E-06	0.024	1.93982
GFRA3	AC_000164.1	80	21	1.20E-05	5.39E-05	0.024	1.93982
EGR1	AC_000164.1	16	87	8.86E-08	5.65E-07	0.357	97.3863
CTNNA1	AC_000164.1	83	0	3.95E-16	6.84E-15	782.826	29.6623
ZNF395	AC_000165.1	85	25	2.09E-05	9.03E-05	0.043	3.82017
MOB3B	AC_000165.1	100	0	2.22E-19	4.69E-18	0.981	2.09704
KLF9	AC_000165.1	80	0	1.24E-15	1.87E-14	0.372	8.86346
RHOBTB2	AC_000165.1	16	100	1.86E-09	1.56E-08	0.129	1.10532
FANCC	AC_000165.1	83	23	1.39E-05	6.16E-05	4.859	2.9906
ASCC3	AC_000166.1	100	17	4.16E-09	3.41E-08	6.901	6.19346
PTPRK	AC_000166.1	83	20	3.33E-06	1.65E-05	2.563	7.58014
LRP11	AC_000166.1	0	100	2.22E-19	4.69E-18	1.06	1.14334
RPS6KA2	AC_000166.1	0	80	1.24E-15	1.87E-14	0.216	1.24944
RPS6KA2	AC_000166.1	0	100	2.22E-19	4.69E-18	0.216	1.24944
GPC3	AC_000187.1	77	0	5.26E-15	7.81E-14	4.36	8.81999
ZNF75D	AC_000187.1	83	0	3.95E-16	6.84E-15	204.013	66.9043
ZNF75D	AC_000187.1	83	11	7.24E-09	5.76E-08	204.013	66.9043
ZNF75D	AC_000187.1	0	75	1.25E-14	1.81E-13	204.013	66.9043
TMEM185A	AC_000187.1	100	0	2.22E-19	4.69E-18	60.753	0.15763
MSN	AC_000187.1	80	0	1.24E-15	1.87E-14	5.118	9.52565
MSN	AC_000187.1	100	6	6.67E-14	9.52E-13	5.118	9.52565
MSN	AC_000187.1	80	7	4.23E-10	3.99E-09	5.118	9.52565

MSN	AC_000187.1	80	16	7.24E-07	4.12E-06	5.118	9.52565
PHEX	AC_000187.1	85	0	1.66E-16	3.11E-15	0.032	1.12563
MOSPD2	AC_000187.1	75	13	4.30E-07	2.51E-06	2.568	6.82811

Table S7.3 Gene expression for DMRs between sperm vs. *in vitro* MII

Gene expression in DMRs from in vitro MII vs. Sperm							
Gene	Chr	In vitr MII_me	Sperm_me	p-value	q-value	In vitr MII expression	Spmer expression
ADCY5	AC_000158.1	0	100	2.22E-19	2.32E-18	0.06	5.65265
BDH1	AC_000158.1	0	100	2.22E-19	2.32E-18	0.802	11.332
XXYLT1	AC_000158.1	0	100	2.22E-19	2.32E-18	9.236	2.88536
KPNA6	AC_000158.1	0	100	2.22E-19	2.32E-18	17.299	3.88082
UBASH3A	AC_000158.1	18	100	7.85E-09	4.28E-08	16.101	0.164468
PFKL	AC_000158.1	0	100	2.22E-19	2.32E-18	0.129	0.197475
PFKL	AC_000158.1	0	100	2.22E-19	2.32E-18	0.129	0.197475
PDXK	AC_000158.1	0	100	2.22E-19	2.32E-18	3.386	1.29524
PDXK	AC_000158.1	0	83	3.95E-16	3.44E-15	3.386	1.29524
COL18A1	AC_000158.1	0	100	2.22E-19	2.32E-18	0.071	19.4062
COL18A1	AC_000158.1	0	100	2.22E-19	2.32E-18	0.071	19.4062
COL18A1	AC_000158.1	0	100	2.22E-19	2.32E-18	0.071	19.4062
COL18A1	AC_000158.1	0	100	2.22E-19	2.32E-18	0.071	19.4062
COL18A1	AC_000158.1	0	100	2.22E-19	2.32E-18	0.071	19.4062
COL18A1	AC_000158.1	0	100	2.22E-19	2.32E-18	0.071	19.4062
COL18A1	AC_000158.1	0	100	2.22E-19	2.32E-18	0.071	19.4062
COL18A1	AC_000158.1	0	100	2.22E-19	2.32E-18	0.071	19.4062
SPATC1L	AC_000158.1	100	18	7.85E-09	4.28E-08	0.019	16.2154
RUNX1	AC_000158.1	20	100	2.92E-08	1.49E-07	0.42	0.393924
RUNX1	AC_000158.1	0	100	2.22E-19	2.32E-18	0.42	0.393924
BTD	AC_000158.1	100	0	2.22E-19	2.32E-18	3.236	2.48654
BTD	AC_000158.1	100	0	2.22E-19	2.32E-18	3.236	2.48654
OXNAD1	AC_000158.1	0	100	2.22E-19	2.32E-18	1.977	10.5107
OXNAD1	AC_000158.1	0	100	2.22E-19	2.32E-18	1.977	10.5107
OXNAD1	AC_000158.1	0	80	1.24E-15	9.79E-15	1.977	10.5107
OXNAD1	AC_000158.1	0	100	2.22E-19	2.32E-18	1.977	10.5107
OXNAD1	AC_000158.1	0	100	2.22E-19	2.32E-18	1.977	10.5107
OXNAD1	AC_000158.1	0	100	2.22E-19	2.32E-18	1.977	10.5107
OXNAD1	AC_000158.1	0	100	2.22E-19	2.32E-18	1.977	10.5107
PLCL2	AC_000158.1	0	100	2.22E-19	2.32E-18	10.364	45.9542
PLCL2	AC_000158.1	0	100	2.22E-19	2.32E-18	10.364	45.9542
PLCL2	AC_000158.1	0	83	3.95E-16	3.44E-15	10.364	45.9542
TXNDC16	AC_000167.1	0	100	2.22E-19	2.32E-18	2.544	5.12414
NOX5	AC_000167.1	0	100	2.22E-19	2.32E-18	0.728	0.104699
BCL2L2	AC_000167.1	0	100	2.22E-19	2.32E-18	5.42	10.4149
TEP1	AC_000167.1	0	92	7.02E-18	7.27E-17	0.165	0.898197
KATNBL1	AC_000167.1	80	14	1.93E-07	8.74E-07	22.924	19.9724
TMEM229B	AC_000167.1	100	0	2.22E-19	2.32E-18	0.197	2.78354

VASH1	AC_000167.1	0	100	2.22E-19	2.32E-18	0.301	2.02373
CNNM4	AC_000168.1	20	92	2.77E-07	1.24E-06	11.71	6.86361
FHL2	AC_000168.1	0	100	2.22E-19	2.32E-18	2.757	8.26512
FHL2	AC_000168.1	0	100	2.22E-19	2.32E-18	2.757	8.26512
FHL2	AC_000168.1	0	100	2.22E-19	2.32E-18	2.757	8.26512
LOXL3	AC_000168.1	0	100	2.22E-19	2.32E-18	0.279	0.975324
DYSF	AC_000168.1	80	20	6.94E-06	2.60E-05	0.44	2.59209
CAMKMT	AC_000168.1	100	5	1.69E-14	1.30E-13	2.258	13.4428
EMILIN1	AC_000168.1	0	100	2.22E-19	2.32E-18	0.05	2.56389
ADCY3	AC_000168.1	0	100	2.22E-19	2.32E-18	0.876	2.50149
RALGPS1	AC_000168.1	80	0	1.24E-15	9.79E-15	2.29	23.5689
ENG	AC_000168.1	0	100	2.22E-19	2.32E-18	0.057	5.34783
NTNG2	AC_000168.1	0	100	2.22E-19	2.32E-18	0.26	0.683614
NTNG2	AC_000168.1	0	100	2.22E-19	2.32E-18	0.26	0.683614
AK8	AC_000168.1	0	85	1.66E-16	1.56E-15	0.032	44.5611
AK8	AC_000168.1	20	100	2.92E-08	1.49E-07	0.032	44.5611
AK8	AC_000168.1	0	100	2.22E-19	2.32E-18	0.032	44.5611
AK8	AC_000168.1	0	80	1.24E-15	9.79E-15	0.032	44.5611
GFI1B	AC_000168.1	0	100	2.22E-19	2.32E-18	0.57	0.0413428
GFI1B	AC_000168.1	0	83	3.95E-16	3.44E-15	0.57	0.0413428
INPP5E	AC_000168.1	0	100	2.22E-19	2.32E-18	0.14	8.13702
INPP5E	AC_000168.1	0	100	2.22E-19	2.32E-18	0.14	8.13702
INPP5E	AC_000168.1	0	100	2.22E-19	2.32E-18	0.14	8.13702
SARDH	AC_000168.1	0	100	2.22E-19	2.32E-18	0.042	0.12003
SARDH	AC_000168.1	0	83	3.95E-16	3.44E-15	0.042	0.12003
SARDH	AC_000168.1	14	100	3.79E-10	2.31E-09	0.042	0.12003
SARDH	AC_000168.1	0	100	2.22E-19	2.32E-18	0.042	0.12003
SARDH	AC_000168.1	0	83	3.95E-16	3.44E-15	0.042	0.12003
CACNA1B	AC_000168.1	100	0	2.22E-19	2.32E-18	0.477	0.0635291
TPRN	AC_000168.1	0	100	2.22E-19	2.32E-18	0.685	1.47106
SLC7A1	AC_000169.1	0	100	2.22E-19	2.32E-18	0.518	16.1771
TNFRSF19	AC_000169.1	0	83	3.95E-16	3.44E-15	0.037	0.107024
DOCK9	AC_000169.1	88	0	3.94E-17	3.96E-16	27.006	5.15748
DOCK9	AC_000169.1	80	11	2.08E-08	1.09E-07	27.006	5.15748
DOCK9	AC_000169.1	75	20	2.62E-05	9.12E-05	27.006	5.15748
RAB20	AC_000169.1	0	100	2.22E-19	2.32E-18	0.304	0.975288
RASA3	AC_000169.1	0	100	2.22E-19	2.32E-18	0.302	1.43627
RASA3	AC_000169.1	0	100	2.22E-19	2.32E-18	0.302	1.43627
PLCB1	AC_000170.1	100	11	2.69E-11	1.74E-10	0.538	1.56312
PLCB1	AC_000170.1	88	10	5.48E-10	3.19E-09	0.538	1.56312
PLCB1	AC_000170.1	100	22	9.72E-08	4.57E-07	0.538	1.56312
PLCB1	AC_000170.1	93	25	2.95E-06	1.17E-05	0.538	1.56312
PLCB1	AC_000170.1	95	2	5.23E-16	4.55E-15	0.538	1.56312
PLCB1	AC_000170.1	100	21	5.72E-08	2.73E-07	0.538	1.56312
ISM1	AC_000170.1	0	100	2.22E-19	2.32E-18	0.191	2.60195

CUBN	AC_000170.1	92	4	6.82E-14	5.22E-13	0.097	4.77637
CUBN	AC_000170.1	83	6	4.28E-11	2.72E-10	0.097	4.77637
CUBN	AC_000170.1	75	14	9.09E-07	3.87E-06	0.097	4.77637
CUBN	AC_000170.1	75	14	9.09E-07	3.87E-06	0.097	4.77637
PFKP	AC_000170.1	0	100	2.22E-19	2.32E-18	0.159	30.7787
SLC4A11	AC_000170.1	80	0	1.24E-15	9.79E-15	0.637	12.4908
PCMTD2	AC_000170.1	0	100	2.22E-19	2.32E-18	30.34	23.5781
OPRL1	AC_000170.1	21	75	3.99E-05	1.35E-04	0.088	2.42345
OPRL1	AC_000170.1	21	75	3.99E-05	1.35E-04	0.088	2.42345
RBM38	AC_000170.1	14	100	3.79E-10	2.31E-09	22.426	3.80514
CHMP4B	AC_000170.1	75	12	2.23E-07	1.01E-06	6.574	17.6036
CHMP4B	AC_000170.1	90	25	6.49E-06	2.48E-05	6.574	17.6036
RBL1	AC_000170.1	0	100	2.22E-19	2.32E-18	2.118	9.51603
RBL1	AC_000170.1	0	80	1.24E-15	9.79E-15	2.118	9.51603
KCNB1	AC_000170.1	0	83	3.95E-16	3.44E-15	0.148	0.595133
DOK5	AC_000170.1	0	100	2.22E-19	2.32E-18	0.076	1.18619
TONSL	AC_000171.1	0	100	2.22E-19	2.32E-18	2.864	1.07664
SLC39A4	AC_000171.1	0	85	1.66E-16	1.56E-15	0.012	0.49789
VAMP2	AC_000171.1	0	100	2.22E-19	2.32E-18	5.115	5.04003
VAMP2	AC_000171.1	0	100	2.22E-19	2.32E-18	5.115	5.04003
VAMP2	AC_000171.1	0	100	2.22E-19	2.32E-18	5.115	5.04003
VAMP2	AC_000171.1	0	100	2.22E-19	2.32E-18	5.115	5.04003
VAMP2	AC_000171.1	100	0	2.22E-19	2.32E-18	5.115	5.04003
VAMP2	AC_000171.1	14	83	8.33E-08	3.95E-07	5.115	5.04003
VAMP2	AC_000171.1	0	100	2.22E-19	2.32E-18	5.115	5.04003
VAMP2	AC_000171.1	0	93	5.27E-18	5.48E-17	5.115	5.04003
VAMP2	AC_000171.1	0	100	2.22E-19	2.32E-18	5.115	5.04003
VAMP2	AC_000171.1	0	100	2.22E-19	2.32E-18	5.115	5.04003
VAMP2	AC_000171.1	0	100	2.22E-19	2.32E-18	5.115	5.04003
VAMP2	AC_000171.1	0	100	2.22E-19	2.32E-18	5.115	5.04003
VAMP2	AC_000171.1	14	100	3.79E-10	2.31E-09	5.115	5.04003
TSNARE1	AC_000171.1	0	100	2.22E-19	2.32E-18	1.863	0.00898524
TSNARE1	AC_000171.1	0	100	2.22E-19	2.32E-18	1.863	0.00898524
TSNARE1	AC_000171.1	0	100	2.22E-19	2.32E-18	1.863	0.00898524
PTP4A3	AC_000171.1	0	100	2.22E-19	2.32E-18	1.208	0.747433
PTP4A3	AC_000171.1	0	100	2.22E-19	2.32E-18	1.208	0.747433
PTP4A3	AC_000171.1	16	100	1.86E-09	1.05E-08	1.208	0.747433
NDRG1	AC_000171.1	0	100	2.22E-19	2.32E-18	0.022	8.90479
NDRG1	AC_000171.1	0	100	2.22E-19	2.32E-18	0.022	8.90479
NDRG1	AC_000171.1	0	100	2.22E-19	2.32E-18	0.022	8.90479
ASAP1	AC_000171.1	0	95	2.22E-18	2.32E-17	38.082	4.84221
ASAP1	AC_000171.1	0	92	7.02E-18	7.27E-17	38.082	4.84221
TTPA	AC_000171.1	100	22	9.72E-08	4.57E-07	0.127	1.44846
PREX2	AC_000171.1	87	10	8.39E-10	4.88E-09	0.204	1.02787
CPQ	AC_000171.1	0	100	2.22E-19	2.32E-18	4.798	65.1425

CPQ	AC_000171.1	0	80	1.24E-15	9.79E-15	4.798	65.1425
MAML2	AC_000172.1	0	100	2.22E-19	2.32E-18	0.035	0.898364
NCAM1	AC_000172.1	0	100	2.22E-19	2.32E-18	0.052	7.27085
NCAM1	AC_000172.1	0	100	2.22E-19	2.32E-18	0.052	7.27085
NCAM1	AC_000172.1	0	100	2.22E-19	2.32E-18	0.052	7.27085
NCAM1	AC_000172.1	0	100	2.22E-19	2.32E-18	0.052	7.27085
UPK2	AC_000172.1	0	100	2.22E-19	2.32E-18	0.076	0.915982
UPK2	AC_000172.1	0	100	2.22E-19	2.32E-18	0.076	0.915982
UPK2	AC_000172.1	0	100	2.22E-19	2.32E-18	0.076	0.915982
PHLDB1	AC_000172.1	0	100	2.22E-19	2.32E-18	0.626	2.4146
MCAM	AC_000172.1	0	100	2.22E-19	2.32E-18	0.287	0.514236
GRAMD1B	AC_000172.1	0	100	2.22E-19	2.32E-18	10.286	9.43855
SPON1	AC_000172.1	100	16	1.86E-09	1.05E-08	5.547	36.0375
HPX	AC_000172.1	0	100	2.22E-19	2.32E-18	0.034	2.16298
APBB1	AC_000172.1	0	100	2.22E-19	2.32E-18	0.01	2.96761
PDE2A	AC_000172.1	0	100	2.22E-19	2.32E-18	0.052	2.68373
PDE2A	AC_000172.1	0	100	2.22E-19	2.32E-18	0.052	2.68373
ARRB1	AC_000172.1	0	100	2.22E-19	2.32E-18	0.553	0.862835
ARRB1	AC_000172.1	0	100	2.22E-19	2.32E-18	0.553	0.862835
CAPN5	AC_000172.1	0	100	2.22E-19	2.32E-18	0.013	2.56793
CAPN5	AC_000172.1	0	100	2.22E-19	2.32E-18	0.013	2.56793
CD82	AC_000172.1	0	100	2.22E-19	2.32E-18	0.012	17.878
CD82	AC_000172.1	0	100	2.22E-19	2.32E-18	0.012	17.878
CD82	AC_000172.1	0	100	2.22E-19	2.32E-18	0.012	17.878
CD82	AC_000172.1	0	100	2.22E-19	2.32E-18	0.012	17.878
CD82	AC_000172.1	0	100	2.22E-19	2.32E-18	0.012	17.878
CD82	AC_000172.1	22	94	4.95E-07	2.18E-06	0.012	17.878
CD82	AC_000172.1	0	100	2.22E-19	2.32E-18	0.012	17.878
MAPK8IP1	AC_000172.1	0	100	2.22E-19	2.32E-18	0.236	6.49307
MAPK8IP1	AC_000172.1	0	100	2.22E-19	2.32E-18	0.236	6.49307
ATG13	AC_000172.1	20	100	2.92E-08	1.49E-07	4.369	17.2482
MYBPC3	AC_000172.1	0	100	2.22E-19	2.32E-18	0.042	0.272787
MYBPC3	AC_000172.1	0	85	1.66E-16	1.56E-15	0.042	0.272787
RAPSN	AC_000172.1	0	100	2.22E-19	2.32E-18	0.068	0.345906
SLC43A3	AC_000172.1	20	100	2.92E-08	1.49E-07	0.271	0.656248
SLC43A3	AC_000172.1	0	100	2.22E-19	2.32E-18	0.271	0.656248
SLC43A3	AC_000172.1	0	80	1.24E-15	9.79E-15	0.271	0.656248
UBE2L6	AC_000172.1	0	85	1.66E-16	1.56E-15	3.465	1.79197
ZDHHC5	AC_000172.1	20	100	2.92E-08	1.49E-07	11.02	9.20832
NCAPD3	AC_000172.1	0	100	2.22E-19	2.32E-18	13.269	29.5086
IKBKE	AC_000173.1	0	80	1.24E-15	9.79E-15	0.026	0.151946
IL10	AC_000173.1	0	100	2.22E-19	2.32E-18	0.598	2.08477
LEFTY2	AC_000173.1	0	83	3.95E-16	3.44E-15	0.091	0.377381
RGS7	AC_000173.1	87	7	3.08E-11	1.96E-10	0.034	0.674704
RGS7	AC_000173.1	100	6	6.67E-14	5.10E-13	0.034	0.674704

RGS7	AC_000173.1	77	10	1.99E-08	1.05E-07	0.034	0.674704
RGS7	AC_000173.1	75	15	1.62E-06	6.65E-06	0.034	0.674704
PLOD1	AC_000173.1	100	0	2.22E-19	2.32E-18	0.255	13.5712
SLC2A5	AC_000173.1	0	90	1.66E-17	1.70E-16	0.043	1.0146
ACOT7	AC_000173.1	0	100	2.22E-19	2.32E-18	6.274	92.1376
NMNAT2	AC_000173.1	0	100	2.22E-19	2.32E-18	0.051	11.5046
NCF2	AC_000173.1	0	100	2.22E-19	2.32E-18	12.602	0.711148
LAMB3	AC_000173.1	0	100	2.22E-19	2.32E-18	0.106	0.36457
PLXNA2	AC_000173.1	0	100	2.22E-19	2.32E-18	0.028	2.16689
PLXNA2	AC_000173.1	0	100	2.22E-19	2.32E-18	0.028	2.16689
PLXNA2	AC_000173.1	0	100	2.22E-19	2.32E-18	0.028	2.16689
PLXNA2	AC_000173.1	0	100	2.22E-19	2.32E-18	0.028	2.16689
PITPNM2	AC_000174.1	0	100	2.22E-19	2.32E-18	3.483	2.33325
PITPNM2	AC_000174.1	0	100	2.22E-19	2.32E-18	3.483	2.33325
PITPNM2	AC_000174.1	0	83	3.95E-16	3.44E-15	3.483	2.33325
PITPNM2	AC_000174.1	0	100	2.22E-19	2.32E-18	3.483	2.33325
PITPNM2	AC_000174.1	0	100	2.22E-19	2.32E-18	3.483	2.33325
PITPNM2	AC_000174.1	0	83	3.95E-16	3.44E-15	3.483	2.33325
RHOF	AC_000174.1	0	100	2.22E-19	2.32E-18	1.357	1.26635
CUX2	AC_000174.1	0	100	2.22E-19	2.32E-18	50.403	0.223335
CUX2	AC_000174.1	0	100	2.22E-19	2.32E-18	50.403	0.223335
RAB35	AC_000174.1	0	90	1.66E-17	1.70E-16	18.804	5.9147
RAB35	AC_000174.1	16	100	1.86E-09	1.05E-08	18.804	5.9147
TRPV4	AC_000174.1	0	100	2.22E-19	2.32E-18	0.085	0.254707
TRPV4	AC_000174.1	0	100	2.22E-19	2.32E-18	0.085	0.254707
TRPV4	AC_000174.1	0	100	2.22E-19	2.32E-18	0.085	0.254707
TRPV4	AC_000174.1	0	100	2.22E-19	2.32E-18	0.085	0.254707
TRPV4	AC_000174.1	0	100	2.22E-19	2.32E-18	0.085	0.254707
TMEM119	AC_000174.1	100	0	2.22E-19	2.32E-18	3.219	0.865139
LIF	AC_000174.1	0	100	2.22E-19	2.32E-18	0.019	0.442617
CCDC157	AC_000174.1	0	100	2.22E-19	2.32E-18	0.086	20.239
CCDC157	AC_000174.1	0	100	2.22E-19	2.32E-18	0.086	20.239
CCDC157	AC_000174.1	0	100	2.22E-19	2.32E-18	0.086	20.239
OSBP2	AC_000174.1	0	100	2.22E-19	2.32E-18	0.359	14.0231
OSBP2	AC_000174.1	0	100	2.22E-19	2.32E-18	0.359	14.0231
OSBP2	AC_000174.1	0	100	2.22E-19	2.32E-18	0.359	14.0231
SMTN	AC_000174.1	0	100	2.22E-19	2.32E-18	0.083	3.96868
SMTN	AC_000174.1	0	100	2.22E-19	2.32E-18	0.083	3.96868
GGT5	AC_000174.1	0	100	2.22E-19	2.32E-18	0.174	0.631976
GGT5	AC_000174.1	0	80	1.24E-15	9.79E-15	0.174	0.631976
GGT5	AC_000174.1	0	100	2.22E-19	2.32E-18	0.174	0.631976
GGT5	AC_000174.1	0	100	2.22E-19	2.32E-18	0.174	0.631976
GGT5	AC_000174.1	16	100	1.86E-09	1.05E-08	0.174	0.631976
SDF2L1	AC_000174.1	0	87	7.02E-17	6.88E-16	2.915	6.17688
CCDC116	AC_000174.1	100	0	2.22E-19	2.32E-18	0.556	8.55385

SLC7A4	AC_000174.1	0	100	2.22E-19	2.32E-18	0.014	0.587754
MZT2B	AC_000174.1	20	100	2.92E-08	1.49E-07	0.19	1.20482
ARVCF	AC_000174.1	0	80	1.24E-15	9.79E-15	0.241	0.0686743
VAC14	AC_000175.1	0	100	2.22E-19	2.32E-18	0.848	5.18937
VAC14	AC_000175.1	0	80	1.24E-15	9.79E-15	0.848	5.18937
PDPR	AC_000175.1	0	100	2.22E-19	2.32E-18	7.187	5.03969
PDPR	AC_000175.1	0	100	2.22E-19	2.32E-18	7.187	5.03969
SLC38A8	AC_000175.1	0	100	2.22E-19	2.32E-18	21.463	0.203353
COTL1	AC_000175.1	0	100	2.22E-19	2.32E-18	0.614	7.3541
COTL1	AC_000175.1	100	0	2.22E-19	2.32E-18	0.614	7.3541
FOXC2	AC_000175.1	100	0	2.22E-19	2.32E-18	0.358	0.366771
SLC7A5	AC_000175.1	0	100	2.22E-19	2.32E-18	0.039	22.6674
SLC7A5	AC_000175.1	0	100	2.22E-19	2.32E-18	0.039	22.6674
SLC7A5	AC_000175.1	0	85	1.66E-16	1.56E-15	0.039	22.6674
DPEP1	AC_000175.1	0	85	1.66E-16	1.56E-15	0.061	5.56081
DPEP1	AC_000175.1	0	83	3.95E-16	3.44E-15	0.061	5.56081
DPEP1	AC_000175.1	11	100	2.69E-11	1.74E-10	0.061	5.56081
ZNF423	AC_000175.1	0	100	2.22E-19	2.32E-18	0.044	1.49701
ZNF423	AC_000175.1	0	85	1.66E-16	1.56E-15	0.044	1.49701
ZNF423	AC_000175.1	0	75	1.25E-14	9.63E-14	0.044	1.49701
ZNF423	AC_000175.1	0	100	2.22E-19	2.32E-18	0.044	1.49701
ZNF423	AC_000175.1	0	100	2.22E-19	2.32E-18	0.044	1.49701
ZNF423	AC_000175.1	0	100	2.22E-19	2.32E-18	0.044	1.49701
ZNF423	AC_000175.1	0	100	2.22E-19	2.32E-18	0.044	1.49701
ZNF423	AC_000175.1	0	100	2.22E-19	2.32E-18	0.044	1.49701
ZNF423	AC_000175.1	0	100	2.22E-19	2.32E-18	0.044	1.49701
ZNF423	AC_000175.1	0	100	2.22E-19	2.32E-18	0.044	1.49701
ZNF423	AC_000175.1	0	100	2.22E-19	2.32E-18	0.044	1.49701
ZNF423	AC_000175.1	0	100	2.22E-19	2.32E-18	0.044	1.49701
MMP2	AC_000175.1	0	100	2.22E-19	2.32E-18	0.043	11.6334
SLC12A3	AC_000175.1	0	100	2.22E-19	2.32E-18	0.912	0.238977
SLC12A3	AC_000175.1	0	88	3.94E-17	3.96E-16	0.912	0.238977
DRC7	AC_000175.1	0	100	2.22E-19	2.32E-18	195.295	14.7228
NDRG4	AC_000175.1	100	20	2.92E-08	1.49E-07	8.888	16.7646
EXOC3L1	AC_000175.1	0	88	3.94E-17	3.96E-16	0.412	1.44007
SMPD3	AC_000175.1	20	100	2.92E-08	1.49E-07	0.034	1.30709
PEPD	AC_000175.1	0	100	2.22E-19	2.32E-18	0.154	3.74324
PEPD	AC_000175.1	0	100	2.22E-19	2.32E-18	0.154	3.74324
PEPD	AC_000175.1	0	100	2.22E-19	2.32E-18	0.154	3.74324
PEPD	AC_000175.1	0	81	9.35E-16	8.12E-15	0.154	3.74324
PEPD	AC_000175.1	0	100	2.22E-19	2.32E-18	0.154	3.74324
GPI	AC_000175.1	80	0	1.24E-15	9.79E-15	86.567	52.6938
IGFLR1	AC_000175.1	100	14	3.79E-10	2.31E-09	1.824	2.01574
SHKBP1	AC_000175.1	100	0	2.22E-19	2.32E-18	7.656	6.43168
CYP2S1	AC_000175.1	0	100	2.22E-19	2.32E-18	2.047	0.065393

CEACAM19	AC_000175.1	80	0	1.24E-15	9.79E-15	6.162	0.0432857
PPP1R37	AC_000175.1	100	0	2.22E-19	2.32E-18	5.595	16.1979
PPP1R37	AC_000175.1	100	9	3.27E-12	2.29E-11	5.595	16.1979
DHX34	AC_000175.1	0	100	2.22E-19	2.32E-18	0.444	7.09385
DHX34	AC_000175.1	0	100	2.22E-19	2.32E-18	0.444	7.09385
TULP2	AC_000175.1	100	0	2.22E-19	2.32E-18	0.794	16.9575
FCGRT	AC_000175.1	0	87	7.02E-17	6.88E-16	1.853	0.128583
RCN3	AC_000175.1	0	100	2.22E-19	2.32E-18	2.171	3.84027
TSKS	AC_000175.1	100	20	2.92E-08	1.49E-07	0.185	40.0046
TBC1D17	AC_000175.1	100	0	2.22E-19	2.32E-18	0.524	5.25401
KLK12	AC_000175.1	0	100	2.22E-19	2.32E-18	0.207	0.021982
FIZ1	AC_000175.1	100	0	2.22E-19	2.32E-18	0.346	0.0353889
NAT14	AC_000175.1	20	100	2.92E-08	1.49E-07	0.065	0.546189
PPP6R1	AC_000175.1	0	83	3.95E-16	3.44E-15	0.638	31.2632
TNNI3	AC_000175.1	100	0	2.22E-19	2.32E-18	0.331	11.6081
TTYH1	AC_000175.1	0	90	1.66E-17	1.70E-16	1.491	53.4688
TTYH1	AC_000175.1	0	83	3.95E-16	3.44E-15	1.491	53.4688
TTYH1	AC_000175.1	0	80	1.24E-15	9.79E-15	1.491	53.4688
MBOAT7	AC_000175.1	20	87	1.14E-06	4.73E-06	4.474	0.113894
TMC4	AC_000175.1	0	80	1.24E-15	9.79E-15	9.292	0.246617
ZIM2	AC_000175.1	0	85	1.66E-16	1.56E-15	39.328	0.068638
ZIM2	AC_000175.1	14	75	9.09E-07	3.87E-06	39.328	0.068638
ZIM2	AC_000175.1	80	0	1.24E-15	9.79E-15	39.328	0.068638
ZNF583	AC_000175.1	14	75	9.09E-07	3.87E-06	57.418	0.178527
MSI2	AC_000176.1	0	100	2.22E-19	2.32E-18	0.929	3.4265
MSI2	AC_000176.1	0	81	9.35E-16	8.12E-15	0.929	3.4265
MSI2	AC_000176.1	0	100	2.22E-19	2.32E-18	0.929	3.4265
MSI2	AC_000176.1	0	100	2.22E-19	2.32E-18	0.929	3.4265
MSI2	AC_000176.1	0	100	2.22E-19	2.32E-18	0.929	3.4265
RNF43	AC_000176.1	0	80	1.24E-15	9.79E-15	0.831	0.584618
RNF43	AC_000176.1	20	100	2.92E-08	1.49E-07	0.831	0.584618
C19H17orf64	AC_000176.1	0	100	2.22E-19	2.32E-18	0.075	32.1067
GAS2L2	AC_000176.1	0	100	2.22E-19	2.32E-18	0.038	0.147563
LGALS9	AC_000176.1	0	100	2.22E-19	2.32E-18	0.127	0.82207
LGALS9	AC_000176.1	0	100	2.22E-19	2.32E-18	0.127	0.82207
NOS2	AC_000176.1	0	100	2.22E-19	2.32E-18	14.803	0.0757853
UNC119	AC_000176.1	0	100	2.22E-19	2.32E-18	37.376	8.00687
TRAF4	AC_000176.1	80	16	7.24E-07	3.14E-06	13.713	2.96348
FLOT2	AC_000176.1	0	81	9.35E-16	8.12E-15	21.125	3.41417
TRPV3	AC_000176.1	0	100	2.22E-19	2.32E-18	0.687	0.436797
CAMKK1	AC_000176.1	0	100	2.22E-19	2.32E-18	0.194	0.879351
CAMKK1	AC_000176.1	20	100	2.92E-08	1.49E-07	0.194	0.879351
ATP2A3	AC_000176.1	0	100	2.22E-19	2.32E-18	0.053	8.57103
SLC13A5	AC_000176.1	0	100	2.22E-19	2.32E-18	0.016	0.0628505
WSCD1	AC_000176.1	0	100	2.22E-19	2.32E-18	0.044	4.50593

SPEM1	AC_000176.1	0	100	2.22E-19	2.32E-18	0.029	12.3162
GUCY2D	AC_000176.1	0	75	1.25E-14	9.63E-14	0.197	0.0841453
NTN1	AC_000176.1	0	100	2.22E-19	2.32E-18	0.574	0.550449
GAS7	AC_000176.1	0	100	2.22E-19	2.32E-18	6.404	3.74942
DNAH9	AC_000176.1	0	100	2.22E-19	2.32E-18	0.097	0.0143802
FAM83G	AC_000176.1	0	100	2.22E-19	2.32E-18	0.022	1.55324
CACNA1G	AC_000176.1	11	100	2.69E-11	1.74E-10	0.054	0.704679
CACNA1G	AC_000176.1	11	100	2.69E-11	1.74E-10	0.054	0.704679
SP2	AC_000176.1	0	100	2.22E-19	2.32E-18	52.222	3.75422
SP2	AC_000176.1	0	100	2.22E-19	2.32E-18	52.222	3.75422
RPL19	AC_000176.1	80	23	3.02E-05	1.03E-04	622.381	133.855
FBXL20	AC_000176.1	77	9	8.67E-09	4.71E-08	27.908	6.7384
FBXL20	AC_000176.1	80	14	1.93E-07	8.74E-07	27.908	6.7384
FBXL20	AC_000176.1	20	83	3.33E-06	1.30E-05	27.908	6.7384
ERBB2	AC_000176.1	0	100	2.22E-19	2.32E-18	0.006	1.35771
RARA	AC_000176.1	100	0	2.22E-19	2.32E-18	5.363	10.1415
KRT19	AC_000176.1	0	100	2.22E-19	2.32E-18	5.702	0.105565
JUP	AC_000176.1	0	100	2.22E-19	2.32E-18	0.111	3.69015
FKBP10	AC_000176.1	0	100	2.22E-19	2.32E-18	0.139	3.3218
DHX58	AC_000176.1	0	85	1.66E-16	1.56E-15	33.229	0.249484
HDAC5	AC_000176.1	0	100	2.22E-19	2.32E-18	0.17	7.63568
MAPT	AC_000176.1	0	100	2.22E-19	2.32E-18	0.795	0.731686
DCXR	AC_000176.1	0	81	9.35E-16	8.12E-15	1.349	2.01575
CCDC137	AC_000176.1	100	0	2.22E-19	2.32E-18	2.166	1.53063
BAIAP2	AC_000176.1	0	100	2.22E-19	2.32E-18	20.545	3.97209
BAIAP2	AC_000176.1	0	80	1.24E-15	9.79E-15	20.545	3.97209
TBC1D16	AC_000176.1	20	100	2.92E-08	1.49E-07	0.174	0.690348
TBC1D16	AC_000176.1	0	100	2.22E-19	2.32E-18	0.174	0.690348
RBFOX3	AC_000176.1	0	85	1.66E-16	1.56E-15	0.362	0.0541617
RBFOX3	AC_000176.1	0	100	2.22E-19	2.32E-18	0.362	0.0541617
RBFOX3	AC_000176.1	0	100	2.22E-19	2.32E-18	0.362	0.0541617
RBFOX3	AC_000176.1	0	100	2.22E-19	2.32E-18	0.362	0.0541617
RBFOX3	AC_000176.1	0	100	2.22E-19	2.32E-18	0.362	0.0541617
RBFOX3	AC_000176.1	0	100	2.22E-19	2.32E-18	0.362	0.0541617
RBFOX3	AC_000176.1	0	100	2.22E-19	2.32E-18	0.362	0.0541617
RBFOX3	AC_000176.1	0	100	2.22E-19	2.32E-18	0.362	0.0541617
RBFOX3	AC_000176.1	0	100	2.22E-19	2.32E-18	0.362	0.0541617
TIMP2	AC_000176.1	25	100	5.20E-07	2.28E-06	1.267	273.458
TRIM47	AC_000176.1	0	100	2.22E-19	2.32E-18	0.015	1.20996
TRIM47	AC_000176.1	0	100	2.22E-19	2.32E-18	0.015	1.20996
TRIM47	AC_000176.1	0	100	2.22E-19	2.32E-18	0.015	1.20996
TRIM47	AC_000176.1	20	100	2.92E-08	1.49E-07	0.015	1.20996
TRIM47	AC_000176.1	0	100	2.22E-19	2.32E-18	0.015	1.20996
GALK1	AC_000176.1	0	100	2.22E-19	2.32E-18	0.572	3.79491
MIF4GD	AC_000176.1	0	100	2.22E-19	2.32E-18	24.332	2.68766

MRPS7	AC_000176.1	0	100	2.22E-19	2.32E-18	16.342	0.682308
CDR2L	AC_000176.1	80	0	1.24E-15	9.79E-15	1.002	0.619825
FADS6	AC_000176.1	0	100	2.22E-19	2.32E-18	0.374	2.77879
RAB37	AC_000176.1	100	22	9.72E-08	4.57E-07	2.856	0.531397
RAB37	AC_000176.1	75	17	5.30E-06	2.04E-05	2.856	0.531397
RAB37	AC_000176.1	85	0	1.66E-16	1.56E-15	2.856	0.531397
RAB37	AC_000176.1	75	7	2.27E-09	1.28E-08	2.856	0.531397
RAB37	AC_000176.1	100	22	9.72E-08	4.57E-07	2.856	0.531397
RAB37	AC_000176.1	23	87	5.11E-06	1.98E-05	2.856	0.531397
RAB37	AC_000176.1	75	22	6.49E-05	2.14E-04	2.856	0.531397
RAB37	AC_000176.1	75	25	2.10E-04	6.22E-04	2.856	0.531397
RAB37	AC_000176.1	75	10	4.51E-08	2.16E-07	2.856	0.531397
TTYH2	AC_000176.1	0	100	2.22E-19	2.32E-18	0.01	2.69215
TTYH2	AC_000176.1	0	100	2.22E-19	2.32E-18	0.01	2.69215
TTYH2	AC_000176.1	0	85	1.66E-16	1.56E-15	0.01	2.69215
TTYH2	AC_000176.1	0	100	2.22E-19	2.32E-18	0.01	2.69215
SLC39A11	AC_000176.1	0	100	2.22E-19	2.32E-18	0.182	10.2451
SLC39A11	AC_000176.1	0	100	2.22E-19	2.32E-18	0.182	10.2451
SLC39A11	AC_000176.1	0	100	2.22E-19	2.32E-18	0.182	10.2451
SLC39A11	AC_000176.1	0	100	2.22E-19	2.32E-18	0.182	10.2451
SLC39A11	AC_000176.1	0	100	2.22E-19	2.32E-18	0.182	10.2451
SLC39A11	AC_000176.1	0	100	2.22E-19	2.32E-18	0.182	10.2451
ARSG	AC_000176.1	0	100	2.22E-19	2.32E-18	0.088	0.503372
ARSG	AC_000176.1	0	83	3.95E-16	3.44E-15	0.088	0.503372
ARSG	AC_000176.1	0	85	1.66E-16	1.56E-15	0.088	0.503372
RGS9	AC_000176.1	83	0	3.95E-16	3.44E-15	0.307	0.266382
RGS9	AC_000176.1	0	100	2.22E-19	2.32E-18	0.307	0.266382
RGS9	AC_000176.1	0	100	2.22E-19	2.32E-18	0.307	0.266382
PRKCA	AC_000176.1	0	100	2.22E-19	2.32E-18	3.412	1.8482
LIMS2	AC_000159.1	0	80	1.24E-15	9.79E-15	0.03	12.1793
BIN1	AC_000159.1	0	100	2.22E-19	2.32E-18	0.059	2.75044
BIN1	AC_000159.1	20	87	1.14E-06	4.73E-06	0.059	2.75044
BIN1	AC_000159.1	0	100	2.22E-19	2.32E-18	0.059	2.75044
BIN1	AC_000159.1	0	100	2.22E-19	2.32E-18	0.059	2.75044
BIN1	AC_000159.1	0	100	2.22E-19	2.32E-18	0.059	2.75044
BIN1	AC_000159.1	0	88	3.94E-17	3.96E-16	0.059	2.75044
BIN1	AC_000159.1	16	100	1.86E-09	1.05E-08	0.059	2.75044
BIN1	AC_000159.1	0	100	2.22E-19	2.32E-18	0.059	2.75044
BIN1	AC_000159.1	0	100	2.22E-19	2.32E-18	0.059	2.75044
GAD1	AC_000159.1	100	0	2.22E-19	2.32E-18	10.777	0.625979
GLI2	AC_000159.1	0	100	2.22E-19	2.32E-18	2.17	0.233586
TFCP2L1	AC_000159.1	0	100	2.22E-19	2.32E-18	0.037	1.95606
TFCP2L1	AC_000159.1	0	100	2.22E-19	2.32E-18	0.037	1.95606
4-Mar	AC_000159.1	0	100	2.22E-19	2.32E-18	0.089	0.0251621
TNS1	AC_000159.1	0	100	2.22E-19	2.32E-18	0.237	8.80054

TNS1	AC_000159.1	0	85	1.66E-16	1.56E-15	0.237	8.80054
TNS1	AC_000159.1	20	100	2.92E-08	1.49E-07	0.237	8.80054
TNS1	AC_000159.1	20	100	2.92E-08	1.49E-07	0.237	8.80054
SPEG	AC_000159.1	0	100	2.22E-19	2.32E-18	0.872	0.286045
OBSL1	AC_000159.1	0	100	2.22E-19	2.32E-18	0.406	1.48814
OBSL1	AC_000159.1	0	100	2.22E-19	2.32E-18	0.406	1.48814
SLC4A3	AC_000159.1	0	100	2.22E-19	2.32E-18	0.033	1.40557
TMEM54	AC_000159.1	0	100	2.22E-19	2.32E-18	0.367	0.0103144
FGR	AC_000159.1	0	100	2.22E-19	2.32E-18	4.108	0.765796
FGR	AC_000159.1	0	85	1.66E-16	1.56E-15	4.108	0.765796
UBXN11	AC_000159.1	0	100	2.22E-19	2.32E-18	1.157	25.2103
RUNX3	AC_000159.1	0	100	2.22E-19	2.32E-18	0.047	1.51401
EPHB2	AC_000159.1	0	100	2.22E-19	2.32E-18	0.42	0.528627
EPHB2	AC_000159.1	0	100	2.22E-19	2.32E-18	0.42	0.528627
EPHB2	AC_000159.1	0	100	2.22E-19	2.32E-18	0.42	0.528627
EPHB2	AC_000159.1	0	100	2.22E-19	2.32E-18	0.42	0.528627
EPHB2	AC_000159.1	0	100	2.22E-19	2.32E-18	0.42	0.528627
RAP1GAP	AC_000159.1	0	100	2.22E-19	2.32E-18	0.052	2.88221
RAP1GAP	AC_000159.1	0	100	2.22E-19	2.32E-18	0.052	2.88221
RAP1GAP	AC_000159.1	0	100	2.22E-19	2.32E-18	0.052	2.88221
RAP1GAP	AC_000159.1	0	100	2.22E-19	2.32E-18	0.052	2.88221
RAP1GAP	AC_000159.1	0	85	1.66E-16	1.56E-15	0.052	2.88221
RAP1GAP	AC_000159.1	16	100	1.86E-09	1.05E-08	0.052	2.88221
KIF17	AC_000159.1	0	83	3.95E-16	3.44E-15	1.718	4.03725
KIF17	AC_000159.1	0	100	2.22E-19	2.32E-18	1.718	4.03725
KIF17	AC_000159.1	0	100	2.22E-19	2.32E-18	1.718	4.03725
AKR7A2	AC_000159.1	0	100	2.22E-19	2.32E-18	20.822	10.6193
AKR7A2	AC_000159.1	0	100	2.22E-19	2.32E-18	20.822	10.6193
PADI1	AC_000159.1	0	100	2.22E-19	2.32E-18	0.039	0.00684407
LCP2	AC_000177.1	80	12	4.35E-08	2.09E-07	1.715	0.857954
LCP2	AC_000177.1	75	20	2.62E-05	9.12E-05	1.715	0.857954
SLC38A9	AC_000177.1	80	0	1.24E-15	9.79E-15	23.787	12.0679
SLC9A3	AC_000177.1	0	100	2.22E-19	2.32E-18	0.518	0.282475
MRPS11	AC_000178.1	75	21	3.99E-05	1.35E-04	5.9	1.91452
SLC28A1	AC_000178.1	100	15	9.23E-10	5.35E-09	23.765	0.0796632
RASGRF1	AC_000178.1	0	100	2.22E-19	2.32E-18	5.526	0.237718
APBA2	AC_000178.1	0	100	2.22E-19	2.32E-18	0.009	0.122996
SNX33	AC_000178.1	0	100	2.22E-19	2.32E-18	0.025	2.69601
LOXL1	AC_000178.1	0	100	2.22E-19	2.32E-18	0.117	5.00407
LOXL1	AC_000178.1	0	100	2.22E-19	2.32E-18	0.117	5.00407
LOXL1	AC_000178.1	0	80	1.24E-15	9.79E-15	0.117	5.00407
FRMD5	AC_000178.1	88	14	1.67E-08	8.86E-08	5.627	0.203298
FRMD5	AC_000178.1	100	25	5.20E-07	2.28E-06	5.627	0.203298
FRMD5	AC_000178.1	80	20	6.94E-06	2.60E-05	5.627	0.203298
IFI27	AC_000178.1	0	100	2.22E-19	2.32E-18	2.061	0.682495

KRTCAP2	AC_000178.1	0	100	2.22E-19	2.32E-18	66.354	13.6621
BEGAIN	AC_000178.1	0	100	2.22E-19	2.32E-18	0.026	0.239427
EXOC3L4	AC_000178.1	0	100	2.22E-19	2.32E-18	0.104	0.202865
TNFAIP2	AC_000178.1	0	100	2.22E-19	2.32E-18	0.041	3.27001
TNFAIP2	AC_000178.1	0	100	2.22E-19	2.32E-18	0.041	3.27001
SCN5A	AC_000179.1	0	100	2.22E-19	2.32E-18	8.015	0.949517
SCN5A	AC_000179.1	0	100	2.22E-19	2.32E-18	8.015	0.949517
SLC25A38	AC_000179.1	0	100	2.22E-19	2.32E-18	6.859	2.83743
SYNPR	AC_000179.1	83	22	9.08E-06	3.37E-05	0.827	0.493366
SYNPR	AC_000179.1	75	20	2.62E-05	9.12E-05	0.827	0.493366
ERC2	AC_000179.1	83	0	3.95E-16	3.44E-15	6.3	0.399069
ERC2	AC_000179.1	80	16	7.24E-07	3.14E-06	6.3	0.399069
POC1A	AC_000179.1	0	83	3.95E-16	3.44E-15	24.123	18.5052
GRM2	AC_000179.1	0	80	1.24E-15	9.79E-15	0.412	0.063472
SLC38A3	AC_000179.1	0	100	2.22E-19	2.32E-18	1.596	0.00938683
LAMB2	AC_000179.1	0	100	2.22E-19	2.32E-18	0.037	0.0489692
LAMB2	AC_000179.1	0	83	3.95E-16	3.44E-15	0.037	0.0489692
LAMB2	AC_000179.1	16	100	1.86E-09	1.05E-08	0.037	0.0489692
CSPG5	AC_000179.1	0	100	2.22E-19	2.32E-18	2.17	21.0075
CSPG5	AC_000179.1	0	100	2.22E-19	2.32E-18	2.17	21.0075
CSPG5	AC_000179.1	0	80	1.24E-15	9.79E-15	2.17	21.0075
PTH1R	AC_000179.1	0	100	2.22E-19	2.32E-18	0.034	1.46063
PTH1R	AC_000179.1	0	80	1.24E-15	9.79E-15	0.034	1.46063
PTH1R	AC_000179.1	0	100	2.22E-19	2.32E-18	0.034	1.46063
PTH1R	AC_000179.1	0	100	2.22E-19	2.32E-18	0.034	1.46063
PTH1R	AC_000179.1	0	100	2.22E-19	2.32E-18	0.034	1.46063
LIMD1	AC_000179.1	0	100	2.22E-19	2.32E-18	0.854	0.771372
ATP2B2	AC_000179.1	0	100	2.22E-19	2.32E-18	0.009	0.118503
ATP2B2	AC_000179.1	0	100	2.22E-19	2.32E-18	0.009	0.118503
ATP2B2	AC_000179.1	0	100	2.22E-19	2.32E-18	0.009	0.118503
RHO	AC_000179.1	0	100	2.22E-19	2.32E-18	0.131	0.102191
SLC6A6	AC_000179.1	0	100	2.22E-19	2.32E-18	0.039	8.29457
SLC6A6	AC_000179.1	0	100	2.22E-19	2.32E-18	0.039	8.29457
SLC6A6	AC_000179.1	0	100	2.22E-19	2.32E-18	0.039	8.29457
SLC6A6	AC_000179.1	0	100	2.22E-19	2.32E-18	0.039	8.29457
SLC6A6	AC_000179.1	0	100	2.22E-19	2.32E-18	0.039	8.29457
SLC6A6	AC_000179.1	0	100	2.22E-19	2.32E-18	0.039	8.29457
TMEM43	AC_000179.1	0	100	2.22E-19	2.32E-18	39.068	14.655
HDAC11	AC_000179.1	0	83	3.95E-16	3.44E-15	4.063	28.2128
NUP210	AC_000179.1	0	100	2.22E-19	2.32E-18	0.36	2.69E-06
NUP210	AC_000179.1	0	100	2.22E-19	2.32E-18	0.36	2.69E-06
NUP210	AC_000179.1	0	100	2.22E-19	2.32E-18	0.36	2.69E-06
NUP210	AC_000179.1	0	100	2.22E-19	2.32E-18	0.36	2.69E-06
NUP210	AC_000179.1	0	100	2.22E-19	2.32E-18	0.36	2.69E-06
NUP210	AC_000179.1	0	100	2.22E-19	2.32E-18	0.36	2.69E-06

NUP210	AC_000179.1	0	100	2.22E-19	2.32E-18	0.36	2.69E-06
NUP210	AC_000179.1	0	100	2.22E-19	2.32E-18	0.36	2.69E-06
NUP210	AC_000179.1	0	100	2.22E-19	2.32E-18	0.36	2.69E-06
GATA2	AC_000179.1	0	100	2.22E-19	2.32E-18	21.446	1.24153
EEFSEC	AC_000179.1	0	100	2.22E-19	2.32E-18	0.386	3.16696
EEFSEC	AC_000179.1	0	100	2.22E-19	2.32E-18	0.386	3.16696
EEFSEC	AC_000179.1	0	100	2.22E-19	2.32E-18	0.386	3.16696
EEFSEC	AC_000179.1	0	100	2.22E-19	2.32E-18	0.386	3.16696
EEFSEC	AC_000179.1	0	100	2.22E-19	2.32E-18	0.386	3.16696
EEFSEC	AC_000179.1	0	85	1.66E-16	1.56E-15	0.386	3.16696
KLF15	AC_000179.1	100	0	2.22E-19	2.32E-18	0.159	2.02475
ITPR3	AC_000180.1	0	100	2.22E-19	2.32E-18	0.419	15.3446
LEMD2	AC_000180.1	20	87	1.14E-06	4.73E-06	0.012	4.92624
NFKBIE	AC_000180.1	0	100	2.22E-19	2.32E-18	13.733	4.98304
MSH5	AC_000180.1	0	100	2.22E-19	2.32E-18	32.708	4.41634
HIST1H1C	AC_000180.1	80	12	4.35E-08	2.09E-07	154.3	0.347191
TFAP2A	AC_000180.1	100	0	2.22E-19	2.32E-18	0.195	0.580145
NRN1	AC_000180.1	0	100	2.22E-19	2.32E-18	0.097	0.237949
PXDC1	AC_000180.1	0	100	2.22E-19	2.32E-18	0.098	0.305641
PXDC1	AC_000180.1	0	100	2.22E-19	2.32E-18	0.098	0.305641
PXDC1	AC_000180.1	0	100	2.22E-19	2.32E-18	0.098	0.305641
SLC22A23	AC_000180.1	0	100	2.22E-19	2.32E-18	0.015	1.59637
SLC22A23	AC_000180.1	0	100	2.22E-19	2.32E-18	0.015	1.59637
SLC22A23	AC_000180.1	0	88	3.94E-17	3.96E-16	0.015	1.59637
GMDS	AC_000180.1	20	100	2.92E-08	1.49E-07	1.399	29.0845
GMDS	AC_000180.1	0	80	1.24E-15	9.79E-15	1.399	29.0845
NFATC1	AC_000181.1	0	100	2.22E-19	2.32E-18	0.291	0.256695
NFATC1	AC_000181.1	0	100	2.22E-19	2.32E-18	0.291	0.256695
NFATC1	AC_000181.1	0	100	2.22E-19	2.32E-18	0.291	0.256695
NFATC1	AC_000181.1	0	100	2.22E-19	2.32E-18	0.291	0.256695
NFATC1	AC_000181.1	0	100	2.22E-19	2.32E-18	0.291	0.256695
NFATC1	AC_000181.1	0	100	2.22E-19	2.32E-18	0.291	0.256695
NFATC1	AC_000181.1	0	87	7.02E-17	6.88E-16	0.291	0.256695
NFATC1	AC_000181.1	0	87	7.02E-17	6.88E-16	0.291	0.256695
NFATC1	AC_000181.1	0	83	3.95E-16	3.44E-15	0.291	0.256695
NFATC1	AC_000181.1	20	100	2.92E-08	1.49E-07	0.291	0.256695
NFATC1	AC_000181.1	0	100	2.22E-19	2.32E-18	0.291	0.256695
CELF4	AC_000181.1	0	100	2.22E-19	2.32E-18	0.169	0.498227
CELF4	AC_000181.1	0	100	2.22E-19	2.32E-18	0.169	0.498227
CELF4	AC_000181.1	0	100	2.22E-19	2.32E-18	0.169	0.498227
CELF4	AC_000181.1	0	100	2.22E-19	2.32E-18	0.169	0.498227
CELF4	AC_000181.1	100	14	3.79E-10	2.31E-09	0.169	0.498227
CELF4	AC_000181.1	0	100	2.22E-19	2.32E-18	0.169	0.498227
CELF4	AC_000181.1	0	100	2.22E-19	2.32E-18	0.169	0.498227
CELF4	AC_000181.1	0	100	2.22E-19	2.32E-18	0.169	0.498227

CELF4	AC_000181.1	0	100	2.22E-19	2.32E-18	0.169	0.498227
CELF4	AC_000181.1	0	100	2.22E-19	2.32E-18	0.169	0.498227
CELF4	AC_000181.1	0	100	2.22E-19	2.32E-18	0.169	0.498227
CELF4	AC_000181.1	0	100	2.22E-19	2.32E-18	0.169	0.498227
CELF4	AC_000181.1	0	100	2.22E-19	2.32E-18	0.169	0.498227
CELF4	AC_000181.1	0	100	2.22E-19	2.32E-18	0.169	0.498227
CELF4	AC_000181.1	0	90	1.66E-17	1.70E-16	0.169	0.498227
RHBDF1	AC_000182.1	100	0	2.22E-19	2.32E-18	1.067	1.15272
RHBDF1	AC_000182.1	100	0	2.22E-19	2.32E-18	1.067	1.15272
ABCA3	AC_000182.1	0	100	2.22E-19	2.32E-18	0.347	5.89378
CORO7	AC_000182.1	0	85	1.66E-16	1.56E-15	0.265	2.71946
CORO7	AC_000182.1	0	83	3.95E-16	3.44E-15	0.265	2.71946
RBFOX1	AC_000182.1	80	22	1.84E-05	6.52E-05	0.646	0.038647
RBFOX1	AC_000182.1	0	100	2.22E-19	2.32E-18	0.646	0.038647
ABAT	AC_000182.1	20	100	2.92E-08	1.49E-07	9.507	13.3077
ABCC6	AC_000182.1	0	100	2.22E-19	2.32E-18	0.027	8.03E-08
RABEP2	AC_000182.1	0	80	1.24E-15	9.79E-15	2.217	3.18206
ELN	AC_000182.1	0	100	2.22E-19	2.32E-18	8.902	89.7002
ELN	AC_000182.1	0	100	2.22E-19	2.32E-18	8.902	89.7002
COL26A1	AC_000182.1	0	100	2.22E-19	2.32E-18	0.018	0.355506
TRIM56	AC_000182.1	0	100	2.22E-19	2.32E-18	0.621	0.267774
TRIM56	AC_000182.1	0	85	1.66E-16	1.56E-15	0.621	0.267774
ACHE	AC_000182.1	0	100	2.22E-19	2.32E-18	0.018	2.36354
MEPCE	AC_000182.1	100	0	2.22E-19	2.32E-18	20.474	134.825
SLC29A4	AC_000182.1	0	100	2.22E-19	2.32E-18	24.313	0.192267
CARD11	AC_000182.1	0	100	2.22E-19	2.32E-18	0.007	0.584971
CARD11	AC_000182.1	20	80	6.94E-06	2.60E-05	0.007	0.584971
CARD11	AC_000182.1	0	100	2.22E-19	2.32E-18	0.007	0.584971
MICALL2	AC_000182.1	0	100	2.22E-19	2.32E-18	0.044	0.182125
C25H7orf50	AC_000182.1	0	83	3.95E-16	3.44E-15	1.02	3.55481
C25H7orf50	AC_000182.1	0	100	2.22E-19	2.32E-18	1.02	3.55481
PRKG1	AC_000183.1	83	0	3.95E-16	3.44E-15	25.31	2.01529
SUFU	AC_000183.1	0	100	2.22E-19	2.32E-18	1.2	3.82115
SUFU	AC_000183.1	0	100	2.22E-19	2.32E-18	1.2	3.82115
SUFU	AC_000183.1	0	87	7.02E-17	6.88E-16	1.2	3.82115
SUFU	AC_000183.1	0	100	2.22E-19	2.32E-18	1.2	3.82115
SUFU	AC_000183.1	0	100	2.22E-19	2.32E-18	1.2	3.82115
NEURL1	AC_000183.1	0	100	2.22E-19	2.32E-18	0.024	2.93028
SORCS3	AC_000183.1	0	100	2.22E-19	2.32E-18	7.95	20.632
SORCS3	AC_000183.1	14	100	3.79E-10	2.31E-09	7.95	20.632
SORCS3	AC_000183.1	0	100	2.22E-19	2.32E-18	7.95	20.632
SORCS3	AC_000183.1	100	12	6.45E-11	4.07E-10	7.95	20.632
SORCS3	AC_000183.1	0	100	2.22E-19	2.32E-18	7.95	20.632
SORCS3	AC_000183.1	0	100	2.22E-19	2.32E-18	7.95	20.632
SORCS3	AC_000183.1	12	100	6.45E-11	4.07E-10	7.95	20.632

LHPP	AC_000183.1	0	83	3.95E-16	3.44E-15	0.303	2.59394
LHPP	AC_000183.1	0	100	2.22E-19	2.32E-18	0.303	2.59394
LHPP	AC_000183.1	0	100	2.22E-19	2.32E-18	0.303	2.59394
MYOM2	AC_000184.1	0	100	2.22E-19	2.32E-18	0.057	0.0286405
MYOM2	AC_000184.1	0	80	1.24E-15	9.79E-15	0.057	0.0286405
MYOM2	AC_000184.1	0	100	2.22E-19	2.32E-18	0.057	0.0286405
MYOM2	AC_000184.1	0	100	2.22E-19	2.32E-18	0.057	0.0286405
MYOM2	AC_000184.1	0	100	2.22E-19	2.32E-18	0.057	0.0286405
MYOM2	AC_000184.1	0	90	1.66E-17	1.70E-16	0.057	0.0286405
WRN	AC_000184.1	87	0	7.02E-17	6.88E-16	20.063	8.79611
WRN	AC_000184.1	75	0	1.25E-14	9.63E-14	20.063	8.79611
WRN	AC_000184.1	77	5	9.69E-11	6.06E-10	20.063	8.79611
WRN	AC_000184.1	100	0	2.22E-19	2.32E-18	20.063	8.79611
WRN	AC_000184.1	85	0	1.66E-16	1.56E-15	20.063	8.79611
WRN	AC_000184.1	75	0	1.25E-14	9.63E-14	20.063	8.79611
WRN	AC_000184.1	84	4	1.55E-12	1.10E-11	20.063	8.79611
WRN	AC_000184.1	100	13	1.74E-10	1.08E-09	20.063	8.79611
WRN	AC_000184.1	93	17	3.16E-08	1.61E-07	20.063	8.79611
WRN	AC_000184.1	75	10	4.51E-08	2.16E-07	20.063	8.79611
WRN	AC_000184.1	94	18	4.57E-08	2.19E-07	20.063	8.79611
WRN	AC_000184.1	100	0	2.22E-19	2.32E-18	20.063	8.79611
WRN	AC_000184.1	100	0	2.22E-19	2.32E-18	20.063	8.79611
WRN	AC_000184.1	87	0	7.02E-17	6.88E-16	20.063	8.79611
WRN	AC_000184.1	75	0	1.25E-14	9.63E-14	20.063	8.79611
WRN	AC_000184.1	100	6	6.67E-14	5.10E-13	20.063	8.79611
WRN	AC_000184.1	100	13	1.74E-10	1.08E-09	20.063	8.79611
WRN	AC_000184.1	92	12	9.13E-10	5.30E-09	20.063	8.79611
WRN	AC_000184.1	93	13	1.56E-09	8.97E-09	20.063	8.79611
WRN	AC_000184.1	100	17	4.16E-09	2.32E-08	20.063	8.79611
WRN	AC_000184.1	87	13	1.05E-08	5.72E-08	20.063	8.79611
WRN	AC_000184.1	100	21	5.72E-08	2.73E-07	20.063	8.79611
WRN	AC_000184.1	93	20	2.22E-07	1.00E-06	20.063	8.79611
WRN	AC_000184.1	78	25	1.11E-04	3.51E-04	20.063	8.79611
WRN	AC_000184.1	93	0	5.27E-18	5.48E-17	20.063	8.79611
WRN	AC_000184.1	100	5	1.69E-14	1.30E-13	20.063	8.79611
WRN	AC_000184.1	100	7	2.90E-13	2.15E-12	20.063	8.79611
WRN	AC_000184.1	85	7	6.35E-11	4.03E-10	20.063	8.79611
WRN	AC_000184.1	100	12	6.45E-11	4.07E-10	20.063	8.79611
WRN	AC_000184.1	86	12	6.41E-09	3.54E-08	20.063	8.79611
WRN	AC_000184.1	83	16	3.25E-07	1.45E-06	20.063	8.79611
WRN	AC_000184.1	80	22	1.84E-05	6.52E-05	20.063	8.79611
RNF122	AC_000184.1	75	0	1.25E-14	9.63E-14	8.137	10.1717
RNF122	AC_000184.1	100	12	6.45E-11	4.07E-10	8.137	10.1717
RNF122	AC_000184.1	100	23	1.80E-07	8.23E-07	8.137	10.1717
RNF122	AC_000184.1	20	83	3.33E-06	1.30E-05	8.137	10.1717

RNF122	AC_000184.1	80	22	1.84E-05	6.52E-05	8.137	10.1717
RNF122	AC_000184.1	85	0	1.66E-16	1.56E-15	8.137	10.1717
RNF122	AC_000184.1	100	11	2.69E-11	1.74E-10	8.137	10.1717
RNF122	AC_000184.1	100	20	2.92E-08	1.49E-07	8.137	10.1717
RNF122	AC_000184.1	80	16	7.24E-07	3.14E-06	8.137	10.1717
RNF122	AC_000184.1	83	0	3.95E-16	3.44E-15	8.137	10.1717
RNF122	AC_000184.1	80	0	1.24E-15	9.79E-15	8.137	10.1717
RNF122	AC_000184.1	77	0	5.26E-15	4.10E-14	8.137	10.1717
RNF122	AC_000184.1	100	0	2.22E-19	2.32E-18	8.137	10.1717
RNF122	AC_000184.1	87	0	7.02E-17	6.88E-16	8.137	10.1717
RNF122	AC_000184.1	80	0	1.24E-15	9.79E-15	8.137	10.1717
RNF122	AC_000184.1	0	91	1.25E-17	1.29E-16	8.137	10.1717
RNF122	AC_000184.1	83	0	3.95E-16	3.44E-15	8.137	10.1717
RNF122	AC_000184.1	100	20	2.92E-08	1.49E-07	8.137	10.1717
RNF122	AC_000184.1	82	25	4.09E-05	1.38E-04	8.137	10.1717
RNF122	AC_000184.1	100	14	3.79E-10	2.31E-09	8.137	10.1717
RNF122	AC_000184.1	80	0	1.24E-15	9.79E-15	8.137	10.1717
RNF122	AC_000184.1	80	7	4.23E-10	2.58E-09	8.137	10.1717
RNF122	AC_000184.1	100	17	4.16E-09	2.32E-08	8.137	10.1717
RNF122	AC_000184.1	100	20	2.92E-08	1.49E-07	8.137	10.1717
RNF122	AC_000184.1	100	0	2.22E-19	2.32E-18	8.137	10.1717
RNF122	AC_000184.1	80	7	4.23E-10	2.58E-09	8.137	10.1717
RNF122	AC_000184.1	75	6	8.00E-10	4.66E-09	8.137	10.1717
RNF122	AC_000184.1	90	14	8.99E-09	4.88E-08	8.137	10.1717
RNF122	AC_000184.1	80	11	2.08E-08	1.09E-07	8.137	10.1717
RNF122	AC_000184.1	100	16	1.86E-09	1.05E-08	8.137	10.1717
RNF122	AC_000184.1	85	11	3.76E-09	2.10E-08	8.137	10.1717
RNF122	AC_000184.1	88	13	7.12E-09	3.90E-08	8.137	10.1717
RNF122	AC_000184.1	75	12	2.23E-07	1.01E-06	8.137	10.1717
RNF122	AC_000184.1	85	18	6.32E-07	2.76E-06	8.137	10.1717
RNF122	AC_000184.1	83	0	3.95E-16	3.44E-15	8.137	10.1717
RNF122	AC_000184.1	87	15	4.73E-08	2.27E-07	8.137	10.1717
RNF122	AC_000184.1	87	17	1.82E-07	8.30E-07	8.137	10.1717
RNF122	AC_000184.1	100	7	2.90E-13	2.15E-12	8.137	10.1717
RNF122	AC_000184.1	87	10	7.04E-10	4.10E-09	8.137	10.1717
RNF122	AC_000184.1	81	20	5.62E-06	2.16E-05	8.137	10.1717
RNF122	AC_000184.1	100	0	2.22E-19	2.32E-18	8.137	10.1717
RNF122	AC_000184.1	100	9	3.27E-12	2.29E-11	8.137	10.1717
RNF122	AC_000184.1	80	23	3.02E-05	1.03E-04	8.137	10.1717
RNF122	AC_000184.1	80	25	7.02E-05	2.30E-04	8.137	10.1717
RNF122	AC_000184.1	83	0	3.95E-16	3.44E-15	8.137	10.1717
RNF122	AC_000184.1	80	8	1.14E-09	6.61E-09	8.137	10.1717
RNF122	AC_000184.1	11	75	9.55E-08	4.50E-07	8.137	10.1717
RNF122	AC_000184.1	80	20	6.94E-06	2.60E-05	8.137	10.1717
RNF122	AC_000184.1	0	75	1.25E-14	9.63E-14	8.137	10.1717

RNF122	AC_000184.1	100	13	1.74E-10	1.08E-09	8.137	10.1717
RNF122	AC_000184.1	80	14	1.93E-07	8.74E-07	8.137	10.1717
RNF122	AC_000184.1	80	20	6.94E-06	2.60E-05	8.137	10.1717
RNF122	AC_000184.1	80	6	1.16E-10	7.26E-10	8.137	10.1717
RNF122	AC_000184.1	80	17	1.41E-06	5.80E-06	8.137	10.1717
RNF122	AC_000184.1	83	20	3.33E-06	1.30E-05	8.137	10.1717
RNF122	AC_000184.1	80	23	3.02E-05	1.03E-04	8.137	10.1717
RNF122	AC_000184.1	0	83	3.95E-16	3.44E-15	8.137	10.1717
RNF122	AC_000184.1	80	0	1.24E-15	9.79E-15	8.137	10.1717
RNF122	AC_000184.1	100	9	3.27E-12	2.29E-11	8.137	10.1717
RNF122	AC_000184.1	100	11	2.69E-11	1.74E-10	8.137	10.1717
RNF122	AC_000184.1	80	14	1.93E-07	8.74E-07	8.137	10.1717
RNF122	AC_000184.1	75	16	3.16E-06	1.24E-05	8.137	10.1717
RNF122	AC_000184.1	86	22	4.04E-06	1.58E-05	8.137	10.1717
RNF122	AC_000184.1	83	23	1.39E-05	5.01E-05	8.137	10.1717
RNF122	AC_000184.1	85	0	1.66E-16	1.56E-15	8.137	10.1717
RNF122	AC_000184.1	80	0	1.24E-15	9.79E-15	8.137	10.1717
RNF122	AC_000184.1	100	16	1.86E-09	1.05E-08	8.137	10.1717
RNF122	AC_000184.1	87	18	3.61E-07	1.61E-06	8.137	10.1717
RNF122	AC_000184.1	83	22	9.08E-06	3.37E-05	8.137	10.1717
RNF122	AC_000184.1	80	0	1.24E-15	9.79E-15	8.137	10.1717
RNF122	AC_000184.1	83	12	1.81E-08	9.56E-08	8.137	10.1717
RNF122	AC_000184.1	16	77	1.60E-06	6.57E-06	8.137	10.1717
RNF122	AC_000184.1	75	20	2.62E-05	9.12E-05	8.137	10.1717
RNF122	AC_000184.1	88	0	3.94E-17	3.96E-16	8.137	10.1717
RNF122	AC_000184.1	80	14	1.93E-07	8.74E-07	8.137	10.1717
RNF122	AC_000184.1	87	24	8.58E-06	3.19E-05	8.137	10.1717
RNF122	AC_000184.1	78	0	2.95E-15	2.32E-14	8.137	10.1717
RNF122	AC_000184.1	88	16	7.03E-08	3.34E-07	8.137	10.1717
RNF122	AC_000184.1	14	80	1.93E-07	8.74E-07	8.137	10.1717
RNF122	AC_000184.1	92	12	9.13E-10	5.30E-09	8.137	10.1717
RNF122	AC_000184.1	83	18	1.10E-06	4.57E-06	8.137	10.1717
RNF122	AC_000184.1	88	21	1.36E-06	5.60E-06	8.137	10.1717
RNF122	AC_000184.1	100	0	2.22E-19	2.32E-18	8.137	10.1717
RNF122	AC_000184.1	85	0	1.66E-16	1.56E-15	8.137	10.1717
RNF122	AC_000184.1	85	0	1.66E-16	1.56E-15	8.137	10.1717
RNF122	AC_000184.1	100	7	2.90E-13	2.15E-12	8.137	10.1717
RNF122	AC_000184.1	83	5	1.01E-11	6.62E-11	8.137	10.1717
RNF122	AC_000184.1	80	15	4.06E-07	1.80E-06	8.137	10.1717
RNF122	AC_000184.1	80	0	1.24E-15	9.79E-15	8.137	10.1717
RNF122	AC_000184.1	100	11	2.69E-11	1.74E-10	8.137	10.1717
RNF122	AC_000184.1	75	9	1.70E-08	8.98E-08	8.137	10.1717
RNF122	AC_000184.1	80	15	4.06E-07	1.80E-06	8.137	10.1717
RNF122	AC_000184.1	80	23	3.02E-05	1.03E-04	8.137	10.1717
RNF122	AC_000184.1	87	14	2.45E-08	1.29E-07	8.137	10.1717

RNF122	AC_000184.1	100	20	2.92E-08	1.49E-07	8.137	10.1717
RNF122	AC_000184.1	77	17	3.06E-06	1.21E-05	8.137	10.1717
RNF122	AC_000184.1	80	20	6.94E-06	2.60E-05	8.137	10.1717
RNF122	AC_000184.1	75	22	6.49E-05	2.14E-04	8.137	10.1717
RNF122	AC_000184.1	88	18	2.56E-07	1.15E-06	8.137	10.1717
RNF122	AC_000184.1	25	75	2.10E-04	6.22E-04	8.137	10.1717
RNF122	AC_000184.1	100	0	2.22E-19	2.32E-18	8.137	10.1717
RNF122	AC_000184.1	100	10	8.84E-12	5.80E-11	8.137	10.1717
RNF122	AC_000184.1	100	10	8.84E-12	5.80E-11	8.137	10.1717
RNF122	AC_000184.1	88	8	6.85E-11	4.32E-10	8.137	10.1717
RNF122	AC_000184.1	85	10	1.65E-09	9.47E-09	8.137	10.1717
RNF122	AC_000184.1	88	12	3.36E-09	1.88E-08	8.137	10.1717
RNF122	AC_000184.1	77	20	1.58E-05	5.68E-05	8.137	10.1717
RNF122	AC_000184.1	100	0	2.22E-19	2.32E-18	8.137	10.1717
RNF122	AC_000184.1	80	12	4.35E-08	2.09E-07	8.137	10.1717
RNF122	AC_000184.1	88	16	7.03E-08	3.34E-07	8.137	10.1717
RNF122	AC_000184.1	75	6	8.00E-10	4.66E-09	8.137	10.1717
RNF122	AC_000184.1	87	10	8.39E-10	4.88E-09	8.137	10.1717
RNF122	AC_000184.1	100	16	1.86E-09	1.05E-08	8.137	10.1717
RNF122	AC_000184.1	88	16	7.03E-08	3.34E-07	8.137	10.1717
RNF122	AC_000184.1	100	18	7.85E-09	4.28E-08	8.137	10.1717
RNF122	AC_000184.1	90	20	4.80E-07	2.11E-06	8.137	10.1717
UNC5D	AC_000184.1	100	5	1.69E-14	1.30E-13	5.798	0.293699
UNC5D	AC_000184.1	96	15	3.22E-09	1.80E-08	5.798	0.293699
UNC5D	AC_000184.1	100	24	2.94E-07	1.32E-06	5.798	0.293699
UNC5D	AC_000184.1	83	24	2.27E-05	7.98E-05	5.798	0.293699
FGFR1	AC_000184.1	0	100	2.22E-19	2.32E-18	1.128	4.27163
FGFR1	AC_000184.1	12	100	6.45E-11	4.07E-10	1.128	4.27163
SFRP1	AC_000184.1	0	100	2.22E-19	2.32E-18	2.73	0.563249
SFRP1	AC_000184.1	0	100	2.22E-19	2.32E-18	2.73	0.563249
CSGALNACT1	AC_000184.1	0	100	2.22E-19	2.32E-18	0.037	2.32425
ADAMTS14	AC_000185.1	0	80	1.24E-15	9.79E-15	0.207	0.0820264
CDH23	AC_000185.1	100	0	2.22E-19	2.32E-18	20.334	0.962554
CDH23	AC_000185.1	0	100	2.22E-19	2.32E-18	20.334	0.962554
ANXA8L1	AC_000185.1	0	100	2.22E-19	2.32E-18	0.02	0.00748011
ANXA8L1	AC_000185.1	0	100	2.22E-19	2.32E-18	0.02	0.00748011
PKNOX2	AC_000186.1	0	100	2.22E-19	2.32E-18	0.007	1.20047
PKNOX2	AC_000186.1	0	100	2.22E-19	2.32E-18	0.007	1.20047
KIRREL3	AC_000186.1	0	83	3.95E-16	3.44E-15	0.014	0.26713
KIRREL3	AC_000186.1	77	7	1.12E-09	6.47E-09	0.014	0.26713
KIRREL3	AC_000186.1	95	14	2.01E-09	1.14E-08	0.014	0.26713
KIRREL3	AC_000186.1	80	18	2.38E-06	9.54E-06	0.014	0.26713
KIRREL3	AC_000186.1	76	18	7.00E-06	2.61E-05	0.014	0.26713
KIRREL3	AC_000186.1	80	22	1.84E-05	6.52E-05	0.014	0.26713
KIRREL3	AC_000186.1	75	22	6.49E-05	2.14E-04	0.014	0.26713

KIRREL3	AC_000186.1	80	18	2.38E-06	9.54E-06	0.014	0.26713
KIRREL3	AC_000186.1	83	22	9.08E-06	3.37E-05	0.014	0.26713
KIRREL3	AC_000186.1	75	9	1.70E-08	8.98E-08	0.014	0.26713
KIRREL3	AC_000186.1	90	16	3.88E-08	1.88E-07	0.014	0.26713
KIRREL3	AC_000186.1	87	22	3.28E-06	1.29E-05	0.014	0.26713
KIRREL3	AC_000186.1	88	24	6.41E-06	2.45E-05	0.014	0.26713
KIRREL3	AC_000186.1	80	25	7.02E-05	2.30E-04	0.014	0.26713
KIRREL3	AC_000186.1	85	9	5.67E-10	3.30E-09	0.014	0.26713
KIRREL3	AC_000186.1	100	15	9.23E-10	5.35E-09	0.014	0.26713
KIRREL3	AC_000186.1	80	10	8.02E-09	4.36E-08	0.014	0.26713
KIRREL3	AC_000186.1	90	16	3.88E-08	1.88E-07	0.014	0.26713
KIRREL3	AC_000186.1	78	11	3.96E-08	1.91E-07	0.014	0.26713
KIRREL3	AC_000186.1	100	22	9.72E-08	4.57E-07	0.014	0.26713
KIRREL3	AC_000186.1	83	17	5.72E-07	2.51E-06	0.014	0.26713
KIRREL3	AC_000186.1	83	17	5.72E-07	2.51E-06	0.014	0.26713
KIRREL3	AC_000186.1	81	25	5.36E-05	1.79E-04	0.014	0.26713
KIRREL3	AC_000186.1	83	10	2.71E-09	1.53E-08	0.014	0.26713
KIRREL3	AC_000186.1	83	14	8.33E-08	3.95E-07	0.014	0.26713
KIRREL3	AC_000186.1	80	15	4.06E-07	1.80E-06	0.014	0.26713
KIRREL3	AC_000186.1	75	16	3.16E-06	1.24E-05	0.014	0.26713
KIRREL3	AC_000186.1	100	0	2.22E-19	2.32E-18	0.014	0.26713
KIRREL3	AC_000186.1	80	7	4.23E-10	2.58E-09	0.014	0.26713
KIRREL3	AC_000186.1	76	10	3.00E-08	1.53E-07	0.014	0.26713
KIRREL3	AC_000186.1	100	24	2.94E-07	1.32E-06	0.014	0.26713
KIRREL3	AC_000186.1	76	16	2.25E-06	9.06E-06	0.014	0.26713
KIRREL3	AC_000186.1	76	6	5.02E-10	3.04E-09	0.014	0.26713
KIRREL3	AC_000186.1	80	8	1.14E-09	6.61E-09	0.014	0.26713
KIRREL3	AC_000186.1	80	11	2.08E-08	1.09E-07	0.014	0.26713
KIRREL3	AC_000186.1	83	0	3.95E-16	3.44E-15	0.014	0.26713
KIRREL3	AC_000186.1	81	21	8.86E-06	3.29E-05	0.014	0.26713
KIRREL3	AC_000186.1	77	11	5.04E-08	2.42E-07	0.014	0.26713
KIRREL3	AC_000186.1	83	10	3.22E-09	1.80E-08	0.014	0.26713
KIRREL3	AC_000186.1	100	18	7.85E-09	4.28E-08	0.014	0.26713
KIRREL3	AC_000186.1	83	24	2.27E-05	7.98E-05	0.014	0.26713
KIRREL3	AC_000186.1	75	22	6.49E-05	2.14E-04	0.014	0.26713
KIRREL3	AC_000186.1	0	100	2.22E-19	2.32E-18	0.014	0.26713
TMEM132A	AC_000186.1	0	100	2.22E-19	2.32E-18	0.101	2.9154
TMEM258	AC_000186.1	0	100	2.22E-19	2.32E-18	6.39	34.137
FADS2	AC_000186.1	0	100	2.22E-19	2.32E-18	0.022	34.409
FADS2	AC_000186.1	0	100	2.22E-19	2.32E-18	0.022	34.409
FADS2	AC_000186.1	0	100	2.22E-19	2.32E-18	0.022	34.409
MACROD1	AC_000186.1	0	100	2.22E-19	2.32E-18	3.035	8.30819
MACROD1	AC_000186.1	0	100	2.22E-19	2.32E-18	3.035	8.30819
MACROD1	AC_000186.1	0	100	2.22E-19	2.32E-18	3.035	8.30819
MACROD1	AC_000186.1	0	100	2.22E-19	2.32E-18	3.035	8.30819

MACROD1	AC_000186.1	0	100	2.22E-19	2.32E-18	3.035	8.30819
MACROD1	AC_000186.1	0	100	2.22E-19	2.32E-18	3.035	8.30819
MACROD1	AC_000186.1	0	80	1.24E-15	9.79E-15	3.035	8.30819
MACROD1	AC_000186.1	0	100	2.22E-19	2.32E-18	3.035	8.30819
MACROD1	AC_000186.1	0	100	2.22E-19	2.32E-18	3.035	8.30819
MACROD1	AC_000186.1	0	100	2.22E-19	2.32E-18	3.035	8.30819
MACROD1	AC_000186.1	0	100	2.22E-19	2.32E-18	3.035	8.30819
MACROD1	AC_000186.1	20	100	2.92E-08	1.49E-07	3.035	8.30819
MACROD1	AC_000186.1	0	100	2.22E-19	2.32E-18	3.035	8.30819
MACROD1	AC_000186.1	0	100	2.22E-19	2.32E-18	3.035	8.30819
MACROD1	AC_000186.1	0	80	1.24E-15	9.79E-15	3.035	8.30819
MACROD1	AC_000186.1	0	100	2.22E-19	2.32E-18	3.035	8.30819
MACROD1	AC_000186.1	0	100	2.22E-19	2.32E-18	3.035	8.30819
FKBP2	AC_000186.1	100	11	2.69E-11	1.74E-10	2.701	43.4495
FKBP2	AC_000186.1	100	11	2.69E-11	1.74E-10	2.701	43.4495
NRXN2	AC_000186.1	0	83	3.95E-16	3.44E-15	0.031	4.57515
NRXN2	AC_000186.1	0	100	2.22E-19	2.32E-18	0.031	4.57515
EHBP1L1	AC_000186.1	0	100	2.22E-19	2.32E-18	0.063	1.11711
ANKRD13D	AC_000186.1	100	25	5.20E-07	2.28E-06	0.273	0.307814
TMEM134	AC_000186.1	0	85	1.66E-16	1.56E-15	1.769	0.00026075
ALDH3B1	AC_000186.1	0	100	2.22E-19	2.32E-18	0.043	1.67588
ALDH3B1	AC_000186.1	0	100	2.22E-19	2.32E-18	0.043	1.67588
ALDH3B1	AC_000186.1	0	85	1.66E-16	1.56E-15	0.043	1.67588
MRGPRF	AC_000186.1	0	100	2.22E-19	2.32E-18	0.028	0.0658296
MRGPRF	AC_000186.1	0	100	2.22E-19	2.32E-18	0.028	0.0658296
ANO1	AC_000186.1	0	100	2.22E-19	2.32E-18	0.11	52.6666
ANO1	AC_000186.1	20	85	1.96E-06	7.96E-06	0.11	52.6666
ANO1	AC_000186.1	0	100	2.22E-19	2.32E-18	0.11	52.6666
ANO1	AC_000186.1	0	85	1.66E-16	1.56E-15	0.11	52.6666
ANO1	AC_000186.1	0	85	1.66E-16	1.56E-15	0.11	52.6666
DHCR7	AC_000186.1	0	100	2.22E-19	2.32E-18	2.574	1.67939
TSSC4	AC_000186.1	0	83	3.95E-16	3.44E-15	0.6	0.0114462
TSSC4	AC_000186.1	0	83	3.95E-16	3.44E-15	0.6	0.0114462
TH	AC_000186.1	0	100	2.22E-19	2.32E-18	0.215	0.230183
TH	AC_000186.1	0	91	1.25E-17	1.29E-16	0.215	0.230183
TH	AC_000186.1	0	83	3.95E-16	3.44E-15	0.215	0.230183
IGF2	AC_000186.1	0	100	2.22E-19	2.32E-18	0.037	31.6633
IGF2	AC_000186.1	0	100	2.22E-19	2.32E-18	0.037	31.6633
IGF2	AC_000186.1	0	100	2.22E-19	2.32E-18	0.037	31.6633
PNPLA2	AC_000186.1	100	25	5.20E-07	2.28E-06	0.752	8.83435
HRAS	AC_000186.1	8	100	9.20E-13	6.56E-12	1.46	1.73E-06
HRAS	AC_000186.1	8	100	9.20E-13	6.56E-12	1.46	1.73E-06
PKP3	AC_000186.1	0	100	2.22E-19	2.32E-18	0.211	0.0558369
PKP3	AC_000186.1	0	100	2.22E-19	2.32E-18	0.211	0.0558369
ADAMTS4	AC_000160.1	0	100	2.22E-19	2.32E-18	8.259	13.4961

PEAR1	AC_000160.1	0	90	1.66E-17	1.70E-16	0.017	3.50785
ATP1A1	AC_000160.1	96	11	1.05E-10	6.54E-10	72.836	148.908
ATP1A1	AC_000160.1	95	18	3.21E-08	1.63E-07	72.836	148.908
SLC44A5	AC_000160.1	83	0	3.95E-16	3.44E-15	26.817	7.84819
EFHD1	AC_000160.1	0	100	2.22E-19	2.32E-18	12.044	61.7899
INPP5D	AC_000160.1	0	100	2.22E-19	2.32E-18	0.005	0.417505
INPP5D	AC_000160.1	0	100	2.22E-19	2.32E-18	0.005	0.417505
BOK	AC_000160.1	0	100	2.22E-19	2.32E-18	0.023	0.290115
BOK	AC_000160.1	0	80	1.24E-15	9.79E-15	0.023	0.290115
BOK	AC_000160.1	20	100	2.92E-08	1.49E-07	0.023	0.290115
THAP4	AC_000160.1	100	9	3.27E-12	2.29E-11	5.406	3.32E-10
ASB4	AC_000161.1	100	2	5.84E-17	5.86E-16	0.059	2.29124
ASB4	AC_000161.1	94	4	3.11E-14	2.39E-13	0.059	2.29124
ASB4	AC_000161.1	83	6	3.47E-11	2.22E-10	0.059	2.29124
ASB4	AC_000161.1	95	18	3.21E-08	1.63E-07	0.059	2.29124
ASB4	AC_000161.1	83	13	3.69E-08	1.88E-07	0.059	2.29124
KIAA1324L	AC_000161.1	80	14	1.93E-07	8.74E-07	8.885	26.3772
KIAA1324L	AC_000161.1	75	19	1.53E-05	5.52E-05	8.885	26.3772
LHFPL3	AC_000161.1	77	0	5.26E-15	4.10E-14	99.227	0.712787
LHFPL3	AC_000161.1	77	0	5.26E-15	4.10E-14	99.227	0.712787
MET	AC_000161.1	100	11	2.69E-11	1.74E-10	0.49	3.35075
MET	AC_000161.1	83	18	1.10E-06	4.57E-06	0.49	3.35075
MET	AC_000161.1	80	17	1.41E-06	5.80E-06	0.49	3.35075
CRHR2	AC_000161.1	100	0	2.22E-19	2.32E-18	0.576	0.21157
GTPBP10	AC_000161.1	0	100	2.22E-19	2.32E-18	28.986	16.8739
ADCY1	AC_000161.1	0	90	1.66E-17	1.70E-16	0.016	2.7462
ADCY1	AC_000161.1	0	100	2.22E-19	2.32E-18	0.016	2.7462
ADCY1	AC_000161.1	0	100	2.22E-19	2.32E-18	0.016	2.7462
CAMK2B	AC_000161.1	0	100	2.22E-19	2.32E-18	0.187	0.127235
CAMK2B	AC_000161.1	0	100	2.22E-19	2.32E-18	0.187	0.127235
CAMK2B	AC_000161.1	16	100	1.86E-09	1.05E-08	0.187	0.127235
CAMK2B	AC_000161.1	0	100	2.22E-19	2.32E-18	0.187	0.127235
CAMK2B	AC_000161.1	0	100	2.22E-19	2.32E-18	0.187	0.127235
CAMK2B	AC_000161.1	0	100	2.22E-19	2.32E-18	0.187	0.127235
CAMK2B	AC_000161.1	0	100	2.22E-19	2.32E-18	0.187	0.127235
CAMK2B	AC_000161.1	0	87	7.02E-17	6.88E-16	0.187	0.127235
CAMK2B	AC_000161.1	16	100	1.86E-09	1.05E-08	0.187	0.127235
CAMK2B	AC_000161.1	20	83	3.33E-06	1.30E-05	0.187	0.127235
CAMK2B	AC_000161.1	0	100	2.22E-19	2.32E-18	0.187	0.127235
GCK	AC_000161.1	0	100	2.22E-19	2.32E-18	0.055	0.419373
CDK13	AC_000161.1	78	15	6.41E-07	2.80E-06	22.109	15.9006
CDK13	AC_000161.1	78	15	6.41E-07	2.80E-06	22.109	15.9006
PLXNA4	AC_000161.1	0	85	1.66E-16	1.56E-15	0.799	0.523385
LRGUK	AC_000161.1	83	0	3.95E-16	3.44E-15	2.29	4.2307
LRGUK	AC_000161.1	94	14	2.56E-09	1.44E-08	2.29	4.2307

LRGUK	AC_000161.1	83	12	1.81E-08	9.56E-08	2.29	4.2307
LRGUK	AC_000161.1	86	25	1.71E-05	6.13E-05	2.29	4.2307
LRGUK	AC_000161.1	83	0	3.95E-16	3.44E-15	2.29	4.2307
LRGUK	AC_000161.1	100	11	2.69E-11	1.74E-10	2.29	4.2307
LRGUK	AC_000161.1	83	16	2.86E-07	1.29E-06	2.29	4.2307
LRGUK	AC_000161.1	80	16	7.24E-07	3.14E-06	2.29	4.2307
LRGUK	AC_000161.1	100	14	3.79E-10	2.31E-09	2.29	4.2307
LRGUK	AC_000161.1	100	17	4.16E-09	2.32E-08	2.29	4.2307
LRGUK	AC_000161.1	83	18	1.10E-06	4.57E-06	2.29	4.2307
LRGUK	AC_000161.1	78	20	1.17E-05	4.26E-05	2.29	4.2307
LRGUK	AC_000161.1	83	19	1.84E-06	7.50E-06	2.29	4.2307
UBN2	AC_000161.1	80	10	8.02E-09	4.36E-08	46.853	3.21039
UBN2	AC_000161.1	100	10	8.84E-12	5.80E-11	46.853	3.21039
UBN2	AC_000161.1	100	11	2.69E-11	1.74E-10	46.853	3.21039
UBN2	AC_000161.1	85	21	3.15E-06	1.24E-05	46.853	3.21039
UBN2	AC_000161.1	75	17	5.30E-06	2.04E-05	46.853	3.21039
UBN2	AC_000161.1	100	6	6.67E-14	5.10E-13	46.853	3.21039
UBN2	AC_000161.1	93	12	6.06E-10	3.53E-09	46.853	3.21039
SSPO	AC_000161.1	0	83	3.95E-16	3.44E-15	0.01	6.73901
SSPO	AC_000161.1	0	83	3.95E-16	3.44E-15	0.01	6.73901
SSPO	AC_000161.1	0	100	2.22E-19	2.32E-18	0.01	6.73901
RARRES2	AC_000161.1	0	83	3.95E-16	3.44E-15	4.624	5.74164
RARRES2	AC_000161.1	0	80	1.24E-15	9.79E-15	4.624	5.74164
RARRES2	AC_000161.1	0	75	1.25E-14	9.63E-14	4.624	5.74164
NOS3	AC_000161.1	0	100	2.22E-19	2.32E-18	0.32	1.16742
TMUB1	AC_000161.1	0	100	2.22E-19	2.32E-18	0.297	0.833155
PAXIP1	AC_000161.1	0	100	2.22E-19	2.32E-18	21.428	1.97E-07
RAPGEF3	AC_000162.1	0	100	2.22E-19	2.32E-18	0.919	1.38967
STAT6	AC_000162.1	0	100	2.22E-19	2.32E-18	0.117	1.92315
PTPN6	AC_000162.1	0	100	2.22E-19	2.32E-18	0.146	0.552625
TNFRSF1A	AC_000162.1	78	20	1.17E-05	4.26E-05	0.649	15.1137
SCNN1A	AC_000162.1	78	20	1.17E-05	4.26E-05	1.772	1.35987
VWF	AC_000162.1	0	85	1.66E-16	1.56E-15	2.671	4.28453
VWF	AC_000162.1	0	85	1.66E-16	1.56E-15	2.671	4.28453
SLC6A12	AC_000162.1	0	100	2.22E-19	2.32E-18	0.009	1.19542
DCP1B	AC_000162.1	0	100	2.22E-19	2.32E-18	0.08	13.4787
DCP1B	AC_000162.1	0	100	2.22E-19	2.32E-18	0.08	13.4787
DCP1B	AC_000162.1	0	100	2.22E-19	2.32E-18	0.08	13.4787
JOSD1	AC_000162.1	80	0	1.24E-15	9.79E-15	29.302	17.061
TBC1D22A	AC_000162.1	0	100	2.22E-19	2.32E-18	0.421	8.54892
HDAC10	AC_000162.1	0	100	2.22E-19	2.32E-18	0.293	3.73E-07
MAPK12	AC_000162.1	0	100	2.22E-19	2.32E-18	0.03	0.340854
PDE5A	AC_000163.1	100	0	2.22E-19	2.32E-18	20.064	14.8399
PDE5A	AC_000163.1	76	0	6.99E-15	5.45E-14	20.064	14.8399
PDE5A	AC_000163.1	10	80	8.02E-09	4.36E-08	20.064	14.8399

PDE5A	AC_000163.1	85	13	1.98E-08	1.04E-07	20.064	14.8399
PDE5A	AC_000163.1	75	0	1.25E-14	9.63E-14	20.064	14.8399
PDE5A	AC_000163.1	88	10	5.48E-10	3.19E-09	20.064	14.8399
PDE5A	AC_000163.1	75	7	2.27E-09	1.28E-08	20.064	14.8399
PDE5A	AC_000163.1	83	15	1.57E-07	7.27E-07	20.064	14.8399
PDE5A	AC_000163.1	80	21	1.20E-05	4.38E-05	20.064	14.8399
PDE5A	AC_000163.1	75	21	3.99E-05	1.35E-04	20.064	14.8399
CASP6	AC_000163.1	100	0	2.22E-19	2.32E-18	214.923	2.46198
CASP6	AC_000163.1	100	16	1.86E-09	1.05E-08	214.923	2.46198
NFKB1	AC_000163.1	93	11	2.63E-10	1.63E-09	6.486	2.82109
NFKB1	AC_000163.1	75	12	2.23E-07	1.01E-06	6.486	2.82109
NFKB1	AC_000163.1	85	25	2.09E-05	7.36E-05	6.486	2.82109
ADAMTS3	AC_000163.1	94	0	2.96E-18	3.08E-17	0.202	0.815374
ADAMTS3	AC_000163.1	100	13	1.74E-10	1.08E-09	0.202	0.815374
ADAMTS3	AC_000163.1	97	13	4.27E-10	2.60E-09	0.202	0.815374
ADAMTS3	AC_000163.1	80	8	1.14E-09	6.61E-09	0.202	0.815374
ADAMTS3	AC_000163.1	87	11	1.94E-09	1.10E-08	0.202	0.815374
ADAMTS3	AC_000163.1	75	9	1.70E-08	8.98E-08	0.202	0.815374
ADAMTS3	AC_000163.1	85	13	1.98E-08	1.04E-07	0.202	0.815374
ADAMTS3	AC_000163.1	100	20	2.92E-08	1.49E-07	0.202	0.815374
ADAMTS3	AC_000163.1	80	13	1.01E-07	4.71E-07	0.202	0.815374
ADAMTS3	AC_000163.1	75	20	2.62E-05	9.12E-05	0.202	0.815374
ADAMTS3	AC_000163.1	83	0	3.95E-16	3.44E-15	0.202	0.815374
ADAMTS3	AC_000163.1	78	2	4.86E-13	3.60E-12	0.202	0.815374
ADAMTS3	AC_000163.1	87	7	3.08E-11	1.96E-10	0.202	0.815374
ADAMTS3	AC_000163.1	83	7	1.31E-10	8.14E-10	0.202	0.815374
ADAMTS3	AC_000163.1	77	11	5.04E-08	2.42E-07	0.202	0.815374
ADAMTS3	AC_000163.1	88	16	7.03E-08	3.34E-07	0.202	0.815374
ADAMTS3	AC_000163.1	77	15	9.12E-07	3.87E-06	0.202	0.815374
ADAMTS3	AC_000163.1	77	25	1.34E-04	4.21E-04	0.202	0.815374
ADAMTS3	AC_000163.1	75	6	8.00E-10	4.66E-09	0.202	0.815374
JAKMIP1	AC_000163.1	0	100	2.22E-19	2.32E-18	0.935	0.04102
JAKMIP1	AC_000163.1	0	100	2.22E-19	2.32E-18	0.935	0.04102
JAKMIP1	AC_000163.1	0	100	2.22E-19	2.32E-18	0.935	0.04102
TNIP2	AC_000163.1	0	100	2.22E-19	2.32E-18	0.492	0.0316418
TNIP2	AC_000163.1	0	100	2.22E-19	2.32E-18	0.492	0.0316418
TNIP2	AC_000163.1	0	100	2.22E-19	2.32E-18	0.492	0.0316418
TNIP2	AC_000163.1	0	100	2.22E-19	2.32E-18	0.492	0.0316418
TNIP2	AC_000163.1	0	100	2.22E-19	2.32E-18	0.492	0.0316418
TNIP2	AC_000163.1	0	100	2.22E-19	2.32E-18	0.492	0.0316418
TNIP2	AC_000163.1	0	100	2.22E-19	2.32E-18	0.492	0.0316418
TNIP2	AC_000163.1	0	100	2.22E-19	2.32E-18	0.492	0.0316418
TNIP2	AC_000163.1	0	80	1.24E-15	9.79E-15	0.492	0.0316418
TBC1D14	AC_000163.1	0	83	3.95E-16	3.44E-15	61.99	13.8021
CRTC1	AC_000164.1	0	100	2.22E-19	2.32E-18	1.328	1.00504

CRTC1	AC_000164.1	0	100	2.22E-19	2.32E-18	1.328	1.00504
MVB12A	AC_000164.1	100	0	2.22E-19	2.32E-18	2.818	2.91305
CACNA1A	AC_000164.1	0	100	2.22E-19	2.32E-18	0.415	0.723295
IER2	AC_000164.1	100	0	2.22E-19	2.32E-18	0.043	16.2488
COL5A3	AC_000164.1	0	100	2.22E-19	2.32E-18	0.1	2.99264
S1PR5	AC_000164.1	83	0	3.95E-16	3.44E-15	0.185	0.920123
LDLR	AC_000164.1	0	100	2.22E-19	2.32E-18	2.294	8.06501
EVI5L	AC_000164.1	0	80	1.24E-15	9.79E-15	1.675	12.5533
ANGPTL4	AC_000164.1	0	100	2.22E-19	2.32E-18	0.067	0.499163
C3	AC_000164.1	0	100	2.22E-19	2.32E-18	0.01	1.40461
RFX2	AC_000164.1	0	100	2.22E-19	2.32E-18	0.075	42.5618
RFX2	AC_000164.1	0	100	2.22E-19	2.32E-18	0.075	42.5618
TJP3	AC_000164.1	20	100	2.92E-08	1.49E-07	0.072	1.60424
PTBP1	AC_000164.1	0	100	2.22E-19	2.32E-18	107.244	6.34773
PTBP1	AC_000164.1	0	100	2.22E-19	2.32E-18	107.244	6.34773
EGR1	AC_000164.1	85	0	1.66E-16	1.56E-15	14.139	97.3863
CTNNA1	AC_000164.1	87	0	7.02E-17	6.88E-16	359.821	29.6623
CTNNA1	AC_000164.1	80	0	1.24E-15	9.79E-15	359.821	29.6623
CTNNA1	AC_000164.1	83	13	3.69E-08	1.88E-07	359.821	29.6623
PCDH1	AC_000164.1	0	100	2.22E-19	2.32E-18	0.542	1.2975
GRIA1	AC_000164.1	85	23	8.46E-06	3.15E-05	0.377	0.551824
EFNA5	AC_000164.1	0	80	1.24E-15	9.79E-15	0.397	29.9675
ZNF395	AC_000165.1	80	0	1.24E-15	9.79E-15	5.019	3.82017
ZNF395	AC_000165.1	80	8	1.14E-09	6.61E-09	5.019	3.82017
ZNF395	AC_000165.1	80	12	4.35E-08	2.09E-07	5.019	3.82017
ZNF395	AC_000165.1	80	18	2.38E-06	9.54E-06	5.019	3.82017
SCARA5	AC_000165.1	100	0	2.22E-19	2.32E-18	0.093	3.45835
SCARA5	AC_000165.1	0	100	2.22E-19	2.32E-18	0.093	3.45835
SHB	AC_000165.1	0	80	1.24E-15	9.79E-15	10.368	0.272166
SHB	AC_000165.1	0	80	1.24E-15	9.79E-15	10.368	0.272166
RHOBTB2	AC_000165.1	0	100	2.22E-19	2.32E-18	0.412	1.10532
RHOBTB2	AC_000165.1	0	100	2.22E-19	2.32E-18	0.412	1.10532
RHOBTB2	AC_000165.1	0	85	1.66E-16	1.56E-15	0.412	1.10532
RHOBTB2	AC_000165.1	0	96	1.25E-18	1.30E-17	0.412	1.10532
AQP7	AC_000165.1	0	85	1.66E-16	1.56E-15	0.018	16.045
AQP7	AC_000165.1	20	100	2.92E-08	1.49E-07	0.018	16.045
CNTFR	AC_000165.1	0	100	2.22E-19	2.32E-18	1.272	0.401799
RPP25L	AC_000165.1	100	20	2.92E-08	1.49E-07	0.022	9.72948
TMEM246	AC_000165.1	78	20	1.17E-05	4.26E-05	0.048	0.61765
COL27A1	AC_000165.1	0	100	2.22E-19	2.32E-18	0.199	1.08769
COL27A1	AC_000165.1	0	100	2.22E-19	2.32E-18	0.199	1.08769
COL27A1	AC_000165.1	0	100	2.22E-19	2.32E-18	0.199	1.08769
COL27A1	AC_000165.1	20	100	2.92E-08	1.49E-07	0.199	1.08769
PHF19	AC_000165.1	0	90	1.66E-17	1.70E-16	0.213	2.04815
GSN	AC_000165.1	0	100	2.22E-19	2.32E-18	0.529	26.6831

GSN	AC_000165.1	0	100	2.22E-19	2.32E-18	0.529	26.6831
GSN	AC_000165.1	0	100	2.22E-19	2.32E-18	0.529	26.6831
GSN	AC_000165.1	0	100	2.22E-19	2.32E-18	0.529	26.6831
GSN	AC_000165.1	0	100	2.22E-19	2.32E-18	0.529	26.6831
GSN	AC_000165.1	0	100	2.22E-19	2.32E-18	0.529	26.6831
LAMA4	AC_000166.1	80	14	1.93E-07	8.74E-07	1.364	2.82183
ASCC3	AC_000166.1	88	14	1.67E-08	8.86E-08	34.241	6.19346
ASCC3	AC_000166.1	83	21	5.30E-06	2.04E-05	34.241	6.19346
ENPP3	AC_000166.1	77	9	8.67E-09	4.71E-08	0.191	2.2943
ENPP3	AC_000166.1	85	20	1.76E-06	7.20E-06	0.191	2.2943
ZDHHC14	AC_000166.1	0	85	1.66E-16	1.56E-15	0.565	6.51905
RPS6KA2	AC_000166.1	0	100	2.22E-19	2.32E-18	0.225	1.24944
RPS6KA2	AC_000166.1	0	100	2.22E-19	2.32E-18	0.225	1.24944
RPS6KA2	AC_000166.1	0	83	3.95E-16	3.44E-15	0.225	1.24944
RPS6KA2	AC_000166.1	0	100	2.22E-19	2.32E-18	0.225	1.24944
RPS6KA2	AC_000166.1	0	100	2.22E-19	2.32E-18	0.225	1.24944
RPS6KA2	AC_000166.1	0	100	2.22E-19	2.32E-18	0.225	1.24944
RPS6KA2	AC_000166.1	0	83	3.95E-16	3.44E-15	0.225	1.24944
RPS6KA2	AC_000166.1	0	80	1.24E-15	9.79E-15	0.225	1.24944
RPS6KA2	AC_000166.1	0	100	2.22E-19	2.32E-18	0.225	1.24944
RPS6KA2	AC_000166.1	0	77	5.26E-15	4.10E-14	0.225	1.24944
RPS6KA2	AC_000166.1	5	100	1.69E-14	1.30E-13	0.225	1.24944
RPS6KA2	AC_000166.1	0	100	2.22E-19	2.32E-18	0.225	1.24944
RPS6KA2	AC_000166.1	0	100	2.22E-19	2.32E-18	0.225	1.24944
THBS2	AC_000166.1	0	100	2.22E-19	2.32E-18	1.311	1.91925
THBS2	AC_000166.1	100	0	2.22E-19	2.32E-18	1.311	1.91925
ERMARD	AC_000166.1	0	88	3.94E-17	3.96E-16	2.539	9.29923
ZNF75D	AC_000187.1	14	85	3.93E-08	1.89E-07	140.532	66.9043
ZNF75D	AC_000187.1	83	0	3.95E-16	3.44E-15	140.532	66.9043
ZNF75D	AC_000187.1	0	85	1.66E-16	1.56E-15	140.532	66.9043
ZNF75D	AC_000187.1	0	100	2.22E-19	2.32E-18	140.532	66.9043
ABCD1	AC_000187.1	0	100	2.22E-19	2.32E-18	0.088	4.01559
TMEM164	AC_000187.1	100	0	2.22E-19	2.32E-18	1.617	2.99726
PAK3	AC_000187.1	14	78	3.50E-07	1.56E-06	12.109	2.90494
MSN	AC_000187.1	91	9	7.07E-11	4.45E-10	34.72	9.52565
MSN	AC_000187.1	77	20	1.58E-05	5.68E-05	34.72	9.52565
MOSPD2	AC_000187.1	18	85	6.32E-07	2.76E-06	27.71	6.82811
STS	AC_000187.1	0	100	2.22E-19	2.32E-18	0.282	0.38815

Table S7.4 Gene expression for DMRs between GV vs. *in vivo* MII

Gene expression in DMRs from GV vs. in vivo MII							
Gene	**Chr**	**GV_me**	**In vivo MII_me**	**p-value**	**q-value**	**GV expression**	**In vivo MII expression**
SENP7	AC_000158.1	20	100	2.92E-08	4.20E-07	28.275	1.328
MYCBP2	AC_000169.1	75	14	9.09E-07	8.19E-06	11.59	6.121
DOCK9	AC_000169.1	14	80	1.93E-07	2.06E-06	21.342	11.036
SERTAD4	AC_000173.1	0	100	2.22E-19	4.19E-17	0.377	0.386
ZNF524	AC_000175.1	0	100	2.22E-19	4.19E-17	3.733	0.517
RPL19	AC_000176.1	77	20	1.58E-05	1.10E-04	1281.436	27.609
RAB37	AC_000176.1	0	80	1.24E-15	8.79E-14	5.424	0.14
RAB37	AC_000176.1	85	16	1.60E-07	1.79E-06	5.424	0.14
RAB37	AC_000176.1	87	21	1.86E-06	1.61E-05	5.424	0.14
TRIM62	AC_000159.1	0	100	2.22E-19	4.19E-17	10.799	0.037
LCP2	AC_000177.1	0	100	2.22E-19	4.19E-17	1.083	0.162
SLC38A9	AC_000177.1	25	80	7.02E-05	4.25E-04	23.88	10.109
MRPS11	AC_000178.1	20	100	2.92E-08	4.20E-07	24.469	1.443
MRPS11	AC_000178.1	22	100	9.72E-08	1.10E-06	24.469	1.443
FRMD5	AC_000178.1	100	25	5.20E-07	5.31E-06	8.882	3.842
FRMD5	AC_000178.1	100	16	1.86E-09	3.35E-08	8.882	3.842
FRMD5	AC_000178.1	80	15	4.06E-07	4.23E-06	8.882	3.842
SLC4A7	AC_000179.1	0	80	1.24E-15	8.79E-14	7.76	11.245
ERC2	AC_000179.1	80	16	7.24E-07	7.27E-06	5.638	1.022
DUSP7	AC_000179.1	0	80	1.24E-15	8.79E-14	129.436	15.385
PTPN23	AC_000179.1	23	80	3.02E-05	1.94E-04	9.137	1.502
MGLL	AC_000179.1	83	0	3.95E-16	4.34E-14	0.776	0.045
HIST1H1C	AC_000180.1	80	20	6.94E-06	5.05E-05	168.516	8.217
ATP9B	AC_000181.1	100	0	2.22E-19	4.19E-17	1.054	0.513
KCTD1	AC_000181.1	100	0	2.22E-19	4.19E-17	3.893	6.366
LOXL4	AC_000183.1	0	100	2.22E-19	4.19E-17	0.014	0.052
SUFU	AC_000183.1	75	0	1.25E-14	8.05E-13	2.698	1.731
SORCS3	AC_000183.1	0	80	1.24E-15	8.79E-14	8.191	2.896
SORCS3	AC_000183.1	0	100	2.22E-19	4.19E-17	8.191	2.896
WRN	AC_000184.1	80	15	4.06E-07	4.23E-06	10.07	1.63
WRN	AC_000184.1	93	16	1.47E-08	2.45E-07	10.07	1.63
RNF122	AC_000184.1	80	0	1.24E-15	8.79E-14	9.872	2.269
RNF122	AC_000184.1	15	80	4.06E-07	4.23E-06	9.872	2.269
RNF122	AC_000184.1	87	0	7.02E-17	1.15E-14	9.872	2.269
RNF122	AC_000184.1	100	14	3.79E-10	8.76E-09	9.872	2.269
RNF122	AC_000184.1	100	7	2.90E-13	1.60E-11	9.872	2.269
RNF122	AC_000184.1	100	20	2.92E-08	4.20E-07	9.872	2.269
RNF122	AC_000184.1	83	20	3.33E-06	2.69E-05	9.872	2.269

RNF122	AC_000184.1	0	100	2.22E-19	4.19E-17	9.872	2.269
RNF122	AC_000184.1	100	0	2.22E-19	4.19E-17	9.872	2.269
RNF122	AC_000184.1	83	11	7.24E-09	1.23E-07	9.872	2.269
RNF122	AC_000184.1	80	20	6.94E-06	5.05E-05	9.872	2.269
RNF122	AC_000184.1	0	80	1.24E-15	8.79E-14	9.872	2.269
RNF122	AC_000184.1	20	80	6.94E-06	5.05E-05	9.872	2.269
RNF122	AC_000184.1	80	20	6.94E-06	5.05E-05	9.872	2.269
RNF122	AC_000184.1	100	0	2.22E-19	4.19E-17	9.872	2.269
RNF122	AC_000184.1	14	83	8.33E-08	9.57E-07	9.872	2.269
RNF122	AC_000184.1	80	20	6.94E-06	5.05E-05	9.872	2.269
RNF122	AC_000184.1	100	20	2.92E-08	4.20E-07	9.872	2.269
RNF122	AC_000184.1	83	20	3.33E-06	2.69E-05	9.872	2.269
RNF122	AC_000184.1	16	80	7.24E-07	7.27E-06	9.872	2.269
RNF122	AC_000184.1	0	83	3.95E-16	4.34E-14	9.872	2.269
RNF122	AC_000184.1	80	0	1.24E-15	8.79E-14	9.872	2.269
RNF122	AC_000184.1	14	100	3.79E-10	8.76E-09	9.872	2.269
RNF122	AC_000184.1	0	100	2.22E-19	4.19E-17	9.872	2.269
RNF122	AC_000184.1	25	90	6.49E-06	5.05E-05	9.872	2.269
RNF122	AC_000184.1	25	85	2.09E-05	1.41E-04	9.872	2.269
RNF122	AC_000184.1	100	0	2.22E-19	4.19E-17	9.872	2.269
RNF122	AC_000184.1	100	20	2.92E-08	4.20E-07	9.872	2.269
RNF122	AC_000184.1	80	0	1.24E-15	8.79E-14	9.872	2.269
RNF122	AC_000184.1	5	80	3.50E-11	9.03E-10	9.872	2.269
RNF122	AC_000184.1	100	20	2.92E-08	4.20E-07	9.872	2.269
RNF122	AC_000184.1	80	20	6.94E-06	5.05E-05	9.872	2.269
RNF122	AC_000184.1	20	80	6.94E-06	5.05E-05	9.872	2.269
RNF122	AC_000184.1	80	20	6.94E-06	5.05E-05	9.872	2.269
RNF122	AC_000184.1	80	0	1.24E-15	8.79E-14	9.872	2.269
RNF122	AC_000184.1	76	16	2.25E-06	1.91E-05	9.872	2.269
RNF122	AC_000184.1	81	0	9.35E-16	8.79E-14	9.872	2.269
RNF122	AC_000184.1	20	100	2.92E-08	4.20E-07	9.872	2.269
RNF122	AC_000184.1	20	100	2.92E-08	4.20E-07	9.872	2.269
RNF122	AC_000184.1	20	80	6.94E-06	5.05E-05	9.872	2.269
RNF122	AC_000184.1	80	16	7.24E-07	7.27E-06	9.872	2.269
RNF122	AC_000184.1	80	14	1.93E-07	2.06E-06	9.872	2.269
RNF122	AC_000184.1	0	100	2.22E-19	4.19E-17	9.872	2.269
RNF122	AC_000184.1	0	80	1.24E-15	8.79E-14	9.872	2.269
RNF122	AC_000184.1	88	0	3.94E-17	6.82E-15	9.872	2.269
RNF122	AC_000184.1	80	0	1.24E-15	8.79E-14	9.872	2.269
RNF122	AC_000184.1	20	80	6.94E-06	5.05E-05	9.872	2.269
RNF122	AC_000184.1	100	25	5.20E-07	5.31E-06	9.872	2.269
UNC5D	AC_000184.1	100	0	2.22E-19	4.19E-17	9.564	3.119
MACROD1	AC_000186.1	0	100	2.22E-19	4.19E-17	5.449	0.955
PC	AC_000186.1	100	0	2.22E-19	4.19E-17	0.961	0.042
CARS	AC_000186.1	77	20	1.58E-05	1.10E-04	3.16	0.776

MAGI3	AC_000160.1	80	0	1.24E-15	8.79E-14	68.672	7.925
KIAA1324L	AC_000161.1	85	9	5.67E-10	1.06E-08	14.742	3.943
KIAA1324L	AC_000161.1	80	25	7.02E-05	4.25E-04	14.742	3.943
KIAA1324L	AC_000161.1	22	83	9.08E-06	6.54E-05	14.742	3.943
MET	AC_000161.1	87	20	1.14E-06	1.00E-05	0.14	0.156
GTPBP10	AC_000161.1	83	0	3.95E-16	4.34E-14	36.996	1.259
LRGUK	AC_000161.1	0	100	2.22E-19	4.19E-17	2.844	0.074
LRGUK	AC_000161.1	20	100	2.92E-08	4.20E-07	2.844	0.074
LRGUK	AC_000161.1	80	14	1.93E-07	2.06E-06	2.844	0.074
LRGUK	AC_000161.1	80	20	6.94E-06	5.05E-05	2.844	0.074
LRGUK	AC_000161.1	77	20	1.58E-05	1.10E-04	2.844	0.074
LRGUK	AC_000161.1	75	20	2.62E-05	1.76E-04	2.844	0.074
LRGUK	AC_000161.1	100	20	2.92E-08	4.20E-07	2.844	0.074
UBN2	AC_000161.1	16	100	1.86E-09	3.35E-08	55.015	3.553
ITPR2	AC_000162.1	23	75	9.52E-05	5.55E-04	2.054	1.345
TNFRSF1A	AC_000162.1	80	16	7.24E-07	7.27E-06	0.315	0.058
SCNN1A	AC_000162.1	80	16	7.24E-07	7.27E-06	4.3	0.279
PDE5A	AC_000163.1	83	0	3.95E-16	4.34E-14	20.575	6.356
PDE5A	AC_000163.1	12	80	4.35E-08	5.03E-07	20.575	6.356
PDE5A	AC_000163.1	80	14	1.93E-07	2.06E-06	20.575	6.356
PDE5A	AC_000163.1	16	80	7.24E-07	7.27E-06	20.575	6.356
PDE5A	AC_000163.1	90	23	2.50E-06	2.11E-05	20.575	6.356
METAP1	AC_000163.1	20	80	6.94E-06	5.05E-05	10.854	11.068
ADAMTS3	AC_000163.1	87	20	1.14E-06	1.00E-05	0.48	0.026
CCDC96	AC_000163.1	20	85	1.96E-06	1.68E-05	0.902	0.013
SLC12A2	AC_000164.1	100	0	2.22E-19	4.19E-17	22.906	9.346
DBN1	AC_000164.1	100	0	2.22E-19	4.19E-17	5.413	2.981
EGR1	AC_000164.1	100	16	1.86E-09	3.35E-08	23.657	0.357
CTNNA1	AC_000164.1	100	20	2.92E-08	4.20E-07	282.447	782.826
CTNNA1	AC_000164.1	85	20	1.96E-06	1.68E-05	282.447	782.826
CTNNA1	AC_000164.1	81	25	5.36E-05	3.34E-04	282.447	782.826
GRIA1	AC_000164.1	81	0	9.35E-16	8.79E-14	0.245	0.088
MSN	AC_000187.1	77	9	8.67E-09	1.45E-07	42.143	5.118

Table S7.5 Gene expression for DMRs between GV vs. *in vitro* MII

Gene expression in DMRs from GV vs. in vitro MII							
Gene	**Chr**	**GV_me**	**In vitro MII_me**	**p-value**	**q-value**	**GV expression**	**In vitro MII expression**
CNNM4	AC_000168.1	85	20	1.96E-06	1.95E-05	23.617	11.71
DYSF	AC_000168.1	20	80	6.94E-06	5.87E-05	0.372	0.44
DYSF	AC_000168.1	80	20	6.94E-06	5.87E-05	0.372	0.44
RALGPS1	AC_000168.1	80	16	7.24E-07	8.28E-06	2.175	2.29
DOCK9	AC_000169.1	14	80	1.93E-07	2.37E-06	21.342	27.006
PLCB1	AC_000170.1	85	0	1.66E-16	1.71E-14	2.134	0.538
MACROD2	AC_000170.1	87	12	4.29E-09	8.34E-08	6.478	6.667
MACROD2	AC_000170.1	77	12	1.04E-07	1.34E-06	6.478	6.667
CUBN	AC_000170.1	25	83	3.36E-05	2.50E-04	0.254	0.097
CUBN	AC_000170.1	100	22	9.72E-08	1.26E-06	0.254	0.097
DEPTOR	AC_000171.1	100	0	2.22E-19	3.28E-17	4.076	1.409
CD82	AC_000172.1	100	0	2.22E-19	3.28E-17	0.07	0.012
RGS7	AC_000173.1	0	100	2.22E-19	3.28E-17	1.014	0.034
PKP1	AC_000173.1	83	0	3.95E-16	3.29E-14	0.483	0.111
CPE	AC_000174.1	75	25	2.10E-04	0.00122266	5.305	5.301
PRODH	AC_000174.1	0	100	2.22E-19	3.28E-17	1.218	0.165
CCDC116	AC_000174.1	0	100	2.22E-19	3.28E-17	0.377	0.556
FOXC2	AC_000175.1	0	100	2.22E-19	3.28E-17	0.521	0.358
MNT	AC_000176.1	100	0	2.22E-19	3.28E-17	4.813	2.52
FAM83G	AC_000176.1	100	0	2.22E-19	3.28E-17	0.014	0.022
FBXL20	AC_000176.1	0	80	1.24E-15	7.34E-14	29.104	27.908
RAB37	AC_000176.1	0	100	2.22E-19	3.28E-17	5.424	2.856
RAB37	AC_000176.1	80	9	3.43E-09	6.69E-08	5.424	2.856
RAB37	AC_000176.1	83	0	3.95E-16	3.29E-14	5.424	2.856
RAB37	AC_000176.1	20	100	2.92E-08	4.73E-07	5.424	2.856
RAB37	AC_000176.1	83	15	1.57E-07	2.01E-06	5.424	2.856
4-Mar	AC_000159.1	100	0	2.22E-19	3.28E-17	0.525	0.089
SLC38A9	AC_000177.1	83	0	3.95E-16	3.29E-14	23.88	23.787
SLC38A9	AC_000177.1	20	80	6.94E-06	5.87E-05	23.88	23.787
SKIV2L2	AC_000177.1	80	0	1.24E-15	7.34E-14	15.244	16.212
MRPS11	AC_000178.1	83	5	1.01E-11	2.96E-10	24.469	5.9
MRPS11	AC_000178.1	20	100	2.92E-08	4.73E-07	24.469	5.9
FRMD5	AC_000178.1	0	80	1.24E-15	7.34E-14	8.882	5.627
FRMD5	AC_000178.1	14	100	3.79E-10	9.40E-09	8.882	5.627
PTPN23	AC_000179.1	80	16	7.24E-07	8.28E-06	9.137	3.856
ATP2B2	AC_000179.1	100	0	2.22E-19	3.28E-17	0.003	0.009
KLF15	AC_000179.1	0	100	2.22E-19	3.28E-17	0.233	0.159
PXDC1	AC_000180.1	80	0	1.24E-15	7.34E-14	0.076	0.098

GMDS	AC_000180.1	0	100	2.22E-19	3.28E-17	1.846	1.399
FBXL16	AC_000182.1	20	100	2.92E-08	4.73E-07	0.915	0.279
PRKG1	AC_000183.1	14	83	8.33E-08	1.09E-06	21.133	25.31
SORCS3	AC_000183.1	0	100	2.22E-19	3.28E-17	8.191	7.95
SORCS3	AC_000183.1	0	100	2.22E-19	3.28E-17	8.191	7.95
RNF122	AC_000184.1	12	100	6.45E-11	1.73E-09	9.872	8.137
RNF122	AC_000184.1	100	14	3.79E-10	9.40E-09	9.872	8.137
RNF122	AC_000184.1	9	100	3.27E-12	1.23E-10	9.872	8.137
RNF122	AC_000184.1	80	16	7.24E-07	8.28E-06	9.872	8.137
RNF122	AC_000184.1	0	85	1.66E-16	1.71E-14	9.872	8.137
RNF122	AC_000184.1	100	20	2.92E-08	4.73E-07	9.872	8.137
RNF122	AC_000184.1	80	15	4.06E-07	4.81E-06	9.872	8.137
RNF122	AC_000184.1	25	87	1.29E-05	1.05E-04	9.872	8.137
RNF122	AC_000184.1	20	83	3.33E-06	3.08E-05	9.872	8.137
RNF122	AC_000184.1	80	16	7.24E-07	8.28E-06	9.872	8.137
RNF122	AC_000184.1	0	80	1.24E-15	7.34E-14	9.872	8.137
RNF122	AC_000184.1	20	100	2.92E-08	4.73E-07	9.872	8.137
RNF122	AC_000184.1	16	83	2.86E-07	3.43E-06	9.872	8.137
RNF122	AC_000184.1	16	80	7.24E-07	8.28E-06	9.872	8.137
RNF122	AC_000184.1	0	100	2.22E-19	3.28E-17	9.872	8.137
RNF122	AC_000184.1	80	0	1.24E-15	7.34E-14	9.872	8.137
RNF122	AC_000184.1	75	0	1.25E-14	6.66E-13	9.872	8.137
RNF122	AC_000184.1	85	12	8.19E-09	1.53E-07	9.872	8.137
RNF122	AC_000184.1	75	20	2.62E-05	2.02E-04	9.872	8.137
RNF122	AC_000184.1	0	100	2.22E-19	3.28E-17	9.872	8.137
RNF122	AC_000184.1	0	90	1.66E-17	2.26E-15	9.872	8.137
RNF122	AC_000184.1	80	0	1.24E-15	7.34E-14	9.872	8.137
RNF122	AC_000184.1	0	83	3.95E-16	3.29E-14	9.872	8.137
RNF122	AC_000184.1	20	80	6.94E-06	5.87E-05	9.872	8.137
RNF122	AC_000184.1	25	86	1.71E-05	1.38E-04	9.872	8.137
RNF122	AC_000184.1	75	0	1.25E-14	6.66E-13	9.872	8.137
RNF122	AC_000184.1	20	100	2.92E-08	4.73E-07	9.872	8.137
RNF122	AC_000184.1	20	85	1.96E-06	1.95E-05	9.872	8.137
RNF122	AC_000184.1	80	0	1.24E-15	7.34E-14	9.872	8.137
RNF122	AC_000184.1	80	11	2.08E-08	3.55E-07	9.872	8.137
RNF122	AC_000184.1	20	100	2.92E-08	4.73E-07	9.872	8.137
RNF122	AC_000184.1	20	85	1.96E-06	1.95E-05	9.872	8.137
RNF122	AC_000184.1	80	14	1.93E-07	2.37E-06	9.872	8.137
RNF122	AC_000184.1	20	80	6.94E-06	5.87E-05	9.872	8.137
RNF122	AC_000184.1	25	85	2.09E-05	1.63E-04	9.872	8.137
RNF122	AC_000184.1	76	25	1.74E-04	0.00110776	9.872	8.137
RNF122	AC_000184.1	16	100	1.86E-09	3.70E-08	9.872	8.137
RNF122	AC_000184.1	16	80	7.24E-07	8.28E-06	9.872	8.137
RNF122	AC_000184.1	20	87	1.14E-06	1.16E-05	9.872	8.137
RNF122	AC_000184.1	100	0	2.22E-19	3.28E-17	9.872	8.137

RNF122	AC_000184.1	80	0	1.24E-15	7.34E-14	9.872	8.137
RNF122	AC_000184.1	0	78	2.95E-15	1.73E-13	9.872	8.137
RNF122	AC_000184.1	0	77	5.26E-15	3.00E-13	9.872	8.137
RNF122	AC_000184.1	16	100	1.86E-09	3.70E-08	9.872	8.137
RNF122	AC_000184.1	80	25	7.02E-05	4.91E-04	9.872	8.137
RNF122	AC_000184.1	0	85	1.66E-16	1.71E-14	9.872	8.137
RNF122	AC_000184.1	0	80	1.24E-15	7.34E-14	9.872	8.137
RNF122	AC_000184.1	0	80	1.24E-15	7.34E-14	9.872	8.137
RNF122	AC_000184.1	0	75	1.25E-14	6.66E-13	9.872	8.137
RNF122	AC_000184.1	16	80	7.24E-07	8.28E-06	9.872	8.137
RNF122	AC_000184.1	83	0	3.95E-16	3.29E-14	9.872	8.137
RNF122	AC_000184.1	83	20	3.33E-06	3.08E-05	9.872	8.137
RNF122	AC_000184.1	0	100	2.22E-19	3.28E-17	9.872	8.137
RNF122	AC_000184.1	0	88	3.94E-17	5.09E-15	9.872	8.137
RNF122	AC_000184.1	83	0	3.95E-16	3.29E-14	9.872	8.137
RNF122	AC_000184.1	20	100	2.92E-08	4.73E-07	9.872	8.137
RNF122	AC_000184.1	0	100	2.22E-19	3.28E-17	9.872	8.137
RNF122	AC_000184.1	80	14	1.93E-07	2.37E-06	9.872	8.137
RNF122	AC_000184.1	16	80	7.24E-07	8.28E-06	9.872	8.137
RNF122	AC_000184.1	20	75	2.62E-05	2.02E-04	9.872	8.137
RNF122	AC_000184.1	16	100	1.86E-09	3.70E-08	9.872	8.137
RNF122	AC_000184.1	100	11	2.69E-11	7.78E-10	9.872	8.137
UNC5D	AC_000184.1	100	20	2.92E-08	4.73E-07	9.564	5.798
MACROD1	AC_000186.1	0	87	7.02E-17	8.06E-15	5.449	3.035
MACROD1	AC_000186.1	0	85	1.66E-16	1.71E-14	5.449	3.035
NRXN2	AC_000186.1	0	100	2.22E-19	3.28E-17	0.23	0.031
KLC2	AC_000186.1	75	0	1.25E-14	6.66E-13	0.59	0.89
MAGI3	AC_000160.1	80	0	1.24E-15	7.34E-14	68.672	59.519
YBX1	AC_000160.1	100	20	2.92E-08	4.73E-07	167.373	157.381
KIAA1324L	AC_000161.1	80	20	6.94E-06	5.87E-05	14.742	8.885
LHFPL3	AC_000161.1	76	14	6.34E-07	7.37E-06	88.447	99.227
MET	AC_000161.1	87	0	7.02E-17	8.06E-15	0.14	0.49
LRGUK	AC_000161.1	85	0	1.66E-16	1.71E-14	2.844	2.29
LRGUK	AC_000161.1	75	0	1.25E-14	6.66E-13	2.844	2.29
LRGUK	AC_000161.1	16	80	7.24E-07	8.28E-06	2.844	2.29
LRGUK	AC_000161.1	75	14	9.09E-07	9.50E-06	2.844	2.29
UBN2	AC_000161.1	88	0	3.94E-17	5.09E-15	55.015	46.853
TOM1	AC_000162.1	83	0	3.95E-16	3.29E-14	4.641	2.929
TNFRSF1A	AC_000162.1	80	20	6.94E-06	5.87E-05	0.315	0.649
SCNN1A	AC_000162.1	80	20	6.94E-06	5.87E-05	4.3	1.772
PDE5A	AC_000163.1	0	76	6.99E-15	3.93E-13	20.575	20.064
PDE5A	AC_000163.1	100	25	5.20E-07	6.07E-06	20.575	20.064
PDE5A	AC_000163.1	20	83	3.33E-06	3.08E-05	20.575	20.064
PDE5A	AC_000163.1	0	87	7.02E-17	8.06E-15	20.575	20.064
PDE5A	AC_000163.1	12	80	4.35E-08	5.78E-07	20.575	20.064

NFKB1	AC_000163.1	80	0	1.24E-15	7.34E-14	5.368	6.486
NSG1	AC_000163.1	100	0	2.22E-19	3.28E-17	12.347	5.216
PRDX2	AC_000164.1	100	0	2.22E-19	3.28E-17	541.593	139.339
SLC12A2	AC_000164.1	100	0	2.22E-19	3.28E-17	22.906	24.104
CTNNA1	AC_000164.1	100	20	2.92E-08	4.73E-07	282.447	359.821
CTNNA1	AC_000164.1	20	83	3.33E-06	3.08E-05	282.447	359.821
GRIA1	AC_000164.1	81	23	2.27E-05	1.78E-04	0.245	0.377
ZNF395	AC_000165.1	14	80	1.93E-07	2.37E-06	6.707	5.019
ZNF395	AC_000165.1	20	80	6.94E-06	5.87E-05	6.707	5.019
RHOBTB2	AC_000165.1	0	100	2.22E-19	3.28E-17	0.079	0.412
RPS6KA2	AC_000166.1	100	0	2.22E-19	3.28E-17	0.203	0.225
THBS2	AC_000166.1	100	0	2.22E-19	3.28E-17	0.046	1.311
HS6ST2	AC_000187.1	85	20	1.96E-06	1.95E-05	0.774	0.364
ZNF75D	AC_000187.1	80	10	8.02E-09	1.50E-07	109.846	140.532
ZNF75D	AC_000187.1	81	20	5.62E-06	5.11E-05	109.846	140.532
TMEM164	AC_000187.1	0	100	2.22E-19	3.28E-17	6.522	1.617

Table S6.6 Gene expression for DMRs between *in vivo* MII vs. *in vitro* MII

Gene expression in DMRs from in vivo MII vs. in vitro MII							
Gene	**Chr**	**In vivo MII_me**	**In vitro MII_me**	**p-value**	**q-value**	**In vivo MII expression**	**In vitro MII expression**
DOCK9	AC_000169.1	14	88	1.67E-08	2.48E-07	11.036	27.006
CHMP4B	AC_000170.1	20	75	2.62E-05	1.79E-04	8.831	6.574
ZW10	AC_000172.1	75	25	2.10E-04	0.00106068	74.41	27.922
PHLDB1	AC_000172.1	100	0	2.22E-19	2.71E-17	0.203	0.626
CAPN5	AC_000172.1	20	100	2.92E-08	4.16E-07	0.013	0.013
OSBP2	AC_000174.1	0	100	2.22E-19	2.71E-17	0.035	0.359
SLC7A5	AC_000175.1	100	0	2.22E-19	2.71E-17	0.029	0.039
ZNF423	AC_000175.1	100	0	2.22E-19	2.71E-17	0.225	0.044
ZNF423	AC_000175.1	100	0	2.22E-19	2.71E-17	0.225	0.044
TTYH1	AC_000175.1	0	100	2.22E-19	2.71E-17	0.017	1.491
COPZ2	AC_000176.1	0	100	2.22E-19	2.71E-17	0.879	2.322
COPZ2	AC_000176.1	0	100	2.22E-19	2.71E-17	0.879	2.322
RPL19	AC_000176.1	20	80	6.94E-06	5.31E-05	27.609	622.381
RARA	AC_000176.1	0	100	2.22E-19	2.71E-17	0.389	5.363
CDR2L	AC_000176.1	0	80	1.24E-15	6.96E-14	0.017	1.002
RAB37	AC_000176.1	20	75	2.62E-05	1.79E-04	0.14	2.856
RAB37	AC_000176.1	80	0	1.24E-15	6.96E-14	0.14	2.856
RAB37	AC_000176.1	16	75	3.16E-06	2.68E-05	0.14	2.856
RAB37	AC_000176.1	21	75	3.99E-05	2.55E-04	0.14	2.856
LCP2	AC_000177.1	100	0	2.22E-19	2.71E-17	0.162	1.715
SKIV2L2	AC_000177.1	20	80	6.94E-06	5.31E-05	0.801	16.212
SKIV2L2	AC_000177.1	100	0	2.22E-19	2.71E-17	0.801	16.212
FRMD5	AC_000178.1	80	0	1.24E-15	6.96E-14	3.842	5.627
FRMD5	AC_000178.1	13	80	1.01E-07	1.17E-06	3.842	5.627
SYNPR	AC_000179.1	87	25	1.29E-05	9.32E-05	3.006	0.827
ERC2	AC_000179.1	16	83	2.86E-07	3.08E-06	1.022	6.3
PTPN23	AC_000179.1	80	18	2.38E-06	2.09E-05	1.502	3.856
KLF15	AC_000179.1	0	100	2.22E-19	2.71E-17	1.162	0.159
HIST1H1C	AC_000180.1	20	80	6.94E-06	5.31E-05	8.217	154.3
LHPP	AC_000183.1	80	0	1.24E-15	6.96E-14	0.171	0.303
LHPP	AC_000183.1	100	0	2.22E-19	2.71E-17	0.171	0.303
RNF122	AC_000184.1	0	100	2.22E-19	2.71E-17	2.269	8.137
RNF122	AC_000184.1	0	83	3.95E-16	3.04E-14	2.269	8.137
RNF122	AC_000184.1	0	80	1.24E-15	6.96E-14	2.269	8.137
RNF122	AC_000184.1	20	77	1.58E-05	1.13E-04	2.269	8.137
RNF122	AC_000184.1	0	81	9.35E-16	6.96E-14	2.269	8.137
RNF122	AC_000184.1	0	100	2.22E-19	2.71E-17	2.269	8.137
RNF122	AC_000184.1	7	81	2.68E-10	5.96E-09	2.269	8.137

RNF122	AC_000184.1	0	100	2.22E-19	2.71E-17	2.269	8.137
RNF122	AC_000184.1	0	80	1.24E-15	6.96E-14	2.269	8.137
RNF122	AC_000184.1	11	100	2.69E-11	7.05E-10	2.269	8.137
RNF122	AC_000184.1	0	90	1.66E-17	1.86E-15	2.269	8.137
RNF122	AC_000184.1	11	100	2.69E-11	7.05E-10	2.269	8.137
RNF122	AC_000184.1	25	80	7.02E-05	4.29E-04	2.269	8.137
RNF122	AC_000184.1	83	8	4.40E-10	9.35E-09	2.269	8.137
RNF122	AC_000184.1	9	85	5.67E-10	1.02E-08	2.269	8.137
RNF122	AC_000184.1	0	83	3.95E-16	3.04E-14	2.269	8.137
RNF122	AC_000184.1	83	20	3.33E-06	2.78E-05	2.269	8.137
RNF122	AC_000184.1	22	75	6.49E-05	4.02E-04	2.269	8.137
RNF122	AC_000184.1	20	100	2.92E-08	4.16E-07	2.269	8.137
RNF122	AC_000184.1	0	100	2.22E-19	2.71E-17	2.269	8.137
RNF122	AC_000184.1	0	100	2.22E-19	2.71E-17	2.269	8.137
RNF122	AC_000184.1	16	100	1.86E-09	3.23E-08	2.269	8.137
RNF122	AC_000184.1	0	100	2.22E-19	2.71E-17	2.269	8.137
RNF122	AC_000184.1	100	0	2.22E-19	2.71E-17	2.269	8.137
RNF122	AC_000184.1	0	80	1.24E-15	6.96E-14	2.269	8.137
RNF122	AC_000184.1	80	0	1.24E-15	6.96E-14	2.269	8.137
RNF122	AC_000184.1	10	83	3.22E-09	5.45E-08	2.269	8.137
RNF122	AC_000184.1	20	100	2.92E-08	4.16E-07	2.269	8.137
RNF122	AC_000184.1	25	83	3.36E-05	2.19E-04	2.269	8.137
RNF122	AC_000184.1	80	25	7.02E-05	4.29E-04	2.269	8.137
RNF122	AC_000184.1	20	83	3.33E-06	2.78E-05	2.269	8.137
RNF122	AC_000184.1	0	88	3.94E-17	4.13E-15	2.269	8.137
RNF122	AC_000184.1	12	100	6.45E-11	1.56E-09	2.269	8.137
RNF122	AC_000184.1	20	87	1.14E-06	1.04E-05	2.269	8.137
RNF122	AC_000184.1	0	100	2.22E-19	2.71E-17	2.269	8.137
RNF122	AC_000184.1	0	100	2.22E-19	2.71E-17	2.269	8.137
RNF122	AC_000184.1	75	7	2.27E-09	3.91E-08	2.269	8.137
RNF122	AC_000184.1	11	80	2.08E-08	3.05E-07	2.269	8.137
RNF122	AC_000184.1	20	100	2.92E-08	4.16E-07	2.269	8.137
RNF122	AC_000184.1	100	0	2.22E-19	2.71E-17	2.269	8.137
RNF122	AC_000184.1	12	100	6.45E-11	1.56E-09	2.269	8.137
RNF122	AC_000184.1	16	85	1.60E-07	1.85E-06	2.269	8.137
RNF122	AC_000184.1	20	80	6.94E-06	5.31E-05	2.269	8.137
RNF122	AC_000184.1	0	85	1.66E-16	1.48E-14	2.269	8.137
RNF122	AC_000184.1	0	80	1.24E-15	6.96E-14	2.269	8.137
RNF122	AC_000184.1	100	25	5.20E-07	5.45E-06	2.269	8.137
RNF122	AC_000184.1	80	16	7.24E-07	7.46E-06	2.269	8.137
RNF122	AC_000184.1	14	83	8.33E-08	9.92E-07	2.269	8.137
RNF122	AC_000184.1	0	88	3.94E-17	4.13E-15	2.269	8.137
RNF122	AC_000184.1	11	100	2.69E-11	7.05E-10	2.269	8.137
RNF122	AC_000184.1	0	88	3.94E-17	4.13E-15	2.269	8.137
RNF122	AC_000184.1	14	75	9.09E-07	8.53E-06	2.269	8.137

FGFR1	AC_000184.1	100	12	6.45E-11	1.56E-09	2.2	1.128
MACROD1	AC_000186.1	100	0	2.22E-19	2.71E-17	0.955	3.035
CARS	AC_000186.1	20	81	5.62E-06	4.60E-05	0.776	4.071
KIAA1324L	AC_000161.1	0	88	3.94E-17	4.13E-15	3.943	8.885
LRGUK	AC_000161.1	12	80	4.35E-08	5.27E-07	0.074	2.29
LRGUK	AC_000161.1	14	83	8.33E-08	9.92E-07	0.074	2.29
LRGUK	AC_000161.1	100	22	9.72E-08	1.14E-06	0.074	2.29
LRGUK	AC_000161.1	20	83	3.33E-06	2.78E-05	0.074	2.29
UBN2	AC_000161.1	100	20	2.92E-08	4.16E-07	3.553	46.853
UBN2	AC_000161.1	16	75	3.16E-06	2.68E-05	3.553	46.853
UBN2	AC_000161.1	85	0	1.66E-16	1.48E-14	3.553	46.853
PDE5A	AC_000163.1	83	16	2.86E-07	3.08E-06	6.356	20.064
PDE5A	AC_000163.1	80	0	1.24E-15	6.96E-14	6.356	20.064
PDE5A	AC_000163.1	14	75	9.09E-07	8.53E-06	6.356	20.064
PDE5A	AC_000163.1	80	10	8.02E-09	1.29E-07	6.356	20.064
ADAMTS3	AC_000163.1	20	83	3.33E-06	2.78E-05	0.026	0.202
EGR1	AC_000164.1	0	85	1.66E-16	1.48E-14	0.357	14.139
EGR1	AC_000164.1	16	100	1.86E-09	3.23E-08	0.357	14.139
CTNNA1	AC_000164.1	0	87	7.02E-17	6.88E-15	782.826	359.821
ZNF395	AC_000165.1	0	80	1.24E-15	6.96E-14	0.043	5.019
RPS6KA2	AC_000166.1	100	0	2.22E-19	2.71E-17	0.216	0.225
RPS6KA2	AC_000166.1	100	0	2.22E-19	2.71E-17	0.216	0.225
HS6ST2	AC_000187.1	83	0	3.95E-16	3.04E-14	0.013	0.364
ZNF75D	AC_000187.1	83	16	2.86E-07	3.08E-06	204.013	140.532
SYN1	AC_000187.1	85	0	1.66E-16	1.48E-14	1.073	15.124
MSN	AC_000187.1	9	91	7.07E-11	1.65E-09	5.118	34.72
MSN	AC_000187.1	80	23	3.02E-05	1.97E-04	5.118	34.72
MSN	AC_000187.1	80	25	7.02E-05	4.29E-04	5.118	34.72

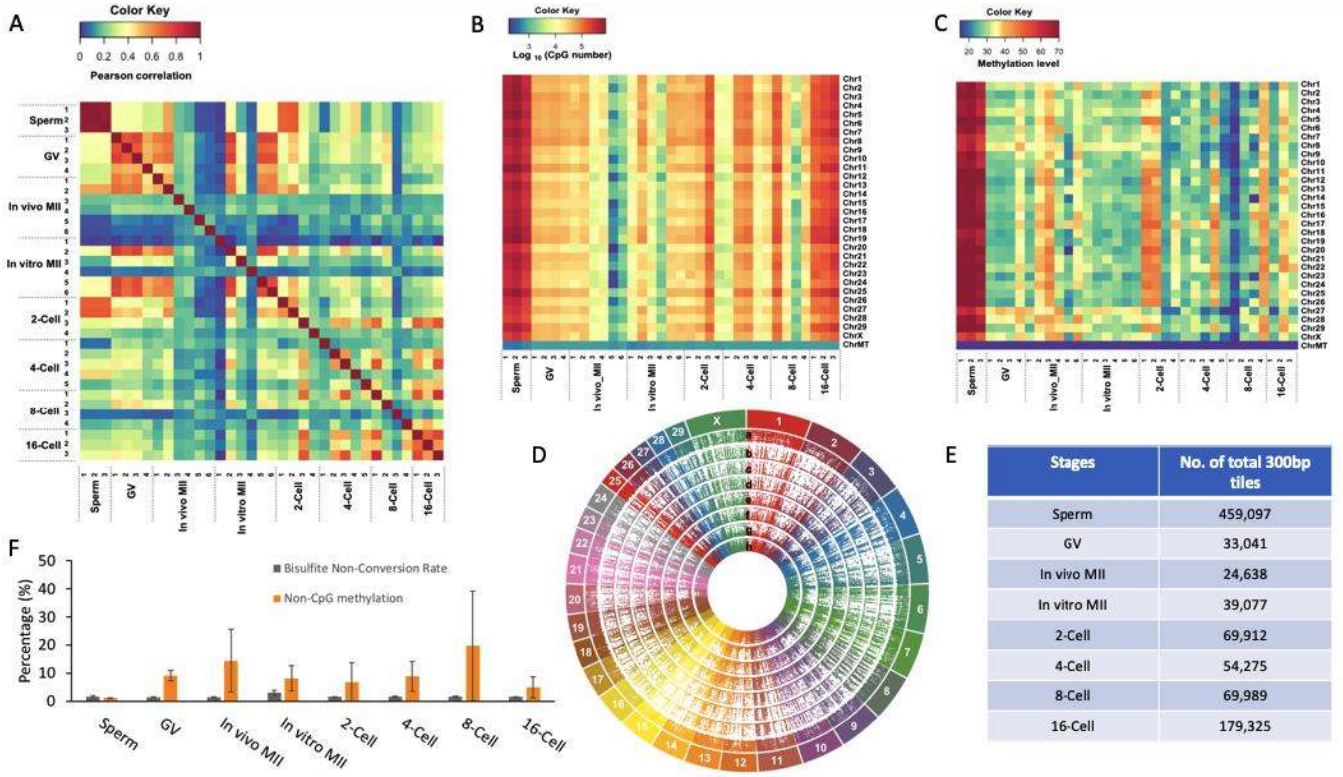

Stages	No. of total 300bp tiles
Sperm	459,097
GV	33,041
In vivo MII	24,638
In vitro MII	39,077
2-Cell	69,912
4-Cell	54,275
8-Cell	69,989
16-Cell	179,325

Figure S1. Methylome profiles of bovine gametes and in vivo developed embryos

The Pearson correlation heatmap (A) between stages. Color key: purple low correlation, red high correlation. Heatmaps of the numbers (Color key: purple: low CpG number, red high CpG numbers) (B) and methylation levels (Color key: purple: hypomethylation, red hypermethylation) (C) of captured CpGs in each chromosome. Circos plot (D) visualization of all methylated 300-bp tiles of each stage of pre-implantation embryonic development. a. sperm, b. GV oocytes, c. *in vivo* MII oocytes, d. *in vitro* MII oocytes, e. 2-cell, f. 4-cell, g. 8-cell, h. 16-cell. The number (E) of total captured 300-bp tiles in each stage. Bar plot (F) of non-CpG methylation level and bisulfite non-conversion rate of each stage. GV: germinal vesicle oocytes; MII: matured oocytes.

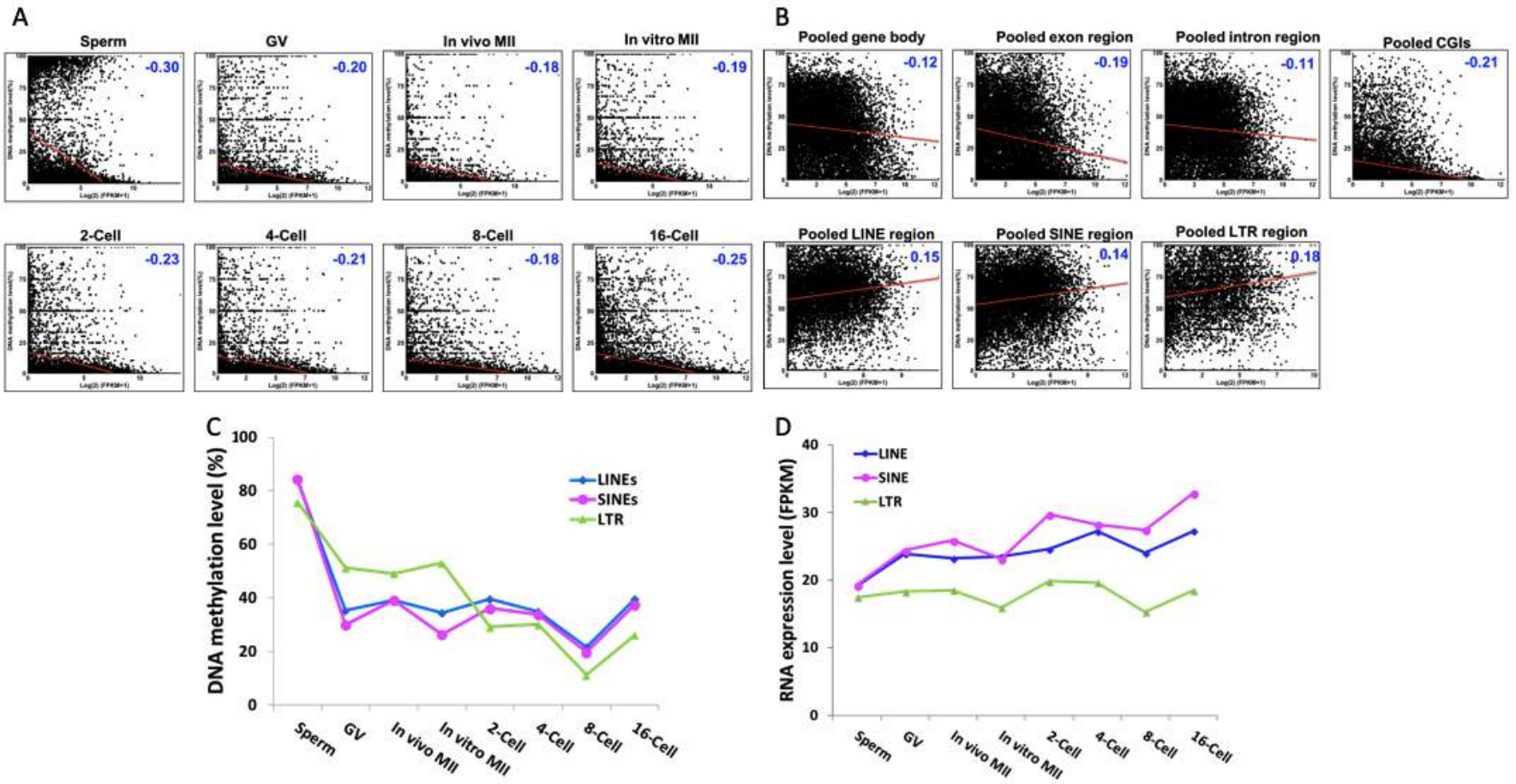

Figure S2. Relationship between transcriptomes and methylomes of bovine gametes and in vivo developed embryos
Correlation between gene expression and methylation of the promoters (A), gene bodies, exons, introns, CGIs (B). Line plots of DNA methylation (C) and RNA expression levels (D) of repetitive elements LINEs, SINEs, and LTR in each development stage. GV: germinal vesicle oocytes; MII: matured oocytes.

A

Stages	No. of unique 300bp tiles
Sperm	276,190
GV	1,089
In vivo MII	877
In vitro MII	2,435
2-Cell	6,091
4-Cell	4,195
8-Cell	6,168
16-Cell	31,628

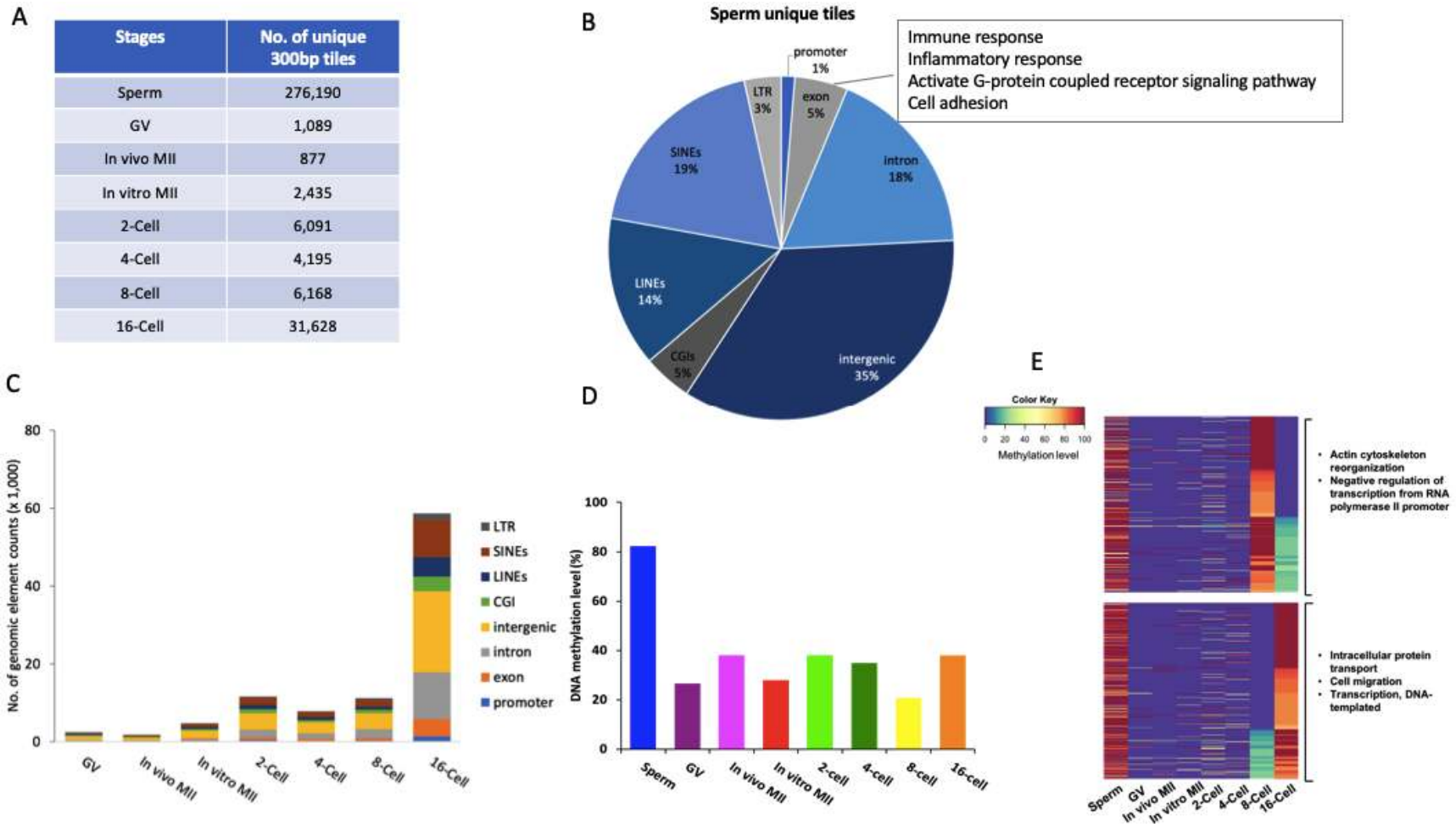

Figure S3. Commonly and uniquely methylated regions in bovine gametes and in vivo developed embryos
The numbers (A) of uniquely methylated 300-bp tiles in each development stage. Pie plot (B) of the distribution of uniquely methylated tiles in sperm categorized by genomic regions and the associated GO terms. Stack bar plot (C) of uniquely methylated 300-bp tiles in each stage categorized by genomic regions. Heatmap (E) of DMRs between the 8- and 16-cell stages that were hypermethylated in the 8-cell (upper) or 16-cell (lower) and their GO term representatives. GV: germinal vesicle oocytes; MII: matured oocytes. (Color key: purple: hypomethylation, red hypermethylation)

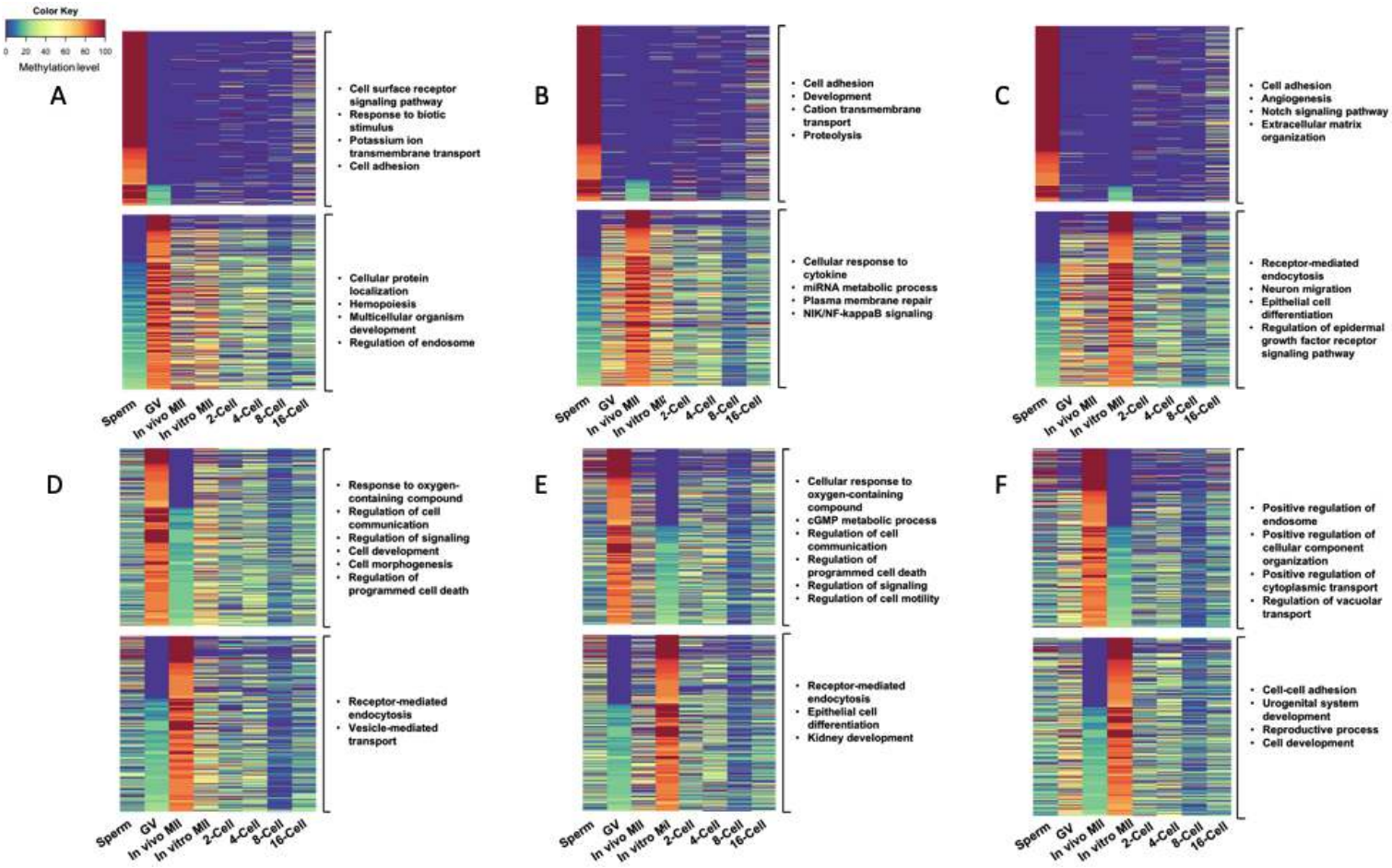

Figure S4. DMRs between different types of gametes and their GO term representatives.
Heatmaps of DMRs: sperm vs. GV (A), sperm vs. *in vivo* MII (B), sperm vs. *in vitro* MII (C), GV vs. *in vivo* MII (D), GV vs. *in vitro* MII (E), and *in vivo* MII vs. *in vitro* MII (F). GV: germinal vesicle oocytes; MII: matured oocytes. (Color key: purple: hypomethylation, red hypermethylation)

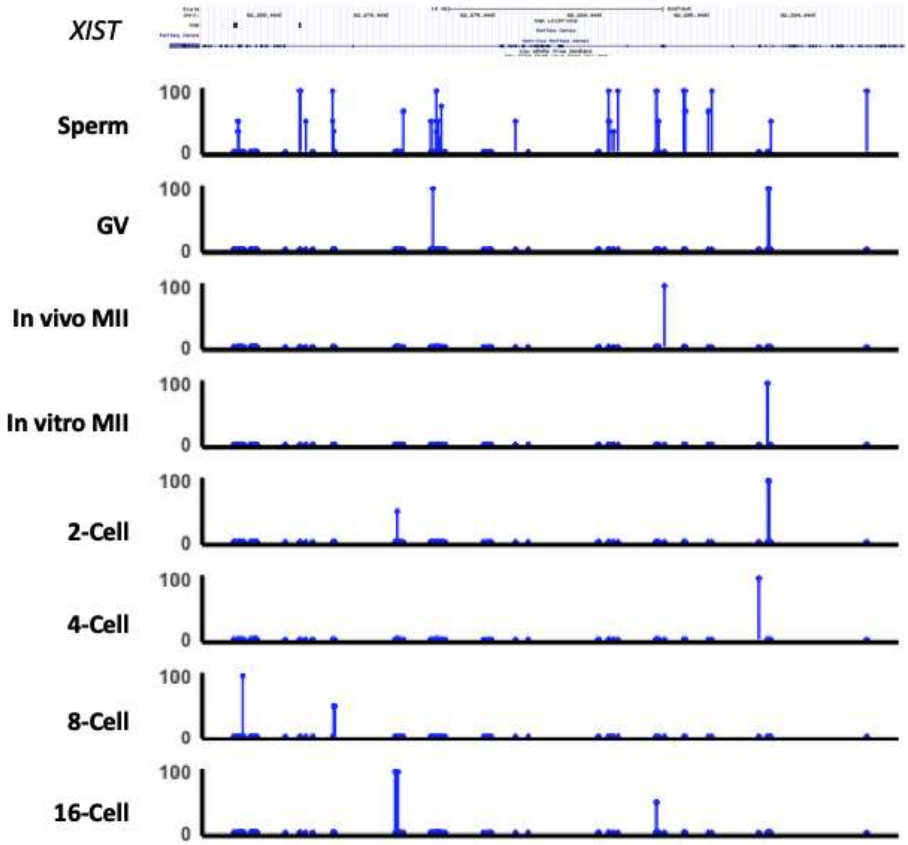

Figure S5. Visualization of gene body methylation of *XIST* gene. GV: germinal vesicle oocytes; MII: matured oocytes.

Chapter Five

Conclusions

This dissertation reported three aspects of epigenetic regulation in domestic ruminants: 1) The effect of maternal nutrition on imprinted gene expression and genomic imprinting pattern in sheep, 2) X chromosome dosage upregulation in bovine germlines, preimplantation embryos, and somatic tissues, 3) Methylome dynamic in bovine early embryos and gametes. Specifically, the following conclusions are made:

1. Maternal diets affected imprinted gene expression while the parental-of-origin expression pattern was not affected. These data suggest that gene expression levels and imprinted patterns may be regulated through different epigenetic mechanisms.

2. In bovine germline, embryos and somatic tissues expression of X-linked genes, especially those that are housekeeping or 'dosage-sensitive' genes were up-regulated, supporting a balanced expression between a single active X and autosome pairs.

3. During bovine embryo development, global demethylation was observed up to the 8-cell stage and de novo methylation at 16-cell stage, refining the current knowledge on bovine embryo DNA methylation dynamics and providing valuable resources for future studies.

Our studies of epigenetic regulations in domestic ruminants will provide insights for animal prenatal nutrition management and optimal *in vitro* culture condition for early embryo development. Future investigations on how the uterine environment influences fetal development, epigenetic regulation, and germline differentiation are needed. Future studies should also include more details in studying the onset of imprinted XCI after fertilization and transition to random XCI during early embryonic development. Moreover, differential genomic markers could be identified from the comparison of epigenetic markers between *in vivo* and *in vitro* produced oocytes and embryos.

Reference

Al Seesi, S., Tiagueu, Y.T., Zelikovsky, A., and Măndoiu, I.I. (2014). Bootstrap-based differential gene expression analysis for RNA-Seq data with and without replicates. BMC Genomics *15*, S2.

Andergassen, D., Dotter, C.P., Wenzel, D., Sigl, V., Bammer, P.C., Muckenhuber, M., Mayer, D., Kulinski, T.M., Theussl, H.-C., Penninger, J.M., et al. (2017). Mapping the mouse Allelome reveals tissue-specific regulation of allelic expression. ELife *6*, e25125.

Andrews, S. (2007). SeqMonk, a tool to visualise and analyse high throughput mapped sequence data. Available online: https://www.bioinformatics.babraham.ac.uk/projects/seqmonk/.

Andrews, S. (2010). FastQC: a quality control tool for high throughput sequence data. Available online at: http://www.bioinformatics.babraham.ac.uk/projects/fastqc.

Auclair, G., and Weber, M. (2012). Mechanisms of DNA methylation and demethylation in mammals. Biochimie *94*, 2202–2211.

Augui, S., Nora, E.P., and Heard, E. (2011). Regulation of X-chromosome inactivation by the X-inactivation centre. Nat. Rev. Genet. *12*, 429–442.

Avner, P., and Heard, E. (2001). X-chromosome inactivation: counting, choice and initiation. Nat. Rev. Genet. *2*, 59–67.

Babak, T., Deveale, B., Armour, C., Raymond, C., Cleary, M.A., van der Kooy, D., Johnson, J.M., and Lim, L.P. (2008). Global survey of genomic imprinting by transcriptome sequencing. Curr. Biol. CB *18*, 1735–1741.

Babak, T., DeVeale, B., Tsang, E.K., Zhou, Y., Li, X., Smith, K.S., Kukurba, K.R., Zhang, R., Li, J.B., van der Kooy, D., et al. (2015). Genetic conflict reflected in tissue-specific maps of genomic imprinting in human and mouse. Nat. Genet. *47*, 544–549.

Bakhtari, A., and P. J. Ross (2014). DPPA3 prevents cytosine hydroxymethylation of the maternal pronucleus and is required for normal development in bovine embryos. Epigenetics 1272–1279.

Balhorn, R., Brewer, L., and Corzett, M. (2000). DNA condensation by protamine and arginine-rich peptides: Analysis of toroid stability using single DNA molecules. Mol. Reprod. Dev. *56*, 230–234.

Bao, J., and Bedford, M.T. (2016). Epigenetic regulation of the histone-to-protamine transition during spermiogenesis. Reprod. Camb. Engl. *151*, R55–R70.

Baran, Y., Subramaniam, M., Biton, A., Tukiainen, T., Tsang, E.K., Rivas, M.A., Pirinen, M., Gutierrez-Arcelus, M., Smith, K.S., Kukurba, K.R., et al. (2015). The landscape of genomic imprinting across diverse adult human tissues. Genome Res. *25*, 927–936.

Barbaux, S., Gascoin-Lachambre, G., Buffat, C., Monnier, P., Mondon, F., Tonanny, M.-B., Pinard, A., Auer, J., Bessières, B., Barlier, A., et al. (2012). A genome-wide approach reveals novel imprinted genes expressed in the human placenta. Epigenetics *7*, 1079–1090.

Barlow, D.P., and Bartolomei, M.S. (2014). Genomic Imprinting in Mammals. Cold Spring Harb. Perspect. Biol. *6*, a018382.

Barry, J.S., and Anthony, R.V. (2008). The Pregnant Sheep as a Model for Human Pregnancy. Theriogenology *69*, 55–67.

Bartolomei, M.S., and Ferguson-Smith, A.C. (2011). Mammalian genomic imprinting. Cold Spring Harb. Perspect. Biol. *3*.

Beaujean, N., Hartshorne, G., Cavilla, J., Taylor, J., Gardner, J., Wilmut, I., Meehan, R., and Young, L. (2004). Non-conservation of mammalian preimplantation methylation dynamics. Curr. Biol. CB *14*, R266-267.

Begum, G., Stevens, A., Smith, E.B., Connor, K., Challis, J.R.G., Bloomfield, F., and White, A. (2012). Epigenetic changes in fetal hypothalamic energy regulating pathways are associated with maternal undernutrition and twinning. FASEB J. *26*, 1694–1703.

Belton, J.-M., McCord, R.P., Gibcus, J.H., Naumova, N., Zhan, Y., and Dekker, J. (2012). Hi-C: a comprehensive technique to capture the conformation of genomes. Methods San Diego Calif *58*, 268–276.

Berletch, J.B., Yang, F., Xu, J., Carrel, L., and Disteche, C.M. (2011). Genes that escape from X inactivation. Hum. Genet. *130*, 237–245.

Bermejo-Alvarez, P., Rizos, D., Lonergan, P., and Gutierrez-Adan, A. (2011). Transcriptional sexual dimorphism in elongating bovine embryos: implications for XCI and sex determination genes. Reproduction *141*, 801–808.

Bhutani, N., Burns, D.M., and Blau, H.M. (2011). DNA demethylation dynamics. Cell 866–872.

Bischoff, S.R., Tsai, S., Hardison, N., Motsinger-Reif, A.A., Freking, B.A., Nonneman, D., Rohrer, G., and Piedrahita, J.A. (2009). Characterization of conserved and nonconserved imprinted genes in swine. Biol. Reprod. *81*, 906–920.

Black, J.C., Van Rechem, C., and Whetstine, J.R. (2012). Histone Lysine Methylation Dynamics: Establishment, Regulation, and Biological Impact. Mol. Cell *48*.

Blake, A., Pickford, K., Greenaway, S., Thomas, S., Pickard, A., Williamson, C.M., Adams, N.C., Walling, A., Beck, T., Fray, M., et al. (2010). MouseBook: an integrated portal of mouse resources. Nucleic Acids Res. *38*, D593-599.

Bock, C., Tomazou, E.M., Brinkman, A.B., Müller, F., Simmer, F., Gu, H., Jäger, N., Gnirke, A., Stunnenberg, H.G., and Meissner, A. (2010). Quantitative comparison of genome-wide DNA methylation mapping technologies. Nat. Biotechnol. *28*, 1106–1114.

Bolger, A.M., Lohse, M., and Usadel, B. (2014). Trimmomatic: a flexible trimmer for Illumina sequence data. Bioinforma. Oxf. Engl. *30*, 2114–2120.

Bostick, M., Kim, J.K., Estève, P.-O., Clark, A., Pradhan, S., and Jacobsen, S.E. (2007). UHRF1 plays a role in maintaining DNA methylation in mammalian cells. Science *317*, 1760–1764.

Bridger, P.S., Haupt, S., Klisch, K., Leiser, R., Tinneberg, H.-R., and Pfarrer, C. (2007). Validation of primary epitheloid cell cultures isolated from bovine placental caruncles and cotyledons. Theriogenology *68*, 592–603.

Canovas, S., and Ross, P.J. (2016). Epigenetics in preimplantation mammalian development. Theriogenology *86*, 69–79.

Canovas, S., Ross, P.J., Kelsey, G., and Coy, P. (2017). DNA Methylation in Embryo Development: Epigenetic Impact of ART (Assisted Reproductive Technologies). BioEssays *39*.

Cao, J., Cusanovich, D.A., Ramani, V., Aghamirzaie, D., Pliner, H.A., Hill, A.J., Daza, R.M., McFaline-Figueroa, J.L., Packer, J.S., Christiansen, L., et al. (2018). Joint profiling of chromatin accessibility and gene expression in thousands of single cells. Science eaau0730.

Chandler Christopher H. (2017). When and why does sex chromosome dosage compensation evolve? Ann. N. Y. Acad. Sci. *1389*, 37–51.

Chédin, F. (2011). Chapter 7 - The DNMT3 Family of Mammalian De Novo DNA Methyltransferases. In Progress in Molecular Biology and Translational Science, X. Cheng, and R.M. Blumenthal, eds. (Academic Press), pp. 255–285.

Chen, Z., Hagen, D.E., Elsik, C.G., Ji, T., Morris, C.J., Moon, L.E., and Rivera, R.M. (2015). Characterization of global loss of imprinting in fetal overgrowth syndrome induced by assisted reproduction. Proc. Natl. Acad. Sci. U. S. A. *112*, 4618–4623.

Chen, Z., Hagen, D.E., Wang, J., Elsik, C.G., Ji, T., Siqueira, L.G., Hansen, P.J., and Rivera, R.M. (2016). Global assessment of imprinted gene expression in the bovine conceptus by next generation sequencing. Epigenetics *11*, 501–516.

Cheng, X., and Blumenthal, R.M. (2011). Chapter 1 - Introduction—Epiphanies in Epigenetics. In Progress in Molecular Biology and Translational Science, X. Cheng, and R.M. Blumenthal, eds. (Academic Press), pp. 1–21.

Choy, J.S., Wei, S., Lee, J.Y., Tan, S., Chu, S., and Lee, T.-H. (2010). DNA Methylation Increases Nucleosome Compaction and Rigidity. J. Am. Chem. Soc. *132*, 1782–1783.

Clayton, A.L., Hazzalin, C.A., and Mahadevan, L.C. (2006). Enhanced histone acetylation and transcription: a dynamic perspective. Mol. Cell *23*, 289–296.

Cooney, C.A., Dave, A.A., and Wolff, G.L. (2002). Maternal methyl supplements in mice affect epigenetic variation and DNA methylation of offspring. J. Nutr. *132*, 2393S-2400S.

Couldrey, C., Johnson, T., Lopdell, T., Zhang, I.L., Littlejohn, M.D., Keehan, M., Sherlock, R.G., Tiplady, K., Scott, A., Davis, S.R., et al. (2017). Bovine mammary gland X chromosome inactivation. J. Dairy Sci. *100*, 5491–5500.

Curradi, M., Izzo, A., Badaracco, G., and Landsberger, N. (2002). Molecular Mechanisms of Gene Silencing Mediated by DNA Methylation. Mol. Cell. Biol. *22*, 3157–3173.

Das, P.J., Chowdhary, B.P., and Raudsepp, T. (2009). Characterization of the Bovine Pseudoautosomal Region and Comparison with Sheep, Goat, and Other Mammalian Pseudoautosomal Regions. Cytogenet. Genome Res. *126*, 139–147.

De La Fuente, R., Hahnel, A., Basrur, P.K., and King, W.A. (1999). X inactive-specific transcript (Xist) expression and X chromosome inactivation in the preattachment bovine embryo. Biol. Reprod. *60*, 769–775.

De Majo, F., and Calore, M. (2018). Chromatin remodelling and epigenetic state regulation by non-coding RNAs in the diseased heart. Non-Coding RNA Res. *3*, 20–28.

De Paepe, C., Krivega, M., Cauffman, G., Geens, M., and Van de Velde, H. (2014). Totipotency and lineage segregation in the human embryo. MHR Basic Sci. Reprod. Med. *20*, 599–618.

Dean, W., Santos, F., Stojkovic, M., Zakhartchenko, V., Walter, J., Wolf, E., and Reik, W. (2001). Conservation of methylation reprogramming in mammalian development: aberrant reprogramming in cloned embryos. Proc. Natl. Acad. Sci. U. S. A. *98*, 13734–13738.

Dekker, J. (2006). The three "C" s of chromosome conformation capture: controls, controls, controls. Nat. Methods *3*, 17–21.

Delaval, K., and Feil, R. (2004). Epigenetic regulation of mammalian genomic imprinting. Curr. Opin. Genet. Dev. *14*, 188–195.

Demetriou, C., Abu-Amero, S., Thomas, A.C., Ishida, M., Aggarwal, R., Al-Olabi, L., Leon, L.J., Stafford, J.L., Syngelaki, A., Peebles, D., et al. (2014). Paternally Expressed, Imprinted Insulin-Like Growth Factor-2 in Chorionic Villi Correlates Significantly with Birth Weight. PLOS ONE *9*, e85454.

Deng, X., Hiatt, J.B., Nguyen, D.K., Ercan, S., Sturgill, D., Hillier, L.W., Schlesinger, F., Davis, C.A., Reinke, V.J., Gingeras, T.R., et al. (2011). Evidence for compensatory upregulation of expressed X-linked genes in mammals, Caenorhabditis elegans and Drosophila melanogaster. Nat. Genet. *43*, 1179–1185.

Denker, A., and Laat, W. de (2016). The second decade of 3C technologies: detailed insights into nuclear organization. Genes Dev. *30*, 1357–1382.

DeVeale, B., van der Kooy, D., and Babak, T. (2012). Critical evaluation of imprinted gene expression by RNA-Seq: a new perspective. PLoS Genet. *8*, e1002600.

Dobbs, K.B., Rodriguez, M., Sudano, M.J., Ortega, M.S., and Hansen, P.J. (2013). Dynamics of DNA Methylation during Early Development of the Preimplantation Bovine Embryo. PLoS ONE *8*.

Doherty, R., and Couldrey, C. (2014). Exploring genome wide bisulfite sequencing for DNA methylation analysis in livestock: a technical assessment. Front. Genet. *5*.

Doi, A., Park, I.-H., Wen, B., Murakami, P., Aryee, M.J., Irizarry, R., Herb, B., Ladd-Acosta, C., Rho, J., Loewer, S., et al. (2009). Differential methylation of tissue- and cancer-specific CpG island shores distinguishes human induced pluripotent stem cells, embryonic stem cells and fibroblasts. Nat. Genet. *41*, 1350–1353.

Dolinoy, D.C., Weidman, J.R., and Jirtle, R.L. (2007). Epigenetic gene regulation: Linking early developmental environment to adult disease. Reprod. Toxicol. *23*, 297–307.

Dominguez-Salas, P., Moore, S.E., Baker, M.S., Bergen, A.W., Cox, S.E., Dyer, R.A., Fulford, A.J., Guan, Y., Laritsky, E., Silver, M.J., et al. (2014). Maternal nutrition at conception modulates DNA methylation of human metastable epialleles. Nat. Commun. *5*, 3746.

Dostie, J., and Dekker, J. (2007). Mapping networks of physical interactions between genomic elements using 5C technology. Nat. Protoc. *2*, 988–1002.

Duitama, J., Srivastava, P.K., and Măndoiu, I.I. (2012). Towards accurate detection and genotyping of expressed variants from whole transcriptome sequencing data. BMC Genomics *13*, S6.

Efron, B., and Tibshirani, R.J. (1994). An Introduction to the Bootstrap (CRC Press).

Engel, N., and Bartolomei, M.S. (2003). Mechanisms of Insulator Function in Gene Regulation and Genomic Imprinting. In International Review of Cytology, (Academic Press), pp. 89–127.

Ercan, S. (2015). Mechanisms of X Chromosome Dosage Compensation. J. Genomics *3*, 1–19.

Erwin, J.A., and Lee, J.T. (2008). New twists in X-chromosome inactivation. Curr. Opin. Cell Biol. *20*, 349–355.

Fagerberg, L., Hallström, B.M., Oksvold, P., Kampf, C., Djureinovic, D., Odeberg, J., Habuka, M., Tahmasebpoor, S., Danielsson, A., Edlund, K., et al. (2014). Analysis of the human tissue-specific expression by genome-wide integration of transcriptomics and antibody-based proteomics. Mol. Cell. Proteomics MCP *13*, 397–406.

Fairbairn, D.J., Blanckenhorn, W.U., and Székely, T. (2007). Sex, Size and Gender Roles (Oxford University Press).

Ferreira, A.R., Machado, G.M., Diesel, T.O., Carvalho, J.O., Rumpf, R., Melo, E.O., Dode, M. a. N., and Franco, M.M. (2010). Allele-specific expression of the MAOA gene and X chromosome inactivation in in vitro produced bovine embryos. Mol. Reprod. Dev. *77*, 615–621.

Freking, B.A., Murphy, S.K., Wylie, A.A., Rhodes, S.J., Keele, J.W., Leymaster, K.A., Jirtle, R.L., and Smith, T.P.L. (2002). Identification of the single base change causing the callipyge muscle hypertrophy phenotype, the only known example of polar overdominance in mammals. Genome Res. *12*, 1496–1506.

Frost, J.M., and Moore, G.E. (2010). The importance of imprinting in the human placenta. PLoS Genet. *6*, e1001015.

Fukuda, A., Tanino, M., Matoba, R., Umezawa, A., and Akutsu, H. (2015). Imbalance between the expression dosages of X-chromosome and autosomal genes in mammalian oocytes. Sci. Rep. *5*, 14101.

Fullwood, M.J., Liu, M.H., Pan, Y.F., Liu, J., Xu, H., Mohamed, Y.B., Orlov, Y.L., Velkov, S., Ho, A., Mei, P.H., et al. (2009). An oestrogen-receptor-alpha-bound human chromatin interactome. Nature *462*, 58–64.

Funaya, S., and Aoki, F. (2017). Regulation of zygotic gene activation by chromatin structure and epigenetic factors. J. Reprod. Dev. *63*, 359–363.

Gao, F., Niu, Y., Sun, Y.E., Lu, H., Chen, Y., Li, S., Kang, Y., Luo, Y., Si, C., Yu, J., et al. (2017). De novo DNA methylation during monkey pre-implantation embryogenesis. Cell Res. *27*, 526–539.

Gene Ontology Consortium (2015). Gene Ontology Consortium: going forward. Nucleic Acids Res. *43*, D1049–D1056.

Gevers, D., Vandepoele, K., Simillon, C., and Van de Peer, Y. (2004). Gene duplication and biased functional retention of paralogs in bacterial genomes. Trends Microbiol. *12*, 148–154.

Godfrey, K.M., and Barker, D.J. (2001). Fetal programming and adult health. Public Health Nutr. *4*, 611–624.

Goldberg, A.D., Allis, C.D., and Bernstein, E. (2007). Epigenetics: a landscape takes shape. Cell *128*, 635–638.

Gordon, D.J., Resio, B., and Pellman, D. (2012). Causes and consequences of aneuploidy in cancer. Nat. Rev. Genet. *13*, 189–203.

Goto, T., and Monk, M. (1998). Regulation of X-Chromosome Inactivation in Development in Mice and Humans. Microbiol. Mol. Biol. Rev. *62*, 362–378.

Goyal, R., Reinhardt, R., and Jeltsch, A. (2006). Accuracy of DNA methylation pattern preservation by the Dnmt1 methyltransferase. Nucleic Acids Res. *34*, 1182–1188.

Graf, A., Krebs, S., Zakhartchenko, V., Schwalb, B., Blum, H., and Wolf, E. (2014). Fine mapping of genome activation in bovine embryos by RNA sequencing. Proc. Natl. Acad. Sci. U. S. A. *111*, 4139–4144.

Graves, J.A.M., and Disteche, C.M. (2007). Does gene dosage really matter? J. Biol. *6*, 1.

Gregg, C., Zhang, J., Weissbourd, B., Luo, S., Schroth, G.P., Haig, D., and Dulac, C. (2010a). High-resolution analysis of parent-of-origin allelic expression in the mouse brain. Science *329*, 643–648.

Gregg, C., Zhang, J., Butler, J.E., Haig, D., and Dulac, C. (2010b). Sex-specific parent-of-origin allelic expression in the mouse brain. Science *329*, 682–685.

Gu, T.-P., Guo, F., Yang, H., Wu, H.-P., Xu, G.-F., Liu, W., Xie, Z.-G., Shi, L., He, X., Jin, S., et al. (2011). The role of Tet3 DNA dioxygenase in epigenetic reprogramming by oocytes. Nature *477*, 606–610.

Guo, H., Zhu, P., Yan, L., Li, R., Hu, B., Lian, Y., Yan, J., Ren, X., Lin, S., Li, J., et al. (2014). The DNA methylation landscape of human early embryos. Nature *511*, 606–610.

Guo, Y., Su, Z.-Y., and Kong, A.-N.T. (2015). Current Perspectives on Epigenetic Modifications by Dietary Chemopreventive and Herbal Phytochemicals. Curr. Pharmacol. Rep. *1*, 245–257.

Gupta, V., Parisi, M., Sturgill, D., Nuttall, R., Doctolero, M., Dudko, O.K., Malley, J.D., Eastman, P.S., and Oliver, B. (2006). Global analysis of X-chromosome dosage compensation. J. Biol. *5*, 3.

Gutiérrez-Aguirre, I., Rački, N., Dreo, T., and Ravnikar, M. (2015). Droplet digital PCR for absolute quantification of pathogens. Methods Mol. Biol. Clifton NJ *1302*, 331–347.

Hackett, J.A., and Surani, M.A. (2013). DNA methylation dynamics during the mammalian life cycle. Philos. Trans. R. Soc. B Biol. Sci. *368*.

Haig, D. (1992). Genomic imprinting and the theory of parent-offspring conflict. Semin Dev Biol *3*, 153–160.

Haig, D., and Graham, C. (1991). Genomic imprinting and the strange case of the insulin-like growth factor II receptor. Cell *64*, 1045–1046.

Handy, D.E., Castro, R., and Loscalzo, J. (2011). Epigenetic Modifications: Basic Mechanisms and Role in Cardiovascular Disease. Circulation *123*, 2145–2156.

Hanna, C.W., and Kelsey, G. (2014). The specification of imprints in mammals. Heredity *113*, 176–183.

Hanna, C.W., Demond, H., and Kelsey, G. (2018). Epigenetic regulation in development: is the mouse a good model for the human? Hum. Reprod. Update *24*, 556–576.

Hansmann, T., Heinzmann, J., Wrenzycki, C., Zechner, U., Niemann, H., and Haaf, T. (2011). Characterization of differentially methylated regions in 3 bovine imprinted genes: a model for studying human germ-cell and embryo development. Cytogenet. Genome Res. *132*, 239–247.

Hassold, T., and Hunt, P. (2001). To err (meiotically) is human: the genesis of human aneuploidy. Nat. Rev. Genet. *2*, 280–291.

Hassold, T., Chen, N., Funkhouser, J., Jooss, T., Manuel, B., Matsuura, J., Matsuyama, A., Wilson, C., Yamane, J.A., and Jacobs, P.A. (1980). A cytogenetic study of 1000 spontaneous abortions. Ann. Hum. Genet. *44*, 151–178.

Hata, K., Okano, M., Lei, H., and Li, E. (2002). Dnmt3L cooperates with the Dnmt3 family of de novo DNA methyltransferases to establish maternal imprints in mice. Development *129*, 1983–1993.

Hayakawa, H., Hirai, T., Takimoto, A., Ideta, A., and Aoyagi, Y. (2009). Superovulation and embryo transfer in Holstein cattle using sexed sperm. Theriogenology *71*, 68–73.

Hayashi, K., Lopes, S.M.C. de S., and Surani, M.A. (2007). Germ Cell Specification in Mice. Science *316*, 394–396.

He, X., and Zhang, J. (2016). X-Chromosome Dosage Compensation. ELS.

He, X., Chen, X., Xiong, Y., Chen, Z., Wang, X., Shi, S., Wang, X., and Zhang, J. (2011). He *et al*. reply. Nat. Genet. *43*, 1171–1172.

Heard, E., Clerc, P., and Avner, P. (1997). X-chromosome inactivation in mammals. Annu. Rev. Genet. *31*, 571–610.

Helena Mangs, A., and Morris, B.J. (2007). The Human Pseudoautosomal Region (PAR): Origin, Function and Future. Curr. Genomics *8*, 129–136.

Hoffman, M.L., Reed, S.A., Pillai, S.M., Jones, A.K., McFadden, K.K., Zinn, S.A., and Govoni, K.E. (2017). PHYSIOLOGY AND ENDOCRINOLOGY SYMPOSIUM:The effects of poor maternal nutrition during gestation on offspring postnatal growth and metabolism. J. Anim. Sci. *95*, 2222–2232.

Holtzman, D.M., Bayney, R.M., Li, Y.W., Khosrovi, H., Berger, C.N., Epstein, C.J., and Mobley, W.C. (1992). Dysregulation of gene expression in mouse trisomy 16, an animal model of Down syndrome. EMBO J. *11*, 619–627.

Hong, E.E., Okitsu, C.Y., Smith, A.D., and Hsieh, C.-L. (2013). Regionally Specific and Genome-Wide Analyses Conclusively Demonstrate the Absence of CpG Methylation in Human Mitochondrial DNA. Mol. Cell. Biol. *33*, 2683–2690.

Huang, D.W., Sherman, B.T., and Lempicki, R.A. (2009a). Bioinformatics enrichment tools: paths toward the comprehensive functional analysis of large gene lists. Nucleic Acids Res. *37*, 1–13.

Huang, D.W., Sherman, B.T., and Lempicki, R.A. (2009b). Systematic and integrative analysis of large gene lists using DAVID bioinformatics resources. Nat. Protoc. *4*, 44–57.

Huang, S., Chang, I.S., Lin, W., Ye, W., Luo, R.Z., Lu, Z., Lu, Y., Zhang, K., Liao, W.S.-L., Tao, T., et al. (2009c). ARHI (DIRAS3), an imprinted tumour suppressor gene, binds to importins and blocks nuclear import of cargo proteins. Biosci. Rep. *30*, 159–168.

Huang, Y., Chavez, L., Chang, X., Wang, X., Pastor, W.A., Kang, J., Zepeda-Martínez, J.A., Pape, U.J., Jacobsen, S.E., Peters, B., et al. (2014). Distinct roles of the methylcytosine oxidases Tet1 and Tet2 in mouse embryonic stem cells. Proc. Natl. Acad. Sci. U. S. A. *111*, 1361–1366.

Hurles, M.E., Dermitzakis, E.T., and Tyler-Smith, C. (2008). The functional impact of structural variation in humans. Trends Genet. TIG *24*, 238–245.

Huynh, K.D., and Lee, J.T. (2003). Inheritance of a pre-inactivated paternal X chromosome in early mouse embryos. Nature *426*, 857–862.

Hyun, K., Jeon, J., Park, K., and Kim, J. (2017). Writing, erasing and reading histone lysine methylations. Exp. Mol. Med. *49*, e324.

Iqbal, K., Jin, S.-G., Pfeifer, G.P., and Szabó, P.E. (2011). Reprogramming of the paternal genome upon fertilization involves genome-wide oxidation of 5-methylcytosine. Proc. Natl. Acad. Sci. *108*, 3642–3647.

Ishida, M., and Moore, G.E. (2013). The role of imprinted genes in humans. Mol. Aspects Med. *34*, 826–840.

Ito, S., Shen, L., Dai, Q., Wu, S.C., Collins, L.B., Swenberg, J.A., He, C., and Zhang, Y. (2011). Tet Proteins Can Convert 5-Methylcytosine to 5-Formylcytosine and 5-Carboxylcytosine. Science *333*, 1300–1303.

Iwasa, Y., and Pomiankowski, A. (2001). The evolution of X-linked genomic imprinting. Genetics *158*, 1801–1809.

Jansson, M.D., and Lund, A.H. (2012). MicroRNA and cancer. Mol. Oncol. *6*, 590–610.

Jennings, L.J., Arcila, M.E., Corless, C., Kamel-Reid, S., Lubin, I.M., Pfeifer, J., Temple-Smolkin, R.L., Voelkerding, K.V., and Nikiforova, M.N. (2017). Guidelines for Validation of Next-Generation Sequencing–Based Oncology Panels: A Joint Consensus Recommendation of the Association for Molecular Pathology and College of American Pathologists. J. Mol. Diagn. *19*, 341–365.

Jeon, Y., Sarma, K., and Lee, J.T. (2012). New and Xisting Regulatory Mechanisms of X Chromosome Inactivation. Curr. Opin. Genet. Dev. *22*, 62–71.

Jia, C.-W., Wang, L., Lan, Y.-L., Song, R., Zhou, L.-Y., Yu, L., Yang, Y., Liang, Y., Li, Y., Ma, Y.-M., et al. (2015). Aneuploidy in Early Miscarriage and its Related Factors. Chin. Med. J. (Engl.) *128*, 2772–2776.

Jiang, C., and Yang, Z. (2009). Characterization, Imprinting Status and Tissue Distribution of Porcine GTL2 Gene. Agric. Sci. China *8*, 216–222.

Jiang, Z., Sun, J., Dong, H., Luo, O., Zheng, X., Obergfell, C., Tang, Y., Bi, J., O'Neill, R., Ruan, Y., et al. (2014). Transcriptional profiles of bovine in vivo pre-implantation development. BMC Genomics *15*, 756.

Jiang, Z., Lin, J., Dong, H., Zheng, X., Marjani, S.L., Duan, J., Ouyang, Z., Chen, J., and Tian, X. (Cindy) (2018). DNA methylomes of bovine gametes and in vivo produced preimplantation embryos. Biol. Reprod.

Johnson, M.H., and Ziomek, C.A. (1981). Induction of polarity in mouse 8-cell blastomeres: specificity, geometry, and stability. J. Cell Biol. *91*, 303–308.

Jones, A.K., Gately, R.E., McFadden, K.K., Zinn, S.A., Govoni, K.E., and Reed, S.A. (2016). Transabdominal ultrasound for detection of pregnancy, fetal and placental landmarks, and fetal age before Day 45 of gestation in the sheep. Theriogenology *85*, 939-945.e1.

Jue, N.K., Murphy, M.B., Kasowitz, S.D., Qureshi, S.M., Obergfell, C.J., Elsisi, S., Foley, R.J., O'Neill, R.J., and O'Neill, M.J. (2013). Determination of dosage compensation of the mammalian X chromosome by RNA-seq is dependent on analytical approach. BMC Genomics *14*, 150.

Ka, S., Ahn, H., Seo, M., Kim, H., Kim, J.N., and Lee, H.-J. (2016). Status of dosage compensation of X chromosome in bovine genome. Genetica *144*, 435–444.

Kaikkonen, M.U., Lam, M.T.Y., and Glass, C.K. (2011). Non-coding RNAs as regulators of gene expression and epigenetics. Cardiovasc. Res. *90*, 430–440.

Kainz, B., Shehata, M., Bilban, M., Kienle, D., Heintel, D., Krömer-Holzinger, E., Le, T., Kröber, A., Heller, G., Schwarzinger, I., et al. (2007). Overexpression of the paternally expressed gene 10 (PEG10) from the imprinted locus on chromosome 7q21 in high-risk B-cell chronic lymphocytic leukemia. Int. J. Cancer *121*, 1984–1993.

Kalantry, S., Purushothaman, S., Bowen, R.B., Starmer, J., and Magnuson, T. (2009). Evidence of *Xist* RNA-independent initiation of mouse imprinted X-chromosome inactivation. Nature *460*, 647–651.

Kharchenko, P.V., Xi, R., and Park, P.J. (2011). Evidence for dosage compensation between the X chromosome and autosomes in mammals. Nat. Genet. *43*, 1167–1169.

Khatib, H. (2005). The COPG2, DCN, and SDHD genes are biallelically expressed in cattle. Mamm. Genome Off. J. Int. Mamm. Genome Soc. *16*, 545–552.

Kim, D., Langmead, B., and Salzberg, S.L. (2015). HISAT: a fast spliced aligner with low memory requirements. Nat. Methods *12*, 357–360.

Kim, J., Bergmann, A., Choo, J.H., and Stubbs, L. (2007). Genomic organization and imprinting of the Peg3 domain in bovine. Genomics *90*, 85–92.

Ko, Y.-G., Yun, J., Park, H.J., Tanaka, S., Shiota, K., and Cho, J.-H. (2013). Dynamic methylation pattern of the methyltransferase1o (Dnmt1o) 5'-flanking region during mouse oogenesis and spermatogenesis. Mol. Reprod. Dev. *80*, 212–222.

Kobayashi, H., Sakurai, T., Imai, M., Takahashi, N., Fukuda, A., Yayoi, O., Sato, S., Nakabayashi, K., Hata, K., Sotomaru, Y., et al. (2012). Contribution of Intragenic DNA Methylation in Mouse Gametic DNA Methylomes to Establish Oocyte-Specific Heritable Marks. PLOS Genet. *8*, e1002440.

Koerner, M.V., Pauler, F.M., Huang, R., and Barlow, D.P. (2009). The function of non-coding RNAs in genomic imprinting. Dev. Camb. Engl. *136*, 1771–1783.

Kohli, R.M., and Zhang, Y. (2013). TET enzymes, TDG and the dynamics of DNA demethylation. Nature *502*, 472–479.

Kono, T., Obata, Y., Yoshimzu, T., Nakahara, T., and Carroll, J. (1996). Epigenetic modifications during oocyte growth correlates with extended parthenogenetic development in the mouse. Nat. Genet. *13*, 91–94.

Krueger, F. (2017). Trim Galore: a wrapper script to automate quality and adapter trimming as well as quality control. Available online at: https://www.bioinformatics.babraham.ac.uk/projects/trim_galore/.

Krueger, F., and Andrews, S.R. (2011). Bismark: a flexible aligner and methylation caller for Bisulfite-Seq applications. Bioinforma. Oxf. Engl. *27*, 1571–1572.

Kues, W.A., Sudheer, S., Herrmann, D., Carnwath, J.W., Havlicek, V., Besenfelder, U., Lehrach, H., Adjaye, J., and Niemann, H. (2008). Genome-wide expression profiling reveals distinct clusters of transcriptional regulation during bovine preimplantation development in vivo. Proc. Natl. Acad. Sci. U. S. A. *105*, 19768–19773.

Lan, X., Cretney, E.C., Kropp, J., Khateeb, K., Berg, M.A., Peñagaricano, F., Magness, R., Radunz, A.E., and Khatib, H. (2013). Maternal Diet during Pregnancy Induces Gene Expression and DNA Methylation Changes in Fetal Tissues in Sheep. Front. Genet. *4*, 49.

Lee, J.T. (2003). Molecular Links between X-Inactivation and Autosomal Imprinting: X-Inactivation as a Driving Force for the Evolution of Imprinting? Curr. Biol. *13*, R242–R254.

Lee, J.T. (2009). Lessons from X-chromosome inactivation: long ncRNA as guides and tethers to the epigenome. Genes Dev. *23*, 1831–1842.

Lee, J.T., and Lu, N. (1999). Targeted Mutagenesis of Tsix Leads to Nonrandom X Inactivation. Cell *99*, 47–57.

Lee, M.T., Bonneau, A.R., and Giraldez, A.J. (2014). Zygotic genome activation during the maternal-to-zygotic transition. Annu. Rev. Cell Dev. Biol. *30*, 581–613.

Lee, Y.J., Park, C.W., Hahn, Y., Park, J., Lee, J., Yun, J.H., Hyun, B., and Chung, J.H. (2000). Mit1/Lb9 and Copg2, new members of mouse imprinted genes closely linked to Peg1/Mest(1). FEBS Lett. *472*, 230–234.

Leitch, H.G., Tang, W.W.C., and Surani, M.A. (2013). Chapter Five - Primordial Germ-Cell Development and Epigenetic Reprogramming in Mammals. In Current Topics in Developmental Biology, E. Heard, ed. (Academic Press), pp. 149–187.

Lepikhov, K., Zakhartchenko, V., Hao, R., Yang, F., Wrenzycki, C., Niemann, H., Wolf, E., and Walter, J. (2008). Evidence for conserved DNA and histone H3 methylation reprogramming in mouse, bovine and rabbit zygotes. Epigenetics Chromatin *1*, 8.

Lesch, B.J., Silber, S.J., McCarrey, J.R., and Page, D.C. (2016). Parallel evolution of male germline epigenetic poising and somatic development in animals. Nat. Genet. *48*, 888–894.

Lewis, A., Green, K., Dawson, C., Redrup, L., Huynh, K.D., Lee, J.T., Hemberger, M., and Reik, W. (2006). Epigenetic dynamics of the Kcnq1 imprinted domain in the early embryo. Dev. Camb. Engl. *133*, 4203–4210.

Lewis, R.M., Cleal, J.K., Ntani, G., Crozier, S.R., Mahon, P.A., Robinson, S.M., Harvey, N.C., Cooper, C., Inskip, H.M., Godfrey, K.M., et al. (2012). Relationship between placental expression of the imprinted PHLDA2 gene, intrauterine skeletal growth and childhood bone mass. Bone *50*, 337–342.

Li, H. (2011). A statistical framework for SNP calling, mutation discovery, association mapping and population genetical parameter estimation from sequencing data. Bioinforma. Oxf. Engl. *27*, 2987–2993.

Li, R., and Albertini, D.F. (2013). The road to maturation: somatic cell interaction and self-organization of the mammalian oocyte. Nat. Rev. Mol. Cell Biol. *14*, 141–152.

Li, E., Bestor, T.H., and Jaenisch, R. (1992). Targeted mutation of the DNA methyltransferase gene results in embryonic lethality. Cell *69*, 915–926.

Li, E., Beard, C., and Jaenisch, R. (1993). Role for DNA methylation in genomic imprinting. Nature *366*, 362–365.

Li, L., Zheng, P., and Dean, J. (2010a). Maternal control of early mouse development. Dev. Camb. Engl. *137*, 859–870.

Li, N., Ye, M., Li, Y., Yan, Z., Butcher, L.M., Sun, J., Han, X., Chen, Q., Zhang, X., and Wang, J. (2010b). Whole genome DNA methylation analysis based on high throughput sequencing technology. Methods San Diego Calif *52*, 203–212.

Li, Y., Zhu, J., Tian, G., Li, N., Li, Q., Ye, M., Zheng, H., Yu, J., Wu, H., Sun, J., et al. (2010c). The DNA methylome of human peripheral blood mononuclear cells. PLoS Biol. *8*, e1000533.

Liao, J., Karnik, R., Gu, H., Ziller, M.J., Clement, K., Tsankov, A.M., Akopian, V., Gifford, C.A., Donaghey, J., Galonska, C., et al. (2015). Targeted disruption of DNMT1, DNMT3A and DNMT3B in human embryonic stem cells. Nat. Genet. *47*, 469–478.

Lin, F., Xing, K., Zhang, J., and He, X. (2012). Expression reduction in mammalian X chromosome evolution refutes Ohno's hypothesis of dosage compensation. Proc. Natl. Acad. Sci. U. S. A. *109*, 11752–11757.

Lister, R., Pelizzola, M., Dowen, R.H., Hawkins, R.D., Hon, G., Tonti-Filippini, J., Nery, J.R., Lee, L., Ye, Z., Ngo, Q.-M., et al. (2009). Human DNA methylomes at base resolution show widespread epigenomic differences. Nature *462*, 315–322.

Liu, B., Du, Q., Chen, L., Fu, G., Li, S., Fu, L., Zhang, X., Ma, C., and Bin, C. (2016). CpG methylation patterns of human mitochondrial DNA. Sci. Rep. *6*, 23421.

Luedi, P.P., Dietrich, F.S., Weidman, J.R., Bosko, J.M., Jirtle, R.L., and Hartemink, A.J. (2007). Computational and experimental identification of novel human imprinted genes. Genome Res. *17*, 1723–1730.

Lyon, M.F. (1961). Gene Action in the X-chromosome of the Mouse (Mus musculus L.). Nature *190*, 372–373.

Lyon, M.F. (1993). Epigenetic inheritance in mammals. Trends Genet. *9*, 123–128.

Maher, E.R., Afnan, M., and Barratt, C.L. (2003). Epigenetic risks related to assisted reproductive technologies: epigenetics, imprinting, ART and icebergs? Hum. Reprod. Oxf. Engl. *18*, 2508–2511.

Mamo, S., Rizos, D., and Lonergan, P. (2012). Transcriptomic changes in the bovine conceptus between the blastocyst stage and initiation of implantation. Anim. Reprod. Sci. *134*, 56–63.

Marikawa, Y., and Alarcón, V.B. (2009). Establishment of trophectoderm and inner cell mass lineages in the mouse embryo. Mol. Reprod. Dev. *76*, 1019–1032.

Meaburn, E., and Schulz, R. (2012). Next generation sequencing in epigenetics: insights and challenges. Semin. Cell Dev. Biol. *23*, 192–199.

Mehlmann, L.M. (2005). Stops and starts in mammalian oocytes: recent advances in understanding the regulation of meiotic arrest and oocyte maturation. Reprod. Camb. Engl. *130*, 791–799.

Memili, E., and First, N.L. (2000). Zygotic and embryonic gene expression in cow: a review of timing and mechanisms of early gene expression as compared with other species. Zygote Camb. Engl. *8*, 87–96.

Messerschmidt, D.M., Knowles, B.B., and Solter, D. (2014). DNA methylation dynamics during epigenetic reprogramming in the germline and preimplantation embryos. Genes Dev. *28*, 812–828.

Misirlioglu, M., Page, G.P., Sagirkaya, H., Kaya, A., Parrish, J.J., First, N.L., and Memili, E. (2006). Dynamics of global transcriptome in bovine matured oocytes and preimplantation embryos. Proc. Natl. Acad. Sci. *103*, 18905–18910.

Monk, D., Wagschal, A., Arnaud, P., Müller, P.-S., Parker-Katiraee, L., Bourc'his, D., Scherer, S.W., Feil, R., Stanier, P., and Moore, G.E. (2008). Comparative analysis of human chromosome 7q21 and mouse proximal chromosome 6 reveals a placental-specific imprinted gene, TFPI2/Tfpi2, which requires EHMT2 and EED for allelic-silencing. Genome Res. *18*, 1270–1281.

Moore, T., and Haig, D. (1991). Genomic imprinting in mammalian development: a parental tug-of-war. Trends Genet. TIG *7*, 45–49.

Moore, L.D., Le, T., and Fan, G. (2013). DNA Methylation and Its Basic Function. Neuropsychopharmacology *38*, 23–38.

Moore, S.G., Pryce, J.E., Hayes, B.J., Chamberlain, A.J., Kemper, K.E., Berry, D.P., McCabe, M., Cormican, P., Lonergan, P., Fair, T., et al. (2016). Differentially Expressed Genes in Endometrium and Corpus Luteum of Holstein Cows Selected for High and Low Fertility Are Enriched for Sequence Variants Associated with Fertility. Biol. Reprod. *94*.

Morales, V., and Richard-Foy, H. (2000). Role of Histone N-Terminal Tails and Their Acetylation in Nucleosome Dynamics. Mol. Cell. Biol. *20*, 7230–7237.

Morison, I.M., Paton, C.J., and Cleverley, S.D. (2001). The imprinted gene and parent-of-origin effect database. Nucleic Acids Res. *29*, 275–276.

Morison, I.M., Ramsay, J.P., and Spencer, H.G. (2005). A census of mammalian imprinting. Trends Genet. *21*, 457–465.

Nakabayashi, K., Makino, S., Minagawa, S., Smith, A., Bamforth, J., Stanier, P., Preece, M., Parker-Katiraee, L., Paton, T., Oshimura, M., et al. (2004). Genomic imprinting of PPP1R9A encoding neurabin I in skeletal muscle and extra-embryonic tissues. J. Med. Genet. *41*, 601–608.

Naumann, A., Hochstein, N., Weber, S., Fanning, E., and Doerfler, W. (2009). A Distinct DNA-Methylation Boundary in the 5′- Upstream Sequence of the FMR1 Promoter Binds Nuclear Proteins and Is Lost in Fragile X Syndrome. Am. J. Hum. Genet. *85*, 606–616.

Nguyen, D.K., and Disteche, C.M. (2006). Dosage compensation of the active X chromosome in mammals. Nat. Genet. *38*, 47–53.

Niakan, K.K., Han, J., Pedersen, R.A., Simon, C., and Pera, R.A.R. (2012). Human pre-implantation embryo development. Dev. Camb. Engl. *139*, 829–841.

Nicolae, M., Mangul, S., Măndoiu, I.I., and Zelikovsky, A. (2011a). Estimation of alternative splicing isoform frequencies from RNA-Seq data. Algorithms Mol. Biol. AMB *6*, 9.

Nicolae, M., Mangul, S., Măndoiu, I.I., and Zelikovsky, A. (2011b). Estimation of alternative splicing isoform frequencies from RNA-Seq data. Algorithms Mol. Biol. AMB *6*, 9.

O'Doherty, A.M., MacHugh, D.E., Spillane, C., and Magee, D.A. (2015a). Genomic imprinting effects on complex traits in domesticated animal species. Front. Genet. *6*, 156.

O'Doherty, A.M., Magee, D.A., O'Shea, L.C., Forde, N., Beltman, M.E., Mamo, S., and Fair, T. (2015b). DNA methylation dynamics at imprinted genes during bovine pre-implantation embryo development. BMC Dev. Biol. *15*, 13.

O'Geen, H., Echipare, L., and Farnham, P.J. (2011). Using ChIP-Seq Technology to Generate High-Resolution Profiles of Histone Modifications. Methods Mol. Biol. Clifton NJ *791*, 265–286.

Ohhata, T., and Wutz, A. (2013). Reactivation of the inactive X chromosome in development and reprogramming. Cell. Mol. Life Sci. CMLS *70*, 2443–2461.

Ohlsson, R., Paldi, A., and Graves, J.A.M. (2001). Did genomic imprinting and X chromosome inactivation arise from stochastic expression? Trends Genet. *17*, 136–141.

Ohno, S. (1966). Sex Chromosomes and Sex-Linked Genes (Berlin Heidelberg: Springer-Verlag).

Ohno, S., Kaplan, W.D., and Kinosita, R. (1959). Formation of the sex chromatin by a single X-chromosome in liver cells of Rattus norvegicus. Exp. Cell Res. *18*, 415–418.

Okamoto, I., and Heard, E. (2006). The dynamics of imprinted X inactivation during preimplantation development in mice. Cytogenet. Genome Res. *113*, 318–324.

Okamoto, I., Patrat, C., Thépot, D., Peynot, N., Fauque, P., Daniel, N., Diabangouaya, P., Wolf, J.-P., Renard, J.-P., Duranthon, V., et al. (2011). Eutherian mammals use diverse strategies to initiate X-chromosome inactivation during development. Nature *472*, 370–374.

O'Neill, C. (2015). The epigenetics of embryo development. Anim. Front. *5*, 42–49.

Ono, R., Shiura, H., Aburatani, H., Kohda, T., Kaneko-Ishino, T., and Ishino, F. (2003). Identification of a large novel imprinted gene cluster on mouse proximal chromosome 6. Genome Res. *13*, 1696–1705.

Oswald, J., Engemann, S., Lane, N., Mayer, W., Olek, A., Fundele, R., Dean, W., Reik, W., and Walter, J. (2000). Active demethylation of the paternal genome in the mouse zygote. Curr. Biol. *10*, 475–478.

Otto, S.P., and Gerstein, A.C. (2008). The evolution of haploidy and diploidy. Curr. Biol. *18*, R1121–R1124.

Papin, C., Ibrahim, A., Gras, S.L., Velt, A., Stoll, I., Jost, B., Menoni, H., Bronner, C., Dimitrov, S., and Hamiche, A. (2017). Combinatorial DNA methylation codes at repetitive elements. Genome Res. *27*, 934–946.

Park, J.I., Hong, J.Y., Yong, H.Y., Hwang, W.S., Lim, J.M., and Lee, E.S. (2005). High oxygen tension during in vitro oocyte maturation improves in vitro development of porcine oocytes after fertilization. Anim. Reprod. Sci. *87*, 133–141.

Park, J.S., Jeong Young Sun, Shin Sang Tae, Lee Kyung-Kwang, and Kang Yong-Kook (2007). Dynamic DNA methylation reprogramming: Active demethylation and immediate remethylation in the male pronucleus of bovine zygotes. Dev. Dyn. *236*, 2523–2533.

Pauler, F.M., Koerner, M.V., and Barlow, D.P. (2007). Silencing by imprinted noncoding RNAs: is transcription the answer? Trends Genet. *23*, 284–292.

Payer, B., and Lee, J.T. (2008). X Chromosome Dosage Compensation: How Mammals Keep the Balance. Annu. Rev. Genet. *42*, 733–772.

Payer, B., Lee, J.T., and Namekawa, S.H. (2011). X-inactivation and X-reactivation: epigenetic hallmarks of mammalian reproduction and pluripotent stem cells. Hum. Genet. *130*, 265–280.

Peñagaricano, F., Wang, X., Rosa, G.J., Radunz, A.E., and Khatib, H. (2014). Maternal nutrition induces gene expression changes in fetal muscle and adipose tissues in sheep. BMC Genomics *15*, 1034.

Perrier, J.-P., Sellem, E., Prézelin, A., Gasselin, M., Jouneau, L., Piumi, F., Al Adhami, H., Weber, M., Fritz, S., Boichard, D., et al. (2018). A multi-scale analysis of bull sperm methylome revealed both species peculiarities and conserved tissue-specific features. BMC Genomics *19*.

Pertea, M., Kim, D., Pertea, G.M., Leek, J.T., and Salzberg, S.L. (2016). Transcript-level expression analysis of RNA-seq experiments with HISAT, StringTie and Ballgown. Nat. Protoc. *11*, 1650–1667.

Pervjakova, N., Kasela, S., Morris, A.P., Kals, M., Metspalu, A., Lindgren, C.M., Salumets, A., and Mägi, R. (2016). Imprinted genes and imprinting control regions show predominant intermediate methylation in adult somatic tissues. Epigenomics *8*, 789–799.

Pessia, E., Makino, T., Bailly-Bechet, M., McLysaght, A., and Marais, G.A.B. (2012). Mammalian X chromosome inactivation evolved as a dosage-compensation mechanism for dosage-sensitive genes on the X chromosome. Proc. Natl. Acad. Sci. U. S. A. *109*, 5346–5351.

Pessia, E., Engelstädter, J., and Marais, G.A.B. (2014). The evolution of X chromosome inactivation in mammals: the demise of Ohno's hypothesis? Cell. Mol. Life Sci. CMLS *71*, 1383–1394.

Pfeifer, K. (2000). Mechanisms of Genomic Imprinting. Am. J. Hum. Genet. *67*, 777–787.

Piedrahita, J.A. (2011). The role of imprinted genes in fetal growth abnormalities. Birt. Defects Res. A. Clin. Mol. Teratol. *91*, 682–692.

Pillai, S.M., Sereda, N.H., Hoffman, M.L., Valley, E.V., Crenshaw, T.D., Park, Y.-K., Lee, J.-Y., Zinn, S.A., and Govoni, K.E. (2016). Effects of Poor Maternal Nutrition during Gestation on Bone Development and Mesenchymal Stem Cell Activity in Offspring. PloS One *11*, e0168382.

Pillai, S.M., Jones, A.K., Hoffman, M.L., McFadden, K.K., Reed, S.A., Zinn, S.A., and Govoni, K.E. (2017). Fetal and organ development at gestational days 45, 90, 135 and at birth of lambs exposed to under- or over-nutrition during gestation,,. Transl. Anim. Sci. *1*, 16–25.

Piskol, R., Ramaswami, G., and Li, J.B. (2013). Reliable identification of genomic variants from RNA-seq data. Am. J. Hum. Genet. *93*, 641–651.

Plasschaert, R.N., and Bartolomei, M.S. (2014). Genomic imprinting in development, growth, behavior and stem cells. Dev. Camb. Engl. *141*, 1805–1813.

Prothero, K.E., Stahl, J.M., and Carrel, L. (2009). Dosage compensation and gene expression on the mammalian X chromosome: one plus one does not always equal two. Chromosome Res. Int. J. Mol. Supramol. Evol. Asp. Chromosome Biol. *17*, 637–648.

Quinlan, A.R., and Hall, I.M. (2010). BEDTools: a flexible suite of utilities for comparing genomic features. Bioinforma. Oxf. Engl. *26*, 841–842.

Rakyan, V.K., Chong, S., Champ, M.E., Cuthbert, P.C., Morgan, H.D., Luu, K.V.K., and Whitelaw, E. (2003). Transgenerational inheritance of epigenetic states at the murine AxinFu allele occurs after maternal and paternal transmission. Proc. Natl. Acad. Sci. *100*, 2538–2543.

Raudsepp, T., and Chowdhary, B.P. (2015). The Eutherian Pseudoautosomal Region. Cytogenet. Genome Res. *147*, 81–94.

Reed, S.A., Raja, J.S., Hoffman, M.L., Zinn, S.A., and Govoni, K.E. (2014). Poor maternal nutrition inhibits muscle development in ovine offspring. J. Anim. Sci. Biotechnol. *5*, 43.

Reik, W. (2007). Stability and flexibility of epigenetic gene regulation in mammalian development. Nature *447*, 425–432.

Reik, W., Constancia, M., Dean, W., Davies, K., Bowden, L., Murrell, A., Feil, R., Walter, J., and Kelsey, G. (2000). Igf2 imprinting in development and disease. Int. J. Dev. Biol. *44*, 145–150.

Reik, W., Dean, W., and Walter, J. (2001). Epigenetic reprogramming in mammalian development. Science *293*, 1089–1093.

Reynolds, L.P., Borowicz, P.P., Caton, J.S., Vonnahme, K.A., Luther, J.S., Hammer, C.J., Maddock Carlin, K.R., Grazul-Bilska, A.T., and Redmer, D.A. (2010). Developmental programming: the concept, large animal models, and the key role of uteroplacental vascular development. J. Anim. Sci. *88*, E61-72.

Robbins, K.M., Chen, Z., Wells, K.D., and Rivera, R.M. (2012). Expression of KCNQ1OT1, CDKN1C, H19, and PLAGL1 and the methylation patterns at the KvDMR1 and H19/IGF2 imprinting control regions is conserved between human and bovine. J. Biomed. Sci. *19*, 95.

Robinson, J.T., Thorvaldsdóttir, H., Winckler, W., Guttman, M., Lander, E.S., Getz, G., and Mesirov, J.P. (2011). Integrative genomics viewer. Nat. Biotechnol. *29*, 24–26.

Rougier, N., Bourc'his, D., Gomes, D.M., Niveleau, A., Plachot, M., Pàldi, A., and Viegas-Péquignot, E. (1998). Chromosome methylation patterns during mammalian preimplantation development. Genes Dev. *12*, 2108–2113.

Rountree, M.R., and Selker, E.U. (2010). DNA methylation and the formation of heterochromatin in *Neurospora crassa*. Heredity *105*, 38–44.

Saadeh, H., and Schulz, R. (2014). Protection of CpG islands against de novo DNA methylation during oogenesis is associated with the recognition site of E2f1 and E2f2. Epigenetics Chromatin *7*, 26.

Salilew-Wondim, D., Fournier, E., Hoelker, M., Saeed-Zidane, M., Tholen, E., Looft, C., Neuhoff, C., Besenfelder, U., Havlicek, V., Rings, F., et al. (2015). Genome-Wide DNA Methylation Patterns of Bovine Blastocysts Developed In Vivo from Embryos Completed Different Stages of Development In Vitro. PLOS ONE *10*, e0140467.

Sangrithi, M.N., Royo, H., Mahadevaiah, S.K., Ojarikre, O., Bhaw, L., Sesay, A., Peters, A.H.F.M., Stadler, M., and Turner, J.M.A. (2017). Non-Canonical and Sexually Dimorphic X Dosage Compensation States in the Mouse and Human Germline. Dev. Cell *40*, 289-301.e3.

Sanz, L.A., Kota, S.K., and Feil, R. (2010). Genome-wide DNA demethylation in mammals. Genome Biol. *11*, 110.

Schaarschmidt, F., and Gerhard, D. (2015). Confidence Intervals for Two Sample Comparisons.

Seisenberger, S., Andrews, S., Krueger, F., Arand, J., Walter, J., Santos, F., Popp, C., Thienpont, B., Dean, W., and Reik, W. (2012). The dynamics of genome-wide DNA methylation reprogramming in mouse primordial germ cells. Mol. Cell *48*, 849–862.

Seisenberger, S., Peat, J.R., Hore, T.A., Santos, F., Dean, W., and Reik, W. (2013). Reprogramming DNA methylation in the mammalian life cycle: building and breaking epigenetic barriers. Phil Trans R Soc B *368*, 20110330.

Seo, M., Caetano-Anolles, K., Rodriguez-Zas, S., Ka, S., Jeong, J.Y., Park, S., Kim, M.J., Nho, W.-G., Cho, S., Kim, H., et al. (2016). Comprehensive identification of sexually dimorphic genes in diverse cattle tissues using RNA-seq. BMC Genomics *17*, 81.

Sharma, S., Kelly, T.K., and Jones, P.A. (2010). Epigenetics in cancer. Carcinogenesis *31*, 27–36.

Sharp, A.J., Stathaki, E., Migliavacca, E., Brahmachary, M., Montgomery, S.B., Dupre, Y., and Antonarakis, S.E. (2011). DNA methylation profiles of human active and inactive X chromosomes. Genome Res. *21*, 1592–1600.

Shen, S., Qu, Y., and Zhang, J. (2014). [The application of next generation sequencing on epigenetic study]. Yi Chuan Hered. *36*, 256–275.

Shi, L., and Wu, J. (2009). Epigenetic regulation in mammalian preimplantation embryo development. Reprod. Biol. Endocrinol. RBE *7*, 59.

Siddiqi, S., Mills, J., and Matushansky, I. (2010). Epigenetic Remodeling of Chromatin Architecture: Exploring Tumor Differentiation Therapies in Mesenchymal Stem Cells and Sarcomas. Curr. Stem Cell Res. Ther. *5*, 63–73.

Siegfried, Z., Eden, S., Mendelsohn, M., Feng, X., Tsuberi, B.Z., and Cedar, H. (1999). DNA methylation represses transcription in vivo. Nat. Genet. *22*, 203–206.

Slotkin, R.K., and Martienssen, R. (2007). Transposable elements and the epigenetic regulation of the genome. Nat. Rev. Genet. *8*, 272–285.

Smallwood, S.A., and Kelsey, G. (2012). De novo DNA methylation: a germ cell perspective. Trends Genet. *28*, 33–42.

Smallwood, S.A., Lee, H.J., Angermueller, C., Krueger, F., Saadeh, H., Peat, J., Andrews, S.R., Stegle, O., Reik, W., and Kelsey, G. (2014). Single-cell genome-wide bisulfite sequencing for assessing epigenetic heterogeneity. Nat. Methods *11*, 817–820.

Smit, M.A., Tordoir, X., Gyapay, G., Cockett, N.E., Georges, M., and Charlier, C. (2005). BEGAIN: a novel imprinted gene that generates paternally expressed transcripts in a tissue- and promoter-specific manner in sheep. Mamm. Genome Off. J. Int. Mamm. Genome Soc. *16*, 801–814.

Smith, S.L., Everts, R.E., Tian, X.C., Du, F., Sung, L.-Y., Rodriguez-Zas, S.L., Jeong, B.-S., Renard, J.-P., Lewin, H.A., and Yang, X. (2005). Global gene expression profiles reveal significant nuclear reprogramming by the blastocyst stage after cloning. Proc. Natl. Acad. Sci. U. S. A. *102*, 17582.

Smith, Z.D., Gu, H., Bock, C., Gnirke, A., and Meissner, A. (2009). High-throughput bisulfite sequencing in mammalian genomes. Methods San Diego Calif *48*, 226–232.

Smith, Z.D., Chan, M.M., Mikkelsen, T.S., Gu, H., Gnirke, A., Regev, A., and Meissner, A. (2012). A unique regulatory phase of DNA methylation in the early mammalian embryo. Nature *484*, 339–344.

Soneson, C., Love, M.I., and Robinson, M.D. (2015). Differential analyses for RNA-seq: transcript-level estimates improve gene-level inferences. F1000Research *4*, 1521.

Stewart, K.R., Veselovska, L., and Kelsey, G. (2016). Establishment and functions of DNA methylation in the germline. Epigenomics *8*, 1399–1413.

Surani, M.A., and Barton, S.C. (1983). Development of gynogenetic eggs in the mouse: implications for parthenogenetic embryos. Science *222*, 1034–1036.

Surani, M.A., Barton, S.C., and Norris, M.L. (1984). Development of reconstituted mouse eggs suggests imprinting of the genome during gametogenesis. Nature *308*, 548–550.

Suzuki, M.M., and Bird, A. (2008). DNA methylation landscapes: provocative insights from epigenomics. Nat. Rev. Genet. *9*, 465–476.

Tadros, W., and Lipshitz, H.D. (2009). The maternal-to-zygotic transition: a play in two acts. Development *136*, 3033–3042.

Takahashi, Y., Wu, J., Suzuki, K., Martinez-Redondo, P., Li, M., Liao, H.-K., Wu, M.-Z., Hernández-Benítez, R., Hishida, T., Shokhirev, M.N., et al. (2017). Integration of CpG-free DNA induces de novo methylation of CpG islands in pluripotent stem cells. Science *356*, 503–508.

Tan, K., An, L., Miao, K., Ren, L., Hou, Z., Tao, L., Zhang, Z., Wang, X., Xia, W., Liu, J., et al. (2016). Impaired imprinted X chromosome inactivation is responsible for the skewed sex ratio following in vitro fertilization. Proc. Natl. Acad. Sci. U. S. A. *113*, 3197–3202.

Telford, N.A., Watson, A.J., and Schultz, G.A. (1990). Transition from maternal to embryonic control in early mammalian development: a comparison of several species. Mol. Reprod. Dev. *26*, 90–100.

Terrenoire, E., McRonald, F., Halsall, J.A., Page, P., Illingworth, R.S., Taylor, A.M.R., Davison, V., O'Neill, L.P., and Turner, B.M. (2010). Immunostaining of modified histones defines high-level features of the human metaphase epigenome. Genome Biol. *11*, R110.

Thurston, A., Taylor, J., Gardner, J., Sinclair, K.D., and Young, L.E. (2008). Monoallelic expression of nine imprinted genes in the sheep embryo occurs after the blastocyst stage. Reprod. Camb. Engl. *135*, 29–40.

Tian, X. (cindy) (2012). Bovine Epigenetics and Epigenomics. In Bovine Genomics, J.E. Womack, ed. (Wiley-Blackwell), pp. 144–168.

Tian, D., Sun, S., and Lee, J.T. (2010). The long noncoding RNA, Jpx, is a molecular switch for X-chromosome inactivation. Cell *143*, 390–403.

Tomizawa, S., Kobayashi, H., Watanabe, T., Andrews, S., Hata, K., Kelsey, G., and Sasaki, H. (2011). Dynamic stage-specific changes in imprinted differentially methylated regions during early mammalian development and prevalence of non-CpG methylation in oocytes. Dev. Camb. Engl. *138*, 811–820.

Turner, J.M.A. (2007). Meiotic sex chromosome inactivation. Dev. Camb. Engl. *134*, 1823–1831.

Umlauf, D., Goto, Y., Cao, R., Cerqueira, F., Wagschal, A., Zhang, Y., and Feil, R. (2004). Imprinting along the Kcnq1 domain on mouse chromosome 7 involves repressive histone methylation and recruitment of Polycomb group complexes. Nat. Genet. *36*, 1296–1300.

Urich, M.A., Nery, J.R., Lister, R., Schmitz, R.J., and Ecker, J.R. (2015). MethylC-seq library preparation for base-resolution whole-genome bisulfite sequencing. Nat. Protoc. *10*, 475–483.

Vakoc, C.R., Sachdeva, M.M., Wang, H., and Blobel, G.A. (2006). Profile of Histone Lysine Methylation across Transcribed Mammalian Chromatin. Mol. Cell. Biol. *26*, 9185–9195.

Valinluck, V., and Sowers, L.C. (2007). Endogenous Cytosine Damage Products Alter the Site Selectivity of Human DNA Maintenance Methyltransferase DNMT1. Cancer Res. *67*, 946–950.

Van Bemmel, J.G., Mira-Bontenbal, H., and Gribnau, J. (2016). Cis- and trans-regulation in X inactivation. Chromosoma *125*, 41–50.

Van Cleve, J., and Feldman, M.W. (2007). Sex-Specific Viability, Sex Linkage and Dominance in Genomic Imprinting. Genetics *176*, 1101–1118.

Varmuza, S., and Mann, M. (1994). Genomic imprinting--defusing the ovarian time bomb. Trends Genet. TIG *10*, 118–123.

Vastenhouw, N.L., Zhang, Y., Woods, I.G., Imam, F., Regev, A., Liu, X.S., Rinn, J., and Schier, A.F. (2010). Chromatin signature of embryonic pluripotency is established during genome activation. Nature *464*, 922–926.

Veitia, R.A., and Potier, M.C. (2015). Gene dosage imbalances: action, reaction, and models. Trends Biochem. Sci. *40*, 309–317.

Veselovska, L., Smallwood, S.A., Saadeh, H., Stewart, K.R., Krueger, F., Maupetit-Méhouas, S., Arnaud, P., Tomizawa, S., Andrews, S., and Kelsey, G. (2015). Deep sequencing and de novo assembly of the mouse oocyte transcriptome define the contribution of transcription to the DNA methylation landscape. Genome Biol. *16*, 209.

Vickers, M.H. (2014). Early life nutrition, epigenetics and programming of later life disease. Nutrients *6*, 2165–2178.

Waddington, C.H. (1942). The epigenotype. 1942. Int. J. Epidemiol. *41*, 10–13.

Waldenström, U., Engström, A.-B., Hellberg, D., and Nilsson, S. (2009). Low-oxygen compared with high-oxygen atmosphere in blastocyst culture, a prospective randomized study. Fertil. Steril. *91*, 2461–2465.

Wan, L., and Bartolomei, M.S. (2008). Chapter 7 Regulation of Imprinting in Clusters: Noncoding RNAs Versus Insulators. In Advances in Genetics, (Academic Press), pp. 207–223.

Wang, H., and Dey, S.K. (2006). Roadmap to embryo implantation: clues from mouse models. Nat. Rev. Genet. *7*, 185–199.

Wang, X., and Clark, A.G. (2014). Using next-generation RNA sequencing to identify imprinted genes. Heredity *113*, 156–166.

Wang, L., Zhang, J., Duan, J., Gao, X., Zhu, W., Lu, X., Yang, L., Zhang, J., Li, G., Ci, W., et al. (2014). Programming and inheritance of parental DNA methylomes in mammals. Cell *157*, 979–991.

Wang, X., Soloway, P.D., and Clark, A.G. (2011). A survey for novel imprinted genes in the mouse placenta by mRNA-seq. Genetics *189*, 109–122.

Waterland, R.A., Travisano, M., Tahiliani, K.G., Rached, M.T., and Mirza, S. (2008). Methyl donor supplementation prevents transgenerational amplification of obesity. Int. J. Obes. 2005 *32*, 1373–1379.

Wei, Y., Su, J., Liu, H., Lv, J., Wang, F., Yan, H., Wen, Y., Liu, H., Wu, Q., and Zhang, Y. (2014). MetaImprint: an information repository of mammalian imprinted genes. Dev. Camb. Engl. *141*, 2516–2523.

Weisstein, A.E., Feldman, M.W., and Spencer, H.G. (2002). Evolutionary genetic models of the ovarian time bomb hypothesis for the evolution of genomic imprinting. Genetics *162*, 425–439.

White, M.D., Bissiere, S., Alvarez, Y.D., and Plachta, N. (2016). Chapter Seven - Mouse Embryo Compaction. In Current Topics in Developmental Biology, M.L. DePamphilis, ed. (Academic Press), pp. 235–258.

Wiley, C.D., Matundan, H.H., Duselis, A.R., Isaacs, A.T., and Vrana, P.B. (2008). Patterns of hybrid loss of imprinting reveal tissue- and cluster-specific regulation. PloS One *3*, e3572.

Wilkins, J.F., and Haig, D. (2003). What good is genomic imprinting: the function of parent-specific gene expression. Nat. Rev. Genet. *4*, 359–368.

Wit, E. de, and Laat, W. de (2012). A decade of 3C technologies: insights into nuclear organization. Genes Dev. *26*, 11–24.

Wolf, J.B., and Hager, R. (2006). A maternal-offspring coadaptation theory for the evolution of genomic imprinting. PLoS Biol. *4*, e380.

Woolliams, J.A. (1996). Economic aspects of animal breeding. Livest. Prod. Sci. *2*, 155.

Wu, X., and Zhang, Y. (2017). TET-mediated active DNA demethylation: mechanism, function and beyond. Nat. Rev. Genet. *18*, 517–534.

Wu, G., Bazer, F.W., Wallace, J.M., and Spencer, T.E. (2006). Board-invited review: intrauterine growth retardation: implications for the animal sciences. J. Anim. Sci. *84*, 2316–2337.

Wutz, A., Smrzka, O.W., Schweifer, N., Schellander, K., Wagner, E.F., and Barlow, D.P. (1997). Imprinted expression of the *Igf2r* gene depends on an intronic CpG island. Nature *389*, 745–749.

Xie, W., Schultz, M.D., Lister, R., Hou, Z., Rajagopal, N., Ray, P., Whitaker, J.W., Tian, S., Hawkins, R.D., Leung, D., et al. (2013). Epigenomic analysis of multilineage differentiation of human embryonic stem cells. Cell *153*, 1134–1148.

Xiong, Y., Chen, X., Chen, Z., Wang, X., Shi, S., Wang, X., Zhang, J., and He, X. (2010). RNA sequencing shows no dosage compensation of the active X-chromosome. Nat. Genet. *42*, 1043–1047.

Xue, F., Tian, X.C., Du, F., Kubota, C., Taneja, M., Dinnyes, A., Dai, Y., Levine, H., Pereira, L.V., and Yang, X. (2002). Aberrant patterns of X chromosome inactivation in bovine clones. Nat. Genet. *31*, 216–220.

Yamasaki, K., Hayashida, S., Miura, K., Masuzaki, H., Ishimaru, T., Niikawa, N., and Kishino, T. (2000). The novel gene, gamma2-COP (COPG2), in the 7q32 imprinted domain escapes genomic imprinting. Genomics *68*, 330–335.

Yang, X., Han, H., De Carvalho, D.D., Lay, F.D., Jones, P.A., and Liang, G. (2014). Gene Body Methylation Can Alter Gene Expression and Is a Therapeutic Target in Cancer. Cancer Cell *26*, 577–590.

Yen, Z.C., Meyer, I.M., Karalic, S., and Brown, C.J. (2007). A cross-species comparison of X-chromosome inactivation in Eutheria. Genomics *90*, 453–463.

Young, L.E., Sinclair, K.D., and Wilmut, I. (1998). Large offspring syndrome in cattle and sheep. Rev. Reprod. *3*, 155–163.

Yu, M., Hon, G.C., Szulwach, K.E., Song, C.-X., Zhang, L., Kim, A., Li, X., Dai, Q., Shen, Y., Park, B., et al. (2012). Base-Resolution Analysis of 5-Hydroxymethylcytosine in the Mammalian Genome. Cell *149*, 1368–1380.

Zechner, U., Wilda, M., Kehrer-Sawatzki, H., Vogel, W., Fundele, R., and Hameister, H. (2001). A high density of X-linked genes for general cognitive ability: a run-away process shaping human evolution? Trends Genet. TIG *17*, 697–701.

Zhang, B., Liu, T., Wu, T., Wang, Z., Rao, Z., and Gao, J. (2015). microRNA-137 functions as a tumor suppressor in human non-small cell lung cancer by targeting SLC22A18. Int. J. Biol. Macromol. *74*, 111–118.

Zhang, S., Chen, X., Wang, F., An, X., Tang, B., Zhang, X., Sun, L., and Li, Z. (2016). Aberrant DNA methylation reprogramming in bovine SCNT preimplantation embryos. Sci. Rep. *6*, 30345.

Zhu, P., Guo, H., Ren, Y., Hou, Y., Dong, J., Li, R., Lian, Y., Fan, X., Hu, B., Gao, Y., et al. (2018). Single-cell DNA methylome sequencing of human preimplantation embryos. Nat. Genet. *50*, 12–19.

Zilberman, D. (2017). An evolutionary case for functional gene body methylation in plants and animals. Genome Biol. *18*, 87.

Picard Tools - By Broad Institute. Available online:http://broadinstitute.github.io/picard/.